

2006

Stable-isotope study of infiltration under stream channels in the Mojave Desert

John C. Radyk
San Jose State University

Follow this and additional works at: https://scholarworks.sjsu.edu/etd_theses

Recommended Citation

Radyk, John C., "Stable-isotope study of infiltration under stream channels in the Mojave Desert" (2006). *Master's Theses*. 2920.
DOI: <https://doi.org/10.31979/etd.pe6j-zgr8>
https://scholarworks.sjsu.edu/etd_theses/2920

This Thesis is brought to you for free and open access by the Master's Theses and Graduate Research at SJSU ScholarWorks. It has been accepted for inclusion in Master's Theses by an authorized administrator of SJSU ScholarWorks. For more information, please contact scholarworks@sjsu.edu.

STABLE-ISOTOPE STUDY OF INFILTRATION UNDER STREAM CHANNELS
IN THE MOJAVE DESERT

A Thesis

Presented to

The Faculty of the Department of Geology

San Jose State University

In Partial Fulfillment

of the Requirements for the Degree

Master of Science

by

John C. Radyk

May 2006

UMI Number: 1436946

INFORMATION TO USERS

The quality of this reproduction is dependent upon the quality of the copy submitted. Broken or indistinct print, colored or poor quality illustrations and photographs, print bleed-through, substandard margins, and improper alignment can adversely affect reproduction.

In the unlikely event that the author did not send a complete manuscript and there are missing pages, these will be noted. Also, if unauthorized copyright material had to be removed, a note will indicate the deletion.

UMI[®]

UMI Microform 1436946

Copyright 2006 by ProQuest Information and Learning Company.

All rights reserved. This microform edition is protected against unauthorized copying under Title 17, United States Code.


ProQuest Information and Learning Company
300 North Zeeb Road
P.O. Box 1346
Ann Arbor, MI 48106-1346

© 2006

John C. Radyk

ALL RIGHTS RESERVED

APPROVED FOR THE DEPARTMENT OF GEOLOGY



Dr. June A. Oberdorfer




Dr. David W. Andersen



Dr. Robert L. Michel, U.S. Geological Survey

APPROVED FOR THE UNIVERSITY

 04/18/06

ABSTRACT

STABLE-ISOTOPE STUDY OF INFILTRATION UNDER STREAM CHANNELS IN THE MOJAVE DESERT

By John C. Radyk

To determine if ephemeral channels in the western Mojave Desert provide groundwater recharge, instrumented boreholes were placed in the upper, middle, and lower reaches of two channels, the Oro Grande Wash and Sheep Creek Wash, and on control surfaces away from the active channels. Stable-isotope data from soil waters, precipitation, lysimeter waters, water vapors, and groundwater were used to study water movement beneath the channels.

The data indicate that recharge probably occurs beneath the upper and middle locations of both channels. The isotopic compositions of soil waters from beneath the channels display little or no evaporative enrichment, indicating rapid infiltration and percolation, when compared to soil waters from beneath the control surfaces. Tritium data indicate that percolation rates are 0.3 to 1.1 m/year beneath the channels. Chloride concentrations of as much as 180 mg/L beneath the lower channels and control surfaces indicate no recharge there under current climatic conditions.

TABLE OF CONTENTS

	Page
INTRODUCTION	1
STABLE ISOTOPES OF WATER.....	4
Isotope Ratio, VSMOW, and δ Values	4
Fractionation	5
Rayleigh Processes.....	6
Precipitation and the Meteoric Water Line	9
The Unsaturated Zone.....	10
Shallow Depth Profile.....	10
Below the Transition Zone.....	13
Applications	15
STUDY AREA	17
Geology.....	18
Hydrology and Hydrogeology	19
Alluvial Aquifer	19
Regional Aquifer.....	19
Ephemeral Stream Channels	20
Oro Grande Wash	20
Sheep Creek Wash.....	23

METHODS	25
Drilling Method and Procedures	28
Borehole Instrumentation.....	30
Precipitation Collection	32
Hand-auger Sampling	32
Sample Collection for Stable-isotope Analysis	33
Precipitation Samples.....	33
Core Samples	34
Hand-auger Samples	34
Lysimeter Samples.....	34
Vapor Samples	35
Groundwater	35
Soil-water Extraction	36
Stable-isotope Analysis.....	40
Gravimetric-water Content	40
Soil-water Potential.....	41
Lithology	42
Particle-size Distribution.....	42
Lithologic Descriptions.....	42
Chloride Concentrations	42
Tritium Concentrations	43
RESULTS	44

Lithology	44
Gravimetric-water Content and Soil-water Potential	44
Gravimetric-water Contents	57
Soil-water Potential	57
Chloride and Tritium Data	58
Chloride Concentrations	58
Tritium Concentrations	69
Stable Isotopes	70
Precipitation	70
Stream Water, Snow, Surface Water, and Groundwater.....	74
Soil Water	75
Core Samples	78
Summit.....	78
UOGW	87
MOGW.....	87
LOGW-1	91
LOGW-2	95
OGF.....	95
USCW	100
MSCW	100
LSCW	104
SCF	104

Hand-auger Samples	110
UOGW	110
MOGW.....	111
OGF.....	111
Lysimeters.....	118
UOGW	118
MOGW	118
LOGW-1	124
USCW	124
LSCW	124
Water Vapor.....	131
UOGW	131
MOGW	133
LOGW-1	133
OGF.....	140
DISCUSSION.....	143
Validity of Soil-water-isotope Data.....	148
Oro Grande Wash	148
Sheep Creek Wash.....	149
Discussions of Specific Sites	151
Summit.....	151
UOGW	152

MOGW	153
LOGW-1	158
LOGW-2	161
OGF.....	163
USCW	167
MSCW	169
LSCW	171
SCF	173
Overview.....	174
CONCLUSIONS.....	177
REFERENCES CITED.....	180
APPENDIX A: QUALITY ASSURANCE INVESTIGATIONS FOR SOIL-WATER STABLE-ISOTOPE ANALYSES.....	186
APPENDIX B: CORE AND HAND-AUGER MATERIAL PARTICLE-SIZE DISTRIBUTIONS	206
APPENDIX C: CORE AND HAND-AUGER SAMPLE DATA	214

LIST OF ILLUSTRATIONS

Figure	Page
1. Study Area Map	2
2. Rayleigh Distillation Plot.....	8
3. Shallow Isotope Depth Profile	11
4. Soil Water Mixing Diagram.....	14
5. Landsat Simulated-natural-color Image of Study Area	21
6. Flow at Middle Oro Grande Wash.....	22
7. Borehole and Precipitation Collector Location Map	27
8. Drilling Operations at MOGW	29
9. Soil-water Extraction Distillation Apparatus.....	37
10. Soil-water Extraction in Progress	38
11. Water Contents for Oro Grande Wash Samples	45
12. Water Contents for Sheep Creek Wash Samples.....	46
13. Water Contents and Soil-water Potentials for Summit Samples	47
14. Water Contents and Soil-water Potentials for UOGW Samples.....	48
15. Water Contents and Soil-water Potentials for MOGW Samples	49
16. Water Contents and Soil-water Potentials for LOGW-1 Samples.....	50
17. Water Contents and Soil-water Potentials for LOGW-2 Samples.....	51
18. Water Contents and Soil-water Potentials for OGF Samples	52
19. Water Contents and Soil-water Potentials for USCW Samples.....	53

20. Water Contents and Soil-water Potentials for MSCW Samples	54
21. Water Contents and Soil-water Potentials for LSCW Samples	55
22. Water Contents and Soil-water Potentials for SCF Samples	56
23. Chloride and Tritium Concentrations for Summit Samples.....	59
24. Chloride and Tritium Concentrations for UOGW Samples.....	60
25. Chloride and Tritium Concentrations for MOGW Samples	61
26. Chloride and Tritium Concentrations for LOGW-1 Samples.....	62
27. Chloride and Tritium Concentrations for LOGW-2 Samples.....	63
28. Chloride and Tritium Concentrations for OGF Samples	64
29. Chloride and Tritium Concentrations for USCW Samples.....	65
30. Chloride and Tritium Concentrations for MSCW Samples	66
31. Chloride and Tritium Concentrations for LSCW Samples	67
32. Chloride and Tritium Concentrations for SCF Samples	68
33. δD vs $\delta^{18}O$ Plot of Precipitation Data	72
34. δD vs $\delta^{18}O$ Plot of Bulk-average-precipitation Data	73
35. δD vs $\delta^{18}O$ Plot of Streamflow, Snow, Groundwater, and Bulk-average Precipitation Data.....	77
36. δD vs $\delta^{18}O$ Plot of Soil-water and Precipitation Data	80
37. δD vs $\delta^{18}O$ Plot of Oro Grande Wash Soil Waters	81
38. δD vs $\delta^{18}O$ Plot of Sheep Creek Wash Soil Waters.....	82
39. Oro Grande Wash Deuterium Offsets.....	83
40. Sheep Creek Wash Deuterium Offsets	84

41. δD vs $\delta^{18}O$ Plot of Summit Samples.....	85
42. δD and $\delta^{18}O$ Depth Profiles for Summit Soil Waters	86
43. δD vs $\delta^{18}O$ Plot of UOGW Samples.....	88
44. δD and $\delta^{18}O$ Depth Profiles for UOGW Soil Waters	89
45. δD vs $\delta^{18}O$ Plot of MOGW Samples	90
46. δD and $\delta^{18}O$ Depth Profiles for MOGW Soil Waters.....	92
47. δD vs $\delta^{18}O$ Plot of LOGW-1 Samples.....	93
48. δD and $\delta^{18}O$ Depth Profiles for LOGW-1 Soil Waters	94
49. δD vs $\delta^{18}O$ Plot of LOGW-2 Samples.....	96
50. δD and $\delta^{18}O$ Depth Profiles for LOGW-2 Soil Waters	97
51. δD vs $\delta^{18}O$ Plot of OGF Samples	98
52. δD and $\delta^{18}O$ Depth Profiles for OGF Soil Waters.....	99
53. δD vs $\delta^{18}O$ Plot of USCW Samples.....	101
54. δD and $\delta^{18}O$ Depth Profiles for USCW Soil Waters	102
55. δD vs $\delta^{18}O$ Plot of MSCW Samples	103
56. δD and $\delta^{18}O$ Depth Profiles for MSCW Soil Waters.....	105
57. δD vs $\delta^{18}O$ Plot of LSCW Samples	106
58. δD and $\delta^{18}O$ Depth Profiles for LSCW Soil Waters.....	107
59. δD vs $\delta^{18}O$ Plot of SCF Samples	108
60. δD and $\delta^{18}O$ Depth Profiles for SCF Soil Waters.....	109
61. δD and $\delta^{18}O$ Depth Profiles for UOGW Shallow Soil Waters	112

62. δD vs $\delta^{18}O$ Plot of UOGW Shallow Soil Waters.....	113
63. δD and $\delta^{18}O$ Depth Profiles for MOGW Shallow Soil Waters.....	114
64. δD vs $\delta^{18}O$ Plot of MOGW Shallow Soil Waters.....	115
65. δD and $\delta^{18}O$ Depth Profiles for OGF Shallow Soil Waters.....	116
66. δD vs $\delta^{18}O$ Plot of OGF Shallow Soil Waters.....	117
67. δD vs $\delta^{18}O$ Plot of UOGW Lysimeter Waters.....	120
68. $\delta^{18}O$ Depth Profile of UOGW Lysimeter Waters	121
69. δD vs $\delta^{18}O$ Plot of MOGW Lysimeter Waters	122
70. $\delta^{18}O$ Depth Profile of MOGW Lysimeter Waters	123
71. δD vs $\delta^{18}O$ Plot of LOGW-1 Lysimeter Waters	125
72. $\delta^{18}O$ Depth Profile of LOGW-1 Lysimeter Waters	126
73. δD vs $\delta^{18}O$ Plot of USCW Lysimeter Waters.....	127
74. $\delta^{18}O$ Depth Profile of USCW Lysimeter Waters.....	128
75. δD vs $\delta^{18}O$ Plot of LSCW Lysimeter Waters	129
76. $\delta^{18}O$ Depth Profile of LSCW Lysimeter Waters	130
77. $\delta^{18}O$ Depth Profile of UOGW Water-vapor Samples.....	134
78. δD vs $\delta^{18}O$ Plot of UOGW Water-vapor Samples.....	135
79. $\delta^{18}O$ Depth Profile of MOGW Water-vapor Samples	136
80. δD vs $\delta^{18}O$ Plot of MOGW Water-vapor Samples.....	137
81. $\delta^{18}O$ Depth Profile of LOGW-1 Water-vapor Samples.....	138
82. δD vs $\delta^{18}O$ Plot of LOGW-1 Water-vapor Samples.....	139

83. $\delta^{18}\text{O}$ Depth Profile of OGF Water-vapor Samples	141
84. δD vs $\delta^{18}\text{O}$ Plot of OGF Water-vapor Samples	142
85. Comparison of Control and Channel Locations.....	144
86. MOGW δD Depth Profile Compared to Victorville Precipitation for Water Years 1952-1994.....	156
87. Oro Grande Wash Overview.....	175
88. Sheep Creek Wash Overview	176
A1. Distillation Yield Histogram	190
A2. Distillation Yield versus Water Content	193
A3. Distillation Yield versus Soil-water Potential.....	193
A4. Distillation Yield versus Percent Fines	194
A5. δD vs $\delta^{18}\text{O}$ Plot of Field-sample Rehydration Results.....	198
A6. Isotopic Depletion versus Distillation Yield.....	199
A7. Isotopic Depletion versus Difference in Isotopic Composition between Field and Laboratory Rehydrating Water	200

LIST OF TABLES

Table	Page
1. Borehole Information.....	26
2. Borehole Instrument Placement Depths.....	31
3. Range and Bulk-average Isotopic Compositions of Precipitation from the Study Area	71
4. Surface-water, Snow, and Groundwater Isotopic Compositions	76
5. Soil-water Isotopic Composition Ranges and D Offsets	79
6. Range of Isotopic Compositions and Enrichment Seen in Shallow Depth Profiles for Soil Waters Extracted from Hand-auger Samples	111
7. Lysimeter-water Data.....	119
8. Water-vapor Data.....	132
A1. Distillation Yields	190
A2. Results of Duplicate Distillations and Isotopic Analyses	192
A3. Results of Water-toluene Distillations	195
A4. Results of Quartz-sand Rehydration Distillations.....	196
A5. Results of Field-sample Rehydration Distillations	197
B1. Particle-size Distributions of Core and Hand-auger Materials	207
C1. Core and Hand-auger Sample Data.....	215

INTRODUCTION

The western Mojave Desert of California, in particular the Victorville area (Fig. 1), has experienced rapid development and population growth over the last several decades. Water consumption has increased along with the population. Like many arid regions of the southwestern United States, the western Mojave Desert is almost entirely dependent upon groundwater. Groundwater in the area is obtained from two aquifers known locally as the alluvial aquifer and the regional aquifer. The shallow alluvial aquifer underlies the Mojave River flood plain and is sustained by recharge from the Mojave River. The deep regional aquifer underlies the entire region and is thought to contain mainly water that was recharged during pluvial times when the climate was cooler and wetter (Smith et al., 1992). Most of the groundwater pumped is taken from the alluvial aquifer, but pumping from the regional aquifer is increasing. The water-table elevation has decreased as much as 0.3 m per year in some areas in response to increased groundwater pumping from the regional aquifer (Mendez and Christensen, 1997).

Work by Izbicki et al. (1995) identified areas near the San Gabriel Mountains and beneath ephemeral channels where recharge to the regional aquifer may be occurring under present-day climatic conditions. The unsaturated zone in the area is up to 300 m thick, and it is not known if waters infiltrating beneath the channels reach the water table.

In 1994, the United States Geological Survey and the Mojave Water Agency began an investigation into the possible recharge contributions of ephemeral channels in the Victorville area. The purpose of the study was to provide data for modeling of the

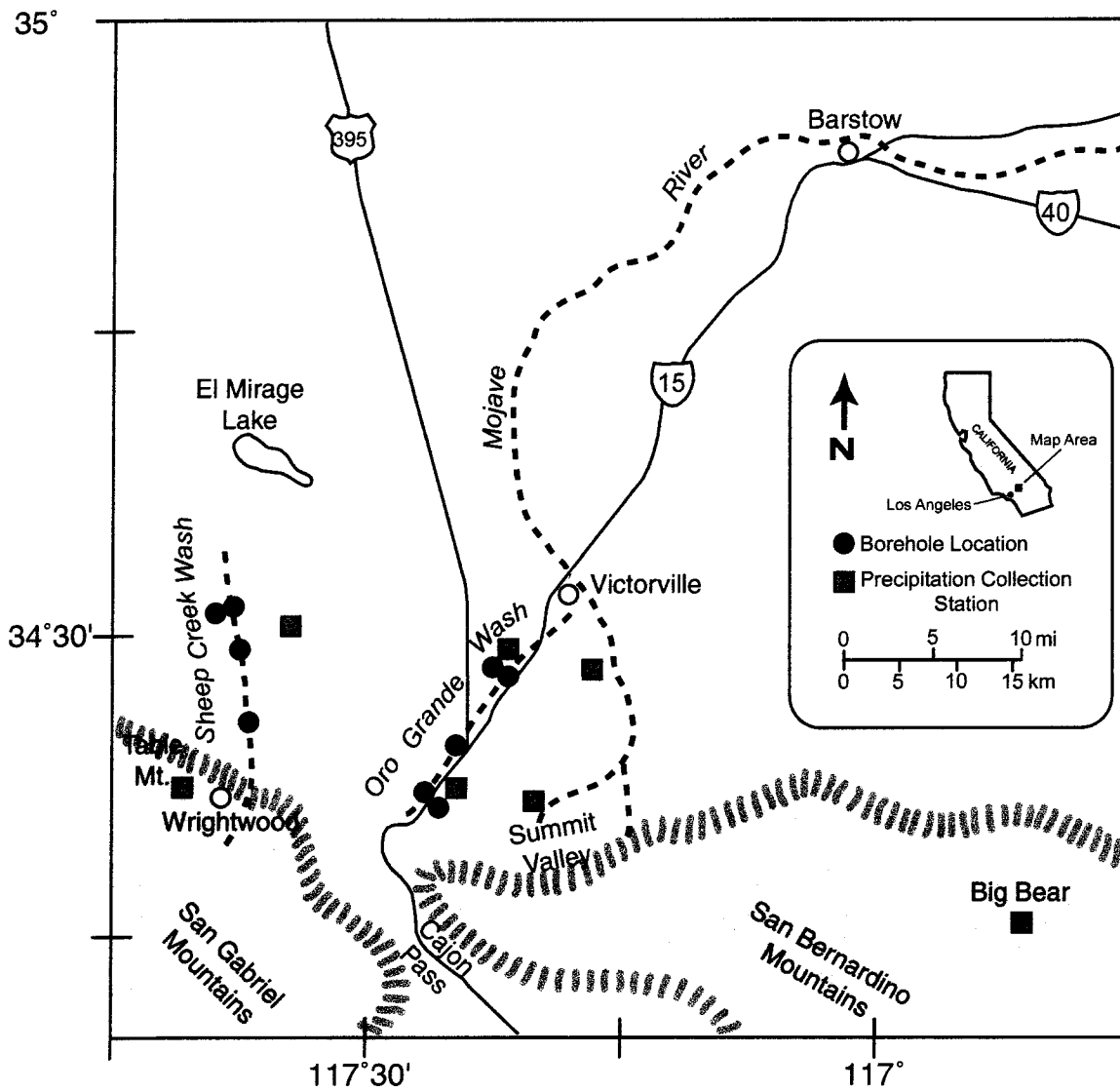


Figure 1. Study area map.

groundwater system and to determine the feasibility of artificial recharge to the regional aquifer through the stream channels.

Two channels, Oro Grande Wash and Sheep Creek Wash (Fig. 1), were chosen for study. Boreholes were placed in the channels and on control surfaces away from the active channels. Cores and cuttings were collected during the drilling process, and the boreholes were instrumented with neutron access tubes, lysimeters, and vapor samplers. The study employed a multi-technique approach involving examination of physical properties and measurement of chemical and isotopic environmental tracer concentrations.

As part of the study, samples of precipitation, stream water, soil water, soil-water vapor, and groundwater collected between 1994 and 1997 were analyzed for their stable-isotope compositions. The stable-isotope data and the interpretations of the data are the subjects of this thesis. The majority of the data are from soil waters extracted from core materials collected in the unsaturated zone beneath the stream channels. The isotopic compositions of the soil waters are compared to the isotopic compositions of precipitation, stream water, and groundwater to determine if infiltrated stream water provides recharge to the regional aquifer. Because the unsaturated zone is a complex environment, the results of gravimetric-water-content, soil-water-potential, chloride, and tritium analyses are included in this thesis and used to support and augment the interpretations of the stable-isotope data.

STABLE ISOTOPES OF WATER

Isotopes are atoms of the same element that have different numbers of neutrons and therefore different masses. Isotopes are either stable or radioactive. Radioactive isotopes decay over time, while stable isotopes do not. Both stable and radioactive isotopes are useful for hydrologic investigations. The subjects of this discussion are the heavy stable isotopes of water, deuterium (D or ^2H) and oxygen-18 (^{18}O). Because D and ^{18}O are part of the water molecule, they can be used as tracers of hydrologic processes. Deuterium is a stable isotope of hydrogen and has an average terrestrial abundance of one deuterium atom for every 6400 protium (^1H) atoms (Kendall and Caldwell, 1998). Oxygen-18 is a stable isotope of oxygen and has an average terrestrial abundance of one ^{18}O atom for every 500 ^{16}O atoms (Kendall and Caldwell, 1998). Although the average abundances of D and ^{18}O are known, their concentrations vary in nature.

Isotope Ratio, VSMOW, and δ Values

The isotopic composition of a substance is denoted by R, the isotope ratio, where R is the ratio of the heavy isotope to the light isotope (for example, $^{18}\text{O}/^{16}\text{O}$). Isotopic composition can be reported as the absolute ratio R, but it normally is reported as a δ (delta) value relative to a standard of known isotopic composition. Delta values for D and ^{18}O are reported in units of parts per thousand (o/oo or per mil) calculated by the following equation:

$$\delta = (R_X / R_S - 1) 1000$$

where R_X and R_S are the isotope ratios of the sample and standard, respectively.

Deuterium and ^{18}O concentrations are reported as δ values relative to Vienna Standard Mean Ocean Water (VSMOW). A positive δ value indicates that the sample contains more of the heavy isotope than VSMOW and is “enriched” relative to VSMOW. A negative δ value indicates that the sample contains less of the heavy isotope than VSMOW and is “depleted” relative to VSMOW. For example, a $\delta^{18}\text{O}$ value of -10 ‰ means that the $^{18}\text{O}/^{16}\text{O}$ of the sample is 10 parts per thousand or 1 % less than the $^{18}\text{O}/^{16}\text{O}$ of VSMOW.

Fractionation

The mass differences, due to the additional neutrons, between D and ^1H , and ^{18}O and ^{16}O , result in slightly different physical and chemical properties. Water molecules containing D or ^{18}O have slightly lower vapor pressures than water molecules containing the lighter isotopes (Gat, 1981). Therefore, water molecules containing the heavy isotopes evaporate less readily and condense more easily. The difference in vapor pressures results in fractionation of the isotopes contained in the liquid and vapor phases of water. Under equilibrium conditions at a particular temperature, the ratio of the isotope ratios of the liquid and vapor phases is constant (Friedman and O’Neil, 1977). This ratio is known as the isotope equilibrium fractionation factor α (alpha):

$$\alpha_{A-B} = R_A / R_B$$

where R is the ratio of the heavy isotope to the light isotope in phases, or compounds, A and B. The values for α are generally close to unity. For example, α_{l-v} values for the

water liquid-vapor phase transition are 1.111 and 1.0117 at 0°C and 1.084 and 1.0098 at 20°C for D and ^{18}O , respectively (Kendall and Caldwell, 1998). Temperature is the most important factor affecting α values; at low temperatures kinetic differences produce larger α values, and with increasing temperatures α approaches unity. The preceding α values are greater than 1, indicating that the liquid phase contains more of the heavy isotope than the vapor phase. The α_{l-v} value of 1.0098 for ^{18}O means the $\delta^{18}\text{O}$ of water is +9.8 ‰ more than the $\delta^{18}\text{O}$ value of vapor with which it is in equilibrium. Another way of expressing fractionation factors is as $10^3 \ln\alpha$, which is a very close estimate of the per mil fractionation between phases or substances. The following formulas can be used to determine $10^3 \ln\alpha$ values for D and ^{18}O for the water liquid-vapor phase transition:

$$\text{D: } 10^3 \ln\alpha = 24.844(10^6 T^{-2}) - 76.248(10^3 T^{-1}) + 52.612,$$

$$^{18}\text{O: } 10^3 \ln\alpha = 1.137(10^6 T^{-2}) - 0.4156(10^3 T^{-1}) - 2.0667,$$

where T is temperature in Kelvin (Friedman and O'Neil, 1977).

Rayleigh Processes

Evaporation and condensation are processes that fractionate D and ^{18}O in water. As water evaporates, the remaining liquid becomes progressively enriched in D and ^{18}O , and, as water condenses, the remaining vapor becomes progressively depleted in D and ^{18}O . For both evaporation and condensation, isotopic fractionation proceeds as a Rayleigh distillation, and the isotopic composition of the remaining water or vapor can be calculated using Rayleigh equations.

For evaporation, an ideal Rayleigh distillation (Fig. 2) would consist of a reservoir of water from which the water vapor is continuously removed from the system; condensation back into the reservoir is not permitted. The fractionation factor remains constant throughout the distillation. As the volume of water remaining in the reservoir decreases, the concentration of the heavy isotopes in the remaining water increases. The isotope ratio of the remaining water is given by:

$$R = R_0 f^{(\alpha - 1)}$$

where R_0 is the initial ratio of the water, f is the fraction of water remaining in the reservoir, and α is the fractionation factor for the temperature of distillation (Kendall and Caldwell, 1998). The distillation described above is known as an "open" system from which vapor is removed continuously under condition of a constant fractionation factor. A "closed" system would involve a second reservoir where removed vapor would accumulate but remain in contact, and therefore in equilibrium, with the water remaining in the first reservoir. Because the water and vapor remain in contact, the range of isotopic composition will be smaller in a closed system than in an open system. Open and closed systems are ideal cases, and natural processes produce fractionations somewhere between the two limiting systems. The preceding discussion of open and closed evaporative systems also applies to condensation. More in-depth discussions of Rayleigh processes can be found in Clark and Fritz (1997) and Kendall and Caldwell (1998).

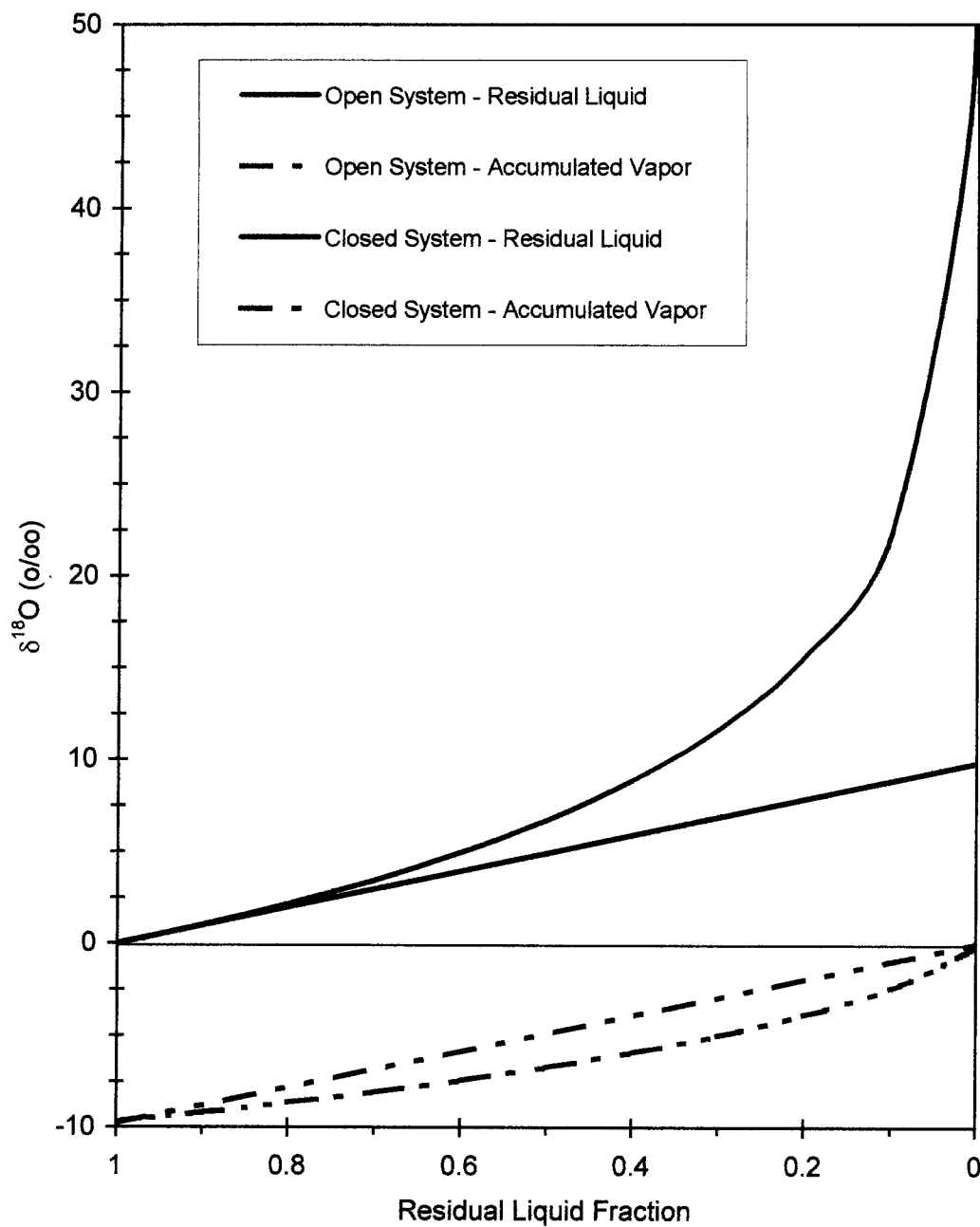


Figure 2. Rayleigh distillation plot for evaporation of water at 20°C. The $\delta^{18}\text{O}$ compositions of residual liquid and accumulated vapor are shown for open and closed systems where initial liquid $\delta^{18}\text{O} = 0$ and fractionation factor $\alpha = 1.0098$.

Precipitation and the Meteoric Water Line

The condensation of vapor in the atmosphere, resulting in precipitation, is a Rayleigh process that results in more negative δ values for the remaining vapor. Plotting precipitation samples from around the world as δD vs $\delta^{18}O$ roughly defines a line with equation:

$$\delta D = 8\delta^{18}O + 10.$$

This line is known as the Global Meteoric Water Line (GMWL) or commonly just the Meteoric Water Line (MWL) (Craig, 1961). The GMWL's slope of 8 approximates the value of equilibrium Rayleigh condensation at 100% humidity. Also, the ratio of fractionation factors for D and ^{18}O is close to 8. The slope of the GMWL is an average and varies from location to location. In arid regions the slope typically is less than 8 because of partial evaporation of precipitation before reaching the ground. Precipitation from a specific area defines a local meteoric water line (LMWL).

The isotopic composition of precipitation is determined by a number of effects, most of which can be explained by Rayleigh processes (Ingraham, 1998). The continental, or rainout effect, occurs as storms move inland from the ocean. The heavier isotopes condense out as precipitation first, and with increasing distance from the ocean the δ values of precipitation tend to become more negative. The altitude effect is the result of adiabatic cooling of an air mass as it moves over mountainous regions. The cooling of the air mass results in precipitation. Cooling and condensation of water vapor continue as altitude increases. Because the heavier isotopes condense out as precipitation first, the isotopic composition of precipitation becomes more negative with altitude.

Because of the altitude effect, precipitation in mountainous regions tends to have more negative δ values than precipitation in nearby lowlands. Seasonal effects upon isotopic composition of precipitation also are common. Winter precipitation typically has more negative δ values than summer precipitation. For any given area, the isotopic composition of local precipitation is determined by a combination of the discussed effects modified by temperature, humidity, and contributions from local evapotranspiration.

The Unsaturated Zone

Shallow Depth Profile

Once precipitation reaches the ground, evaporation, particularly in arid regions, can have a large effect upon isotopic composition. The development of shallow isotope depth profiles has been the subject of much research (Allison et al., 1983; Barnes and Allison, 1983, 1984, 1988; Barnes and Walker, 1989). Shallow soil water undergoes evaporation, and the isotopic composition of shallow soil water develops a characteristic profile that is similar over a wide range of climatic conditions (Fig. 3). From relatively negative δ values near the surface, the δ values increase, reaching a maximum at the depth where the transition from vapor-phase transport to liquid-phase transport occurs. At this “drying front” the capillary upward movement of water in the liquid phase ceases to be the dominant mode of water transport and upward movement of water in the vapor phase becomes the dominant mode. At depths shallower than the isotope maximum, the δ values are more negative due to condensation of vapor and exchange between vapor and the evaporated soil water. Depending upon temperature and the time of day,

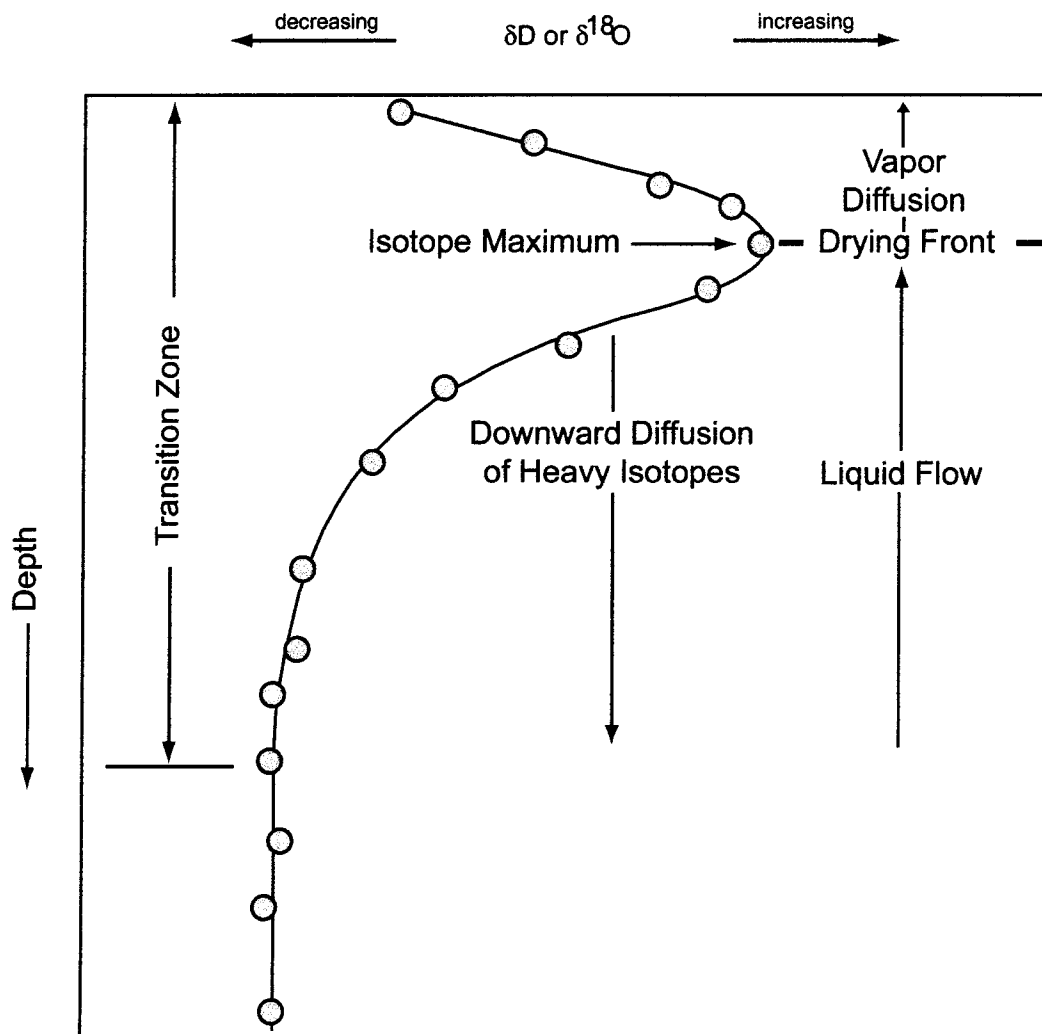


Figure 3. Shallow isotope depth profile (modified from Clark and Fritz, 1997).

evaporation and condensation occur within the region between the land surface and the isotope maximum (Yamanaka and Yonetani, 1999). Below the isotope maximum, the δ values decrease exponentially until they reach a relatively constant value. The decrease in δ values beneath the maximum is the result of downward diffusion of the heavy isotopes within the liquid and upward movement of water in the liquid phase. The depth interval between land surface and the depth at which δ values have reached a relatively constant value is a zone of transition below which evaporative processes cease to modify the isotopic composition of soil water. The depth of the transition zone and the amplitude of the isotope maximum are determined by evaporation rate, water content, and soil properties.

Within the transition zone, the isotopic compositions of soil water plot below the LMWL on an evaporative trend line with a slope less than that of the LMWL. The slope of the evaporative line is dependent upon the relative humidity (Kendall and Caldwell, 1998). With greater humidity, there is less change in δD and $\delta^{18}O$ during evaporation due to molecular exchange between the water and the vapor, and the slope of the evaporative line remains near 8. In arid regions, with low humidities and therefore less molecular exchange between water and vapor, the slopes of evaporative trend lines typically are between 4 and 6. The degree of evaporative enrichment, the displacement from the LMWL, can be numerically expressed as the deuterium or D offset (in ‰) from the LMWL. Greater evaporative enrichment produces larger, more negative, D offsets.

Below the Transition Zone

In the unsaturated zone beneath the transition zone, isotopic compositions of soil water commonly are very similar to precipitation even though the water has journeyed through the transition zone. Infiltrated water from precipitation events of sufficient volume or duration can move through the transition zone, mix with or move past evaporated soil water, and travel through the unsaturated zone with little or no evaporative enrichment. If infiltration is not of high enough volume or sufficient duration, evaporative enrichment will occur and soil water, and groundwater, if climatic conditions remain constant, will be offset from the LMWL. In arid regions the soil water will commonly plot on a line parallel to, but below the LMWL. This is explained by mixing of evaporated water within the transition zone with newly infiltrated water (Fig. 4). Mixing of waters of different isotopic composition will result in water of intermediate isotopic composition. Plotted as δD vs $\delta^{18}O$, the mixture will plot on a line between the two waters, the position (the isotopic composition) determined by the relative proportions of the two waters. Under the proper conditions, the average deuterium offset of the soil water from the LMWL can be used to calculate the average recharge rate for the location (Barnes and Allison, 1983).

Depending upon infiltration rate and amount, the isotopic composition of water moving through the unsaturated zone may or may not be altered by evaporative effects. Once below the transition zone, the isotopic composition of infiltrated water may remain relatively unchanged until it reaches the water table. However, effects such as mixing,

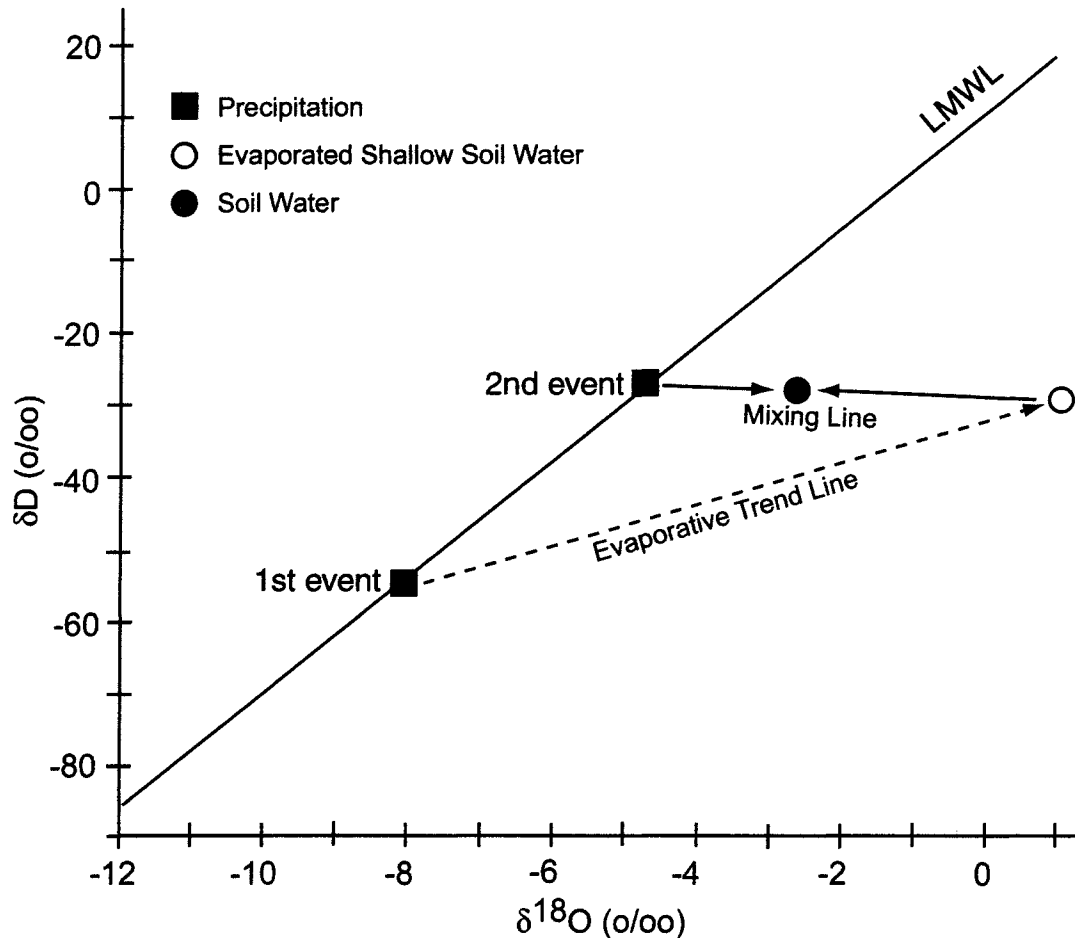


Figure 4. Soil water mixing diagram (modified from Clark and Fritz, 1997). Precipitation (red squares) plots along the local meteoric water line (LMWL). Infiltrated precipitation (1st event) remaining at shallow depths becomes evaporatively enriched shallow soil water (yellow circle). The next precipitation (2nd event) that infiltrates mixes with the evaporatively enriched shallow soil water to produce water with isotopic composition between that of the infiltrated precipitation and the evaporated shallow soil water (blue circle on mixing line) before moving to depths beyond the effects of evaporation. This process is repeated with each infiltration event, and over time, under constant conditions, the soil waters will define a linear trend, parallel to, but below the LMWL.

dispersion, exchange with non-mobile soil waters, water-rock interaction, and vapor transport can all contribute to the modification of the original isotopic composition.

Depth profiles of the isotopic compositions of soil waters in the unsaturated zone can provide evidence of recharge history (Cook et al., 1992). Depending upon conditions, it is possible that thousands of years of recharge history can be recorded in the unsaturated zone. The effects of dispersion and diffusion ultimately will smooth out the profile, but the time interval over which this occurs is dependent upon the recharge rate, the amplitude of the isotope peaks displayed in the profile, the length of time represented by each peak, the moisture content, and the depth of the unsaturated zone. Cook et al. (1992) predicted that evidence of climatic events of 4-5 years duration may be preserved in the unsaturated zone for more than 50 years and that century-scale fluctuations could be preserved for over 1000 years.

Applications

Applications for the stable isotopes of water include identification of water source and flow paths, determination of infiltration and recharge rates, and interpretation of past climatic conditions.

Smith et al. (1992) compared isotopic data on modern groundwater recharge, estimated from a 7-year collection of precipitation samples, to the isotopic compositions of groundwater in southeastern California. More than half of the groundwater samples had δD values at least 10 ‰ more negative than the modern recharge estimates. Their

interpretation was that the more negative groundwaters were recharged under colder, wetter conditions present during pluvial periods more than 10,000 years ago.

Saxena and Dressie (1983) used the difference between winter rains, with more negative δ values, and summer rains, with more positive δ values, to identify peaks in an unsaturated-zone depth profile in glacial sand in Sweden. The infiltration rate, obtained from the isotope profile and independently supported with tritium data, and the moisture content of the sand were used to estimate recharge. The $\delta^{18}\text{O}$ of summer and winter precipitation in their study area differed by 6 to 8 ‰, making identification of seasonal inputs straightforward. Even so, they observed that the amplitude of isotopic variations was rapidly dampened by dispersion, diffusion, and exchange between soil carbon dioxide and soil moisture.

The distance a soil-water sample plots below the LMWL is related to the amount of evaporation the water has undergone. The amount of evaporation can be used as an indication of recharge rate. In a study of four sand dune areas in Australia, where recharge rates had been previously determined using chloride and tritium, Allison et al. (1984) demonstrated that the groundwater recharge rate was inversely proportional to the square of the deuterium offset from the meteoric water line. Phillips et al. (1986) used this relationship to obtain paleoclimatic and recharge information about the central San Juan Basin in New Mexico. In their study, they used the deuterium offset from the meteoric water line and water ages determined from carbon-14 to determine the relative recharge in the basin over a 35,000-year period.

STUDY AREA

The study area is located in the Mojave River basin, part of the western Mojave Desert, about 130 km east of Los Angeles (Fig. 1). It is part of the high desert, with elevations ranging from 1400 m, near the Cajon Pass, to 960 m, near Victorville. The climate is characterized by low precipitation, low humidity, and high summer temperatures. Precipitation occurs mainly during the winter and averages about 15 cm per year in the Victorville area (National Oceanic and Atmospheric Administration), but it can exceed 75 cm per year near the Cajon Pass where cool, damp air from the Pacific Ocean enters the Mojave Desert (Izbicki et al., 1998). Average annual temperature for the Victorville area is 21°C with summer temperatures commonly over 38°C (National Oceanic and Atmospheric Administration). The geology of the area consists mainly of alluvial fan deposits shed from the San Gabriel Mountains to the south (Weldon and Sieh, 1985). The main hydrologic feature of the area is the Mojave River, which flows north from the San Bernardino Mountains to Barstow, where it turns to the east. The Mojave River is an ephemeral stream with perennial surface flow occurring only where shallow bedrock forces water to the surface. The river is the major source of recharge for shallow groundwater in the area (Izbicki et al., 1995).

First settlement of the area occurred along the river, where surface water and shallow groundwater allowed irrigation of crops. In 1960, the city of Victorville had a population of approximately 8,000, alfalfa and pasture were the main crops, and mining and cement manufacture were the main industries (California State Department of Water

Resources, 1967). In 2004, the population of the city of Victorville had increased to approximately 78,000 (City of Victorville, 2004). The growth in population resulted in a 400 percent increase in water usage between 1980 and 2002 (Victor Valley Water District News, 2002).

Numerous ephemeral stream channels extend into the basin from the mountains south of the study area. Work by Izbicki et al. (1995) suggests that some of these channels may provide recharge to the groundwater system. Two channels, Oro Grande Wash and Sheep Creek Wash (Fig. 1), were selected for study. Oro Grande Wash begins near the summit of Cajon Pass and parallels Highway 15 north toward Victorville. Sheep Creek Wash originates in the San Gabriel Mountains, near the town of Wrightwood, and flows into the basin toward El Mirage dry lake.

Geology

The western Mojave Desert is a basin filled primarily with sediment shed from the mountains to the south. The sediment consists mainly of coalesced alluvial fan deposits that have formed a northward-sloping plain. In the area of the Cajon Pass, extending from the base of the San Gabriel Mountains, Quaternary alluvial sediment has formed a broad, northward-sloping alluvial apron. Near the Cajon Pass, the alluvial fan surface is not in contact with the San Gabriel Mountains. Movement along the San Andreas fault and headward erosion by a south-flowing drainage system has beheaded the alluvial fan surface. The beheading of the alluvial fan surface is estimated to have occurred 500,000 years ago (Weldon and Sieh, 1985).

Hydrology and Hydrogeology

Groundwater in the area is obtained from two aquifers: the alluvial aquifer, which is the source of most of the groundwater pumped in the area, and the regional aquifer, the source of deeper groundwater that underlies the entire region.

Alluvial Aquifer

The alluvial aquifer is composed of approximately 80 m of river deposits underlying the floodplain of the Mojave River. It is up to 2.5 km in width and is recharged by floodwaters of the river. Deuterium and tritium data indicate that the waters of the alluvial aquifer have been recently recharged by water from the river (Izbicki et al., 1995). The alluvial aquifer is underlain by older alluvium and fan deposits that compose the regional aquifer.

Regional Aquifer

The regional aquifer underlies the entire study area and is more than 300 m thick. The water table lies more than 300 m below land surface near the base of the mountains and about 100 m below land surface near Victorville. The regional aquifer supplies a small portion of the water used in the study area, but water usage is increasing, and in recent years the water table has dropped as much as 0.3 m per year in some areas (Mendez and Christensen, 1997). Stable-isotope composition and carbon-14 ages indicate that most of the water in the regional aquifer was recharged as long as 20,000 years ago (Izbicki et al., 1995). However, in some parts of the regional aquifer, near

Summit Valley (near the front of the San Bernardino Mountains) and underlying some ephemeral channels, stable-isotope compositions and carbon-14 ages ranging from 500 to 2400 years indicate recharge under current climatic conditions (Izbicki et al., 1995). These findings suggest that infiltration of flow from ephemeral stream channels overlying the regional aquifer may currently be a source of recharge.

Ephemeral Stream Channels

Oro Grande Wash

Oro Grande Wash is incised into a beheaded alluvial fan surface (Fig. 5). Since the beheading of the fan surface, an estimated 500,000 years ago (Weldon and Sieh, 1985), the channel has incised into the fan surface as much as 30 m, and its location has remained relatively constant. The active channel averages 3 m wide. No longer in contact with the San Gabriel Mountains, flow in the channel consists solely of local runoff. Flow in the channel (Fig. 6) occurs a few days a year in response to heavy precipitation near the Cajon Pass. Flow after summer thunderstorms has also been observed in the lower reaches of the channel in the vicinity of Victorville (John Izbicki, personal communication, 1996). Summer flow is believed to be due to local runoff from paved surfaces. Flow in the lower channel has also been observed after draining of a water storage tank located west of the channel (John Izbicki, personal communication, 1996). Average annual flow in Oro Grande Wash is estimated to be 500 acre-ft (Izbicki et al., 2000a). The confinement of the channel over time suggests that infiltration

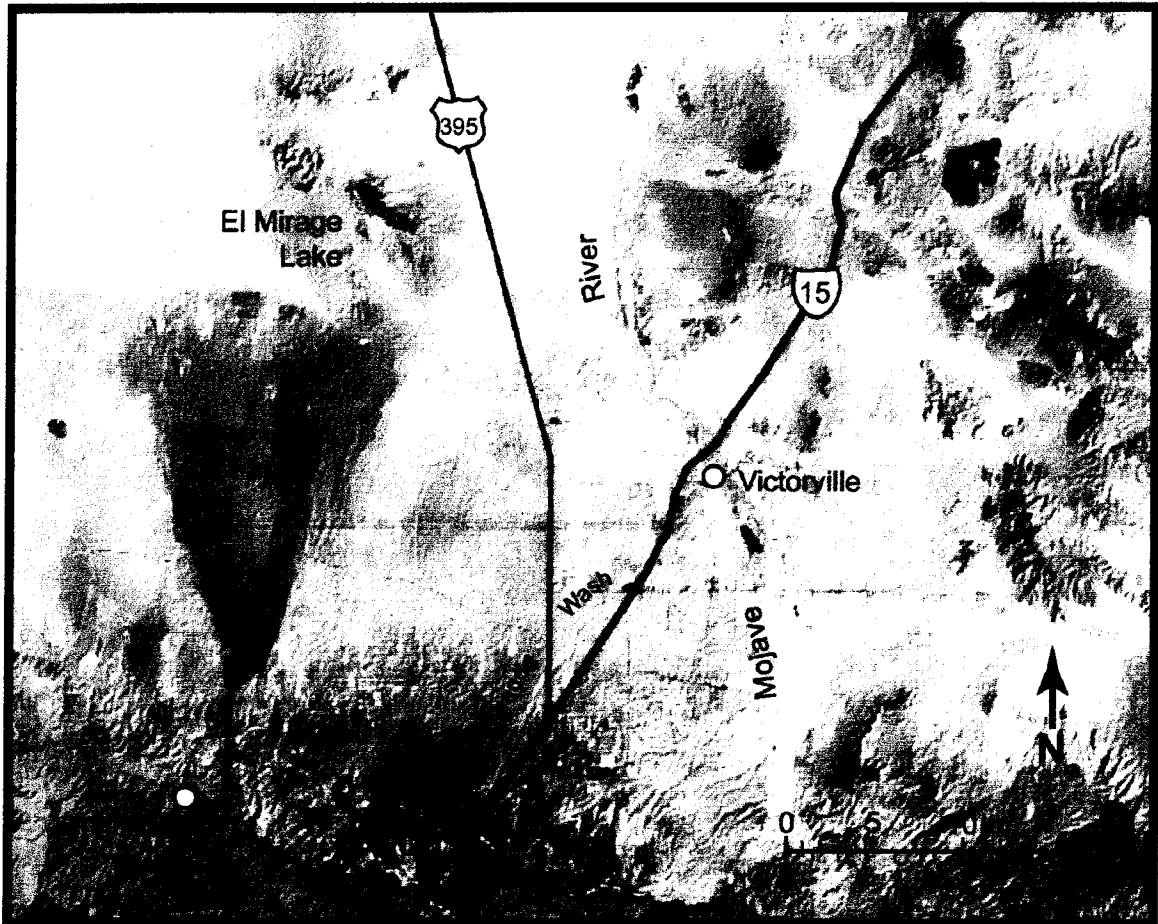


Figure 5. Landsat simulated-natural-color image of study area (modified from U.S. Geological Survey Mojave Desert Satellite Image Map, 1998).



Figure 6. Flow at Middle Oro Grande Wash, 1/9/95. Channel incision into the fan surface can be seen in the background of this view toward the south. The borehole casing in the middle of the photo stands about 1 m (3.3 ft) high.

beneath Oro Grande Wash may be more concentrated, and therefore recharge, if any, may be more likely there than beneath an unconfined channel.

Sheep Creek Wash

Sheep Creek Wash, located to the west of the Oro Grande Wash, flows from the San Gabriel Mountains toward El Mirage dry lake upon the surface of Sheep Creek Fan (Fig. 5). Attempts have been made to confine the channel, but flood warning signs on the highway indicate that this has not been completely successful. Most recently, in 1995, the channel broke through the flood control levees (John Izbicki, personal communication, 1996). The present-day location of the active channel, compared to the channel location shown in air photos taken in the 1950's, indicates that the active channel has changed location within the last 40 years (John Izbicki, personal communication, 1996). Sheep Creek Fan is easily seen in air photos, satellite images, and on the ground due to the color of its sediment (Fig. 5). The sediment from the mountains is derived mainly from the gray Pelona schist, whereas the older alluvium in the basin is brown in color. Channel width is as much as 100 m near the San Gabriel Mountains and gradually decreases to about 3 m over a distance of about 15 km. Flow in the channel is derived mainly from the San Gabriel Mountains, but local runoff does contribute a small amount. Sheep Creek flows more frequently than Oro Grande Wash. Unlike Oro Grande Wash, flow in Sheep Creek is very muddy and viscous, and can occur as a debris flow. The drainage of Sheep Creek includes outcrops of Pelona schist that have been thoroughly pulverized by movement of the San Andreas fault. Rain and snowmelt mobilize the

schist as large debris flows. In May 1941, large debris flows, which occurred daily for more than a week, traveled as much as 24 km (15 mi) into the basin; water runoff continued another 14 km (9 mi) to El Mirage dry lake (Sharp and Nobles, 1953). Average annual flow in Sheep Creek is estimated to be 2,200 acre-ft (Izbicki et al., 2000a). Because the channel of Sheep Creek migrates, infiltration of streamflow beneath the channel is spread over a wide area. Movement of infiltrated stream water through the unsaturated zone may be slower and recharge could be less than under a confined channel such as Oro Grande Wash, even though flow is greater and more frequent in Sheep Creek.

METHODS

The study of infiltration beneath Oro Grande Wash and Sheep Creek Wash was accomplished by drilling and instrumenting boreholes located within the active channel of each wash and on control surfaces away from the active channels. The boreholes within the channels provided information on infiltration of stream water beneath the channels, and the boreholes on the control surfaces provided comparisons between the channels and surrounding areas receiving only direct precipitation. The names, locations, elevations, and depths of each borehole are given in Table 1. Borehole locations are shown in Figure 7. Note that there were two boreholes at Lower Oro Grande Wash. LOGW-2 was located near LOGW-1, 45 m east of the active channel, to investigate the lateral extent of high chloride concentrations found at depth beneath the channel at LOGW-1. There were also two boreholes at Middle Sheep Creek Wash: the first, MSCW-2, was sampled, but collapsed below 85 m (280 ft) before it could be fully instrumented; the second, MSCW-1, was successfully completed. For data interpretation in the study of Sheep Creek Wash the data from MSCW-2 and MSCW-1 were combined and treated as one location. Two control boreholes, Summit and OGF, were associated with Oro Grande Wash because the upper reaches of Oro Grande Wash, near the Cajon Pass, receive much more precipitation than the lower wash. The Summit control borehole represented the wetter environment near the Cajon Pass and the OGF control borehole represented the drier lower wash.

Table 1. Borehole information.

Name	Location	North Latitude	West Longitude	Elevation	Completed Depth	Date Completed
Summit	Fan, control Surface	34°21'37"	117°25'52"	1256 m (4120 ft)	15.2 m (50 ft)	1/97
Upper Oro Grande Wash (UOGW)	Channel	34°22'08"	117°25'51"	1219 m (4000 ft)	32 m (105 ft)	1/95
Middle Oro Grande Wash (MOGW)	Channel	34°25'19"	117°24'07"	1076 m (3530 ft)	201 m (660 ft)	1/95
Lower Oro Grande Wash-1 (LOGW-1)	Channel	34°28'03"	117°21'25"	973 m (3190 ft)	31.4 m (103 ft)	11/94
Lower Oro Grande Wash-2 (LOGW-2)	45 m from channel	34°28'02"	117°21'28"	977 m (3205 ft)	31.4 m (103 ft)	1/97
Oro Grande Fan (OGF)	Fan, control surface	34°28'04"	117°21'33"	983 m (3225 ft)	31.4 m (103 ft)	11/94
Upper Sheep Creek Wash (USCW)	Channel	34°25'51"	117°36'35"	1274 m (4180 ft)	30.5 m (100 ft)	12/95
Middle Sheep Creek Wash-2 (MSCW-2)	Channel	34°29'25"	117°37'07"	1069 m (3505 ft)	85.4 m (280 ft)	4/96
Middle Sheep Creek Wash-1 (MSCW-1)	Channel	34°29'23"	117°37'06"	1069 m (3505 ft)	190.9 m (626 ft)	4/96
Lower Sheep Creek Wash (LSCW)	Channel	34°31'06"	117°37'55"	1002 m (3288 ft)	32.9 m (108 ft)	12/95
Sheep Creek Fan (SCF)	Fan, control surface	34°30'54"	117°37'49"	1009 m (3308 ft)	24.4 m (80 ft)	12/95

Cores and cuttings were collected during drilling operations. Holes were logged after completion of drilling and then were instrumented with neutron access tubes, suction lysimeters, and vapor samplers. In addition to the boreholes, five precipitation collection stations were established in the study area. Hand-auger samples were also collected at several sites along Oro Grande Wash to investigate recent infiltration and the shallow isotope depth profile.

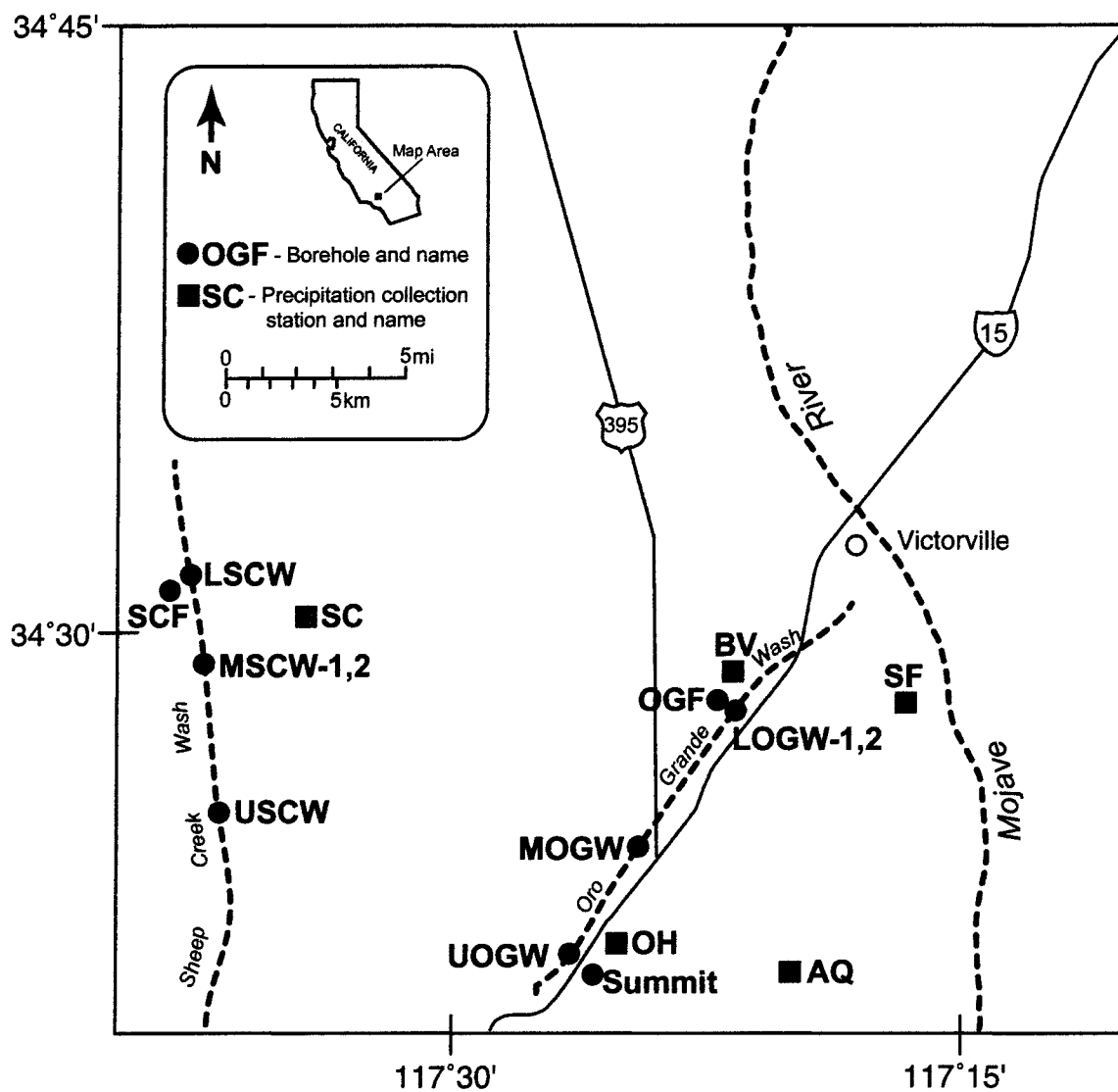


Figure 7. Borehole and precipitation collector location map. Precipitation collection station names are Aqueduct (AQ), Bear Valley Road (BV), Oak Hill (OH), Santa Fe (SF), and Sheep Creek (SC).

Drilling Method and Procedures

All drilling operations (Fig. 8) were conducted at the end of the dry season before the beginning of winter rains so that comparisons between the different boreholes could be made. With the exception of MOGW and MSCW-1, -2, boreholes were drilled entirely using the ODEX air-hammer method (Driscoll, 1986; Hammermeister et al., 1986). This method uses an air hammer and a steel casing that advances with the hammer. Drilling foam or mud is not used, so contamination of dry samples is prevented, and the casing allows drilling in unconsolidated sediment, which would otherwise collapse without drilling fluid or mud. For each 1.5-m (5-ft) segment of borehole, cuttings were collected at 0.3-m (1-ft) intervals for the first 0.9 m (3 ft), and then a 0.6-m (2-ft) core was collected. Coring was performed using a piston core barrel. The deep boreholes, MOGW and MSCW-1, -2, reached the water table at 195 m (640 ft), 166 m (544 ft), and 166 m (544 ft), respectively. For the first 30 m (100 ft) in these three boreholes, cuttings and cores were collected as described above, below 30 m (100 ft) cuttings and cores were collected at greater intervals as drilling conditions permitted. MOGW was drilled to 61 m (200 ft) using the ODEX method and completed using air drilling and foam. MSCW-2 was drilled to 61 m (200 ft) using the ODEX method, and reached the water table using air drilling and foam, but collapsed below 85 m (280 ft) before it could be fully instrumented. MSCW-1 was drilled to 122 m (400 ft) using the ODEX method, reached the water table using air drilling and foam, and instruments were installed. To prevent contamination of the deeper core samples, drilling foam was not used when drilling the final 1.5 m (5 ft) before each coring operation.

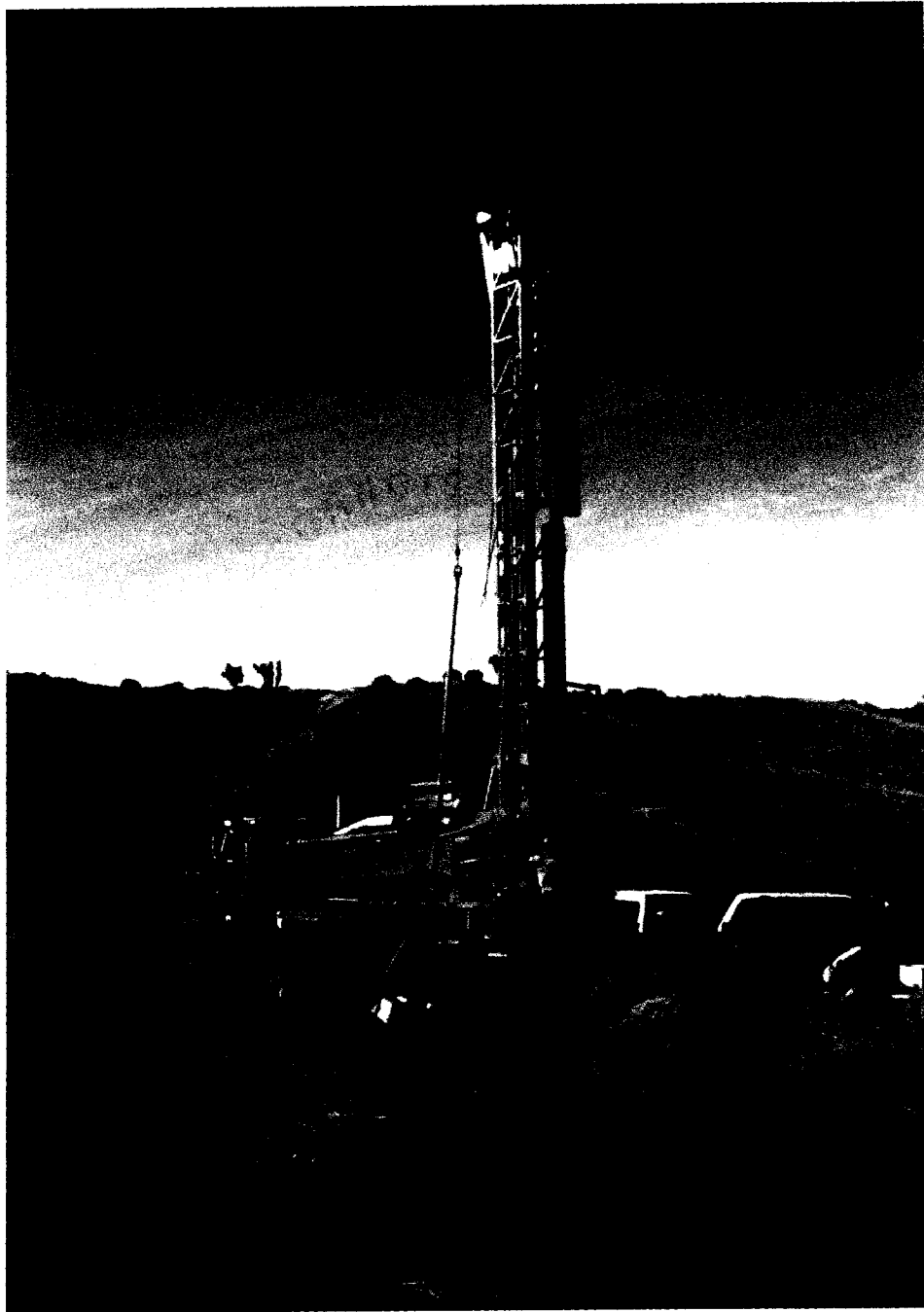


Figure 8. Drilling operations at MOGW (Fig. 7). View is to the west.

Borehole Instrumentation

Boreholes were instrumented with neutron access tubes, suction lysimeters, and vapor samplers (Table 2). Lithologic descriptions from cuttings, specific-conductance measurements taken from cuttings, and neutron and gamma logs were used to determine instrument placement. Logging was performed through the ODEX casing, after the completion of drilling. The results of logging, prior to instrument placement, were used only for instrument placement. Neutron access tubes were installed in each borehole. Suction lysimeters were placed at depths where neutron logging indicated higher water content, and vapor samplers were installed where lower water contents were indicated. Instruments were also located above and below areas of high electro-conductivity. The OGF and SCF boreholes received only vapor samplers because water contents were judged to be too low for lysimeter collection of water.

Neutron access tubes consisted of 5-cm- (2-in.-) diameter galvanized-steel pipe inserted into each borehole. In the deeper holes, MOGW and MSCW-1, stainless-steel screen was attached to the end of the pipe, allowing it to also serve as a water-table well.

The suction-cup lysimeters installed were commercially available units made of 0.46-m- (1.5-ft-) long, 5-cm- (2-in.-) diameter PVC with porous ceramic cups. Units installed at depths of less than 18 m (60 ft) were single chamber, and those installed at greater depths were two-chamber units with stainless-steel one-way valves. The lysimeters were installed in diatomaceous earth. For most of the boreholes, pressure and vacuum-line connections between the lysimeter and the surface were made using 6-mm- (0.25-in.-) diameter refrigeration-grade copper tubing. For MOGW and MSCW-1, the

Table 2. Borehole instrument placement depths.

Site Name	Lysimeter Depths	Vapor Sampler Depths	Neutron Access Tube
Summit	2.1, 6.1 m (7, 20 ft)	2.7, 10.7, 14.9 m (9, 35, 49 ft)	0-15.2 m (0-50 ft)
UOGW	3.4, 11.6, 25 m (11, 38, 82 ft)	6.7, 15.9, 21, 27.7, 32 m (22, 52, 69, 91, 105 ft)	0-31.4 m (0-103 ft)
MOGW	6.7, 13.1, 19.8, 27.1, 42.7 m (22, 43, 65, 89, 140 ft)	7.9, 15.2, 24.4, 45.7, 91.5, 152.4 m (26, 50, 80, 150, 300, 500 ft)	0-201.2 m (0-660 ft) Screened from 189-201.2 m (620-660 ft) to serve as well.
LOGW-1	5.8, 8.2, 21, 24.4 m (19, 27, 69, 80 ft)	13.1, 19.5, 23.8, 27.7, 31.4 m (43, 64, 78, 91, 103 ft)	0-31.4 m (0-103 ft)
LOGW-2	16.8, 22.6, 30.5 m (55, 74, 100 ft)	4.6, 12.2, 25, 31.4 m (15, 40, 82, 103 ft)	0-31.4 m (0-103 ft)
OGF	None Installed	3.7, 9.1, 15.2, 21.3, 25.3 m (12, 30, 50, 70, 83 ft)	0-31.4 m (0-103 ft)
USCW	4.6, 8.5, 14.6, 17.7, 28.7 m (15, 28, 48, 58, 94 ft)	6.1, 11.6, 19.2, 24.4, 29.9 m (20, 38, 63, 80, 98 ft)	0-30.5 m (0-100 ft)
MSCW-2	4.3, 9.1, 15.9, 30.2, 37.2 m (14, 30, 52, 99, 122 ft)	14.6, 25.3, 45.1, 68.9 m (48, 83, 148, 226 ft)	0-85.4 m (0-280 ft)
MSCW-1	48.8, 82.3 m (160, 270 ft)	91.5, 123.5, 152.7 m (300, 405, 501 ft)	0-190.9 m (0-626 ft) Screened from 184.8-190.9 m (606-626 ft) to serve as well.
LSCW	3.4, 8.2, 12.5, 17.7, 27.4 m (11, 27, 41, 58, 90 ft)	6.1, 9.8, 14, 19.8, 32.9 m (20, 32, 46, 65, 108 ft)	0-32 m (0-105 ft)
SCF	None Installed	2.4, 6.1, 15.2, 23.5 m (8, 20, 50, 77 ft)	0-24.4 m (0-80 ft)

deep boreholes, nylon tubing was used for the deeper installations. Graded number 3 Monterey sand was used for backfilling between instruments.

Gas samplers were commercially available 25-cm- (10-in.-) long, 12.7-mm- (0.5-in.-) diameter, stainless-steel units with 0.1-mm (0.004-in.) slotting. Gas samplers were installed in graded number 3 Monterey sand. Gas samplers installed at different depths in the same borehole were isolated from each other by a layer of grout and bentonite chips

installed across a fine-grained sediment layer between the instruments. As with the lysimeters, the connection to the surface for shallower installations was made using copper tubing, with nylon tubing used for the deeper installations. Graded number 3 Monterey sand was used for backfilling between instruments.

Precipitation Collection

Five precipitation collection stations were established in the study area (Fig. 7). They were located in secure areas, such as Caltrans maintenance yards, to prevent vandalism. They were named Aqueduct (AQ), Bear Valley Road (BV), Oak Hill (OH), Santa Fe (SF), and Sheep Creek (SC) for the most significant nearby feature or landmark. Precipitation collection and analysis provided the amount and spatial variation of precipitation within the study area, bulk isotopic composition of precipitation, and chloride deposition data.

Hand-auger Sampling

Shallow soil samples were collected at UOGW, MOGW, and OGF using a hand auger. Samples were collected in January 1996, a year after completion of the boreholes. Samples were collected to compare the isotopic composition of the shallow soil waters with the isotopic composition of precipitation from the previous winter and for examination of the shallow isotope depth profiles. Hand augering was performed within 7 m (23 ft) of each borehole location and within the active channel in the case of MOGW and UOGW. Samples from as deep as 2.7 m (9 ft) were collected.

Sample Collection for Stable-isotope Analysis

Precipitation Samples

Precipitation in the study area was collected from five stations between December of 1994 and October of 1998. Collectors were based on a design by Friedman et al. (1992) and consisted of a 75-mm- (3-in.-) diameter, straight-sided Buchner funnel supported on a stake about 1 m (3.3 ft) above the ground. The funnel was connected to a 1-liter plastic bottle placed below the ground. To prevent evaporation, and resulting fractionation of stable isotopes, a small amount of mineral oil was added to each bottle. Bulk precipitation was collected in April, the end of the rainy season, and November, the end of the dry season. During wet winters samples were collected more frequently to prevent overflow of the collection bottle. After collection, the volume of the sample was measured to determine precipitation amount. Subsamples for stable-isotope analysis were placed in vials with poly-seal caps and shipped to the U.S. Geological Survey Stable Isotope Laboratory in Menlo Park, California. Before analysis, the samples were poured into small separatory funnels and drained into new vials to remove any residual mineral oil.

Because the drainage basin of Sheep Creek lies in the San Gabriel Mountains, at higher altitudes than the study area, precipitation data from two mountain locations (Fig. 1), Big Bear (BB) and Table Mountain (TM), were added to the precipitation data collected in the study area. The data from Big Bear and Table Mountain were obtained from Friedman et al. (1992) and samples were collected between 1982 and 1989.

Core Samples

Cores were collected in a 0.6-m- (2-ft-) long piston core barrel containing four 0.15-m- (6-in.-) long aluminum or brass liners of 0.1-m (4-in.) diameter. After retrieving the core barrel from the borehole, the liners were extruded from the core barrel using a hydraulic ram. Plastic caps were immediately placed on each end of the liner, the caps were wrapped with vinyl tape, the liner was wrapped in plastic, and the entire package was sealed in a labeled, airtight, foil pouch. For stable-isotope analysis either of the two deeper liner sections from each core were used. Use of the deepest sections minimized the possibility of drying or contamination as a result of drilling operations.

Hand-auger Samples

Sample material was removed from the auger bit with a trowel and placed into plastic containers with tight-fitting lids. The lids were sealed with vinyl tape and each container was wrapped in plastic and sealed in a labeled, airtight, foil pouch, in the same manner as the core samples.

Lysimeter Samples

To collect water from the suction lysimeters, a vacuum of about 60 kPa was applied to the vacuum line of the lysimeter using a hand pump. Vacuum was applied at least two weeks before sample collection was attempted. For most of the lysimeters it was necessary to repeat the application of vacuum many times before any water was collected. Water was collected by hooking a compressed nitrogen cylinder to the

pressure line of the lysimeter. Subsamples for stable-isotope analysis were collected and stored in glass vials with poly-seal caps.

Vapor Samples

Vapor was collected in evacuated glass bulbs of 1- to 2-liter capacity. Each gas sampler was purged for several hours prior to sample collection using a peristaltic pump. A bulb was then placed in-line between the vapor sampler tube and the peristaltic pump. The bulb's stopcock was opened slowly and the bulb filled with air. The bulb was allowed to equilibrate for 5 minutes before the stopcock was closed. Bulbs were shipped to the Desert Research Institute Isotope Laboratory in Las Vegas, Nevada, for further processing. At the laboratory, bulbs were placed in liquid nitrogen and non-condensable gases were pumped from the bulb. After warming to room temperature, carbon dioxide gas was collected from the bulb in glass tubes for ^{18}O analysis. Liquid water, for deuterium analysis, was collected in glass capillary tubes.

Groundwater

Groundwater samples from MOGW and MSCW-1 were collected using a positive-displacement piston pump. Samples were collected after at least 3 casing volumes were pumped and temperature, specific conductance, and pH stabilized. Samples for stable-isotope analysis were collected in glass vials with poly-seal caps.

Soil-water Extraction

Soil water was extracted from core and hand-auger samples by means of azeotropic distillation with toluene. The extraction procedure was performed as detailed by Revesz and Woods (1990). Depending upon the apparent moisture content of the sample, between 100 and 300 g of material was weighed, placed into a 500-ml round-bottom boiling flask, and covered with 200 ml of toluene. This operation was performed as rapidly as possible to prevent evaporation that would fractionate the sample. The flask was then connected to the distillation apparatus (Figs. 9 and 10). Distillation time was 75 minutes unless visual examination of the collection funnel revealed water droplets in the chamber above the boiling flask. Residual water indicated that the distillation was not yet complete and additional time was required. Fine-grained materials sometimes required as much as 45 additional minutes of distillation. After cooling, the condenser barrel and collection funnel were gently tapped and toluene from a squirt bottle was sprayed down the condenser barrel to collect any water drops that may have stuck to the side of the condenser or funnel. The extracted water was decanted into a pre-weighed vial with care taken to decant only water. The vial and water were then weighed. The yield of each distillation was determined from the mass of sample used, the mass of water extracted by the distillation, and the gravimetric-water content of the core material, determined from a small subsample of the core material. The water was treated with paraffin wax to remove any residual toluene that could affect the operation of the mass spectrometer. Approximately 1 g of paraffin wax was added to the water and the vial was placed in a 65°C water bath. After the paraffin melted, the vial was shaken so that

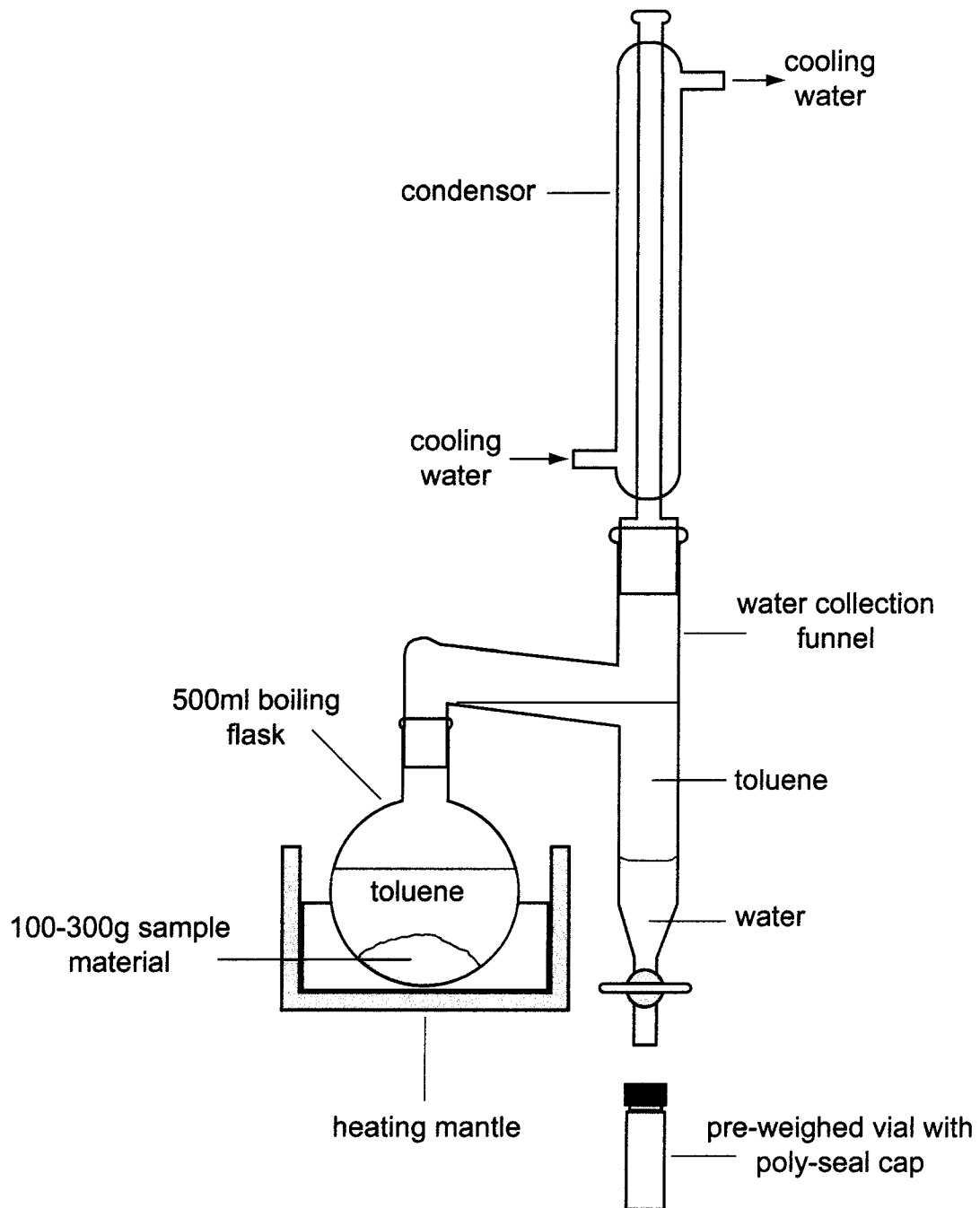


Figure 9. Soil-water extraction distillation apparatus (modified from Revesz and Woods, 1990).

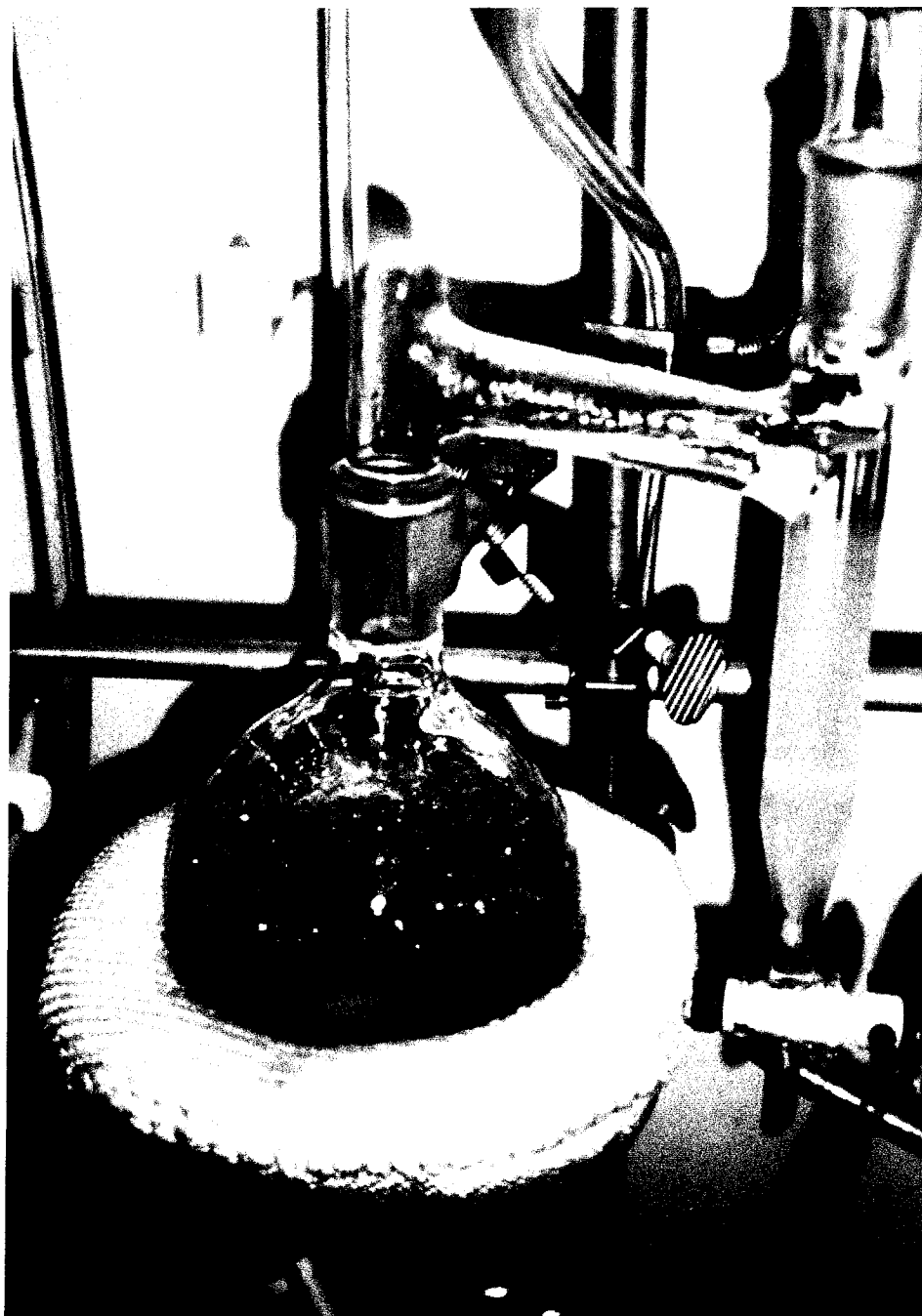


Figure 10. Soil-water extraction in progress.

any residual toluene was absorbed by the paraffin. The vial was allowed to cool and the solidified paraffin was removed. The paraffin treatment was performed twice to ensure that all toluene was removed from the sample.

The extraction of water from soil materials for stable-isotope analysis is a straightforward procedure, but the accuracy of the stable-isotope data obtained from the extracted waters is a matter of some controversy. Revesz and Woods (1990) reported decreased accuracy when dealing with samples with low water content or high clay content. An interlaboratory comparison conducted by Walker et al. (1994) showed that the isotopic compositions of waters extracted by different laboratories differ by several per mil. The differences were attributed to incomplete extraction of soil water. The accuracy of the stable-isotope data obtained from the extracted soil waters in this study was a matter of concern, because they would be compared with precipitation, groundwater, and surface-water data in an attempt to identify the source and recharge history of the soil water. To assess the validity of the stable-isotope data, a quality control program involving the measurement of sample properties, determination of distillation yields, the performance of a series of rehydration experiments, and a literature study were undertaken. The details and results of the quality control program are reported in Appendix A.

As part of the quality control program, soil-water extractions for 36 core samples were performed in duplicate. The duplicate extraction distillations were performed simultaneously on separate subsamples from the same core liner. The distillation yields and isotopic compositions of the waters extracted in duplicate are reported in Appendix

A. For plotting and data interpretation in the study of Oro Grande Wash and Sheep Creek Wash the averages of the duplicates were used.

Stable-isotope Analysis

Precipitation, surface-water, groundwater, lysimeter-water, and extracted soil-water samples were analyzed for stable-isotope composition at the U.S. Geological Survey Stable Isotope Laboratory in Menlo Park, California. Waters collected from soil-vapor samples were analyzed for stable-isotope composition at the Desert Research Institute Isotope Laboratory in Las Vegas, Nevada. Samples were analyzed for ^{18}O content using the carbon dioxide equilibration method of Epstein and Mayeda (1953). The carbon dioxide gas was analyzed with a MAT-251 mass spectrometer. Deuterium content was determined using the zinc reduction method of Kendall and Coplen (1985). Deuterium was measured as hydrogen gas with a Delta E mass spectrometer. Precision of the analyses was +/- 0.05 per mil and +/- 1.5 per mil at the 1-sigma level for ^{18}O and D, respectively. Data are reported in δ (delta) values in per mil (parts per thousand, o/oo) differences in isotope ratio relative to Vienna Standard Mean Ocean Water (VSMOW).

Gravimetric-water Content

Gravimetric-water content was determined using 20- to 40-g subsamples of the core and hand-auger materials. The materials were weighed, oven-dried at 105°C for a minimum of 24 hours, and then reweighed. The water contents of these subsamples were used for determination of azeotropic distillation yields as well as for water-content depth

profiles. The water contents of the small subsamples were determined at the U.S. Geological Survey Isotope Laboratory in Menlo Park, California. The gravimetric-water contents of entire core segments were determined at the Desert Research Institute Laboratory in Las Vegas, Nevada. Gravimetric-water content data from both sources were combined to plot depth profiles for each borehole.

Soil-water Potential

Soil-water potential was obtained by measuring the water activity of small subsamples of the core and hand-auger materials (Gee et al., 1992). The water-activity meter, an AquaLab CX-2, Decagon Devices Inc., utilized a cooled mirror to measure the dew point of the water vapor above a small soil sample. Water activity, A_w , was converted to soil-water potential, ψ , using the Kelvin equation (Rawlins and Campbell, 1986) as follows:

$$\psi = (RT/M)\ln(A_w)$$

where R is the gas constant, T is the temperature in Kelvin, and M is the molecular mass of water. The value of R/M is 461 kPa/K (kilopascals per Kelvin). The soil-water potential expressed here is the total of matric potential and solute potential. These measurements were taken as part of the investigation into the effectiveness of the soil-water extraction technique and were performed at the U.S. Geological Survey Isotope Laboratory in Menlo Park, California. Water activity was also measured on core materials at the Desert Research Institute Laboratory in Las Vegas, Nevada. Soil-water potential data from both sources were combined to plot depth profiles for each borehole.

Lithology

Particle-size Distribution

The sieve technique (Blatt, 1982) was used to determine the particle-size distribution of each subsample of core material used for determination of gravimetric-water content. U.S. Standard Series sieves in sizes 16, 4, 2, 0.35, and 0.074 mm were used. Results are accurate to +/- 0.1 percent.

Lithologic Descriptions

Descriptions of the cuttings collected during drilling operations were made by personnel at the U.S. Geological Survey office in San Diego, California (Izbicki et al., 2000a).

Chloride Concentrations

Cuttings collected during drilling operations were analyzed for their chloride concentrations. The cuttings were sieved to obtain 50 g of material of less than 1 mm size. The sieved material was mixed with 50 ml of distilled water, shaken vigorously for 30 seconds, and allowed to stand for 24 hours. Each sample was then centrifuged at 4,000 rpm for 20 minutes, and filtered through a 0.45- μ m pore-size filter. The chloride concentration of the filtered solution was measured by ion chromatography. These analyses were performed at the U.S. Geological Survey laboratory in San Diego, California.

Tritium Concentrations

Water for tritium measurement was extracted from core materials using a vacuum oven. The material from a core liner, typically between 1.5 and 2 kg, was put into a metal pan and placed in a vacuum oven. A vacuum of about -100 kPa was applied at a temperature of 85°C. Water was collected in cold fingers located in-line between the oven and vacuum pump. Depending upon sample texture, the water extraction process took as long as 8 hours. Finer-grained material usually required longer extraction times. Tritium content was determined by liquid scintillation (Thatcher et al., 1977). Depending upon the volume of water collected, samples were counted directly or were electrolytically enriched prior to counting. Precision of the technique depended upon sample volume and whether or not the sample had been electrolytically enriched. Analyses were performed at the U.S. Geological Survey Tritium Laboratory in Menlo Park.

RESULTS

Lithology

Overall, most of the sediment from beneath both washes and their control surfaces is composed of medium- and coarse-sand-sized material. The primary difference between the two washes is in mineralogy. Sheep Creek Wash sediment is derived largely from Pelona Schist, resulting in gray and grayish-green sediment, whereas the Oro Grande Wash sediment is generally brown and yellowish-brown in color (Izbicki et al., 2000a). The general trend at both washes is one of fining of sediment with greater distance from the mountains, typical of alluvial fan sediments (Rust, 1979). Particle-size analyses for the core samples and hand-auger samples from which soil water was extracted are reported in Appendix B. Lithologic descriptions of drill cuttings and additional particle-size analyses can be found in Izbicki et al. (2000a).

Gravimetric-water Content and Soil-water Potential

The gravimetric-water-content and soil-water-potential data presented in Figures 11 through 22 are the combined results of measurements made at the U.S. Geological Survey and Desert Research Institute laboratories. The gravimetric-water contents and soil-water potentials of core and hand-auger samples from which soil water was extracted for isotopic analysis at the U.S. Geological Survey laboratory are reported in Appendix C. The gravimetric-water contents and soil-water potentials of core samples measured at the Desert Research Institute laboratory are reported in Izbicki et al. (2000a). Figures 11

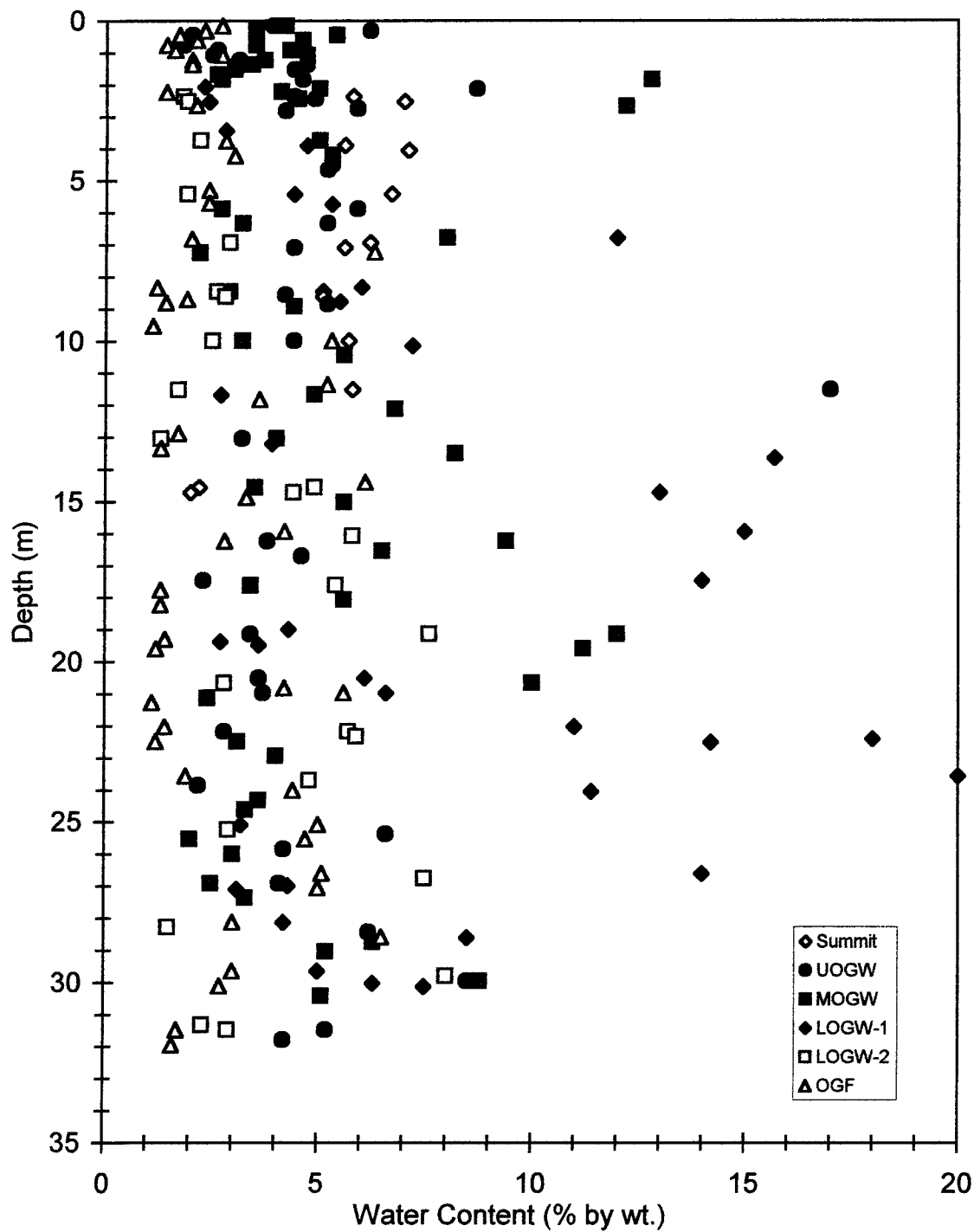


Figure 11. Water contents for Oro Grande Wash samples.

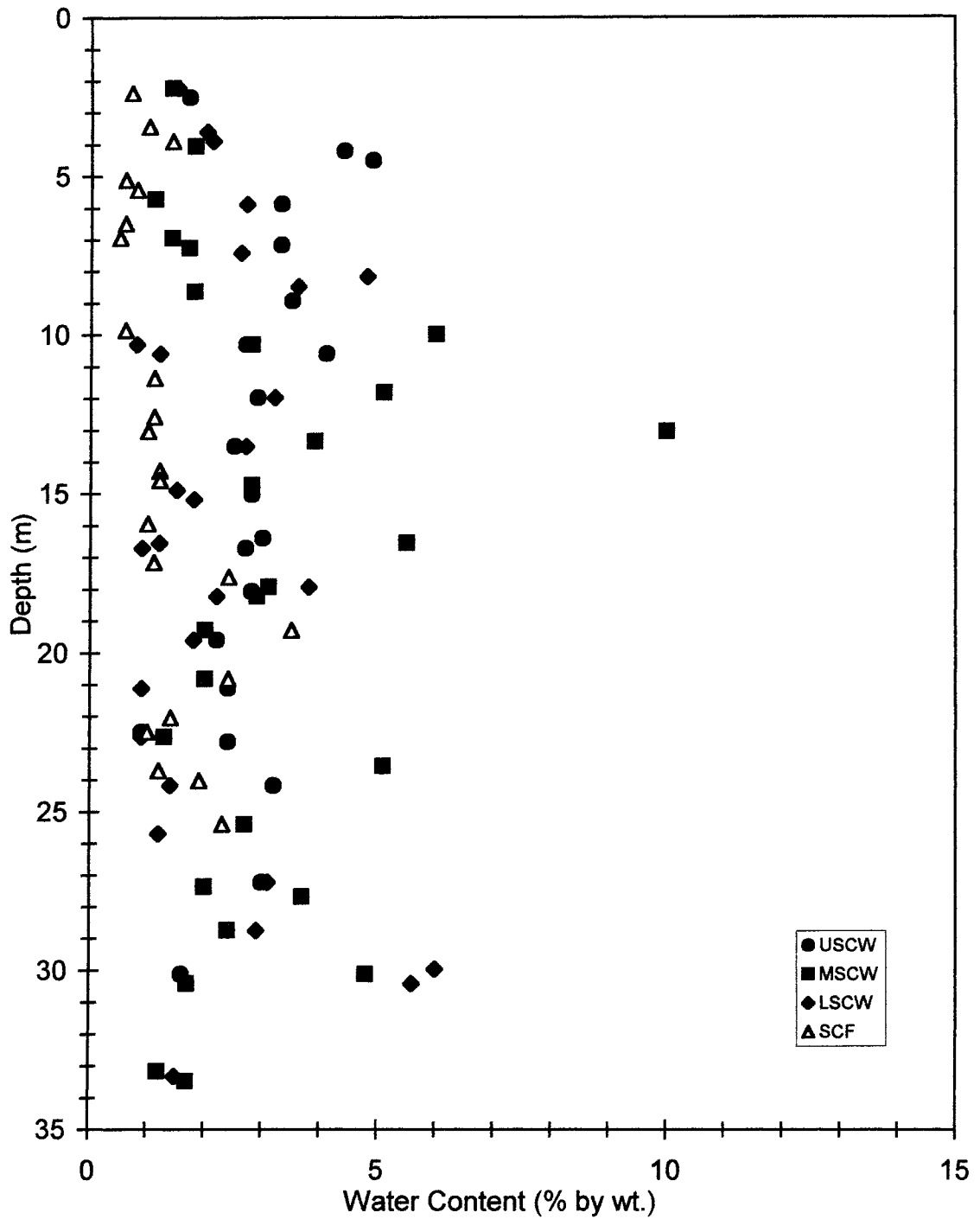


Figure 12. Water contents for Sheep Creek Wash samples.

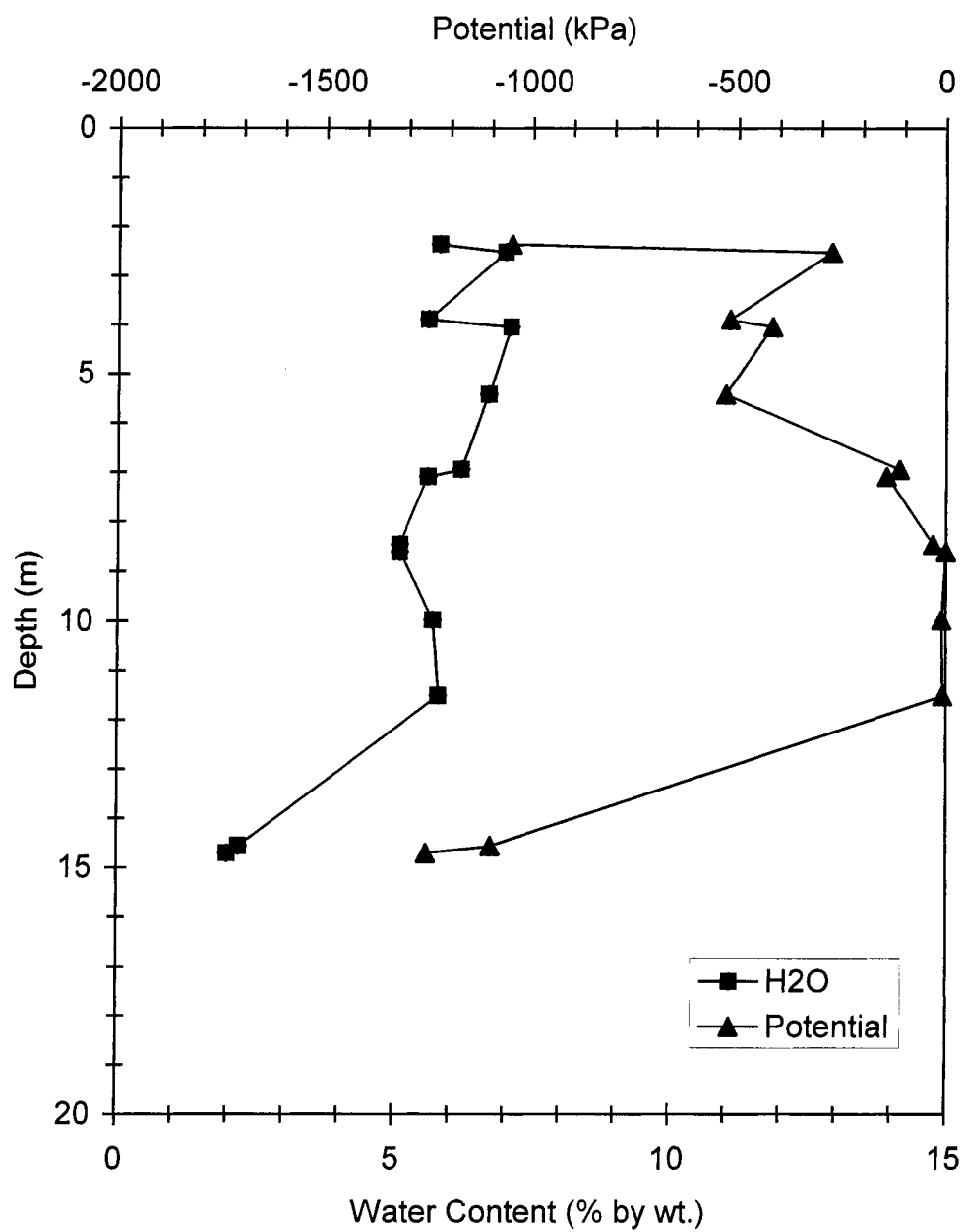


Figure 13. Water contents and soil-water potentials for Summit samples.

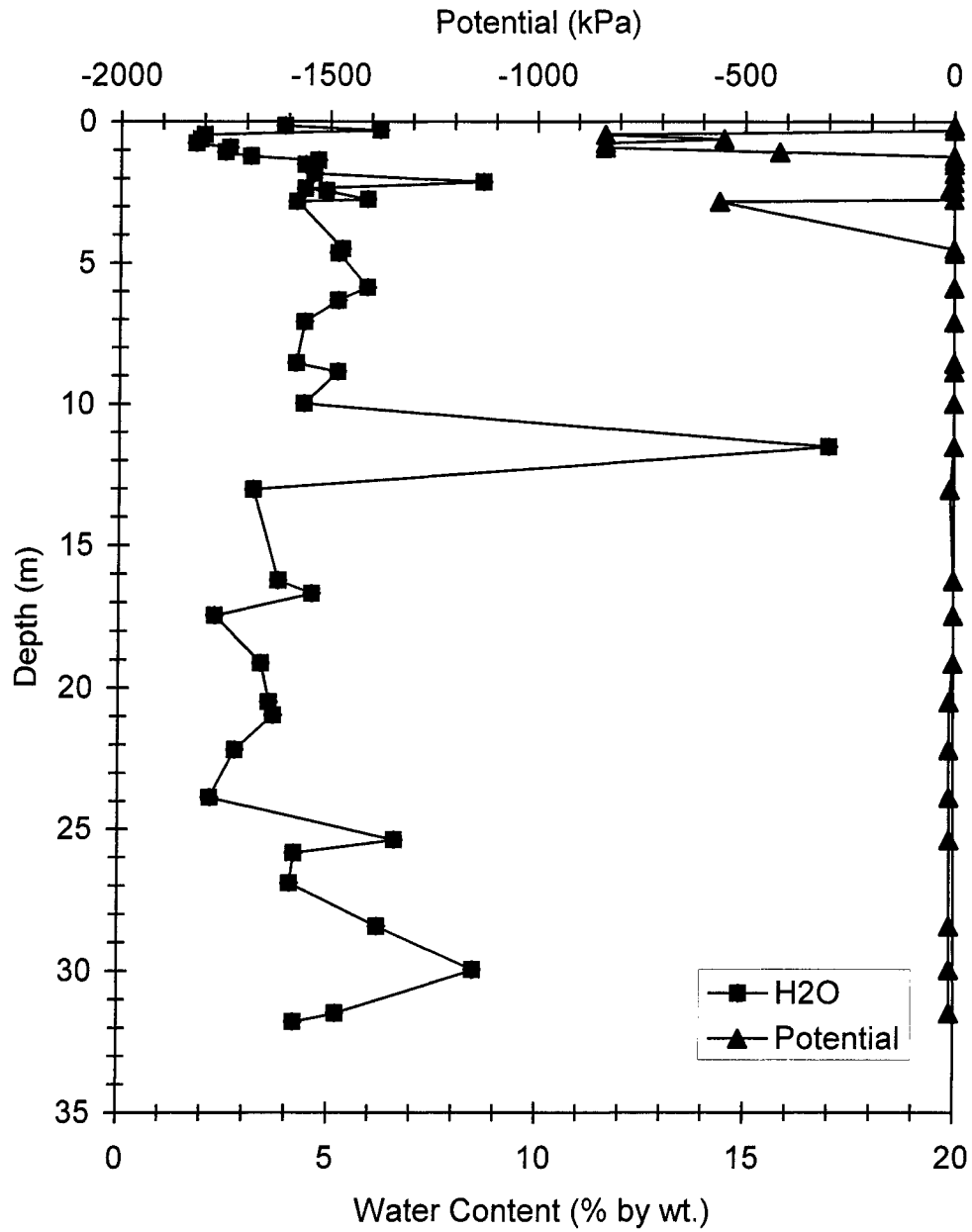


Figure 14. Water contents and soil-water potentials for UOGW samples.

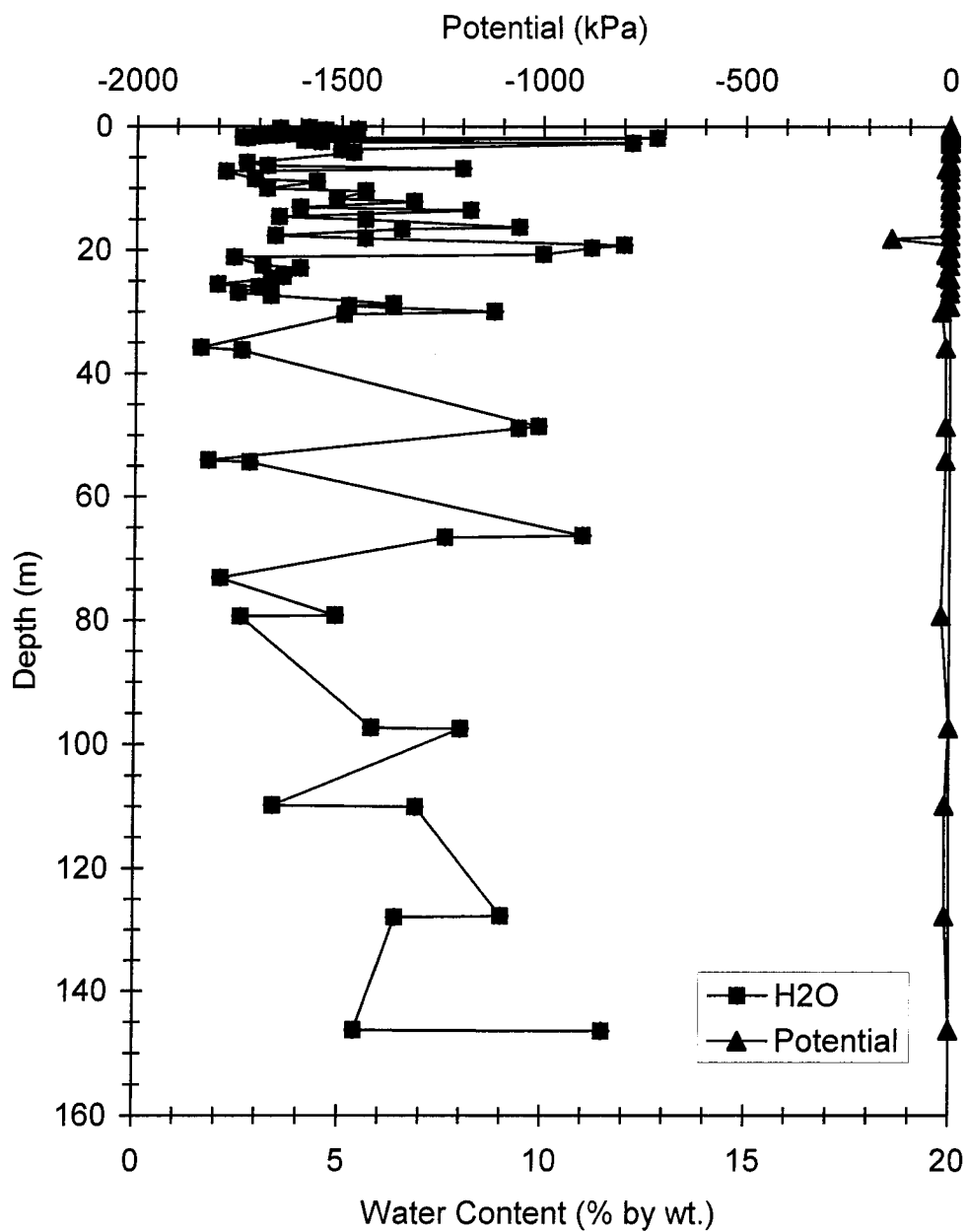


Figure 15. Water contents and soil-water potentials for MOGW samples.

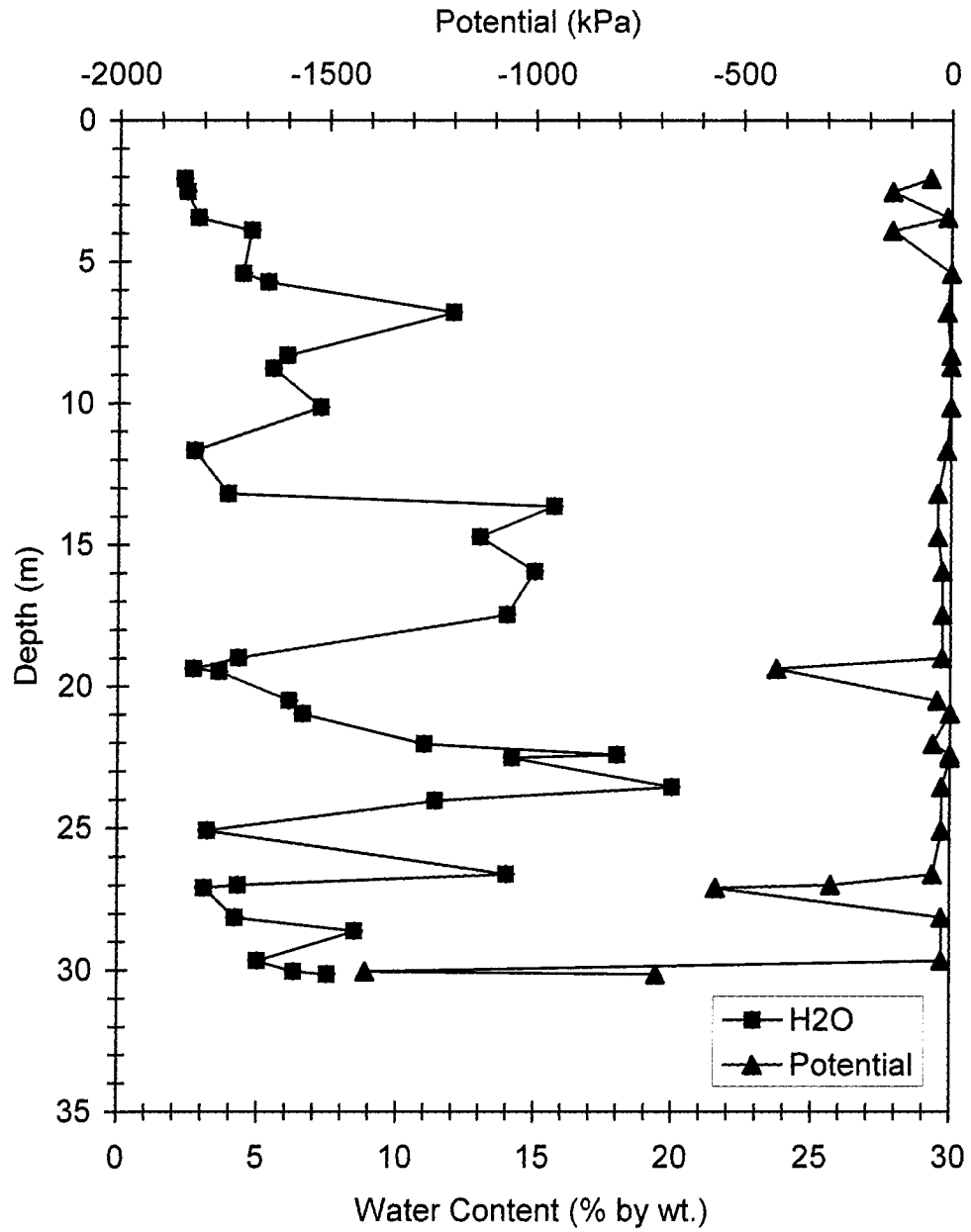


Figure 16. Water contents and soil-water potentials for LOGW-1 samples.

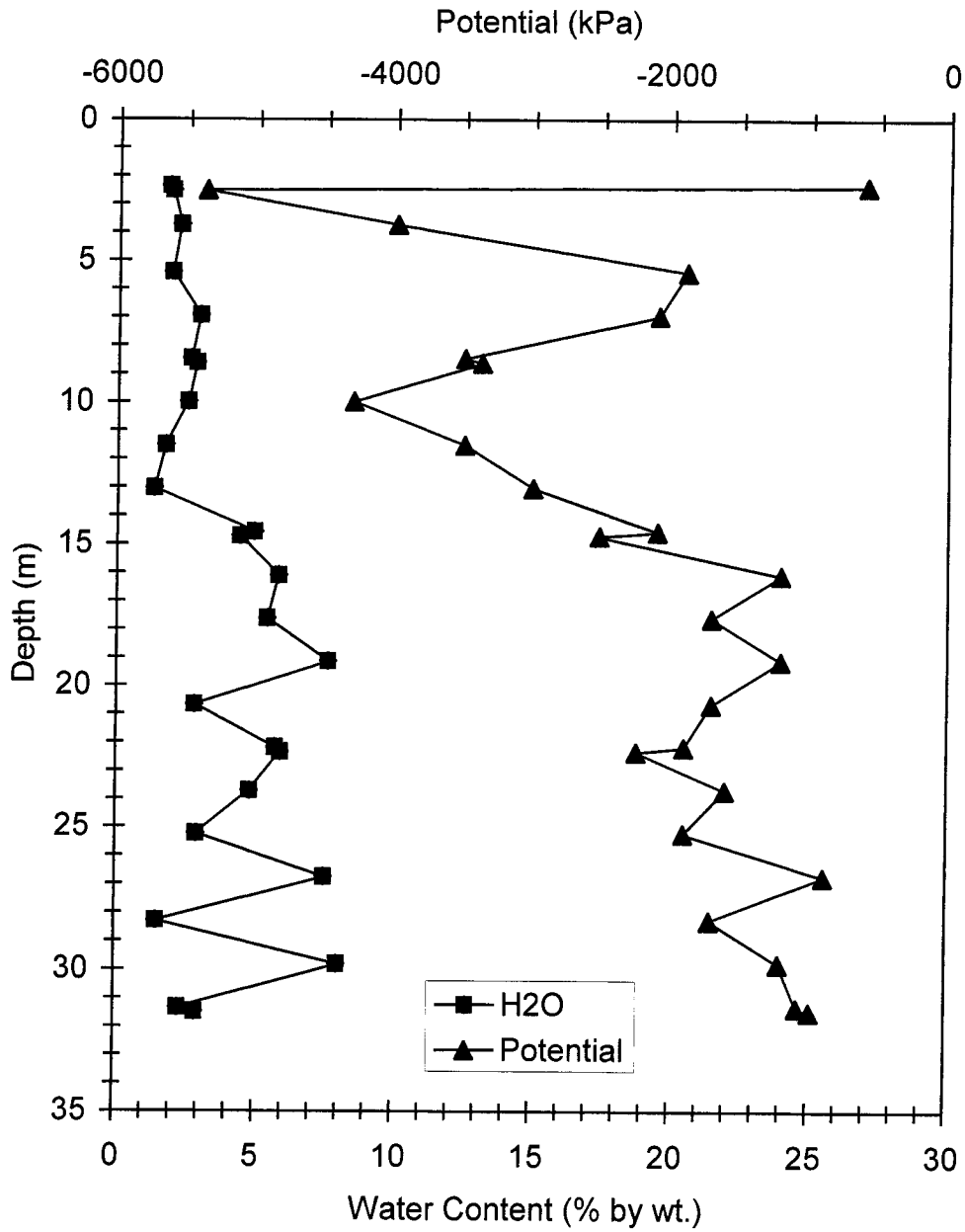


Figure 17. Water contents and soil-water potentials for LOGW-2 samples.

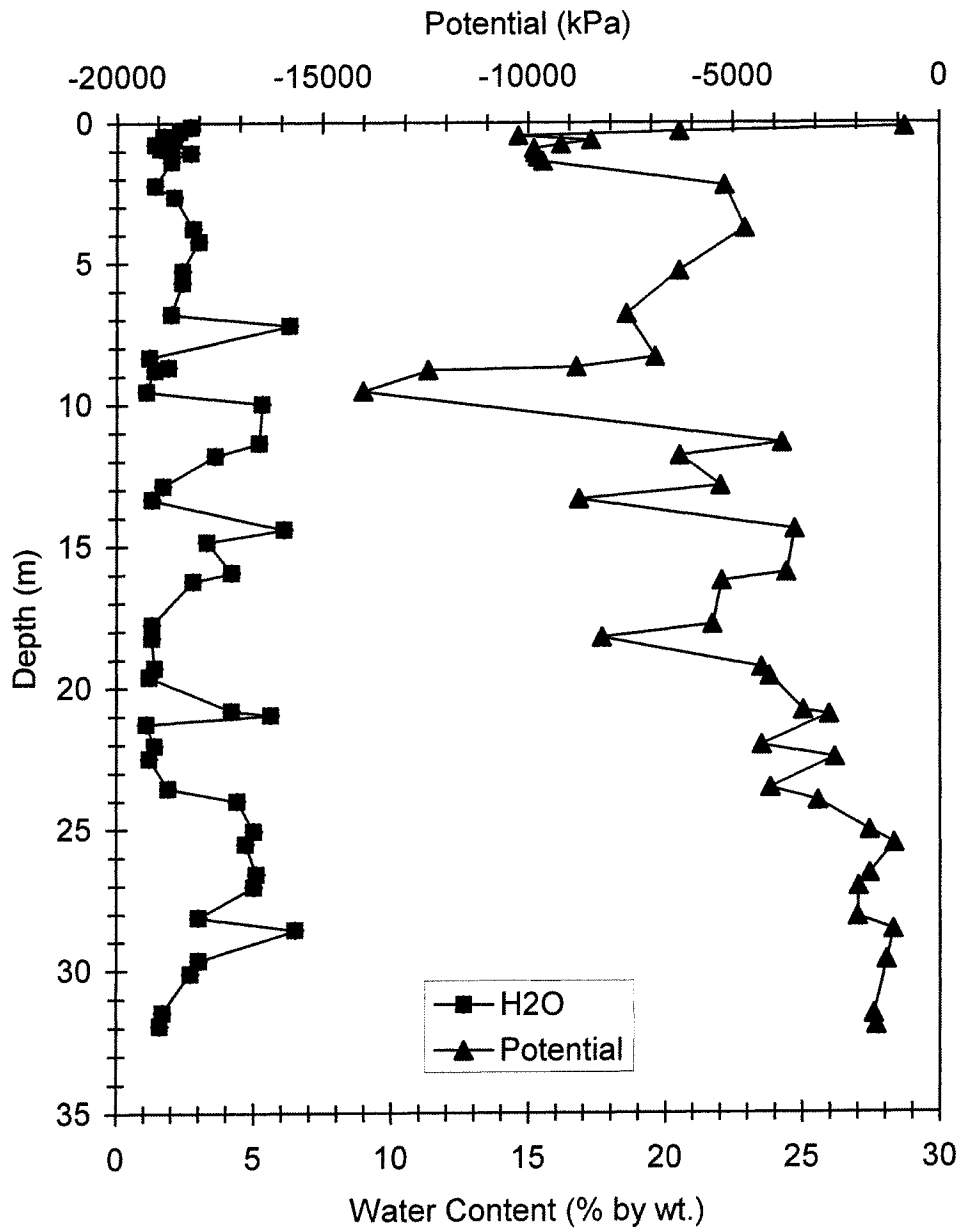


Figure 18. Water contents and soil-water potentials for OGF samples.

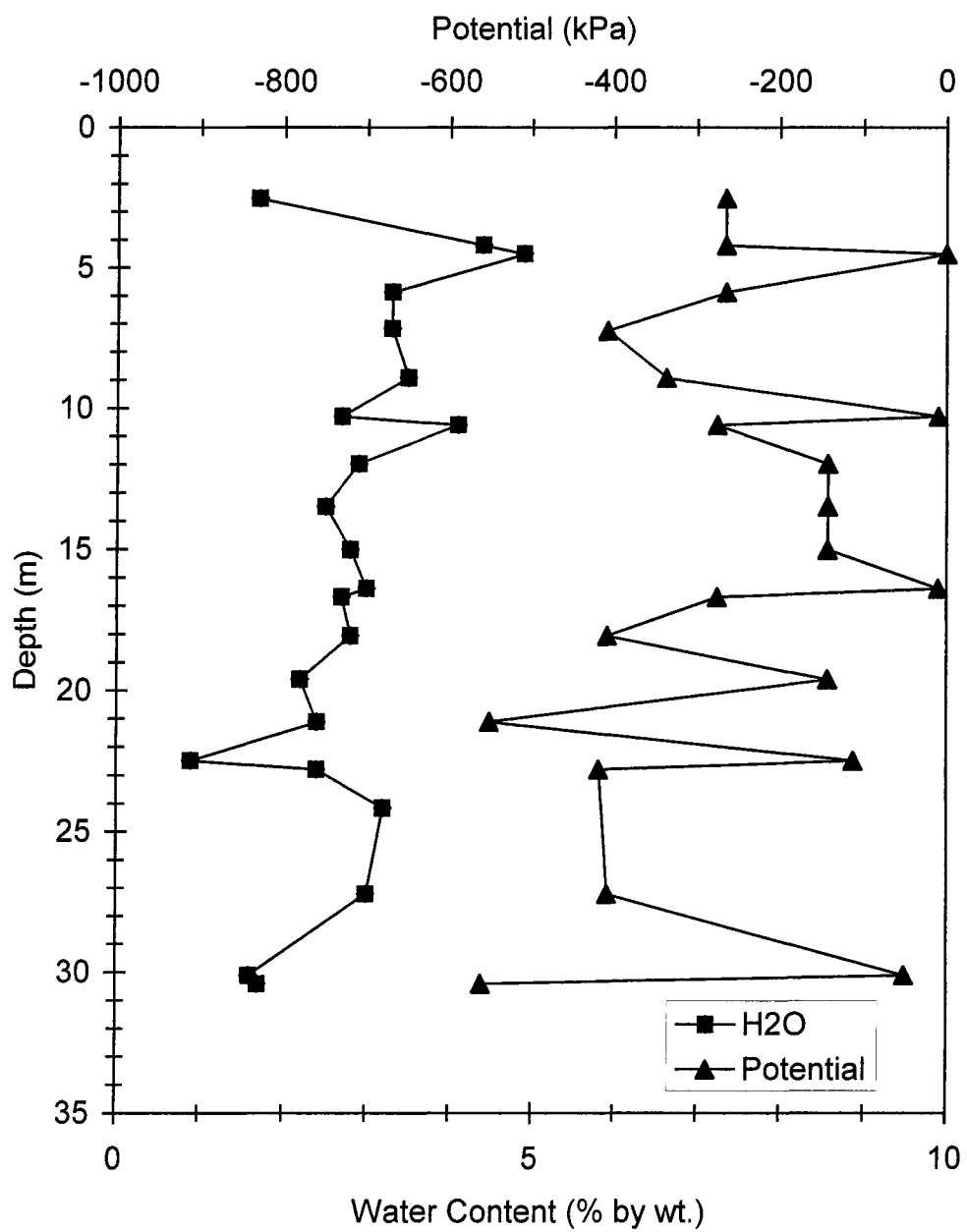


Figure 19. Water contents and soil-water potentials for USCW samples.

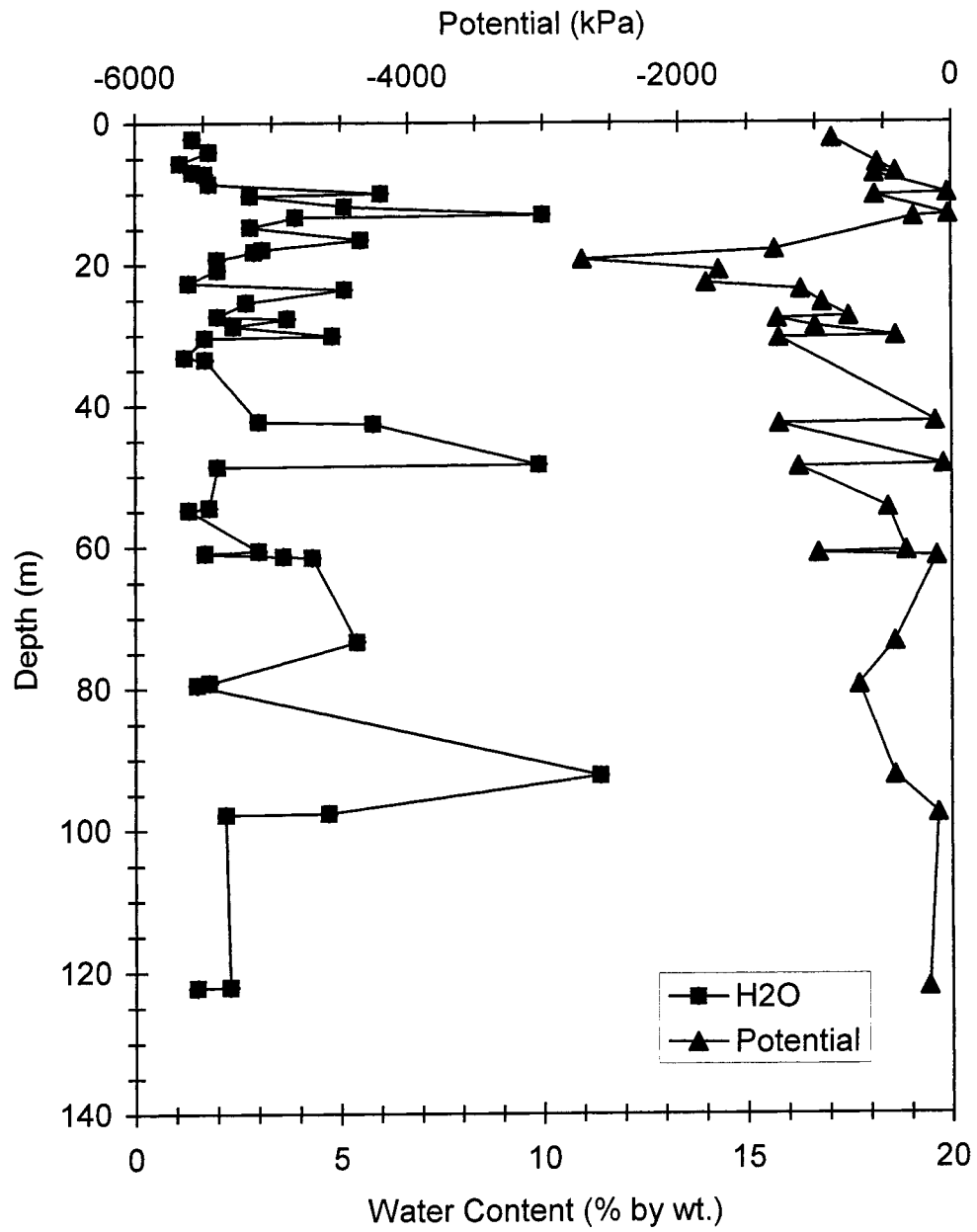


Figure 20. Water contents and soil-water potentials for MSCW samples.

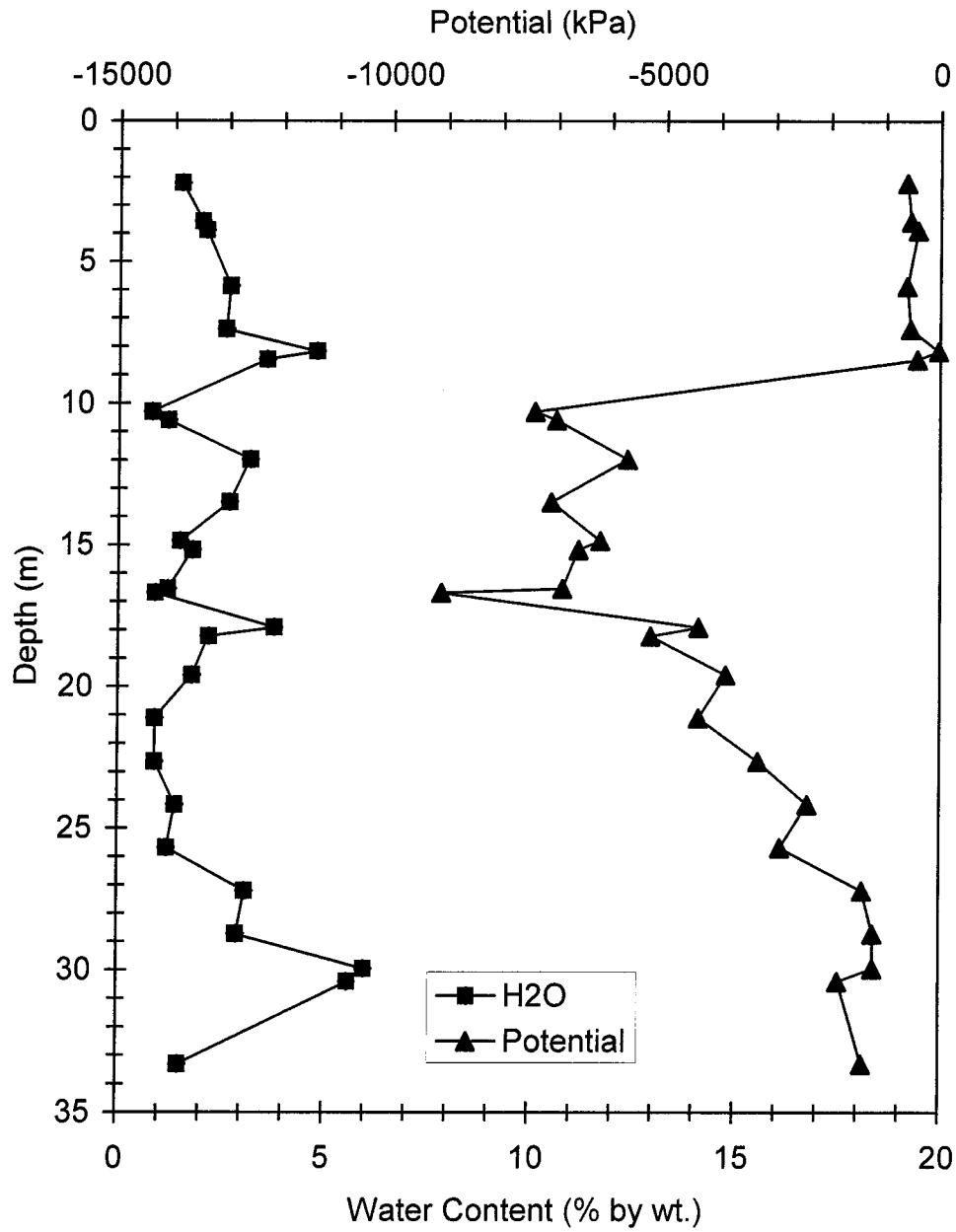


Figure 21. Water contents and soil-water potentials for LSCW samples.

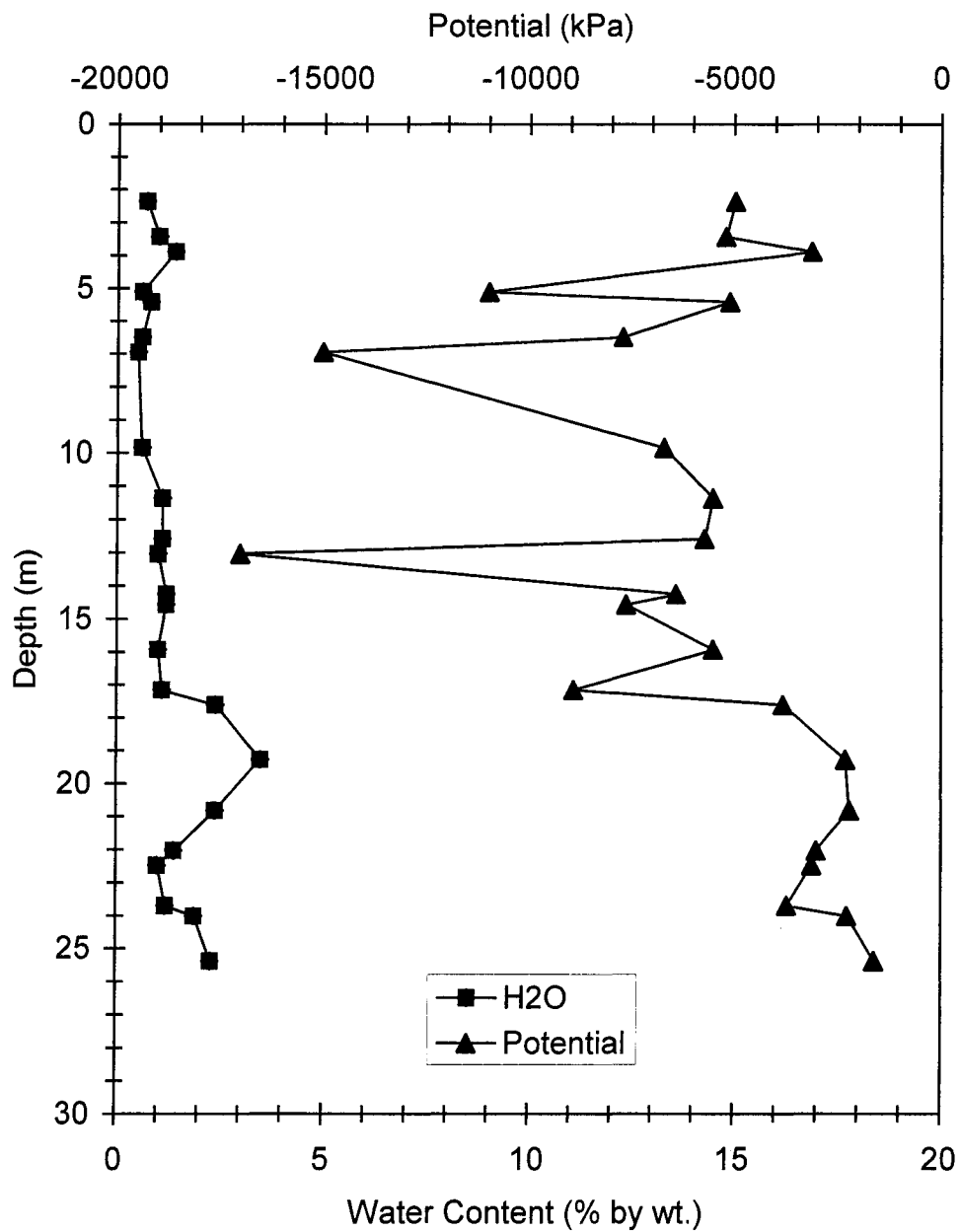


Figure 22. Water contents and soil-water potentials for SCF samples.

and 12 show the gravimetric-water contents for Oro Grande Wash and Sheep Creek Wash, respectively. Figures 13 through 22 show both gravimetric-water content and soil-water potential profiles for each borehole.

Gravimetric-water Contents

In Figures 11 and 12 it can be seen that, in general, the water contents beneath the control surfaces of both washes are lower than the water contents of the sites located within the channels. Beneath Oro Grande Wash, the water contents increase with distance downstream. Beneath Sheep Creek Wash, MSCW generally has the highest water contents. Oro Grande Wash is the wetter location, and water contents of 10 % are relatively common. In contrast, few water contents in samples from Sheep Creek Wash exceed 5 %. Water-content depth profiles for each location are presented in Figures 13 through 22.

Soil-water Potential

Under unsaturated conditions, water is held in the soil matrix. Soil-water potential is a measure of how tightly the water is held. The soil-water potentials discussed here, converted from water-activity measurements, are a combined total of matric and solute potential. Matric potential is a measure of the capillary and adsorptive forces with which water is held by the soil matrix. Solute potential, the result of chemicals dissolved in water, reduces the potential energy of water by reducing the vapor pressure of water. These forces attract and bind water in the soil, reducing the potential

energy of the water and resulting in a negative potential (Hillel, 1982). The lower (more negative) the potential, the more strongly water is held in the soil matrix. As with flow under saturated conditions, flow in the unsaturated zone is in the direction of decreasing total potential.

The results of the soil-water-potential measurements (Figs. 13 through 22) indicate that sediment beneath the control surfaces, with the exception of the Summit location, generally has much lower potentials than sediment beneath the channels. Soil-water potentials for the channel locations are, for the most part, greater than -500 kPa, whereas those of the control locations are in some cases lower than -10,000 kPa. It should be noted that the water-activity meter used for these measurements, with an uncertainty of +/- 400 kPa, is best suited for measurement of dry materials. The potentials of 0 kPa seen in the channel locations reflect the limitations of the meter when used to measure wetter materials.

Chloride and Tritium Data

Figures 23 through 32 combine both chloride and tritium data for each borehole.

Chloride Concentrations

Chloride is deposited upon the surface of the Earth in precipitation and as dryfall. The long-term sources of chloride include seaspray and terrestrial dust, but in recent times industrial sources and fertilizers have also become sources of chloride. Chloride is highly soluble and, once deposited upon the surface, readily moves below the surface

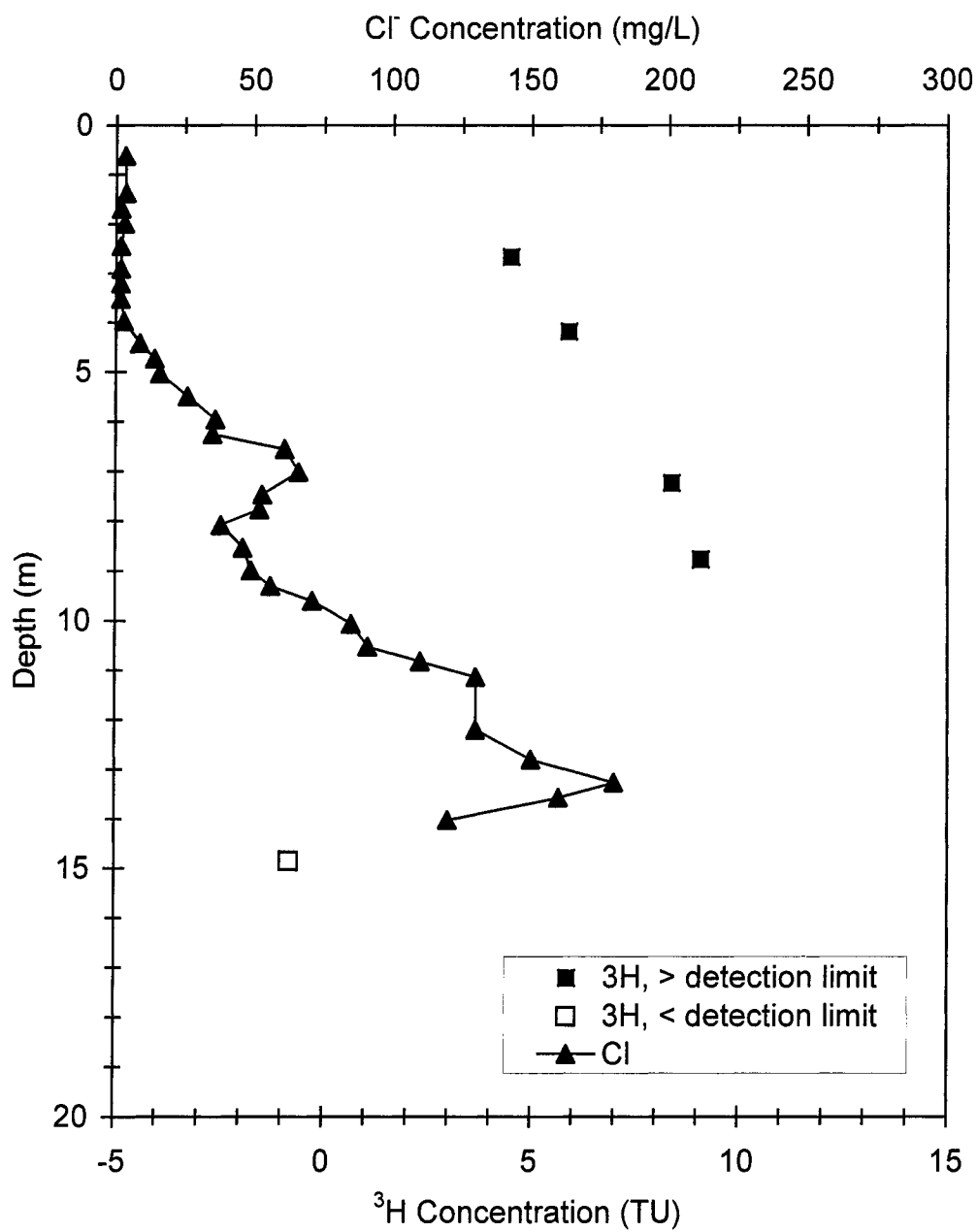


Figure 23. Chloride and tritium concentrations for Summit samples.

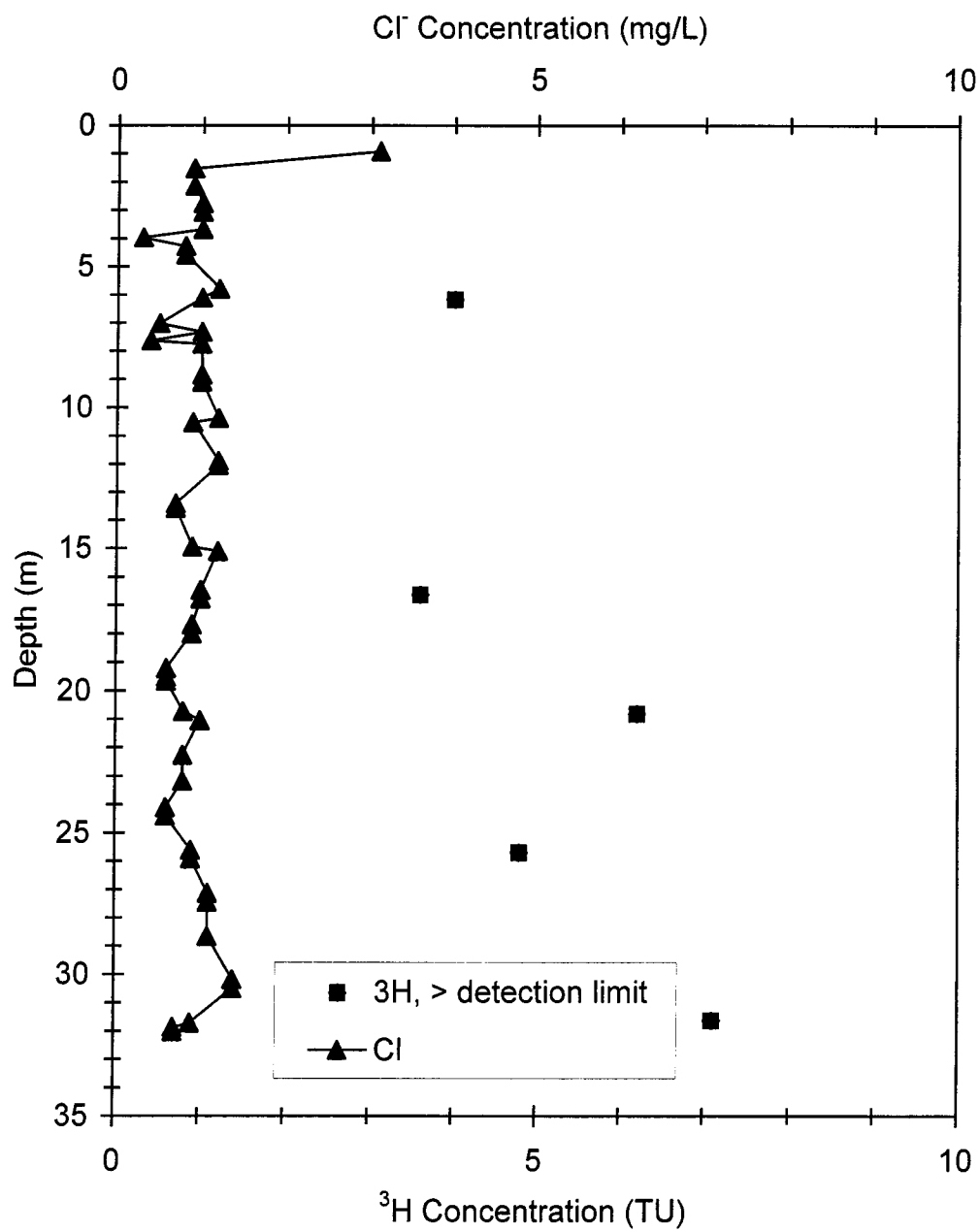


Figure 24. Chloride and tritium concentrations for UOGW samples.

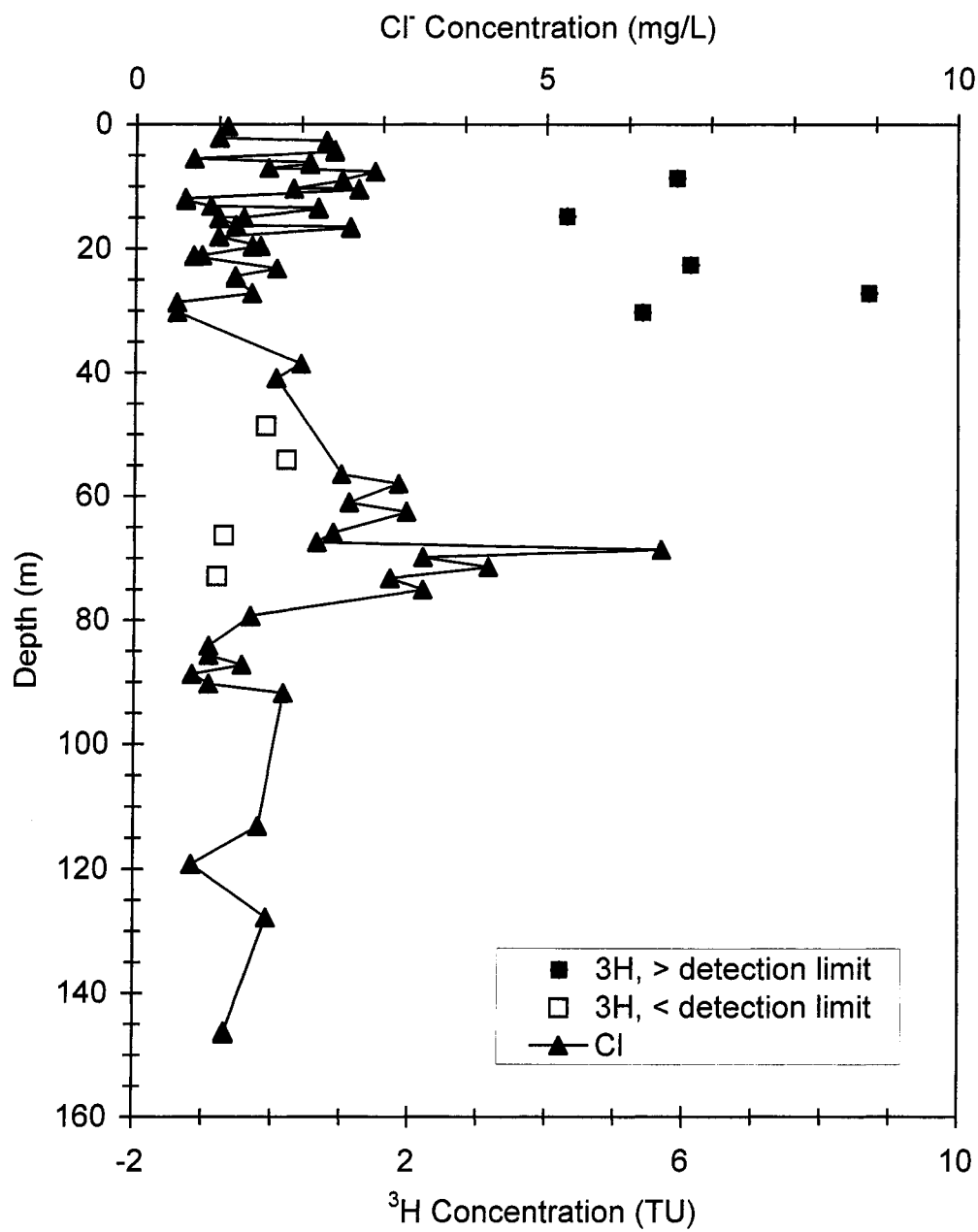


Figure 25. Chloride and tritium concentrations for MOGW samples.

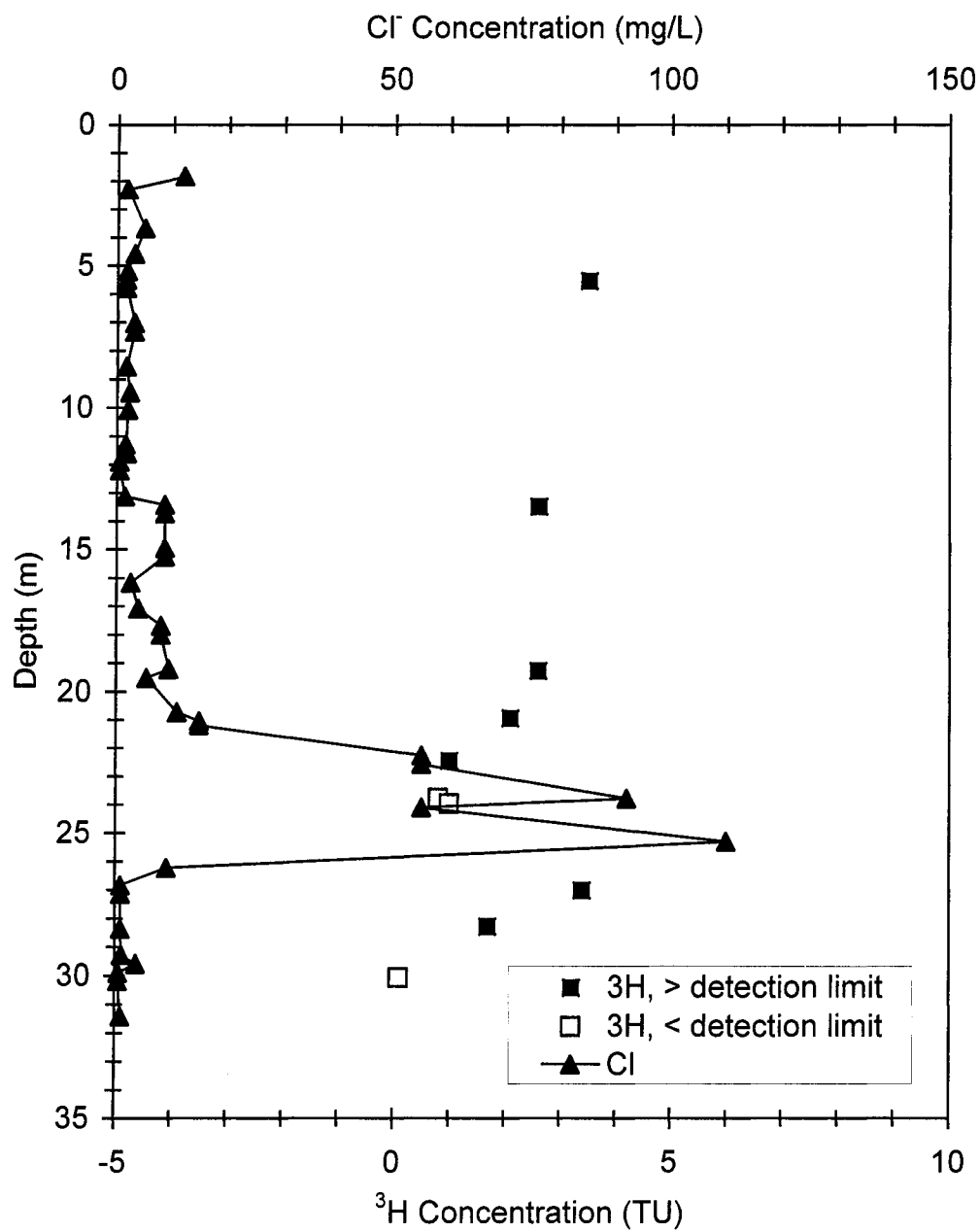


Figure 26. Chloride and tritium concentrations for LOGW-1 samples.

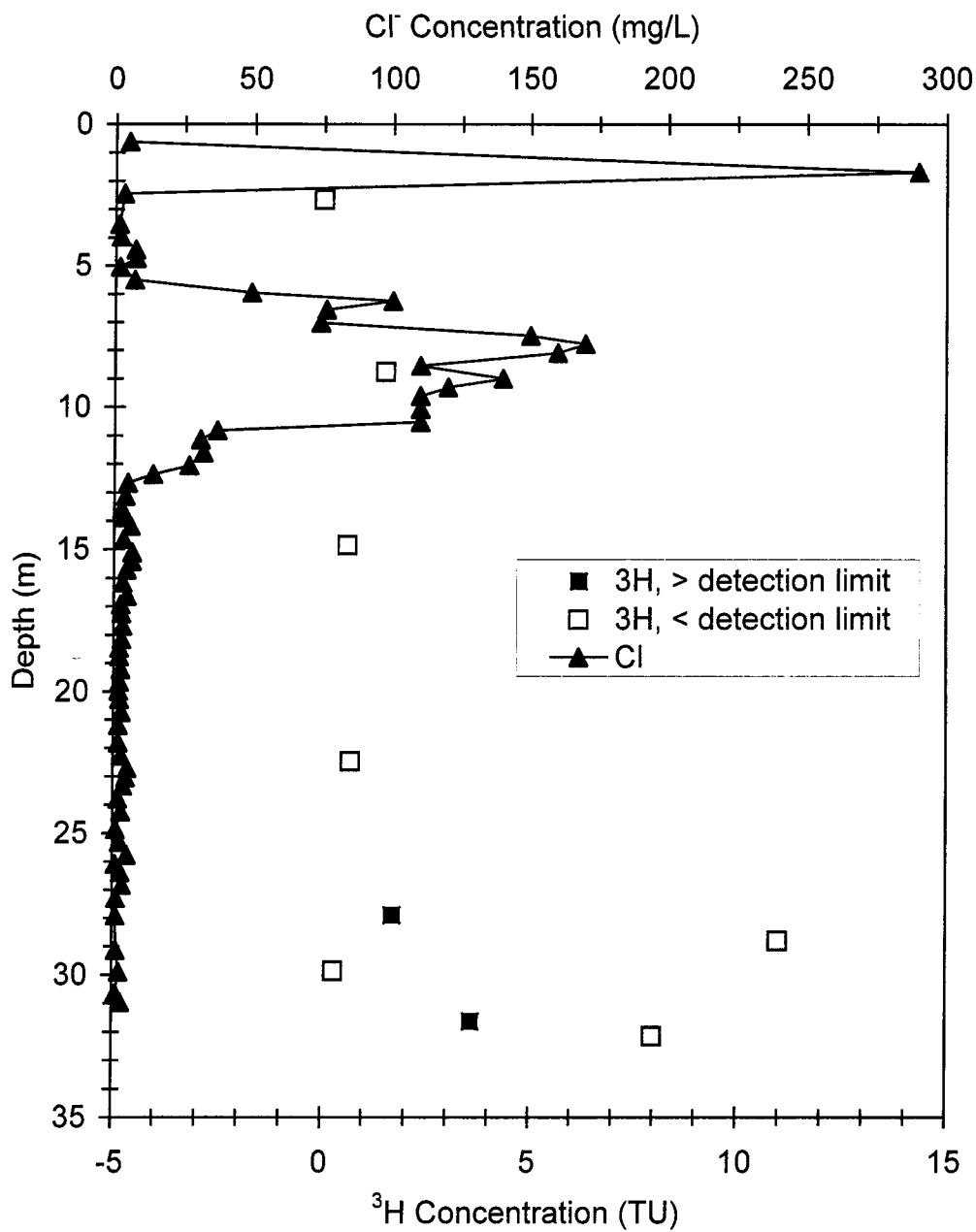


Figure 27. Chloride and tritium concentrations for LOGW-2 samples.

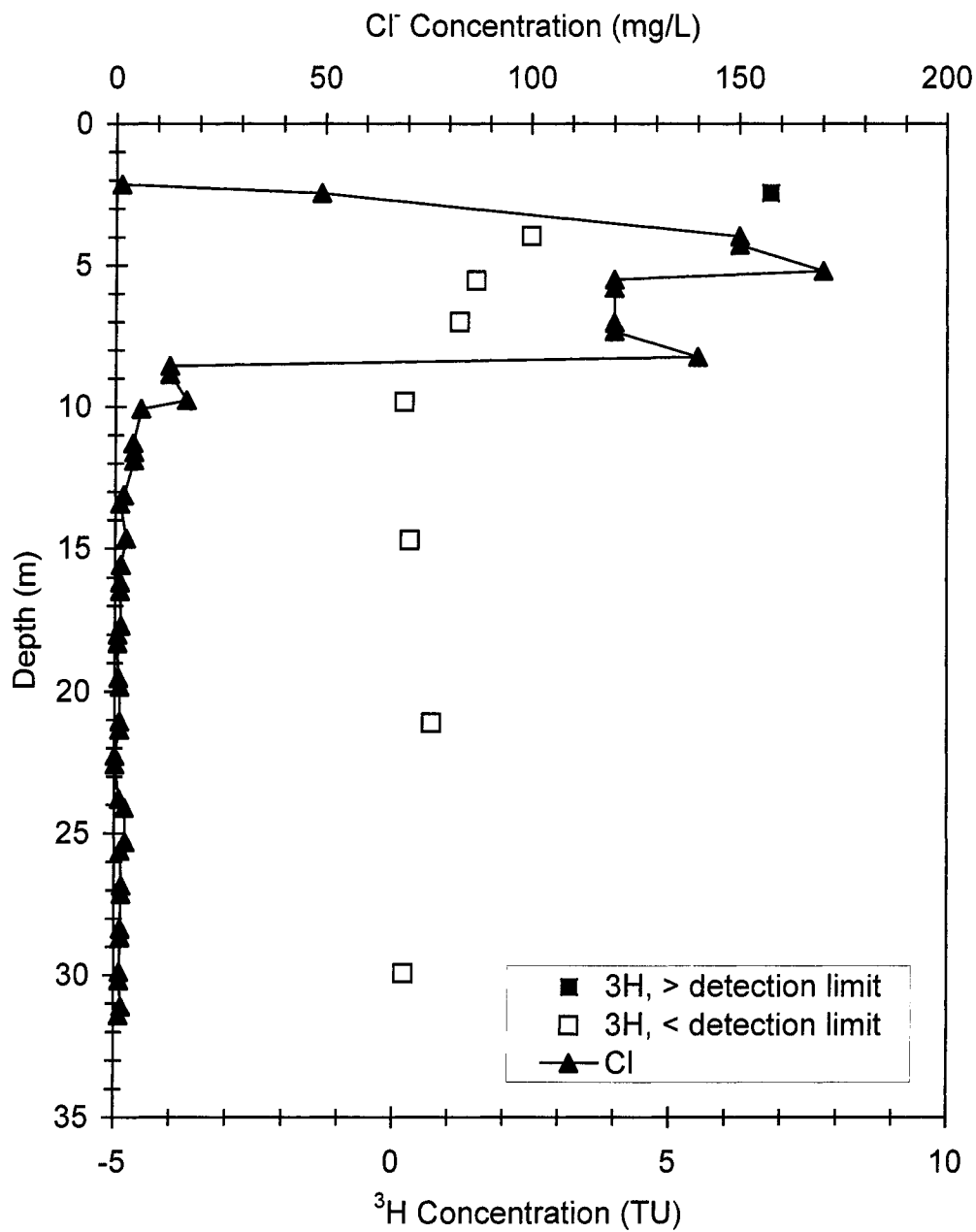


Figure 28. Chloride and tritium concentrations for OGF samples.

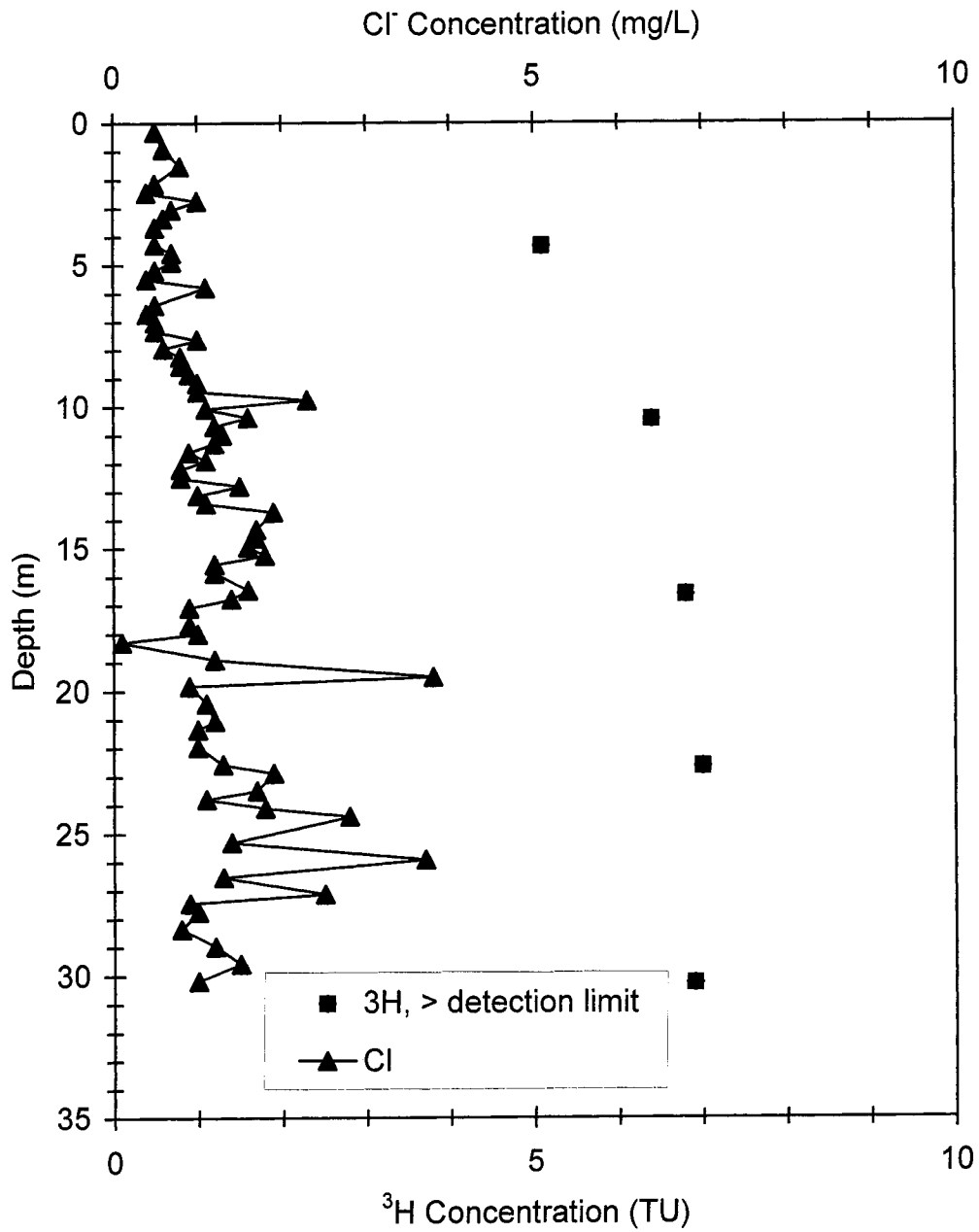


Figure 29. Chloride and tritium concentrations for USCW samples.

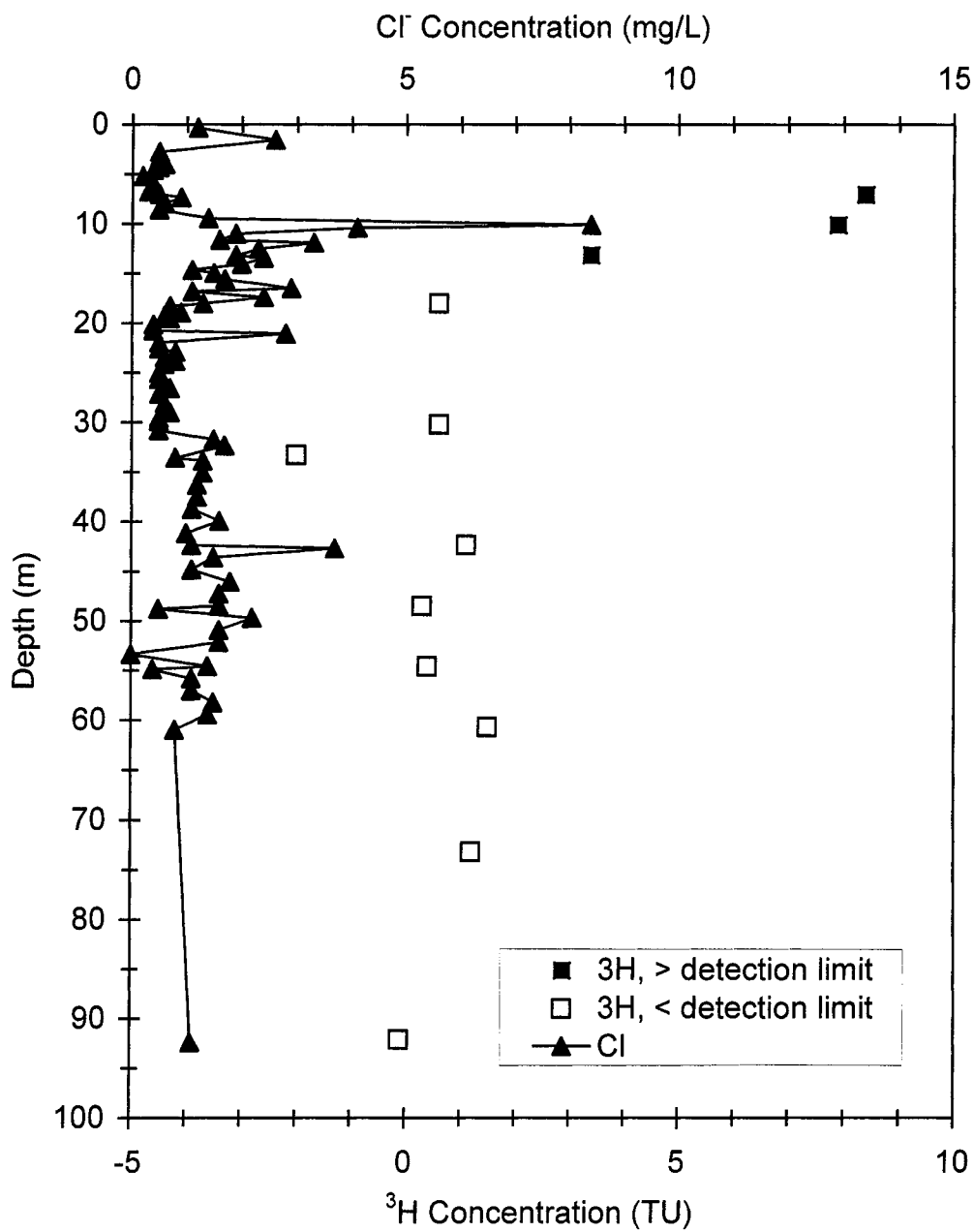


Figure 30. Chloride and tritium concentrations for MSCW samples.

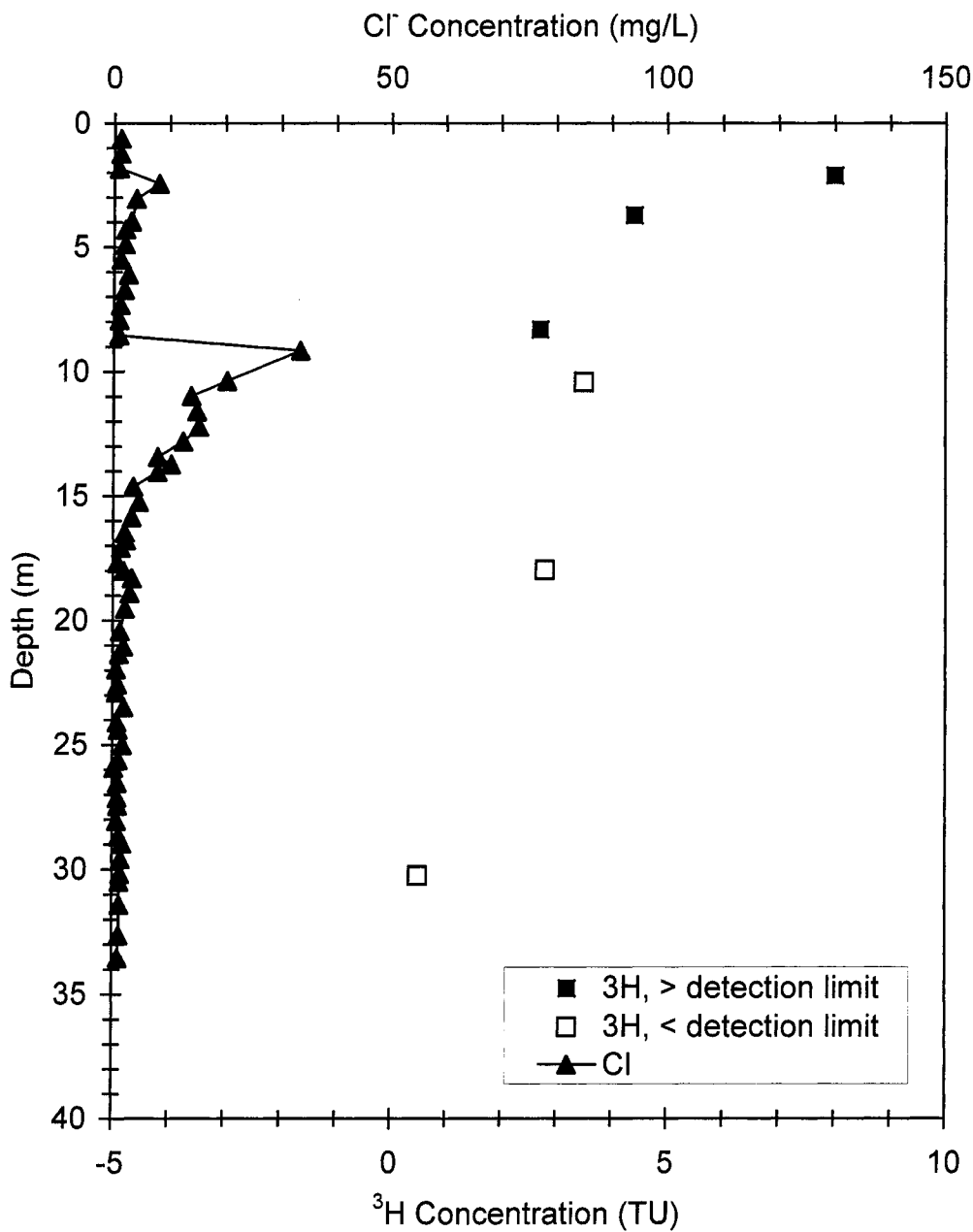


Figure 31. Chloride and tritium concentrations for LSCW samples.

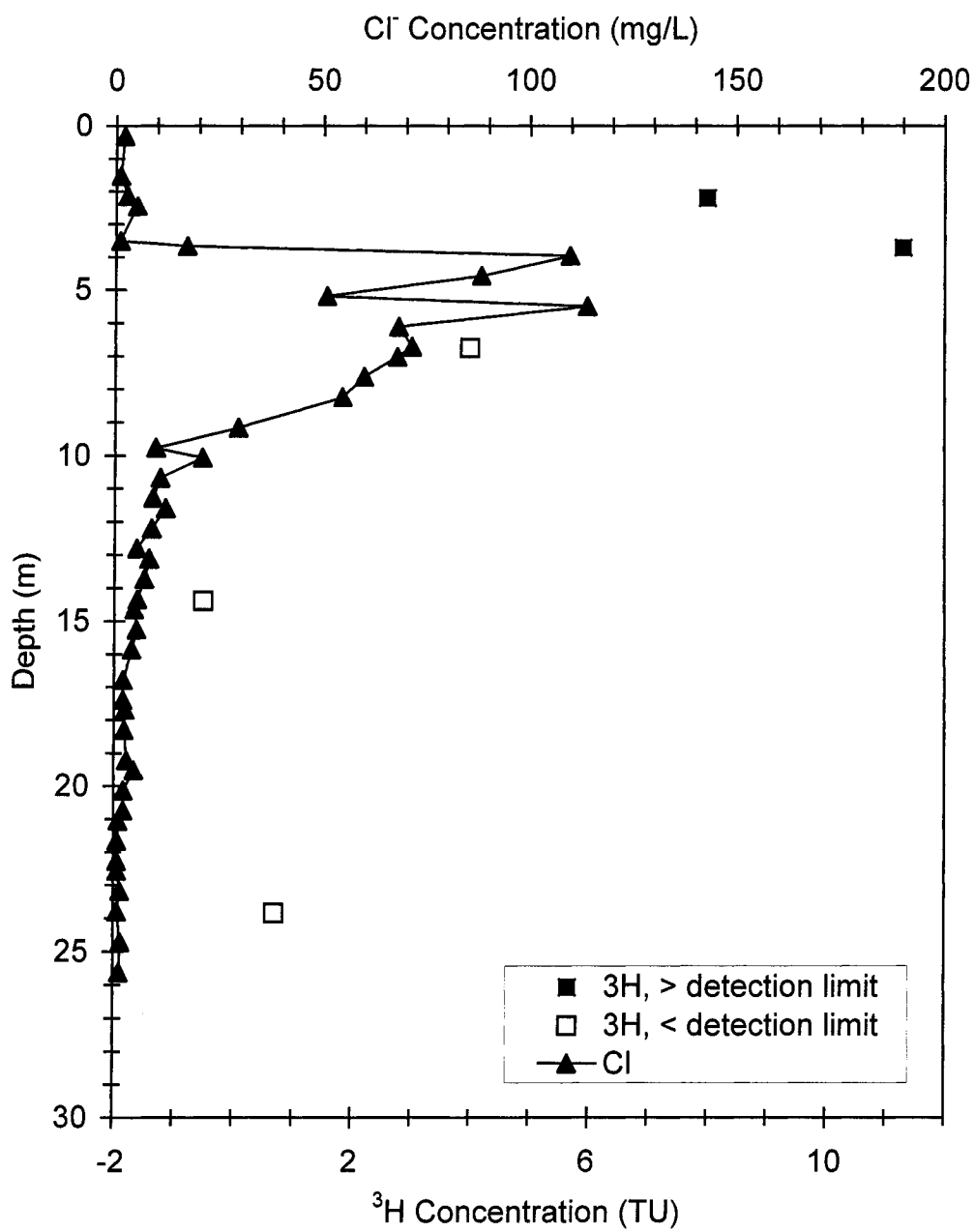


Figure 32. Chloride and tritium concentrations for SCF samples.

with infiltrating water. In areas where water is moving through the unsaturated zone, chloride concentrations will be low. Where water does not move through the unsaturated zone, chloride will accumulate at the maximum depth of infiltration. In many desert areas, high chloride concentrations commonly are found at shallow depths in the unsaturated zone, indicating that recharge is not occurring under present-day climatic conditions. Numerous workers have used chloride accumulation as a way of calculating recharge rate (e.g., Scanlon, 1991; Liu et al., 1995). Given the mass of chloride in the unsaturated zone and the deposition rate, the amount of time since water has moved through the unsaturated zone can be calculated. The accuracy of the technique is based upon the dual assumptions of piston-flow and a constant chloride deposition rate.

High chloride concentrations are present at shallow depths beneath the control surfaces associated with both Oro Grande Wash and Sheep Creek Wash (Figs. 23 through 32). For both channels, chloride concentrations are very low beneath the upper and middle locations. Beneath both lower channel locations, higher chloride concentrations are found. However, the intervals of high chloride concentration beneath the lower channel locations are of lower concentration and/or located at greater depths than the intervals of high chloride concentration beneath the control locations.

Tritium Concentrations

Tritium, ^3H , a radioisotope of hydrogen with a half-life of 12.41 years, is an excellent tracer of water movement because it is part of the water molecule. Tritium content is reported as tritium units (TU). One tritium unit is equal to one tritium atom in

10^{18} hydrogen atoms. Although tritium is produced naturally as a result of cosmic-ray spallation in the upper atmosphere, the present concentrations are primarily the result of atmospheric nuclear testing from 1952-1963 (Plummer et al., 1993). In the unsaturated zone tritium can be used to estimate infiltration rates. The presence of detectable tritium in soil waters indicates that they are less than 50 years old. Assuming piston-flow, the deepest occurrence of tritium will indicate water that entered the unsaturated zone after 1952, and the point of maximum tritium content will be in those waters that entered the unsaturated zone in 1963-64 (Plummer et al., 1993).

In the study area, analyses of soil waters extracted from core materials indicate that tritium has not infiltrated beyond 9 m (30 ft) beneath the control surfaces associated with either Oro Grande Wash or Sheep Creek Wash (Figs. 23 through 32). Beneath several of the channel locations, tritium has infiltrated to depths of greater than 30 m (98 ft). Tritium concentrations indicated as below the detection limit are those with measured concentrations less than 2 standard deviations above zero. Sample size and the average number of disintegrations per minute recorded by the scintillation counter determine the standard deviation for each sample.

Stable Isotopes

Precipitation

Isotopic compositions of bulk precipitation from the 7 stations vary as much as 90 o/oo and 15 o/oo for δD and $\delta^{18}O$, respectively (Table 3). There are large spatial and temporal variations in amount and isotopic composition of the precipitation, but most of

Table 3. Range and bulk-average isotopic compositions of precipitation from the study area.

Station	Range δD (o/oo)	Range $\delta^{18}O$ (o/oo)	Bulk-average δD (o/oo)	Bulk-average $\delta^{18}O$ (o/oo)
Aqueduct (AQ)	-73.9 to -28.0	-10.87 to -1.65	-62.6	-9.00
Oak Hill (OH)	-85.7 to -17.8	-11.67 to +0.36	-64.8	-9.41
Santa Fe (SF)	-89.1 to -18.9	-12.02 to -4.83	-69.7	-10.06
Bear Valley (BV)	-94.7 to -16.1	-12.66 to -4.33	-72.2	-10.32
Sheep Creek (SC)	-94.5 to -24.9	-12.49 to -4.43	-75.7	-10.50
Table Mountain (TM)	-104.1 to -64.0	-14.26 to -7.16	-75.7	-11.18
Big Bear (BB)	-109.0 to -34.0	-15.1 to -5.05	-76.0	-11.00

the samples plot close to the GMWL (Fig. 33). Precipitation collected during the wet season, November to April, accounts for 75% or more of the total precipitation received at each station and, in general, has more negative δ values than precipitation collected during the dry season. The stations located nearest to the Cajon Pass, AQ and OH, received much greater amounts of precipitation, with a less negative isotopic composition, than the other stations. The Cajon Pass is a topographic low area within the mountain barrier through which storm clouds from the coast enter the desert. The bulk-average isotopic compositions for the 5 collection stations (AQ, OH, SF, BV, and SC) located in the desert (Fig. 34) display a trend of decreasing δ values, a rainout effect, with increasing distance from the Cajon Pass. The AQ station, closest to the Cajon Pass, has

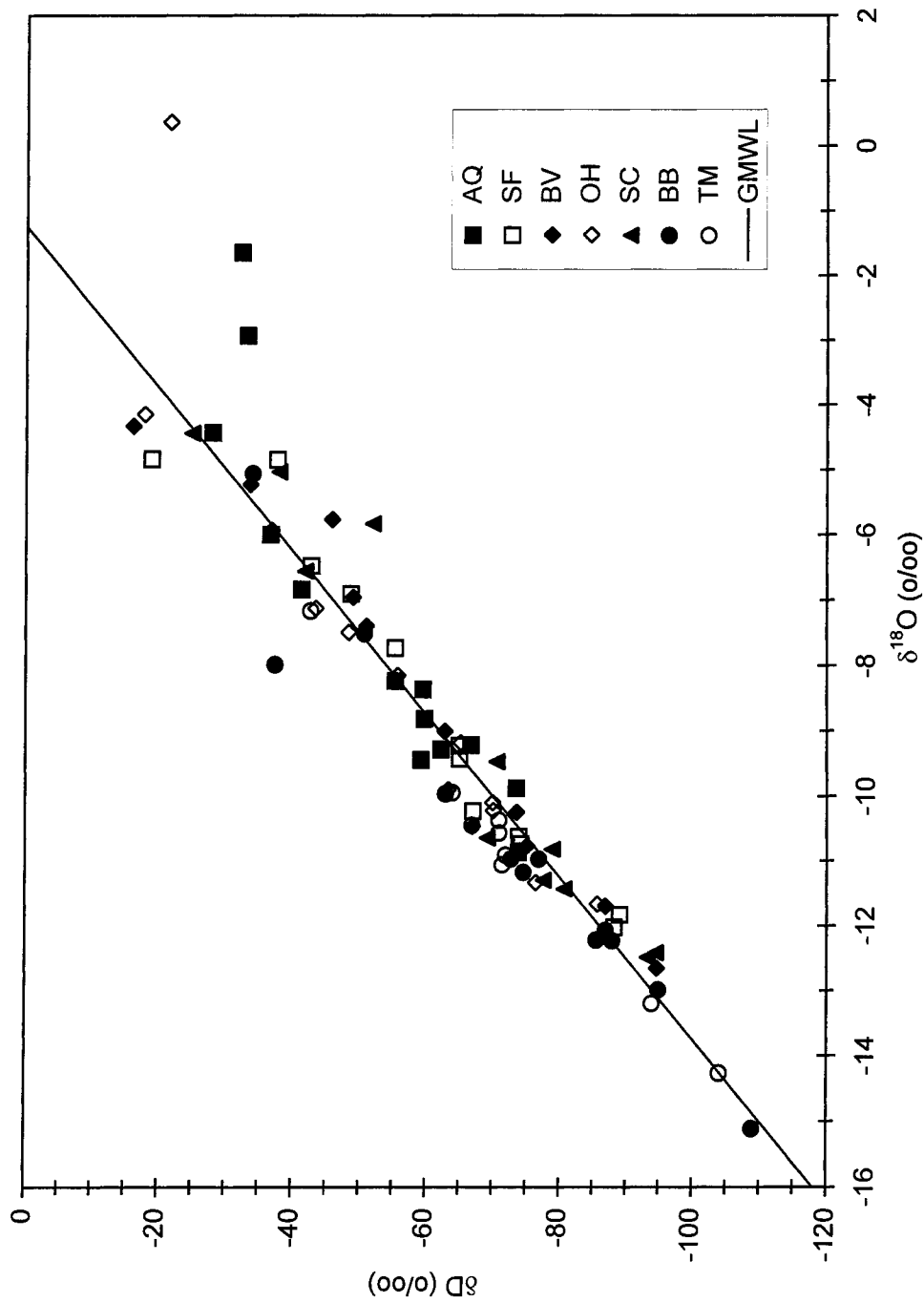


Figure 33. δD vs $\delta^{18}O$ plot of precipitation data with the Global Meteoric Water Line (GMWL). Data are from collection stations Aqueeduct (AQ), Sante Fe (SF), Bear Valley Road (BV), Oak Hill (OH), Sheep Creek (SC), Big Bear (BB), and Table Mountain (TM).

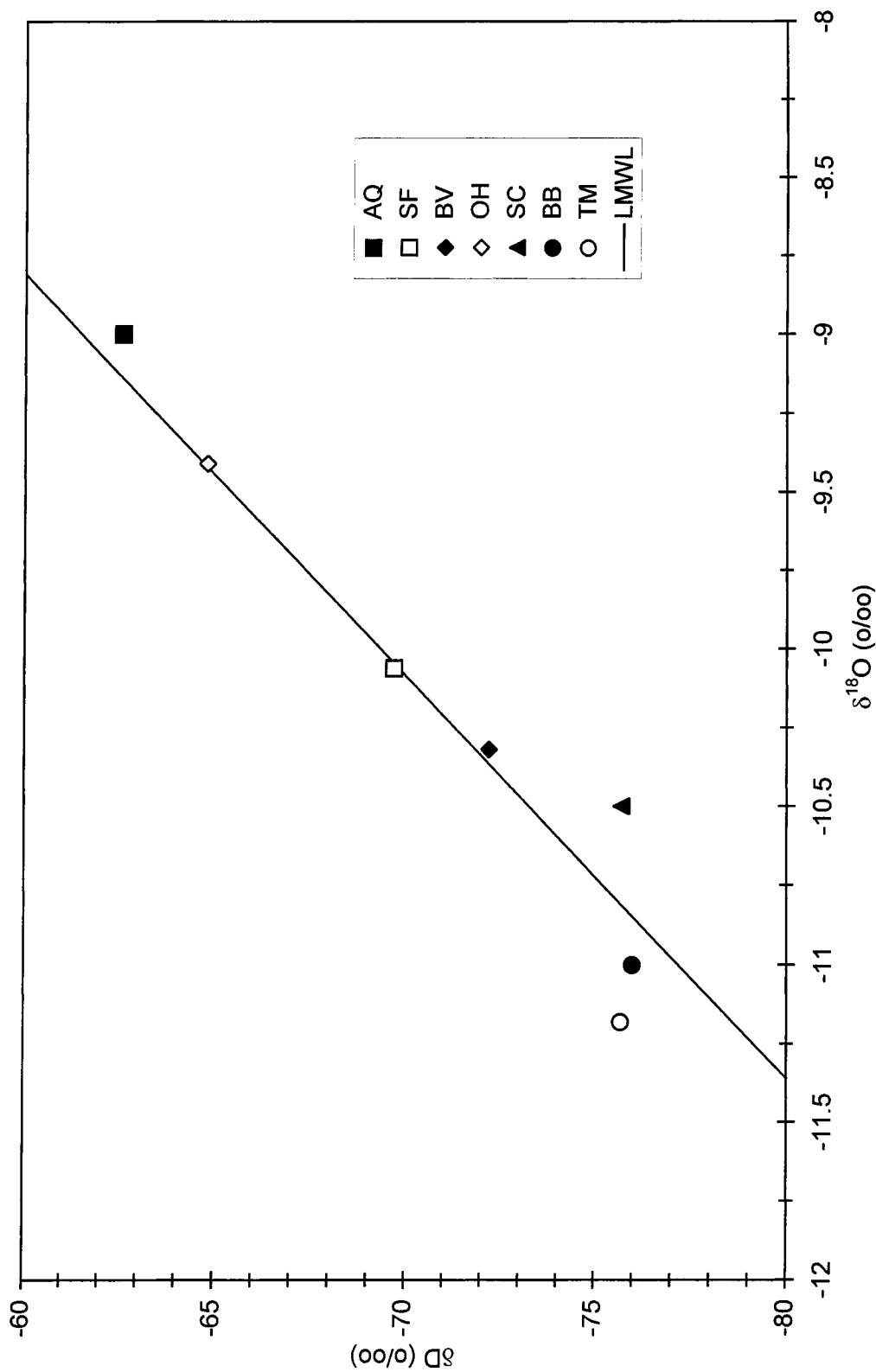


Figure 34. δD vs $\delta^{18}\text{O}$ plot of bulk-average-precipitation data with the local meteoric water line (LMWL). Data are from collection stations Aqueeduct (AQ), Santa Fe (SF), Bear Valley Road (BV), Oak Hill (OH), Sheep Creek (SC), Big Bear (BB), and Table Mountain (TM).

the least negative bulk-average isotopic composition, and the SC station, being the greatest distance from the pass, has the most negative bulk-average isotopic composition of the 5 sites. The bulk-average isotopic compositions for the TM and BB stations located in the mountains have more negative δ values, as would be expected due to the altitude effect, than the 5 stations located in the desert. Further details regarding amounts and isotopic compositions of precipitation collected during the study can be found in Izbicki et al. (2000b).

The majority of the bulk-precipitation data plot very close to the GMWL (Fig. 33). Most of the data lie along the GMWL between $\delta^{18}\text{O}$ values of -12 and -4 ‰. For calculation of the local meteoric water line (LMWL), the 3 data points with $\delta^{18}\text{O}$ values greater than -4 ‰ were not used. These 3 points represented very small amounts of precipitation and were not within the range of soil waters collected from Oro Grande Wash and Sheep Creek Wash. The data used define the following equation for the LMWL:

$$\delta\text{D} = 7.83\delta^{18}\text{O} + 8.95, n = 81, r^2 = 0.9503,$$

similar to the equation for the GMWL.

Stream Water, Snow, Surface Water, and Groundwater

Samples of stream water were collected at both Oro Grande Wash (LOGW-1) and Sheep Creek Wash (LSCW). Snow samples were collected at the Summit and USCW locations. Water was also collected from a puddle at USCW. Groundwater samples were collected from depths of 195 m (640 ft) and 166 m (544 ft) at MOGW and MSCW,

respectively. The isotopic compositions and dates of collection for these samples are given in Table 4. In Figure 35, the isotopic compositions of these samples are compared to the bulk-average isotopic compositions of precipitation from the study area. Stream water from LOGW-1 has a less negative composition while stream water from LSCW has a more negative composition than the bulk-average precipitation compositions. The snow samples are more negative in composition than bulk-average precipitation. The puddle water from USCW plots farther from the LMWL with a less negative $\delta^{18}\text{O}$ than the bulk-average precipitation compositions. Both groundwater samples plot very close to the LMWL. Groundwater from MOGW has a composition within the range of the bulk-average precipitation, whereas the MSCW groundwater has a more negative composition than the bulk-average precipitation.

Soil Water

Water extracted by azeotropic distillation from 118 core samples and 38 hand-auger samples was analyzed for isotopic composition. Core samples analyzed were from depths ranging from 1.5 m (5 ft) to 146 m (480 ft), and the hand-auger samples were from land surface to depths of up to 2.7 m (9 ft). Eighty-five of the core samples and the 38 hand-auger samples were from Oro Grande Wash and its control sites, Summit and OGF. The remaining 33 core samples were from Sheep Creek Wash and its control site SCF. Delta values for the extracted soil waters, from core and shallow hand-auger samples, range from -96.8 to -36.6 ‰ and -11.93 to -1.16 ‰ for δD and $\delta^{18}\text{O}$, respectively. Distillation yields, determined from the mass of sample used, the mass of

Table 4. Surface-water, snow, and groundwater isotopic compositions.

Location	Sample Type	Date	δD (o/oo)	$\delta^{18}O$ (o/oo)
LOGW-1	Stream Water	2/20/96	-56.9	-7.56
LSCW	Stream Water	2/20/96	-89.1	-11.79
Summit	Snow	1/8/97	-112.4	-15.61
USCW	Snow	1/7/97	-106.5	-14.20
USCW	Puddle Water	1/7/97	-73.0	-8.63
MOGW	Groundwater	6/9/95	-75.1	-10.46
MSCW	Groundwater	7/18/96	-83.5	-11.75

water extracted by the distillation, and the gravimetric-water content of the core material, range from 56.4 to 135.8 % with an average of 100.5 % and standard deviation of 11.6 %. Distillations for 36 of the samples were performed in duplicate. The average absolute difference between the distillation yields of the duplicate pairs is 7.4 % with a standard deviation of 6.2 %. The average absolute difference in isotopic composition between the duplicate pairs is 1.5 o/oo with a standard deviation of 1.3 o/oo, and 0.16 o/oo with a standard deviation of 0.12 o/oo for δD and $\delta^{18}O$, respectively. The average isotopic compositions of the duplicate pairs were used for data interpretation. Full results of the duplicate distillations and analyses as well as the results of related distillation experiments are reported in Appendix A. The results of all distillations and isotopic analyses of the core and hand-auger samples are reported in Appendix C.

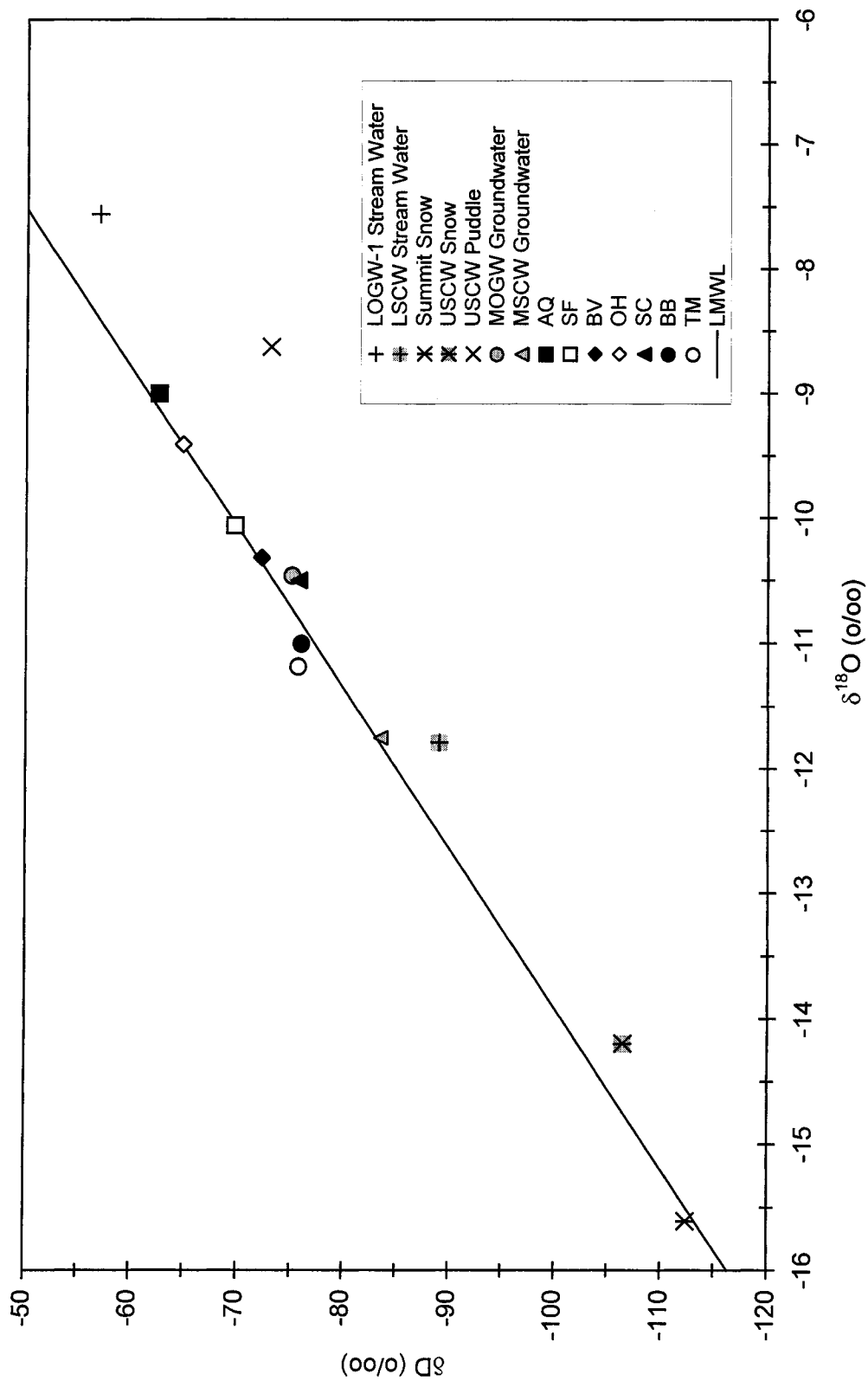


Figure 35. δD vs $\delta^{18}O$ plot of stream water, snow, groundwater, and bulk-average-precipitation data with the local meteoric water line (LMWL). Precipitation data are from collection stations Aqueduct (AQ), Santa Fe (SF), Bear Valley Road (BV), Oak Hill (OH), Sheep Creek (SC), Big Bear (BB), and Table Mountain (TM).

Core Samples. The range of isotopic compositions of the extracted soil waters and average D offsets for each location are given in Table 5. On a δD vs $\delta^{18}O$ plot of soil water and precipitation data, the soil waters lie within the range of recent precipitation for the area (Fig. 36). The plot also shows that there is very little overlap in isotopic composition for the soil waters from the two washes. Many of the soil waters from the Oro Grande Wash locations plot very near to the LMWL, indicating little or no evaporative enrichment. In contrast, soil waters from Sheep Creek Wash plot well off the LMWL and have more negative δD values than the OGW soil waters. A δD vs $\delta^{18}O$ plot of the Oro Grande Wash data (Fig. 37) shows that the soil waters from UOGW and MOGW plot very near to the LMWL. Waters from Summit, LOGW-1, LOGW-2, and OGF plot progressively farther from the LMWL. The δD vs $\delta^{18}O$ plot of Sheep Creek Wash soil waters (Fig. 38) shows that they plot well off the LMWL, indicating substantial evaporative enrichment.

A depth profile of D offset for Oro Grande Wash (Fig. 39) shows that the soil waters from beneath the channel locations have less negative D offsets than the soil waters from beneath the control surfaces. The depth profile of D offset for Sheep Creek Wash (Fig. 40) also shows that the soil waters from beneath the channel locations have less negative D offsets than soil waters beneath the control surface location, but the channel locations have more negative D offsets than their Oro Grande Wash counterparts.

Summit. On a plot of δD vs $\delta^{18}O$ (Fig. 41), the 5 soil waters plot just below the LMWL. Compared to precipitation from the OH station, the nearest precipitation

Table 5. Soil-water isotopic composition ranges and D offsets.

Location	Range δD (o/oo)	Range $\delta^{18}O$ (o/oo)	Average D Offset (o/oo)
Summit	-76.6 to -70.6	-10.24 to -9.37	-6.5 +/- 1.6
UOGW	-64.8 to -51.9	-9.56 to -7.90	+0.6 +/- 1.6
MOGW	-81.8 to -55.4	-11.26 to -8.04	<30m: -1.2 +/- 2.1 30-100m: -5.6 +/- 2.0 >100m: -2.4 +/- 0.9
LOGW-1	-83.5 to -60.9	-10.72 to -7.37	-10.6 +/- 4.1
LOGW-2	-83.6 to -76.9	-10.80 to -8.39	-13.4 +/- 5.7
OGF	-81.9 to -47.4	-10.2 to -5.62	-18.0 +/- 5.4
USCW	-80.3 to -67.9	-8.97 to -6.35	-21.6 +/- 4.3
MSCW	-96.8 to -78.4	-11.93 to -7.71	<54m: -22.3 +/- 7.3 >54m: -11.2 +/- 3.9
LSCW	-87.8 to -69.6	-8.95 to -7.16	-24.9 +/- 11.5
SCF	-92.4 to -77.3	-8.59 to -6.51	-34.8 +/- 3.5

collection station, the soil waters plot farther from the LMWL. The isotopic compositions of the soil waters are within the range of precipitation, but most have more negative compositions than the bulk average. Snow collected at this location is of significantly more negative isotopic composition than the soil waters. The depth profiles for δD and $\delta^{18}O$ (Fig. 42) are similar in shape and display the same trends with depth.

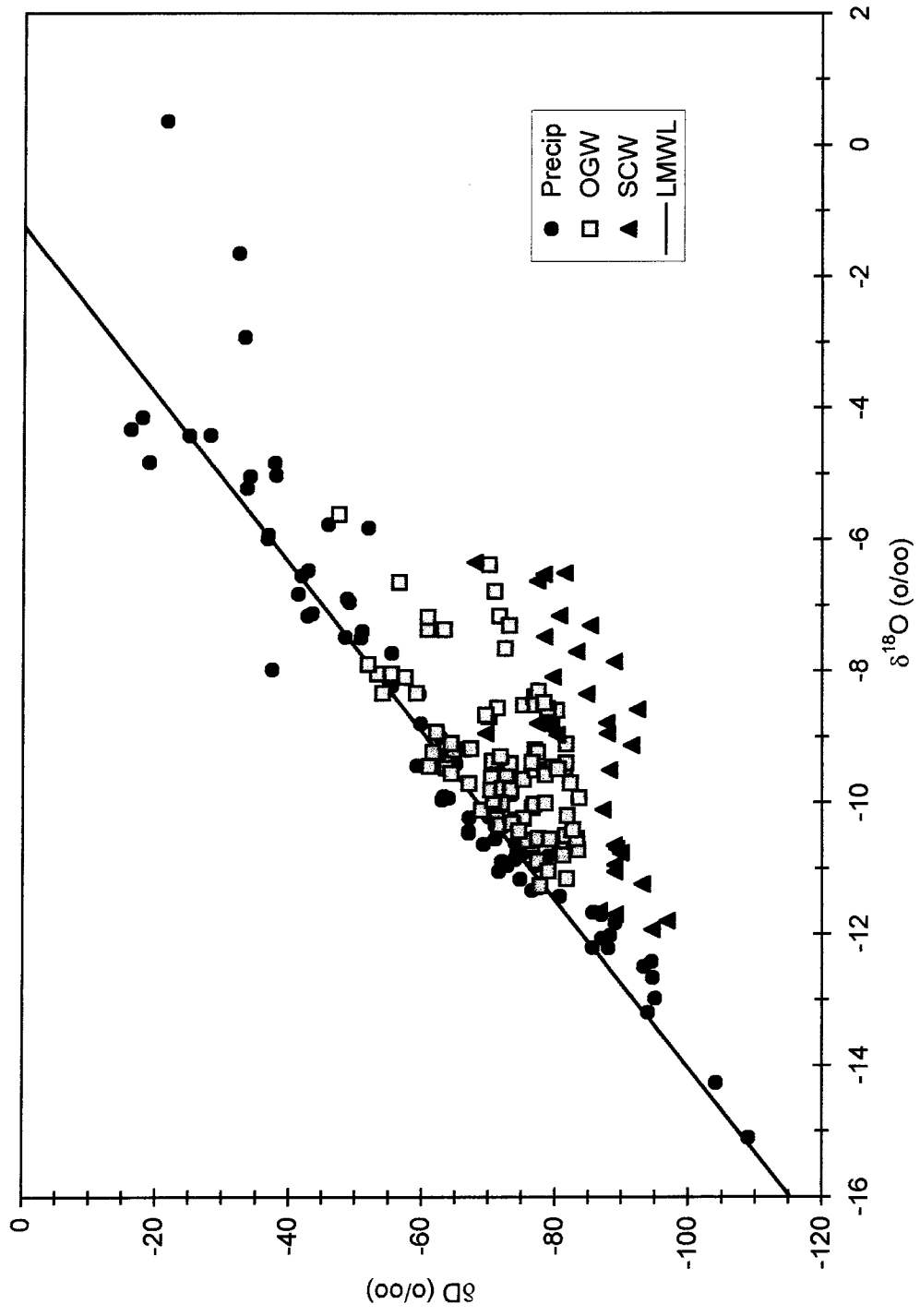


Figure 36. δD vs $\delta^{18}O$ plot of soil-water and precipitation data with the local meteoric water line (LMWL).

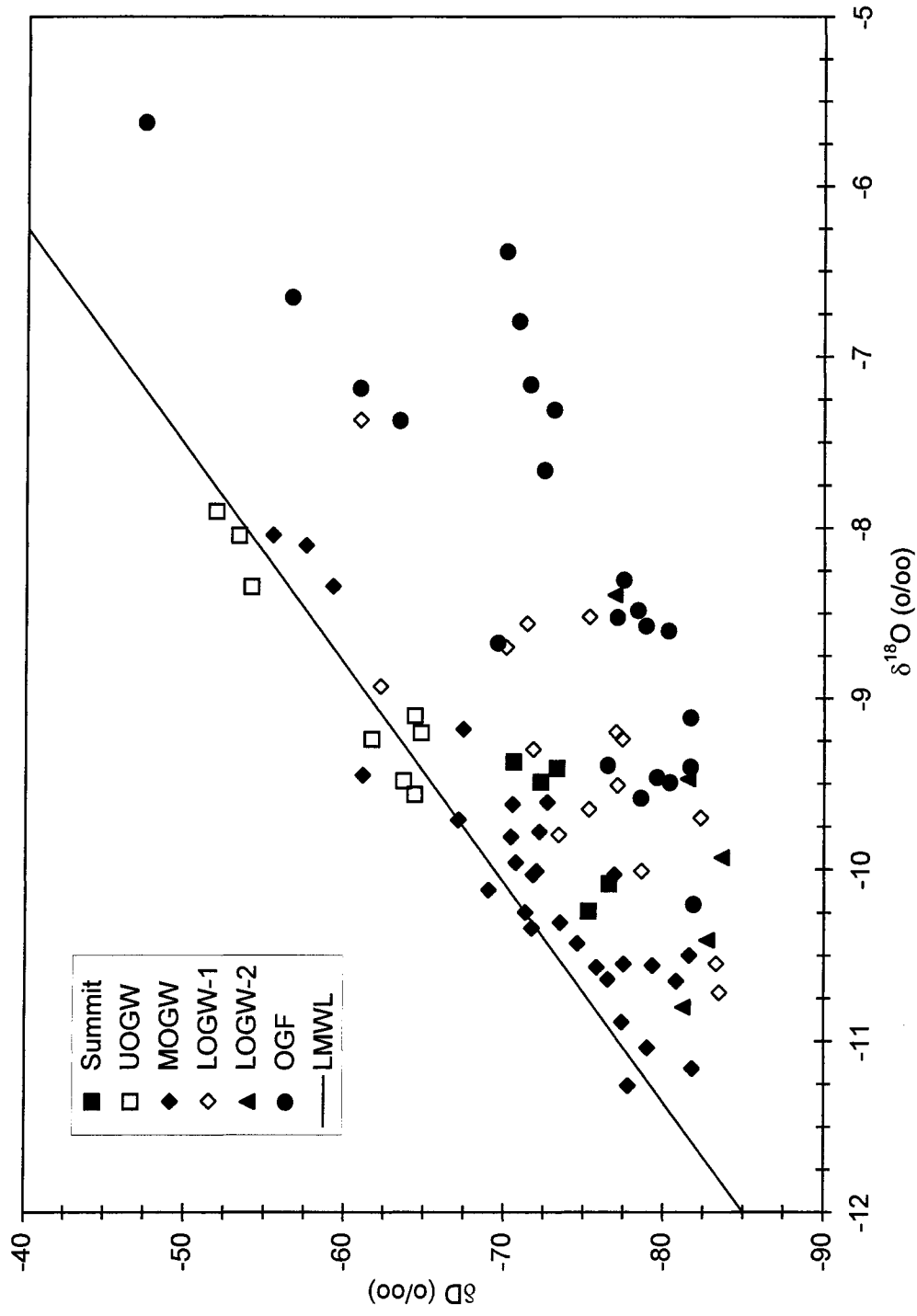


Figure 37. δD vs $\delta^{18}O$ plot of Oro Grande Wash soil waters with the local meteoric water line (LMWL).

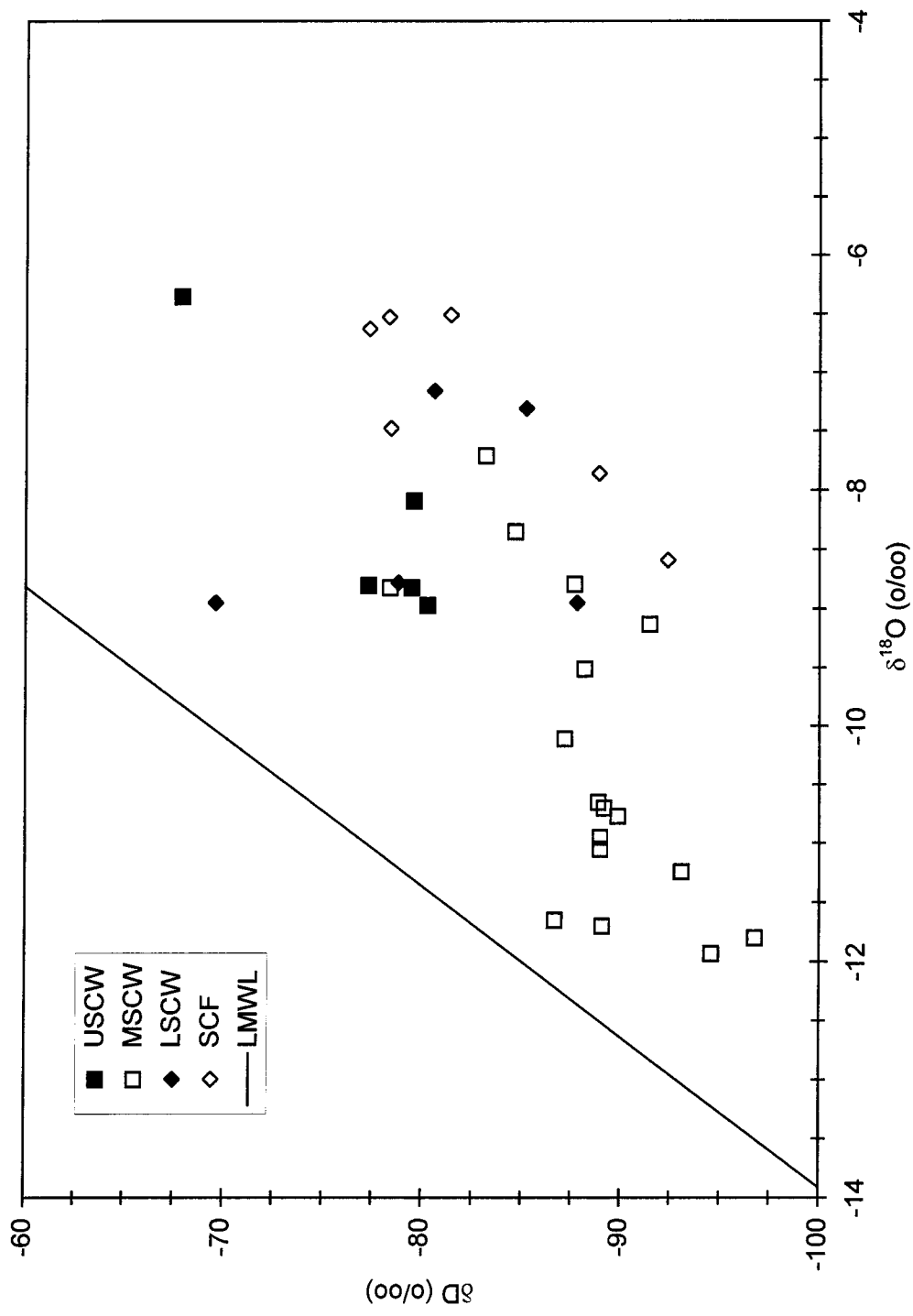


Figure 38. δD vs $\delta^{18}\text{O}$ plot of Sheep Creek Wash soil waters with the local meteoric water line (LMWL).

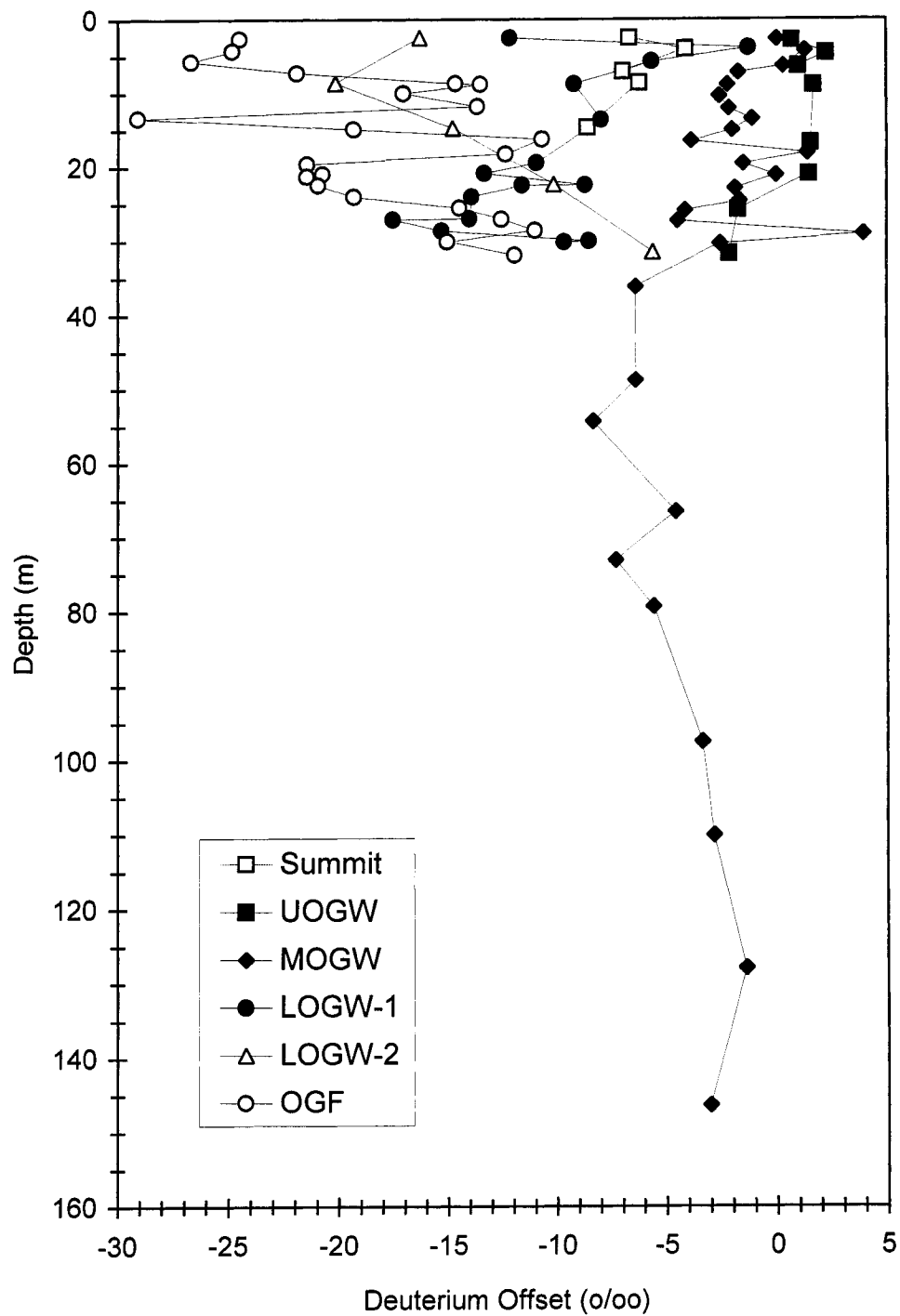


Figure 39. Oro Grande Wash deuterium offsets from the local meteoric water line (LMWL).

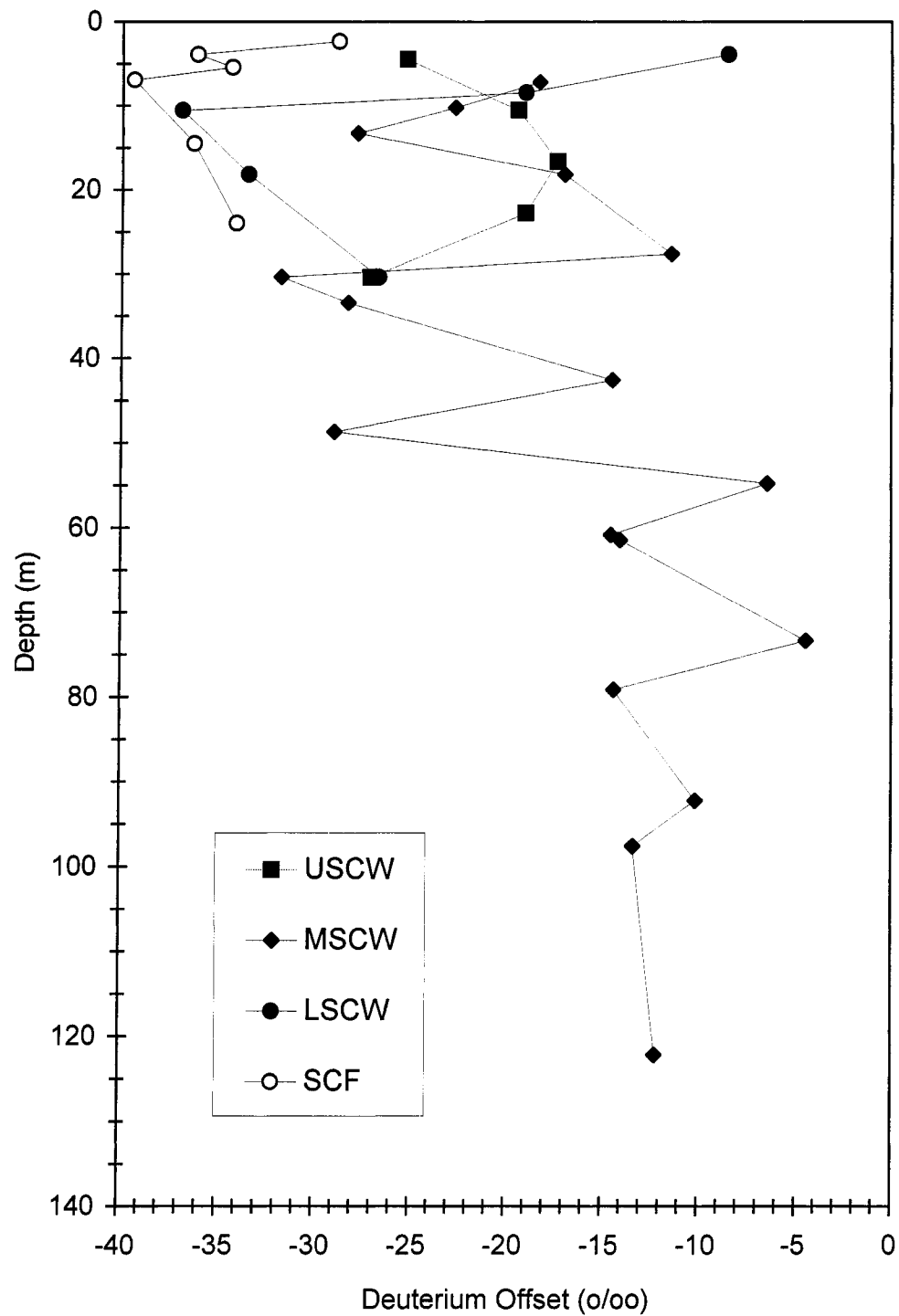


Figure 40. Sheep Creek Wash deuterium offsets from the local meteoric water line (LMWL).

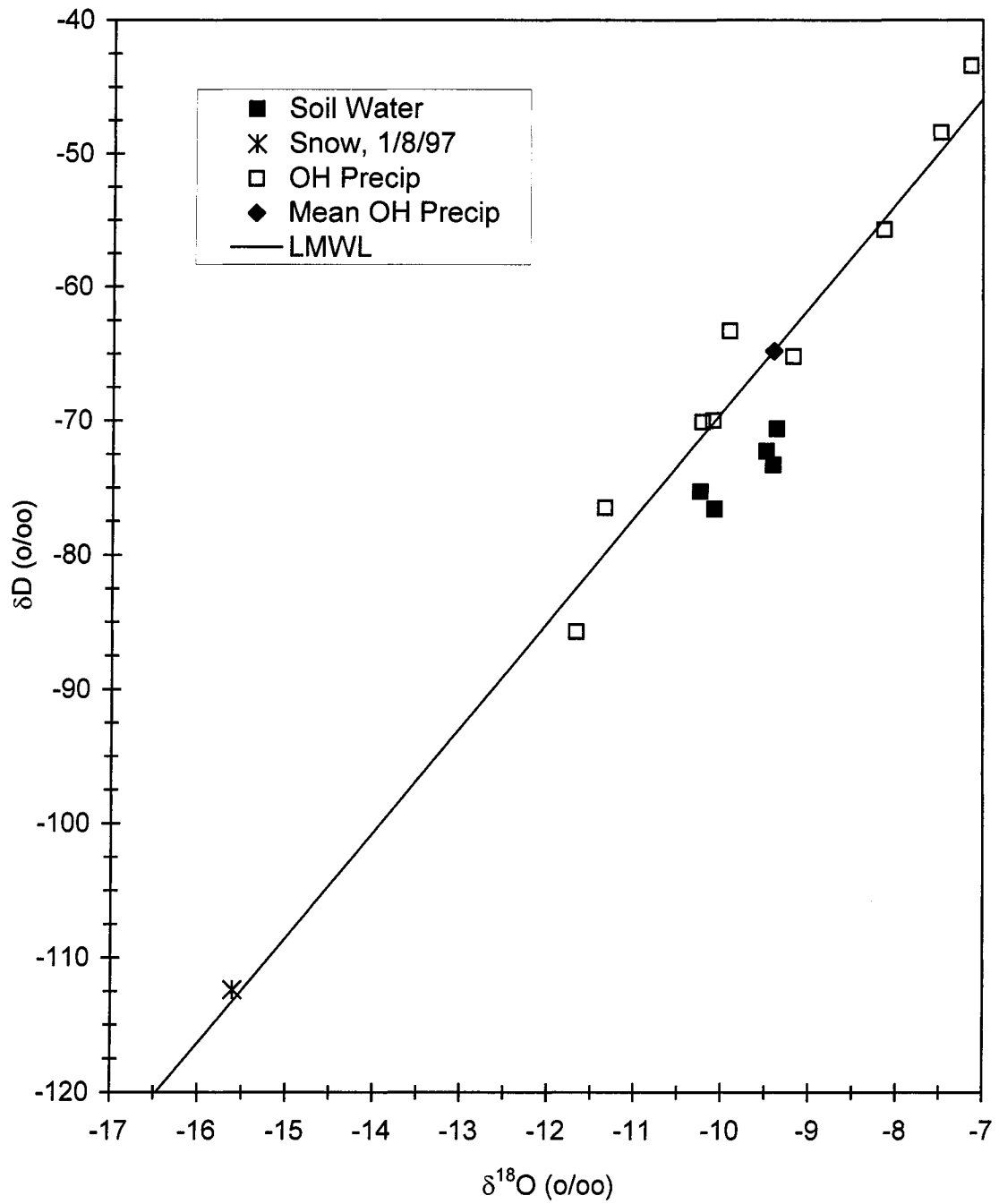


Figure 41. δD vs $\delta^{18}\text{O}$ plot of Summit samples with the local meteoric water line (LMWL).

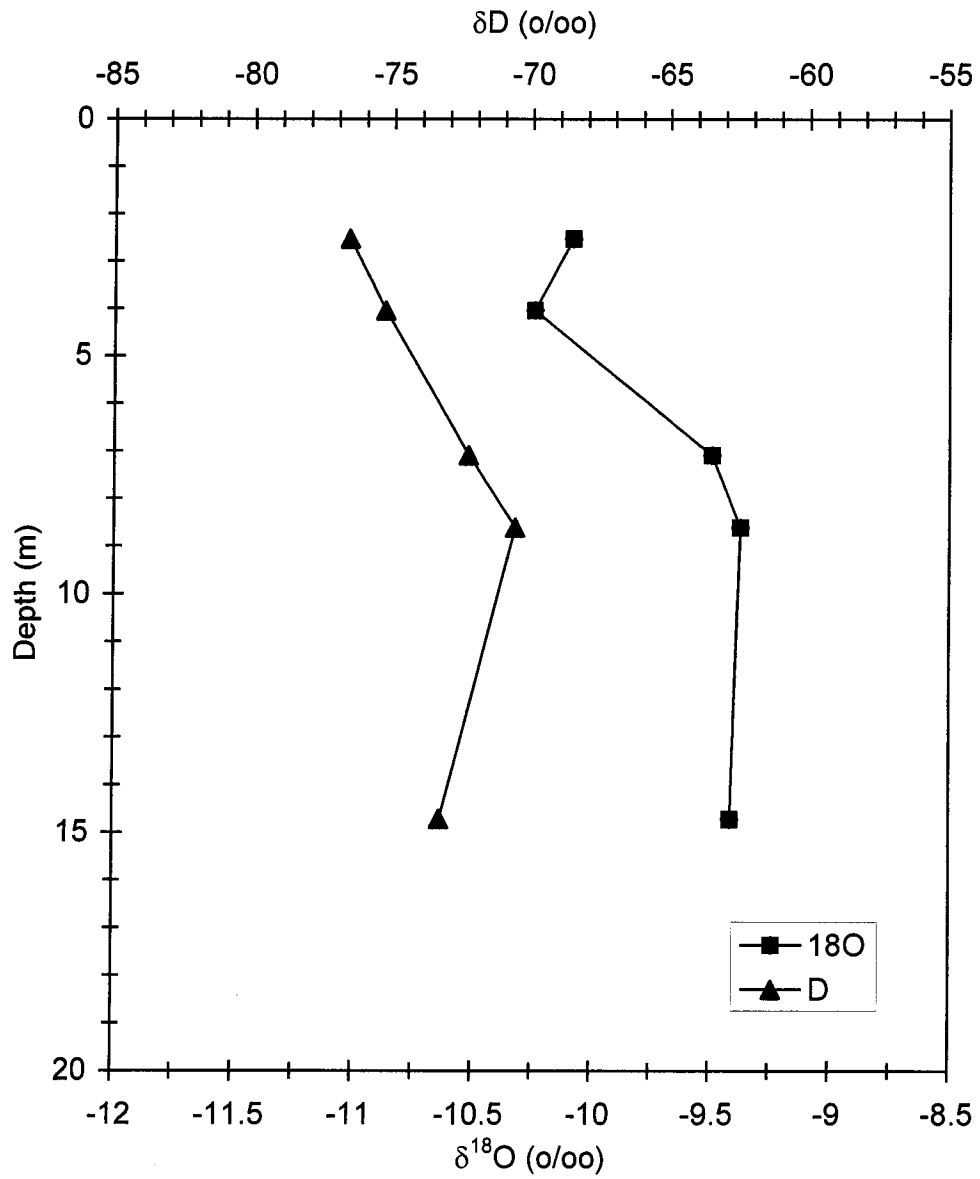


Figure 42. δD and $\delta^{18}O$ depth profiles for Summit soil waters.

UOGW. On a plot of δD vs $\delta^{18}O$ (Fig. 43), the 8 soil waters plot along the LMWL within the range of precipitation samples collected from the OH station. The 3 shallowest soil waters from depths of 6.3 m (21 ft) or less have the least negative δ values and plot higher along the LMWL. The 5 remaining samples, from 8.8 m (29 ft), 16.5 m (54 ft), 20.7 m (68 ft), 25.6 m (84 ft), and 31.7 m (104 ft), cluster around the bulk-average precipitation composition for the OH station. The soil waters plot so close to the LMWL that they are virtually indistinguishable from the precipitation samples. A t-test comparison of the D offsets of the precipitation and the soil waters indicates no statistical difference between them. Depth profiles for δD and $\delta^{18}O$ (Fig. 44) are similar in shape and display the same trends with depth.

MOGW. The MOGW dataset is the largest dataset from the two channels. Soil water was extracted from a sample from each cored interval to provide maximum resolution in the depth profiles. A plot of δD vs $\delta^{18}O$ (Fig. 45) for the 29 soil waters shows that they lie close to the LMWL. The soil-water isotopic compositions are within the range of precipitation for the OH site, but most are of more negative isotopic compositions than bulk-average precipitation. Based on D offset, the soil waters can be split into three groups (Table 5): soil waters from less than 30 m; soil waters from between 30 m and 100 m; and the three deepest samples, from 109.8 m (360 ft), 127.7 m (419 ft), and 146 m (480 ft). Results of t-tests between the D offsets of the soil waters and precipitation indicate that the soil waters from depths of less than 30 m are indistinguishable from precipitation. Groundwater is very similar in isotopic composition

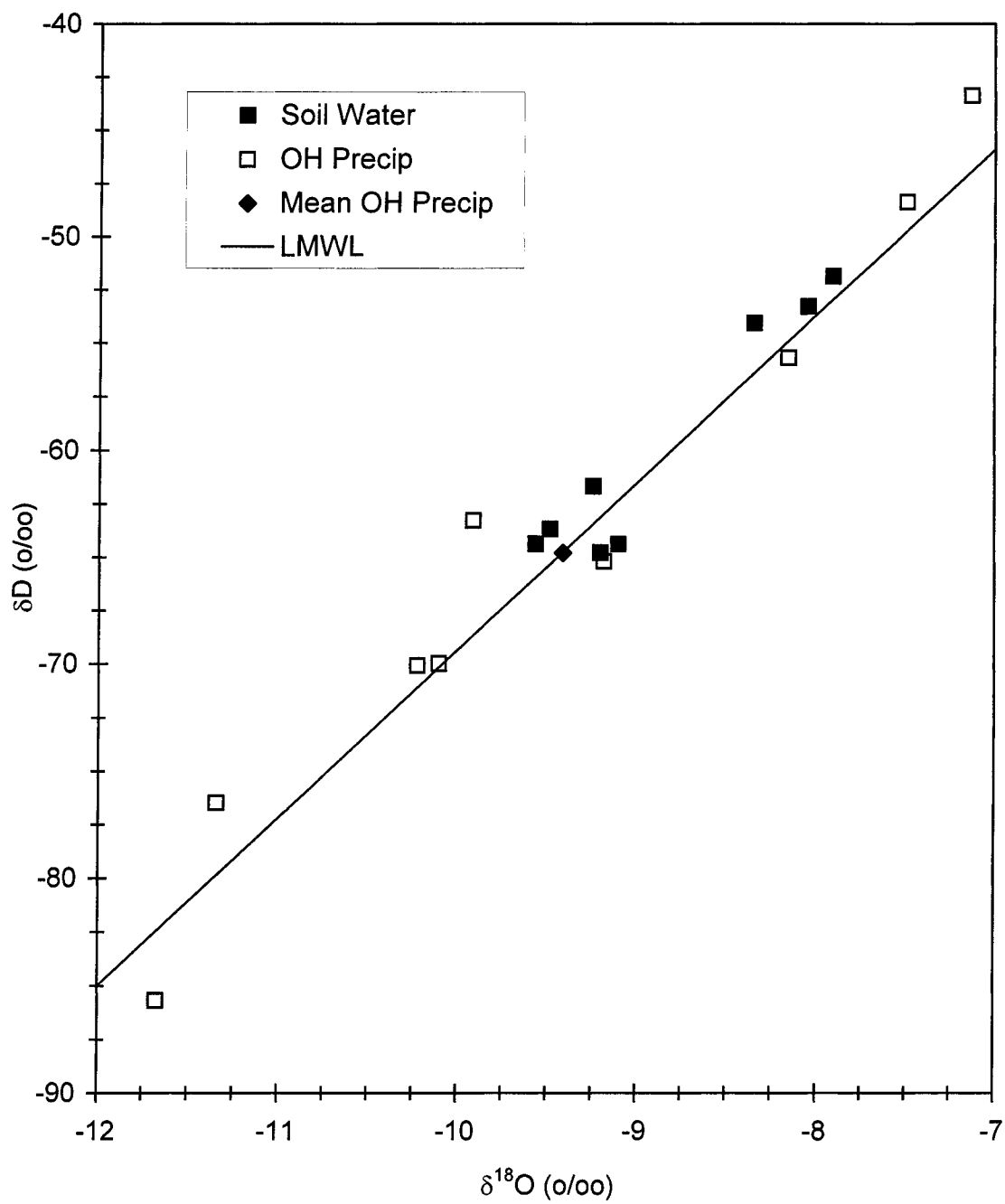


Figure 43. δD vs $\delta^{18}\text{O}$ plot of UOGW samples with the local meteoric water line (LMWL).

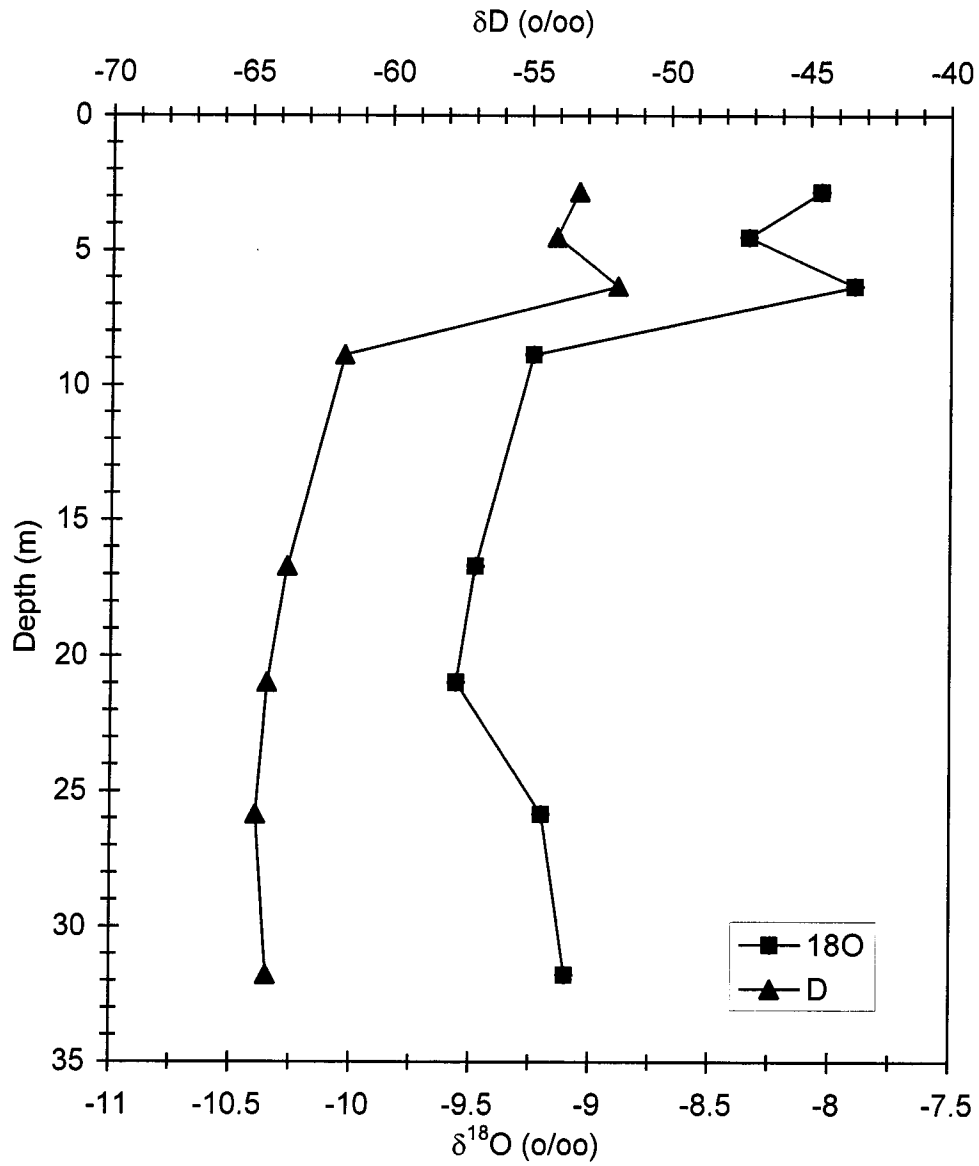


Figure 44. δD and $\delta^{18}O$ depth profiles for UOGW soil waters.

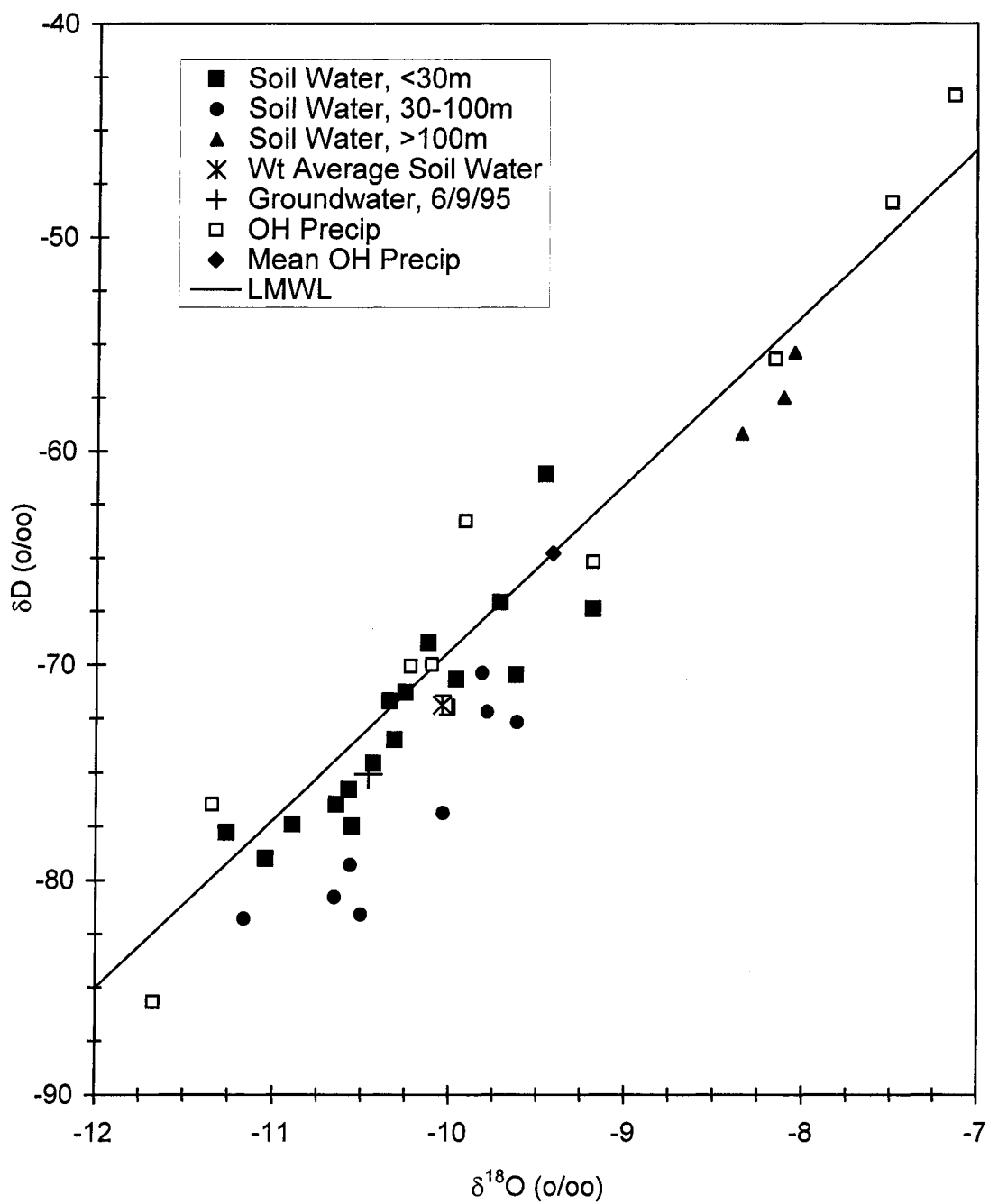


Figure 45. δD vs $\delta^{18}\text{O}$ plot of MOGW samples with the local meteoric water line (LMWL).

to the shallow soil waters and the weighted average of all of the soil waters (gravimetric water content used as the weighting factor). The weighted-average isotopic composition of the soil waters represents an estimate of the isotopic composition of recharge to the aquifer. The δD and $\delta^{18}O$ depth profiles (Fig. 46) are similar in shape and display the same trends with depth. The depth profiles also display considerable variation, indicating that dispersion and diffusion have not smoothed out the profile. The most significant feature of both the δD and $\delta^{18}O$ profiles is a shift toward less negative δ values in the 3 deepest soil waters. The shift seen in the deepest soil waters, away from the groundwater composition, is more than 15 ‰ for δD and more than 2 ‰ for $\delta^{18}O$.

LOGW-1. On a plot of δD vs $\delta^{18}O$ (Fig. 47), the isotopic compositions of all but one of the 15 soil waters lie well below the LMWL. The soil waters from this location have more negative D offsets than those from UOGW and MOGW. Although the soil waters plot off the LMWL, their isotopic compositions are within the range of precipitation collected from the BV station. An estimate of their original isotopic compositions (see Fig. 4), achieved by projecting each data point back to the LMWL along an evaporative trend line (with a slope between 4 and 6) would result in most of them intersecting the LMWL at more negative δ values than bulk-average precipitation. The one sample of stream water collected has a less negative isotopic composition than both the soil waters and bulk-average precipitation from the BV station. Depth profiles for δD and $\delta^{18}O$ (Fig. 48) are similar in shape and display the same trends with depth.

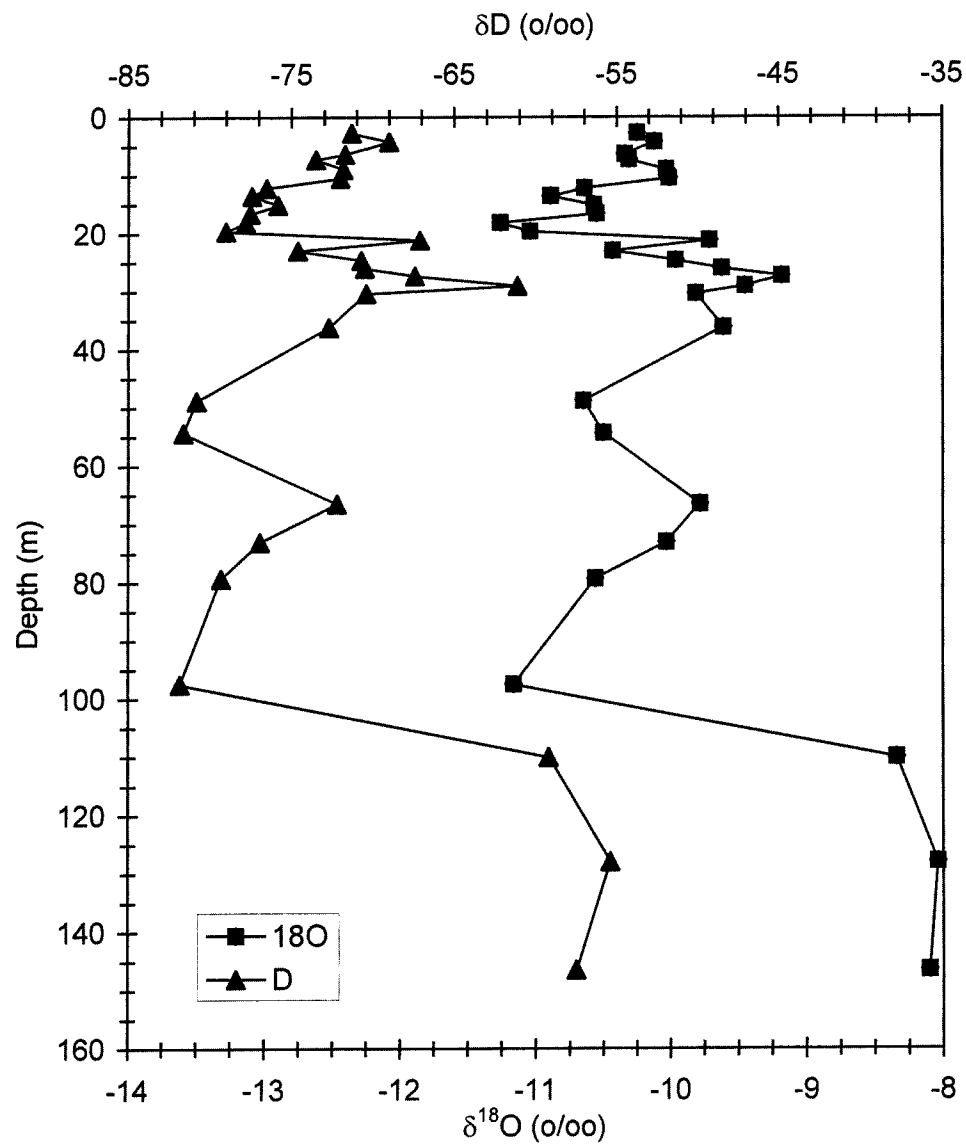


Figure 46. δD and $\delta^{18}O$ depth profiles for MOGW soil waters.

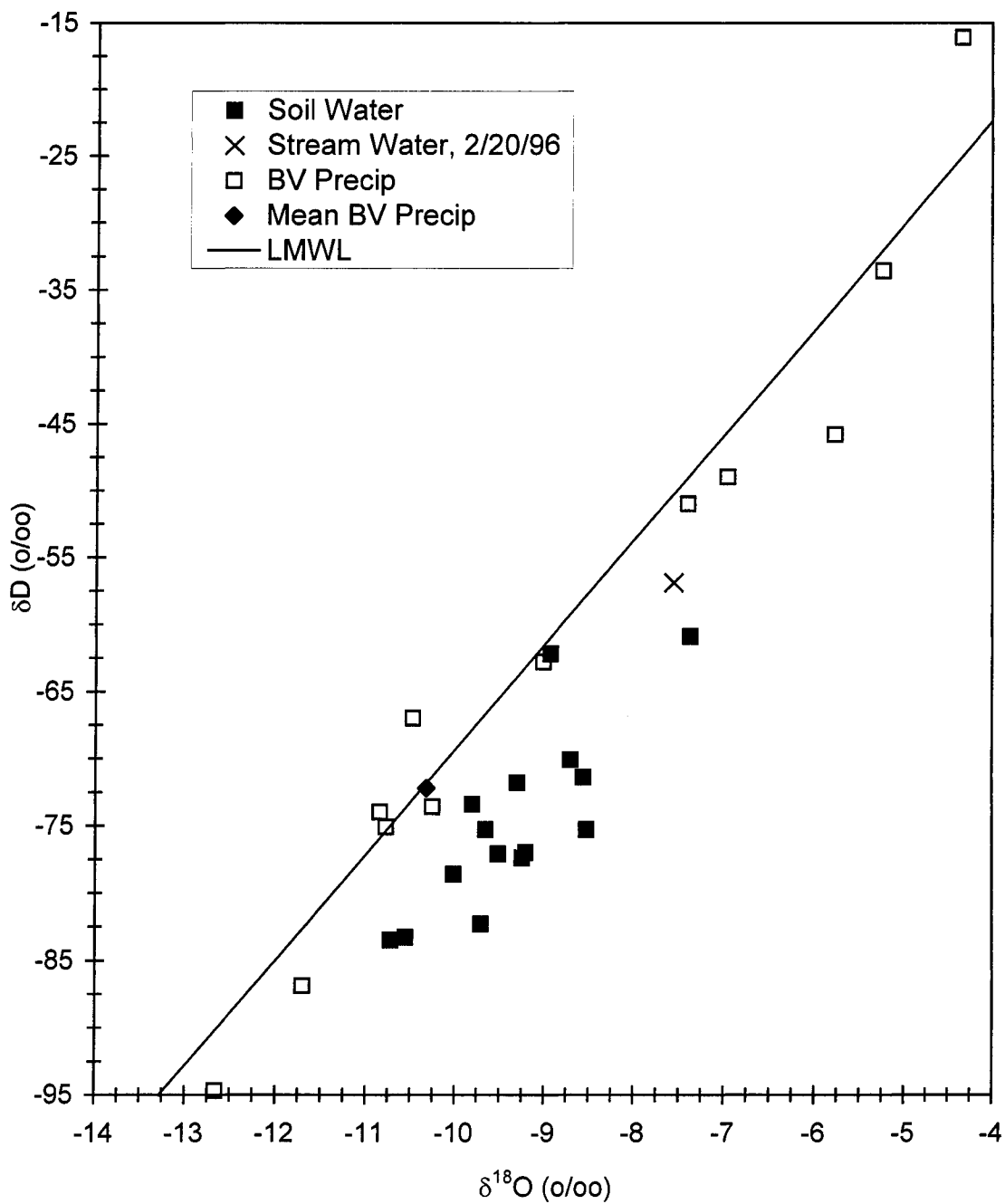


Figure 47. δD vs $\delta^{18}\text{O}$ plot of LOGW-1 samples with the local meteoric water line (LMWL).

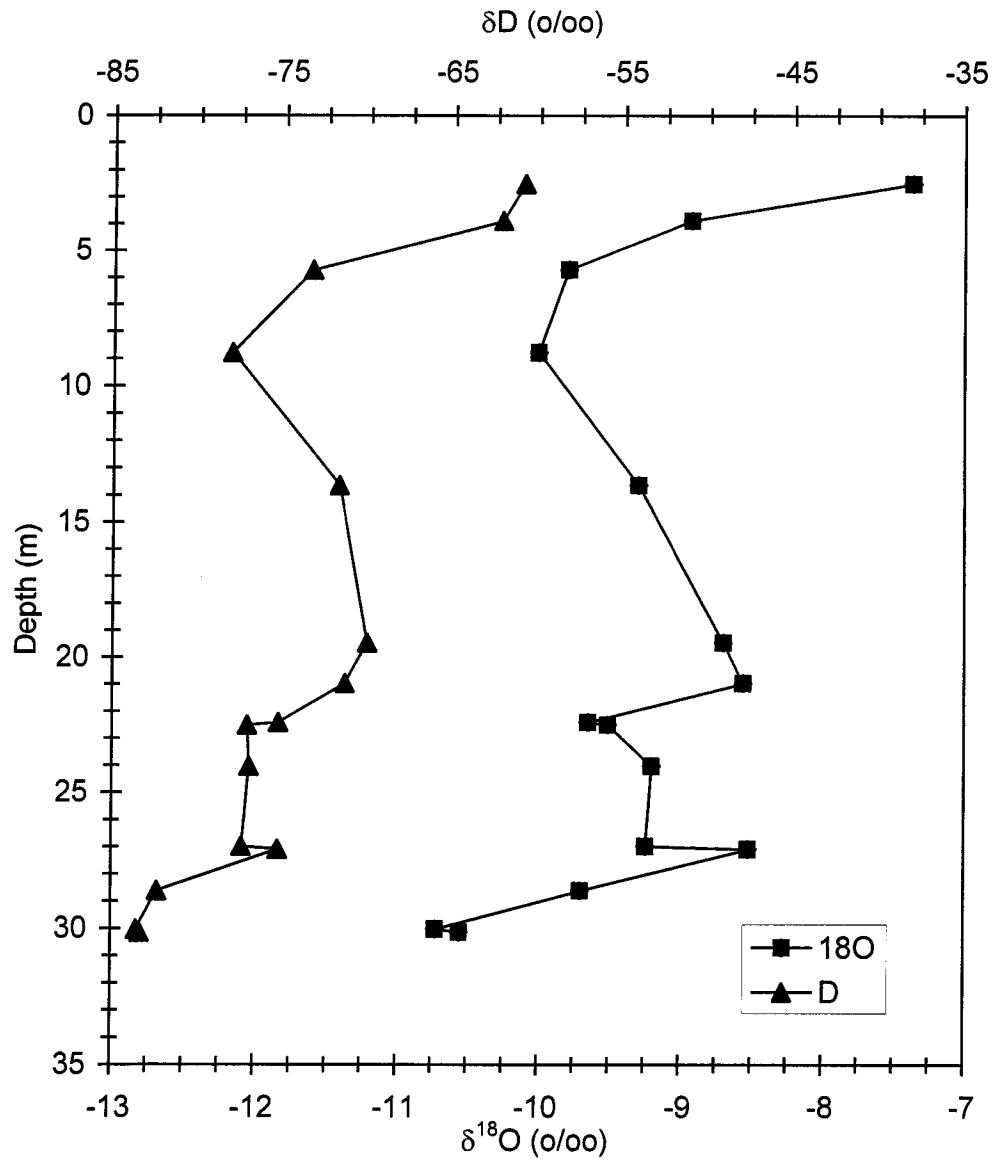


Figure 48. δD and $\delta^{18}O$ depth profiles for LOGW-1 soil waters.

LOGW-2. On a plot of δD vs $\delta^{18}O$ (Fig. 49), the 5 soil waters plot below the LMWL, but within the range of precipitation collected at the BV station. The deepest soil waters (22.3 m (73 ft) and 31.5 m (103 ft)) lie closer to the LMWL than the shallower samples. Projecting the soil waters back to the LMWL along evaporative trend lines would result in their intersecting the LMWL at isotopic compositions considerably more negative than bulk-average precipitation from the BV station. The δD and $\delta^{18}O$ depth profiles (Fig. 50) are similar in shape, but below 15 m the δD values of the soil waters become less negative while the $\delta^{18}O$ values become more negative.

OGF. The OGF dataset is the largest dataset from the three control surfaces with 22 soil waters analyzed for isotopic composition. Soil water from each cored interval was analyzed to provide maximum resolution in the depth profiles. A δD vs $\delta^{18}O$ plot (Fig. 51) shows the soil waters to be within the range of precipitation collected from the BV station, although they plot below the LMWL. On the plot, the soil waters can be separated into three groups: 1) a cluster of soil waters plotting below the LMWL with $\delta^{18}O$ values less than -8 ‰; 2) 5 soil waters with $\delta^{18}O$ values greater than -9 ‰ defining a linear trend roughly parallel to, but below the LMWL; and 3) 5 soil waters with $\delta^{18}O$ values greater than -8 ‰ that define a linear trend with a slope less than that of the LMWL. Most, but not all, of the deeper samples are included in the first group. The δD and $\delta^{18}O$ depth profiles (Fig. 52) display considerable variations, and some differences, but both display an overall trend toward more negative δ values with depth.

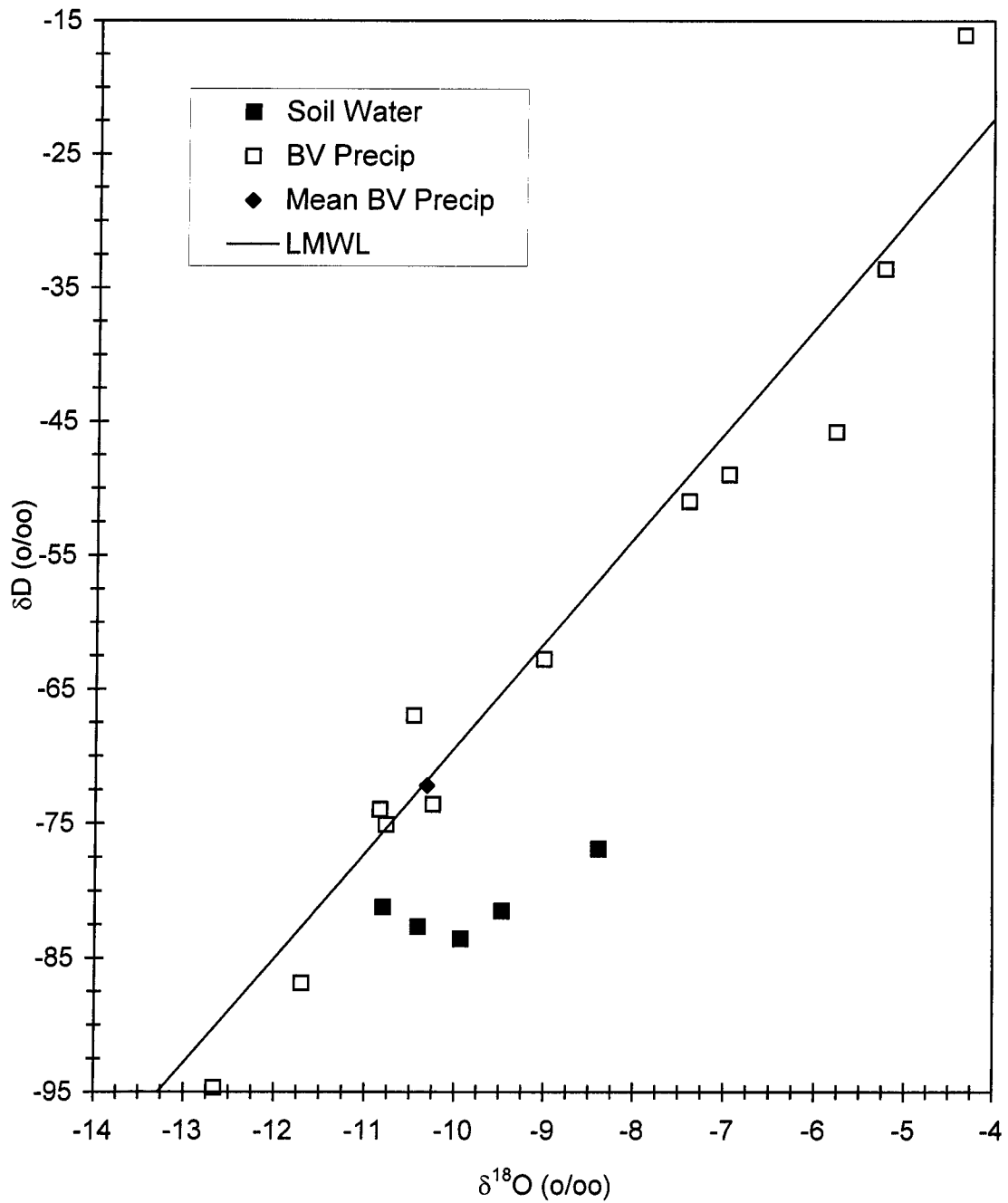


Figure 49. δD vs $\delta^{18}\text{O}$ plot of LOGW-2 samples with the local meteoric water line (LMWL).

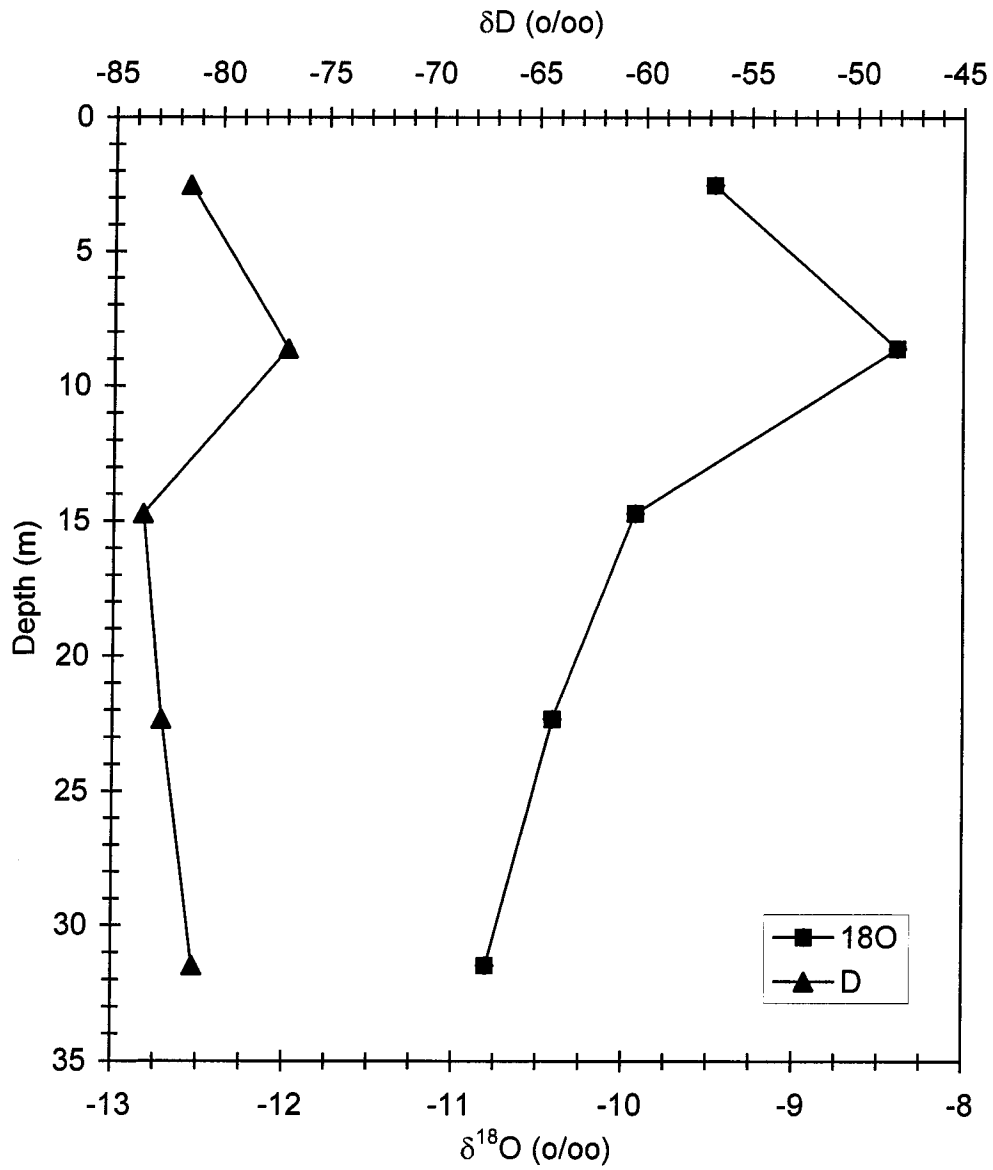


Figure 50. δD and $\delta^{18}O$ depth profiles for LOGW-2 soil waters.

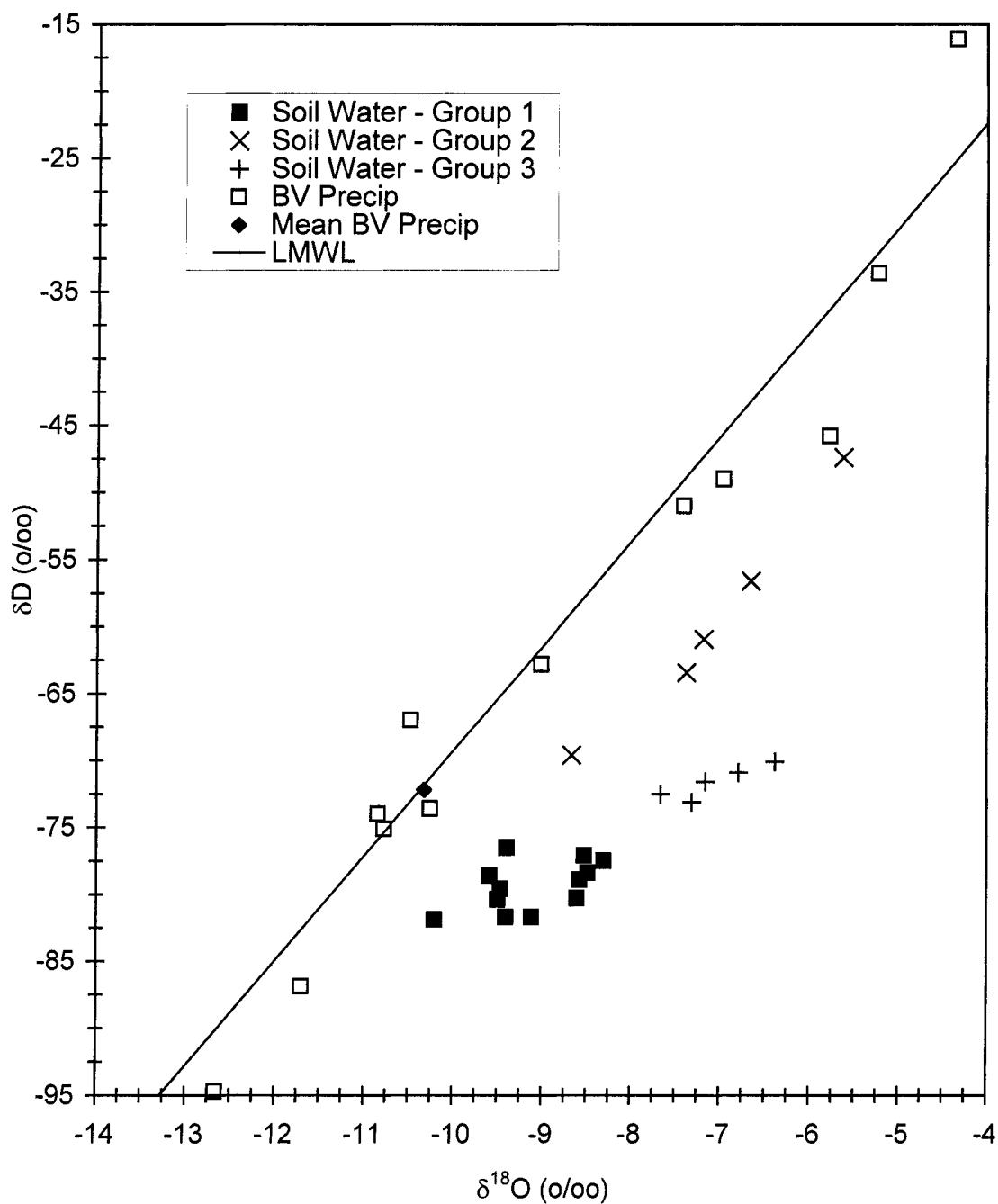


Figure 51. δD vs $\delta^{18}\text{O}$ plot of OGF samples with the local meteoric water line (LMWL). See text for explanation of soil-water groups.

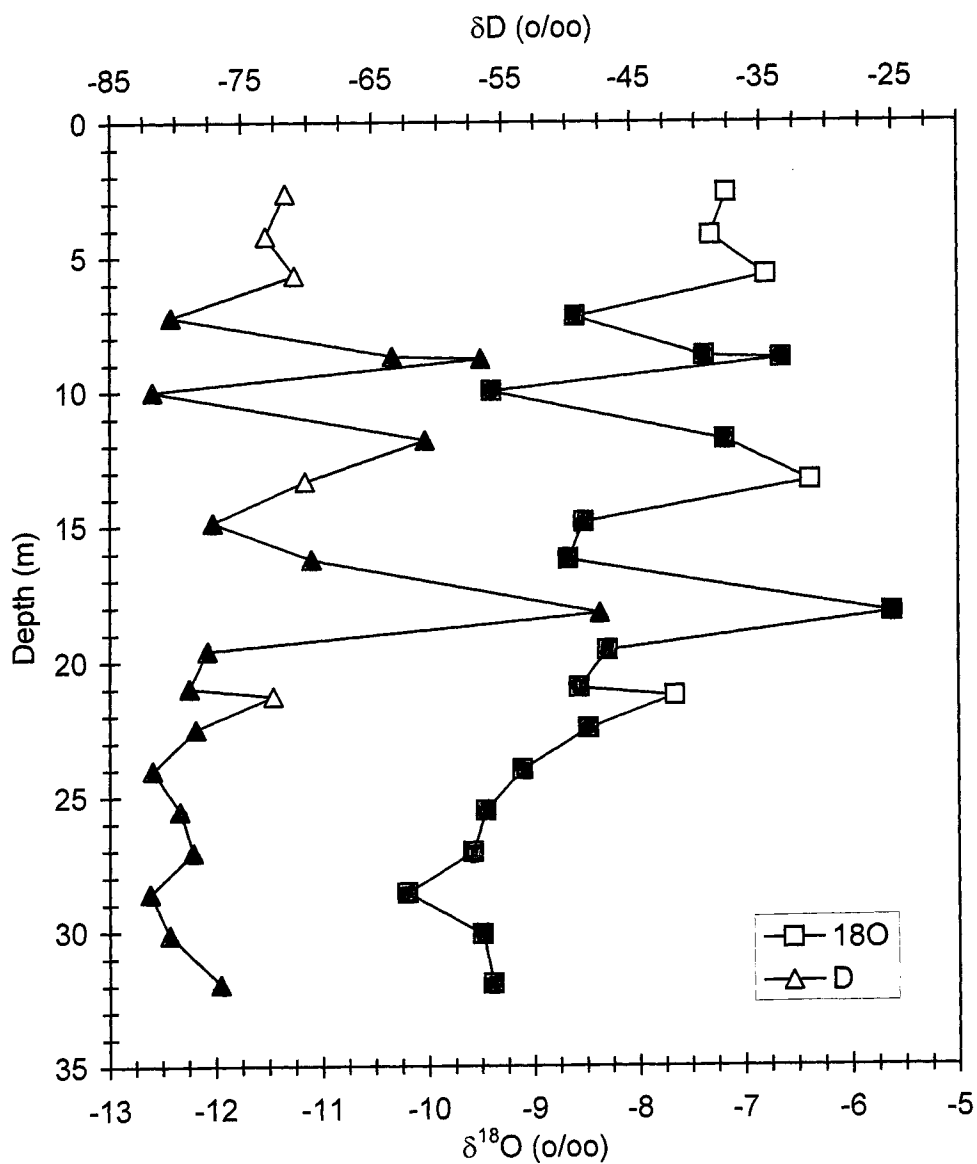


Figure 52. δD and $\delta^{18}O$ depth profiles for OGF soil waters. Fill color of symbol indicates soil-water group: Group 1 in red, Group 2 in blue, and Group 3 in white. See text for explanation of soil-water groups.

USCW. On a plot of δD vs $\delta^{18}O$ (Fig. 53), the 5 soil waters plot well off of the LMWL. Four of the soil waters are similar in composition, and the deepest soil water from 30.4 m (100 ft) has less negative δ values. Projecting the soil waters back to the LMWL along evaporative trend lines (slopes between 4 to 6) would result in their intersecting the LMWL at isotopic compositions more negative than bulk-average precipitation from the TM station. The isotopic composition of snow collected at the site is more negative than bulk precipitation from the TM station. Surface water collected from a puddle at the site is similar in composition to the soil waters. Depth profiles for δD and $\delta^{18}O$ (Fig. 54) are similar in shape and display the same trends with depth.

MSCW. The MSCW dataset is the largest dataset from Sheep Creek Wash with 17 soil waters analyzed for isotopic composition. On a plot of δD vs $\delta^{18}O$ (Fig. 55) the soil waters can be separated into two groups: those from depths of less than 42 m, and those from depths of more than 42 m. The soil waters from depths of less than 42 m, with the exception of one at 27.7 m (91 ft), have $\delta^{18}O$ values greater than -10.5 o/oo and more negative D offsets than most of the deeper soil waters. The soil waters from depths of more than 42 m, with the exception of one at 48.7 m (160 ft), have $\delta^{18}O$ values less than -10.5 o/oo and less negative D offsets than the shallower soil waters. Projecting the soil waters back to the LMWL along evaporative trend lines would result in their intersecting the LMWL at δ values more negative than most bulk precipitation from the SC station. Groundwater has an isotopic composition that is similar to some of the bulk precipitation samples from the SC station, and some of the deeper soil waters (>42 m).

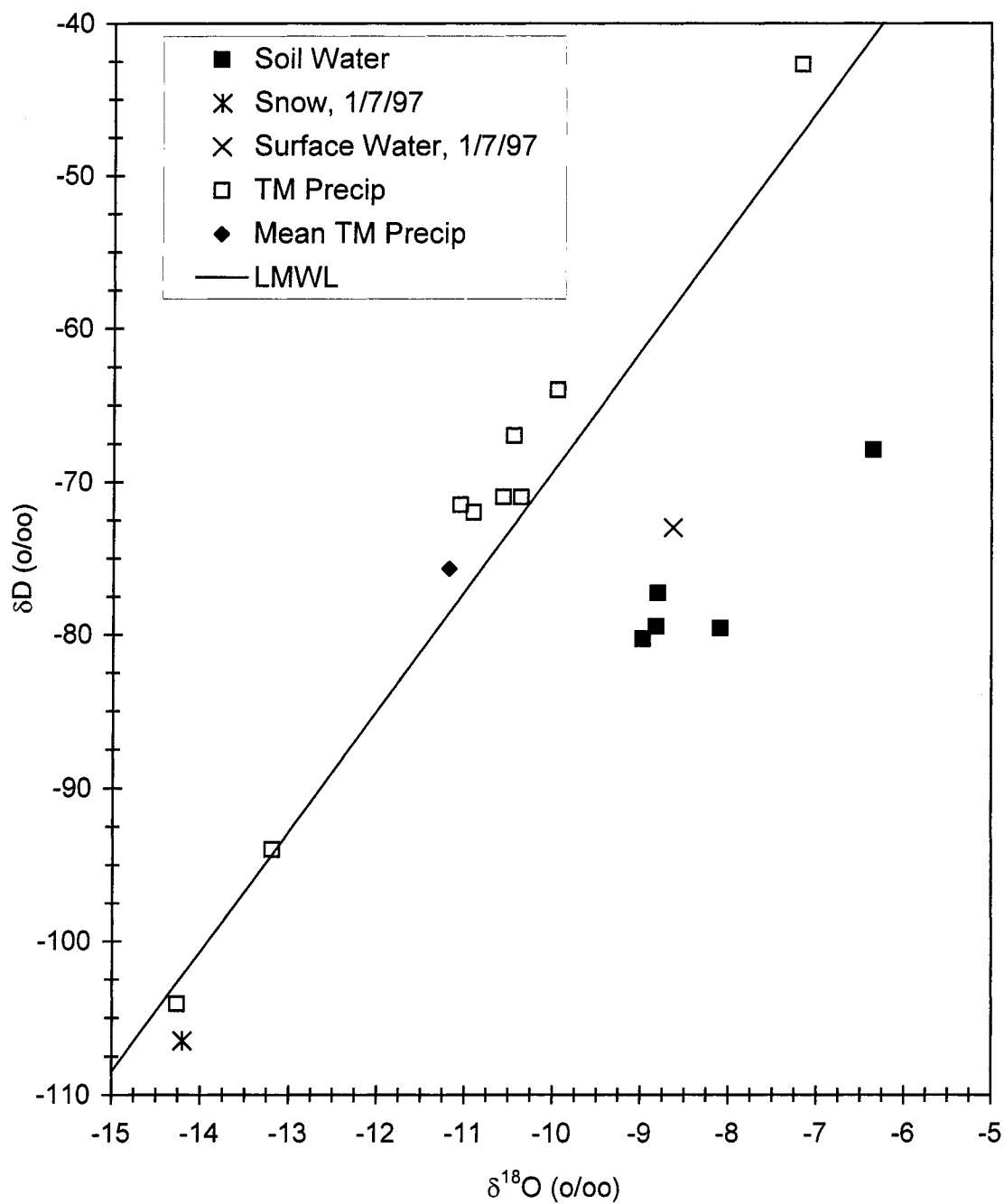


Figure 53. δD vs $\delta^{18}\text{O}$ plot of USCW samples with the local meteoric water line (LMWL).

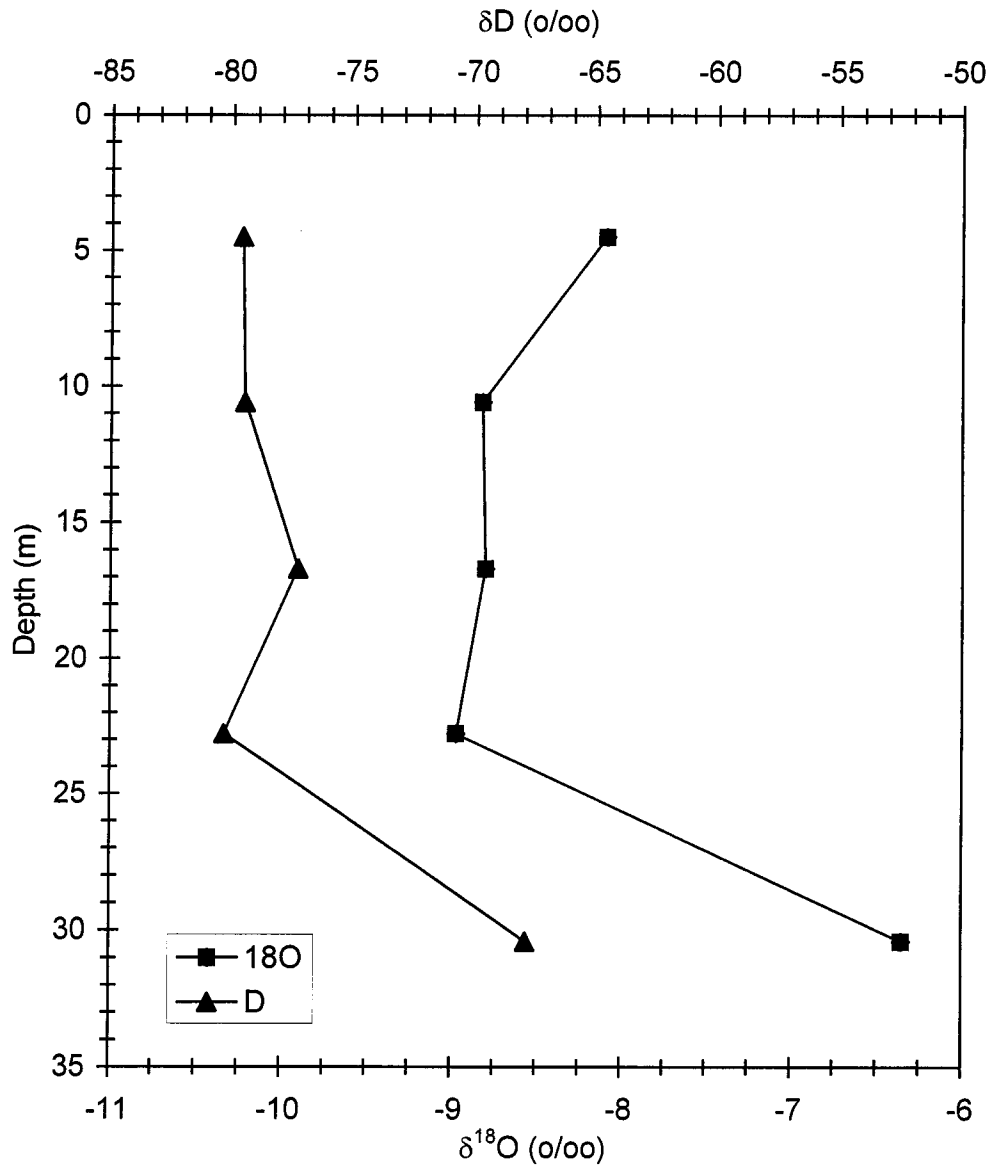


Figure 54. δD and $\delta^{18}O$ depth profiles for USCW soil waters.

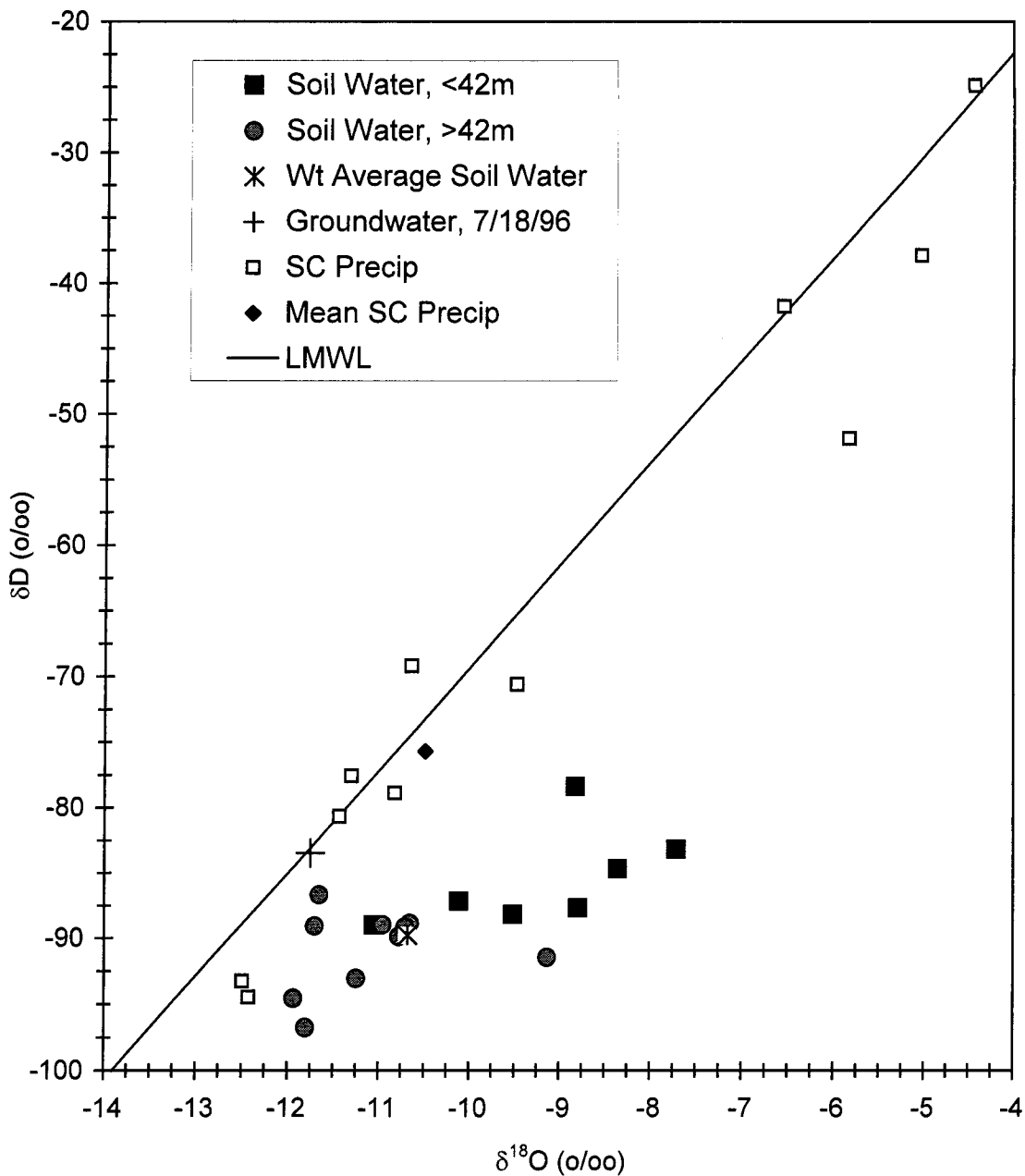


Figure 55. δD vs $\delta^{18}O$ plot of MSCW samples with the local meteoric water line (LMWL).

The groundwater isotopic composition is also close to the weighted-average isotopic composition of all of the soil waters (gravimetric water content used as the weighting factor), which represents an estimate of the isotopic composition of recharge to the aquifer. The δD and $\delta^{18}O$ depth profiles (Fig. 56) are not similar in appearance, but both display an overall trend toward slightly more negative isotopic compositions with depth.

LSCW. On a δD vs $\delta^{18}O$ plot (Fig. 57), the 5 soil waters, except the shallowest water from 3.9 m (13 ft), plot well off the LMWL. The water from 3.9 m (13 ft) has an isotopic composition similar to bulk precipitation from the SC station, but with a less negative composition than the bulk average. The four deeper soil waters, if projected back to the LMWL along evaporative trend lines, would intersect it at more negative δ values than the bulk average from the SC station. Stream water has an isotopic composition within the range of bulk precipitation and plots near the LMWL. Depth profiles for δD and $\delta^{18}O$ (Fig. 58) show the δD values becoming more negative to 10 m and the $\delta^{18}O$ values becoming less negative. Below 10 m both profiles are similar and display the same trends.

SCF. On a δD vs $\delta^{18}O$ plot (Fig. 59), the 6 soil waters plot well below and roughly parallel to the LMWL. The two deepest waters, from 14.6 m (48 ft) and 24 m (79 ft), have more negative isotopic compositions than the shallower waters. Depth profiles for δD and $\delta^{18}O$ (Fig. 60) display a trend toward more negative δ values with depth.

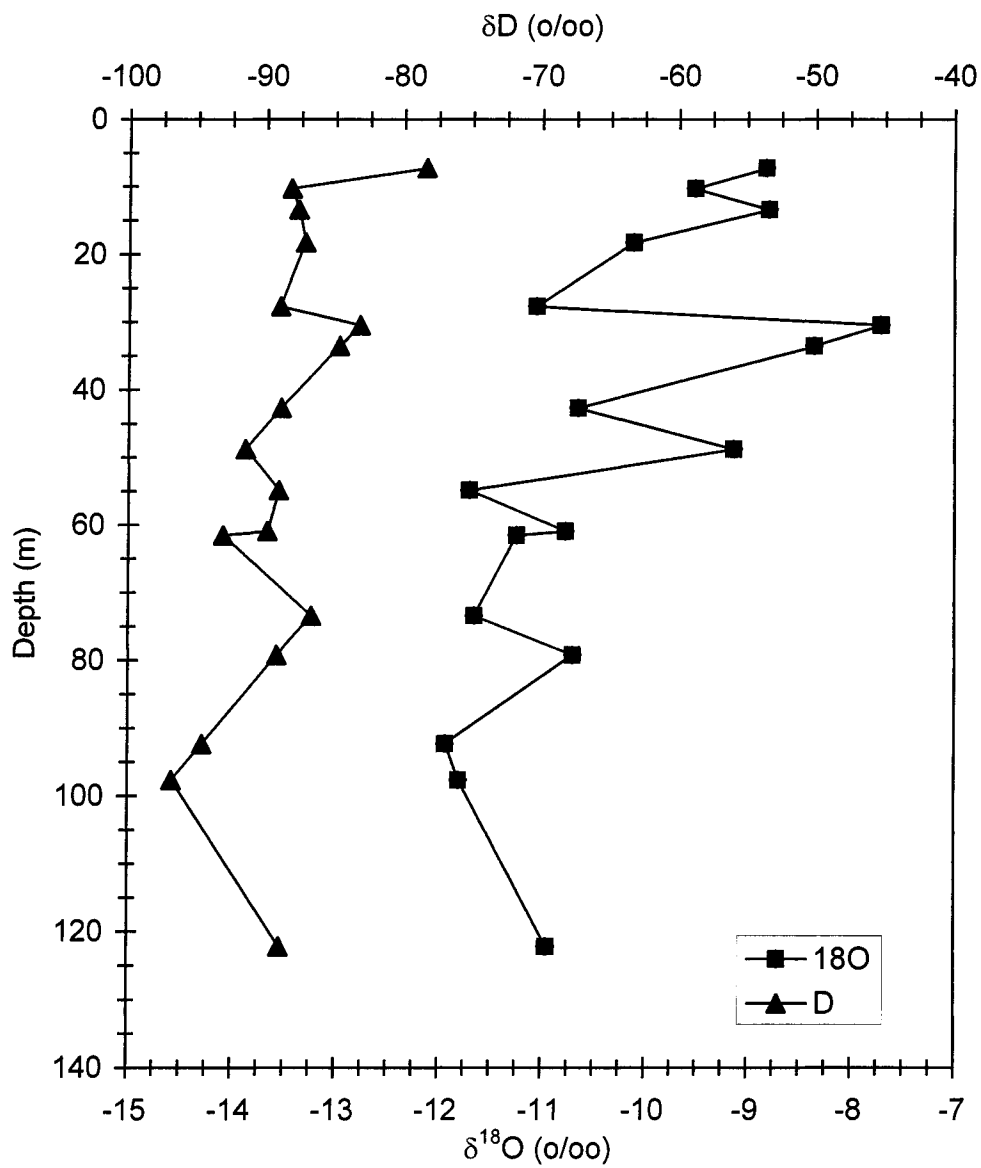


Figure 56. δD and $\delta^{18}O$ depth profiles for MSCW soil waters.

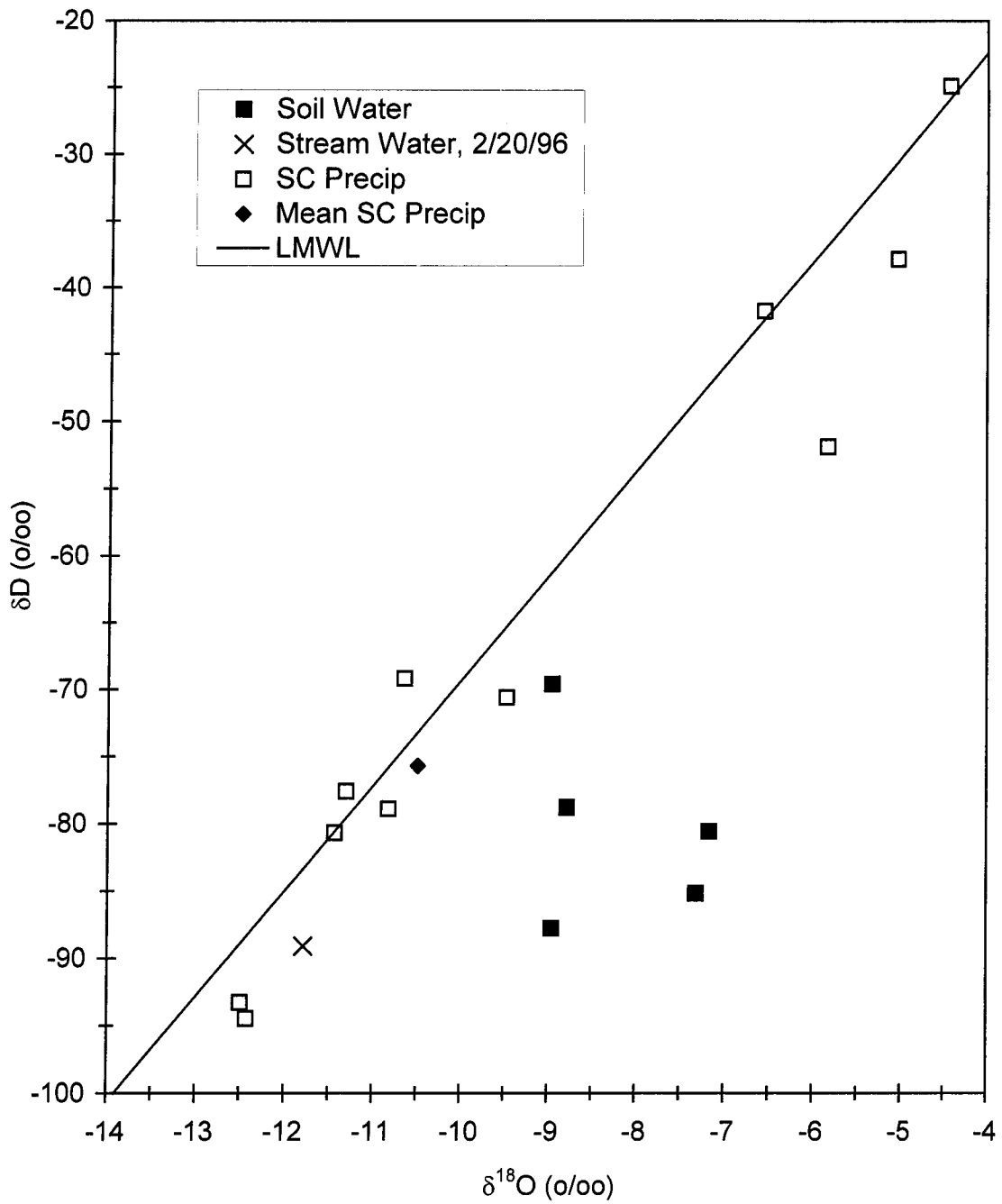


Figure 57. δD vs $\delta^{18}\text{O}$ plot of LSCW samples with the local meteoric water line (LMWL).

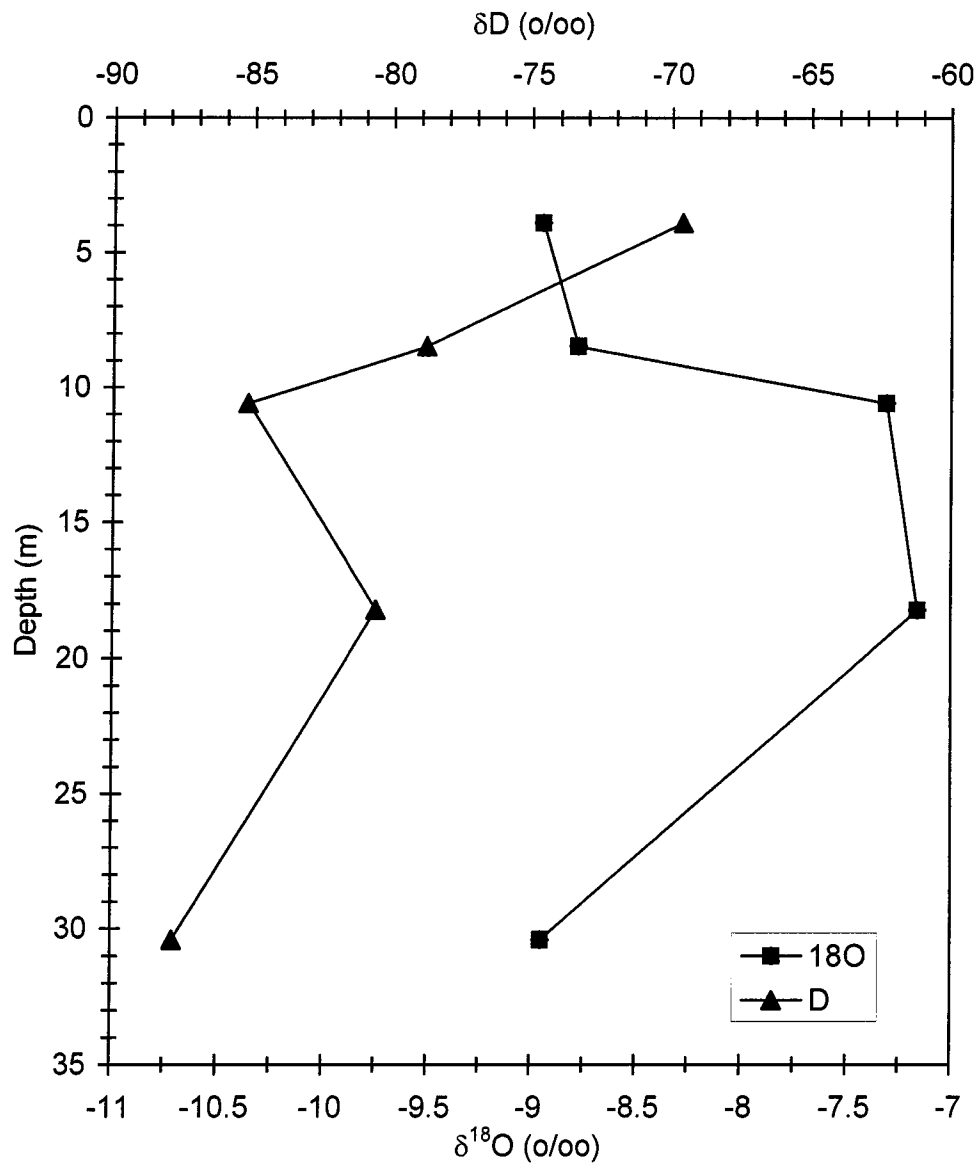


Figure 58. δD and $\delta^{18}O$ depth profiles for LSCW soil waters.

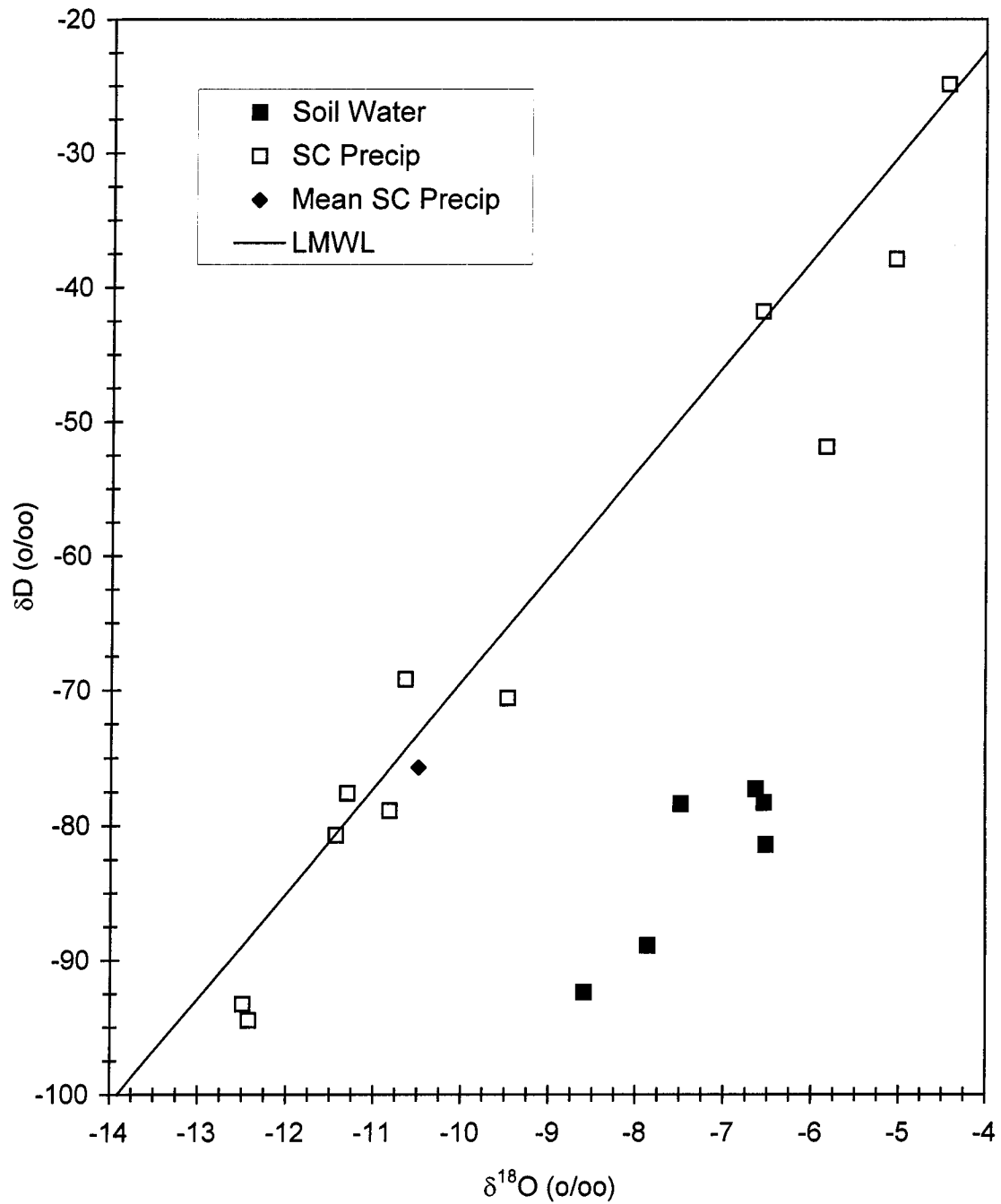


Figure 59. δD vs $\delta^{18}\text{O}$ plot of SCF samples with the local meteoric water line (LMWL).

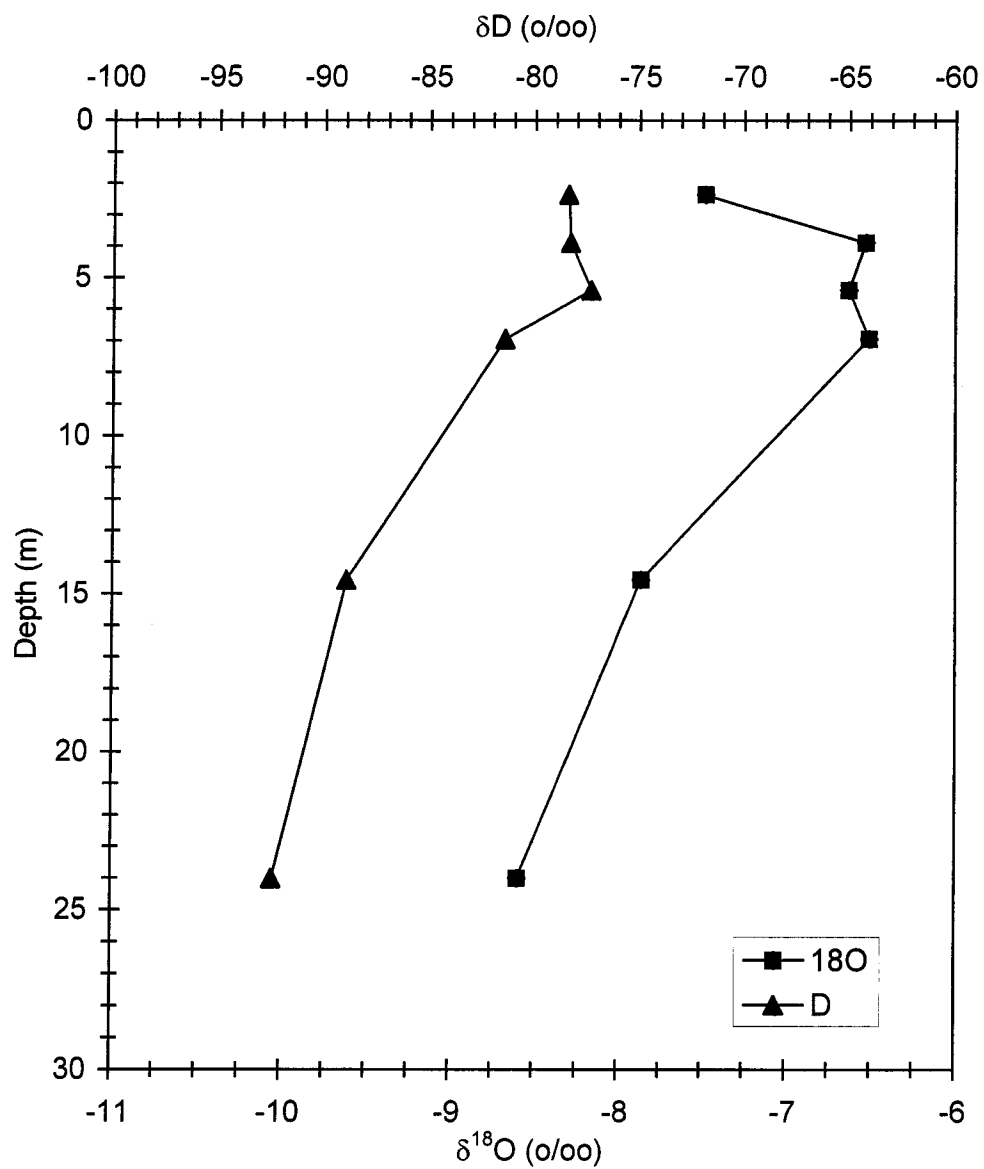


Figure 60. δD and $\delta^{18}O$ depth profiles for SCF soil waters.

Hand-auger Samples. Hand-auger samples were collected at UOGW, MOGW, and OGF in January 1996, a year after the drilling operations were conducted along OGW. The samples were collected to investigate the shallow isotope depth profiles and to compare the isotopic composition of shallow soil water to the previous winter's precipitation. Samples were collected at 0.15-m (6-in.) intervals to depths of up to 2.7 m (9 ft). The range of isotopic compositions for the soil waters and the approximate amount of enrichment at the isotope maximum (see Fig. 3) in each depth profile are given in Table 6 for each location.

UOGW. The δD and $\delta^{18}O$ depth profiles (Fig. 61) are similar and have maximum δ values (indicating the location of the drying front, see Fig. 3) at 0.3 m (1 ft). On a plot of δD vs $\delta^{18}O$ (Fig. 62), the evaporatively enriched waters associated with the isotope maximum plot well off the LMWL and the deeper waters plot near the LMWL. It can also be seen that the soil waters extracted from hand-auger samples collected in January 1996 have more negative isotopic compositions than soil waters extracted from core samples collected in January 1995. Soil water from a depth of 2.7 m (9 ft), extracted from core material collected in January 1995, has an isotopic composition of -53.3 o/oo and -8.04 o/oo for δD and $\delta^{18}O$, respectively. Soil water from the same depth, extracted from a hand-auger sample collected in January 1996, has an isotopic composition of -72.3 o/oo and -10.32 o/oo for δD and $\delta^{18}O$, respectively. The isotopic compositions of the January 1996 soil waters are very similar to that of winter 1995 bulk-average

Table 6. Range of isotopic compositions and enrichment seen in shallow depth profiles for soil waters extracted from hand-auger samples.

Location	Range δD (o/oo)	Range $\delta^{18}O$ (o/oo)	Enrichment at δ Maximum (approximate, in o/oo)
UOGW	-77.3 to -63.4	-10.76 to -6.33	δD : 10, $\delta^{18}O$: 4
MOGW	-73.4 to -50.6	-9.02 to -3.93	δD : 17, $\delta^{18}O$: 5
OGF	-85.3 to -36.6	-9.56 to -1.16	δD : 35, $\delta^{18}O$: 8

precipitation from the OH station, which has an isotopic composition of -73.9 o/oo and -10.23 o/oo for δD and $\delta^{18}O$, respectively.

MOGW. The δD and $\delta^{18}O$ depth profiles (Fig. 63) are similar and have maximum δ values at 0.3 m (1 ft). On a plot of δD vs $\delta^{18}O$ (Fig. 64), the shallowest soil waters (associated with the drying front and diffusion effects) plot well off the LMWL, and the soil waters from depths greater than 1 m are similar in composition to the deeper January 1995 soil waters extracted from the core materials, although they have less negative compositions than the majority of them.

OGF. The δD and $\delta^{18}O$ depth profiles (Fig. 65) are similar and have maximum δ values at 0.3 m (1 ft). At this location, a control site, the amplitude of the isotope maximum, the amount of enrichment seen in the isotope maximum (Table 6) compared to soil waters deeper in the profile, is considerably greater than the isotope maximum amplitudes from the channel locations, UOGW and MOGW. A plot of δD vs $\delta^{18}O$ (Fig. 66) shows that the shallow soil waters from depths greater than 1 m (below the drying

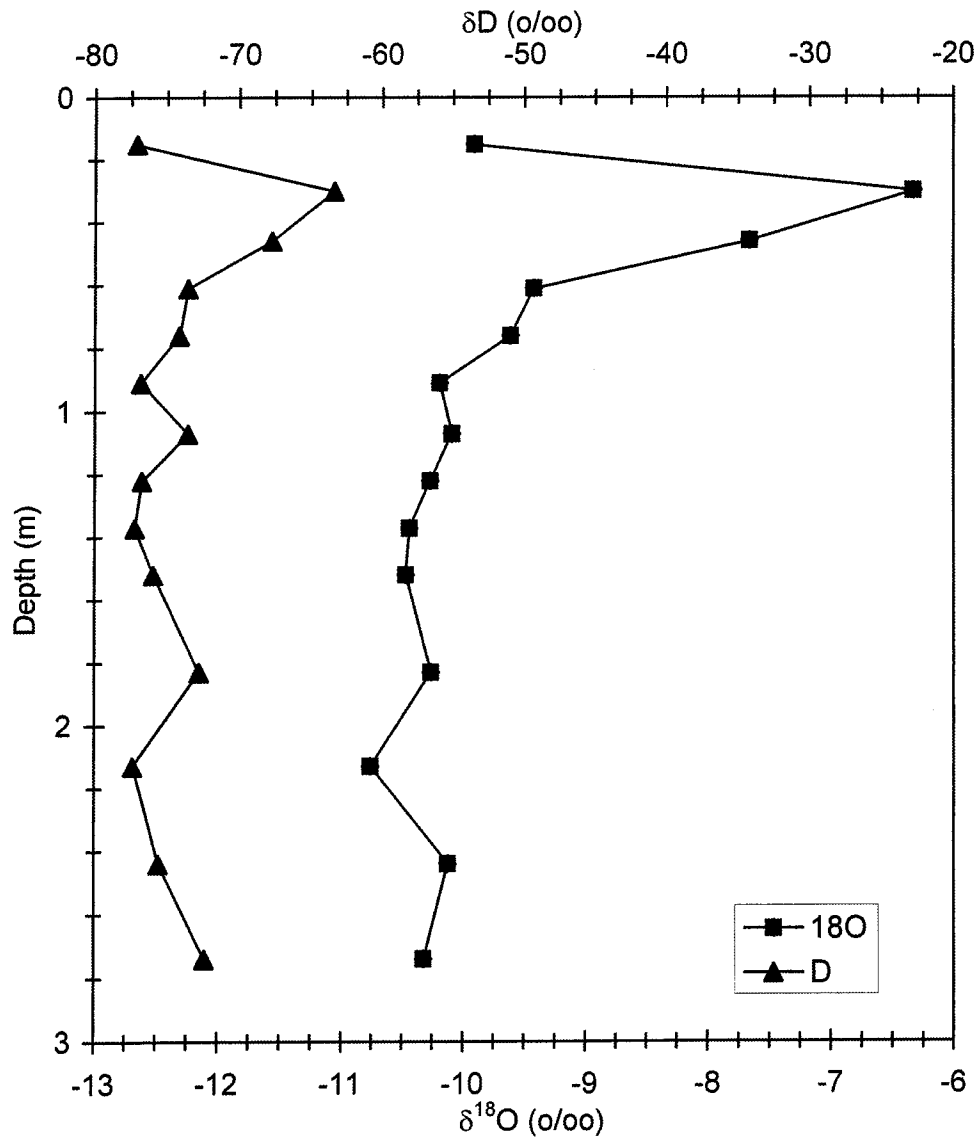


Figure 61. δD and $\delta^{18}O$ depth profiles for UOGW shallow soil waters.

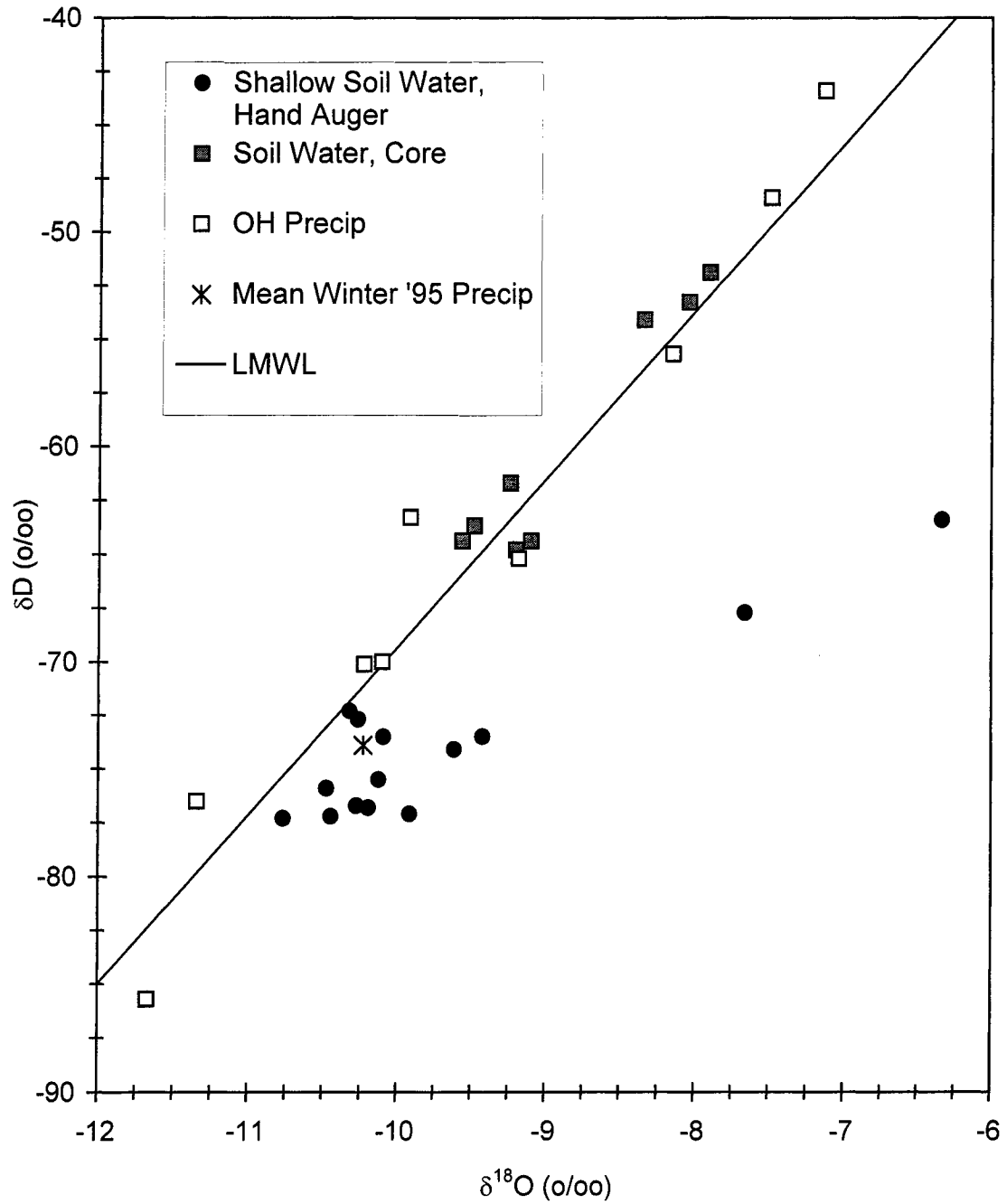


Figure 62. δD vs $\delta^{18}O$ plot of UOGW shallow soil waters with the local meteoric water line (LMWL).

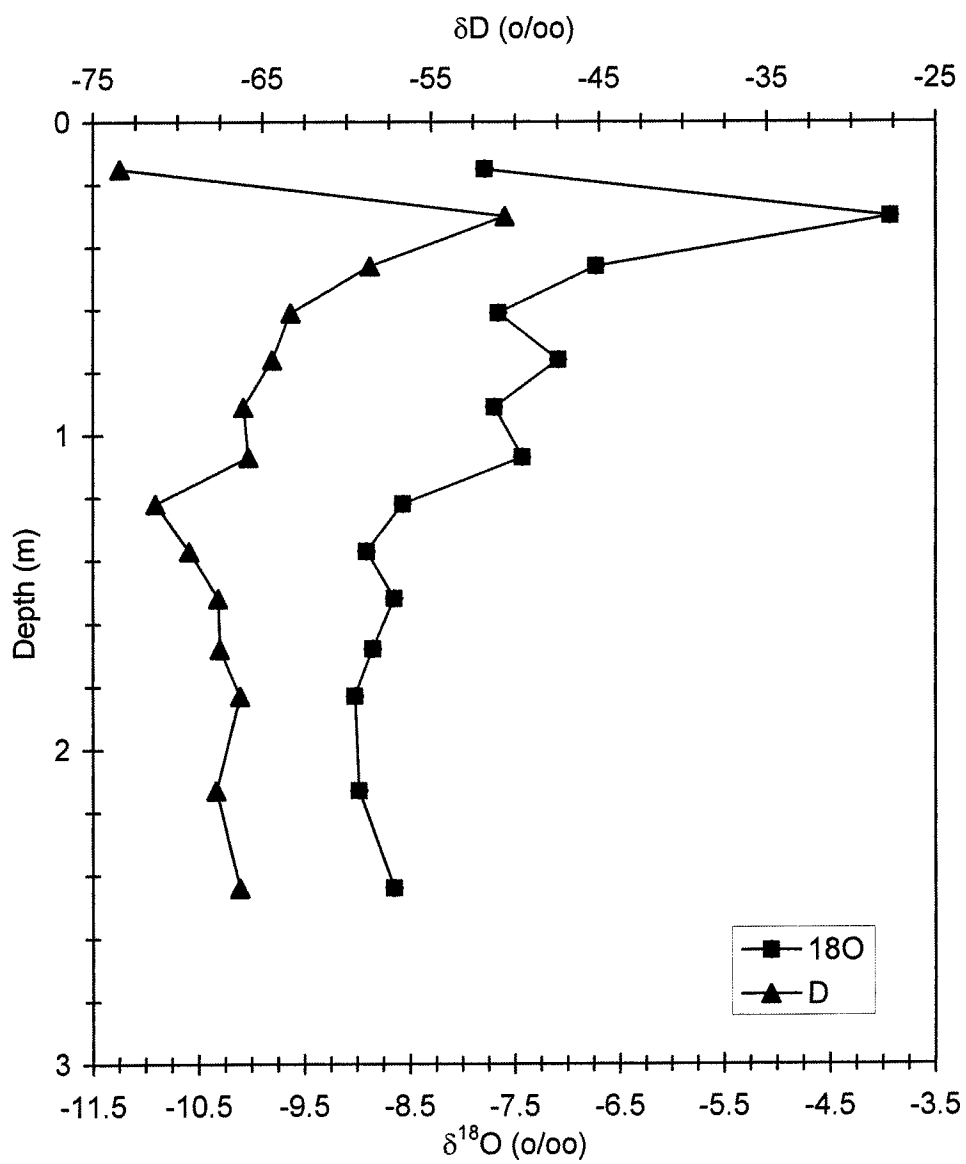


Figure 63. δD and $\delta^{18}O$ depth profiles for MOGW shallow soil waters.

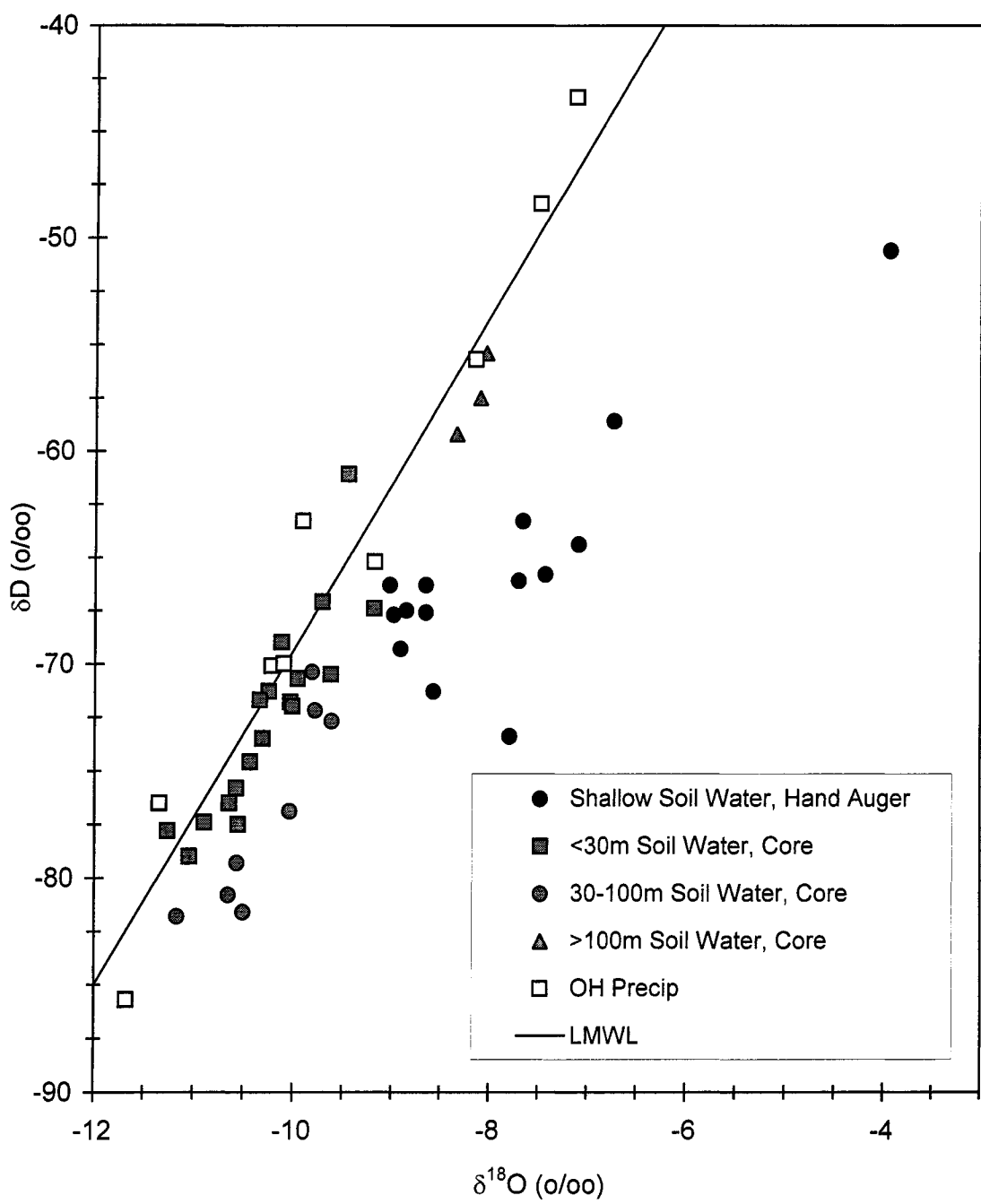


Figure 64. δD vs $\delta^{18}O$ plot of MOGW shallow soil waters with the local meteoric water line (LMWL).

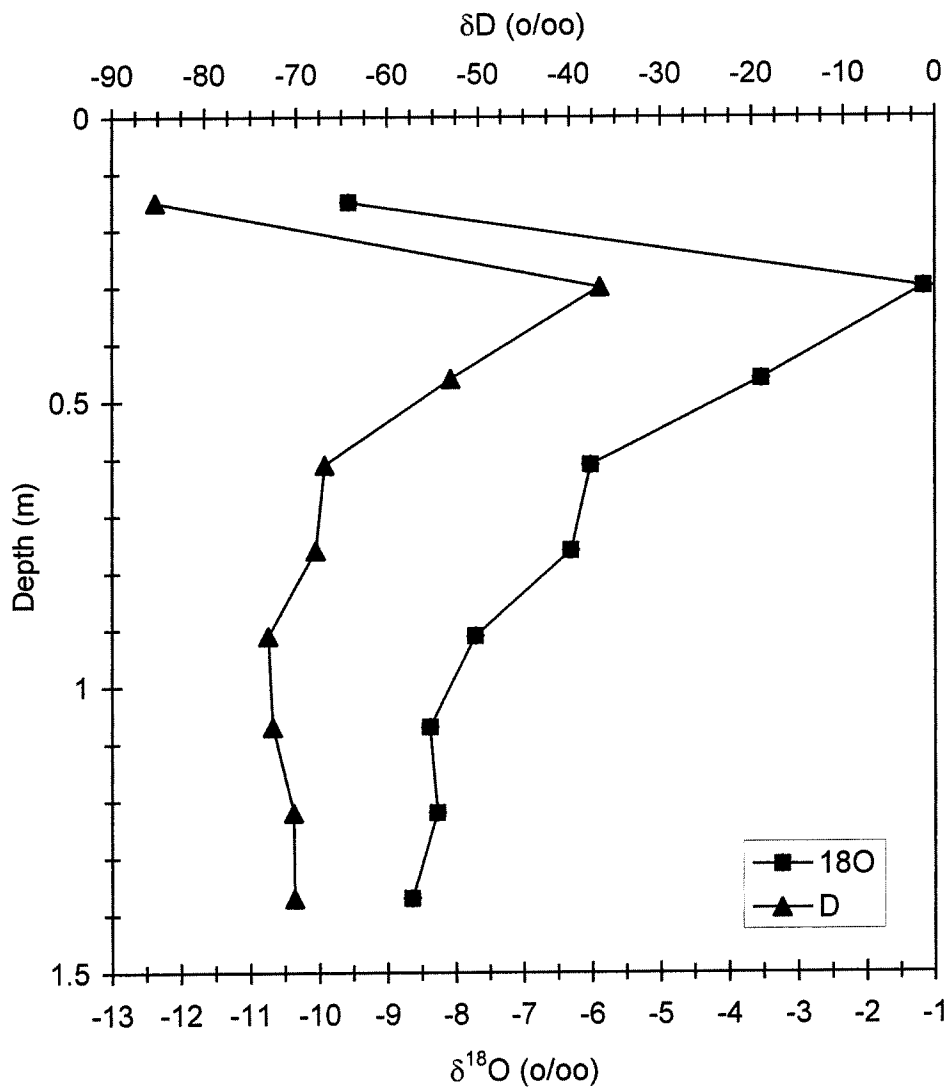


Figure 65. δD and $\delta^{18}O$ depth profiles for OGF shallow soil waters.

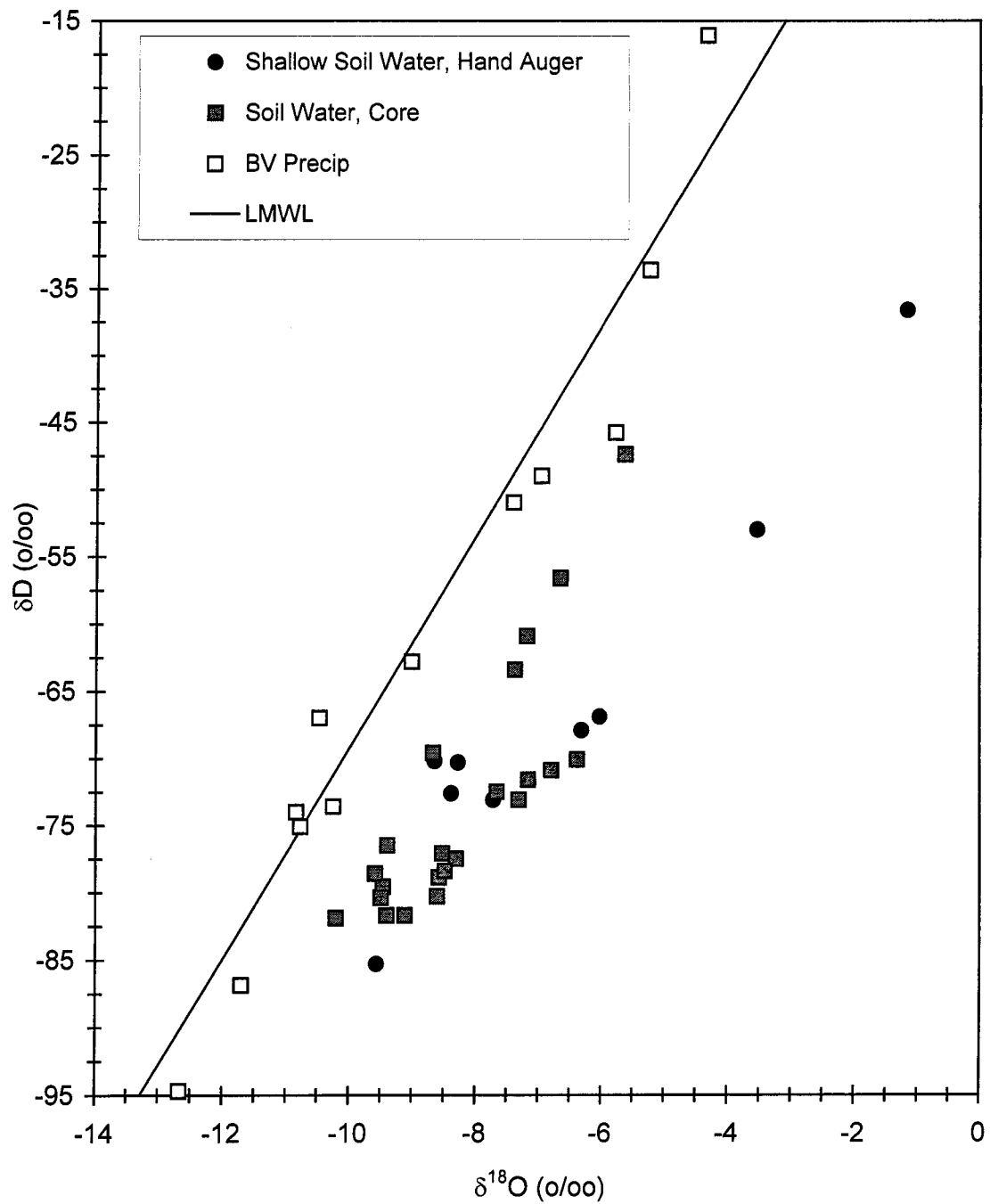


Figure 66. δD vs $\delta^{18}\text{O}$ plot of OGF shallow soil waters with the local meteoric water line (LMWL).

front and diffusion effects) are similar in composition to January 1995 soil waters extracted from core materials. The shallower waters, associated with the isotope maximum, extend the evaporative trend (Group 3 in Fig. 51) of the January 1995 soil waters.

Lysimeters

Water was collected from lysimeters at UOGW, MOGW, LOGW-1, USCW, and LSCW. Not all of the lysimeters at these locations yielded water for analysis, and none of the lysimeters at MSCW yielded water. The isotopic compositions, depth, and date of collection for the waters collected from the lysimeters are given in Table 7.

UOGW. The lysimeter installed at 3.35 m (11 ft) failed to yield water. The isotopic compositions of water collected from the deeper lysimeters are essentially identical. The lysimeter waters are very similar in composition to the soil waters extracted from core materials and bulk-average precipitation from the OH station (Fig. 67). Plotted on a $\delta^{18}\text{O}$ depth profile (Fig. 68) of the soil water samples, they fit the profile well.

MOGW. The lysimeter installed at 13.11 m (43 ft) failed to yield water. A plot of δD vs $\delta^{18}\text{O}$ (Fig. 69) shows that the lysimeter waters are similar in composition to the soil waters extracted from core materials. Plotted on a $\delta^{18}\text{O}$ depth profile (Fig. 70) with the soil-water samples, the lysimeter waters from the shallowest lysimeter (6.7 m) and

Table 7. Lysimeter-water data.

Location	Depth	Date	δD (o/oo)	$\delta^{18}O$ (o/oo)
UOGW	11.6 m (38 ft)	5/3/95	-61.6	-9.42
UOGW	11.6 m (38 ft)	6/22/95	-62.4	-9.42
UOGW	25 m (82 ft)	6/22/95	-65.0	-9.42
MOGW	6.7 m (22 ft)	6/22/95	-67.1	-9.30
MOGW	19.8 m (65 ft)	4/20/95	-72.4	-10.18
MOGW	19.8 m (65 ft)	7/25/95	-76.8	-10.68
MOGW	28.1 m (92 ft)	3/12/96	-68.4	-9.94
MOGW	42.7 m (140 ft)	3/12/96	-60.2	-8.73
MOGW	42.7 m (140 ft)	6/12/96	-64.9	-8.69
LOGW-1	4.3 m (14 ft)	6/23/95	-67.5	-9.06
LOGW-1	6.7 m (22 ft)	9/14/95	-68.3	-9.73
LOGW-1	19.5 m (64 ft)	6/23/95	-72.8	-9.20
LOGW-1	23.2 m (76 ft)	7/25/95	-79.7	-11.37
USCW	4.6 m (15 ft)	6/13/96	-83.4	-11.30
USCW	8.5 m (28 ft)	6/13/96	-75.1	-10.08
USCW	8.5 m (28 ft)	1/7/97	-77.0	-10.50
USCW	14.6 m (48 ft)	6/13/96	-68.8	-9.92
USCW	17.7 m (58 ft)	6/13/96	-74.1	-10.60
USCW	17.7 m (58 ft)	1/7/97	-73.4	-10.62
LSCW	8.2 m (27 ft)	6/11/96	-72.3	-9.21
LSCW	8.2 m (27 ft)	6/13/96	-72.1	-9.32
LSCW	8.2 m (27 ft)	1/8/97	-75.2	-9.36

deepest lysimeter (42.7 m) are less negative in composition than the nearest soil waters and are not a good fit to the profile.

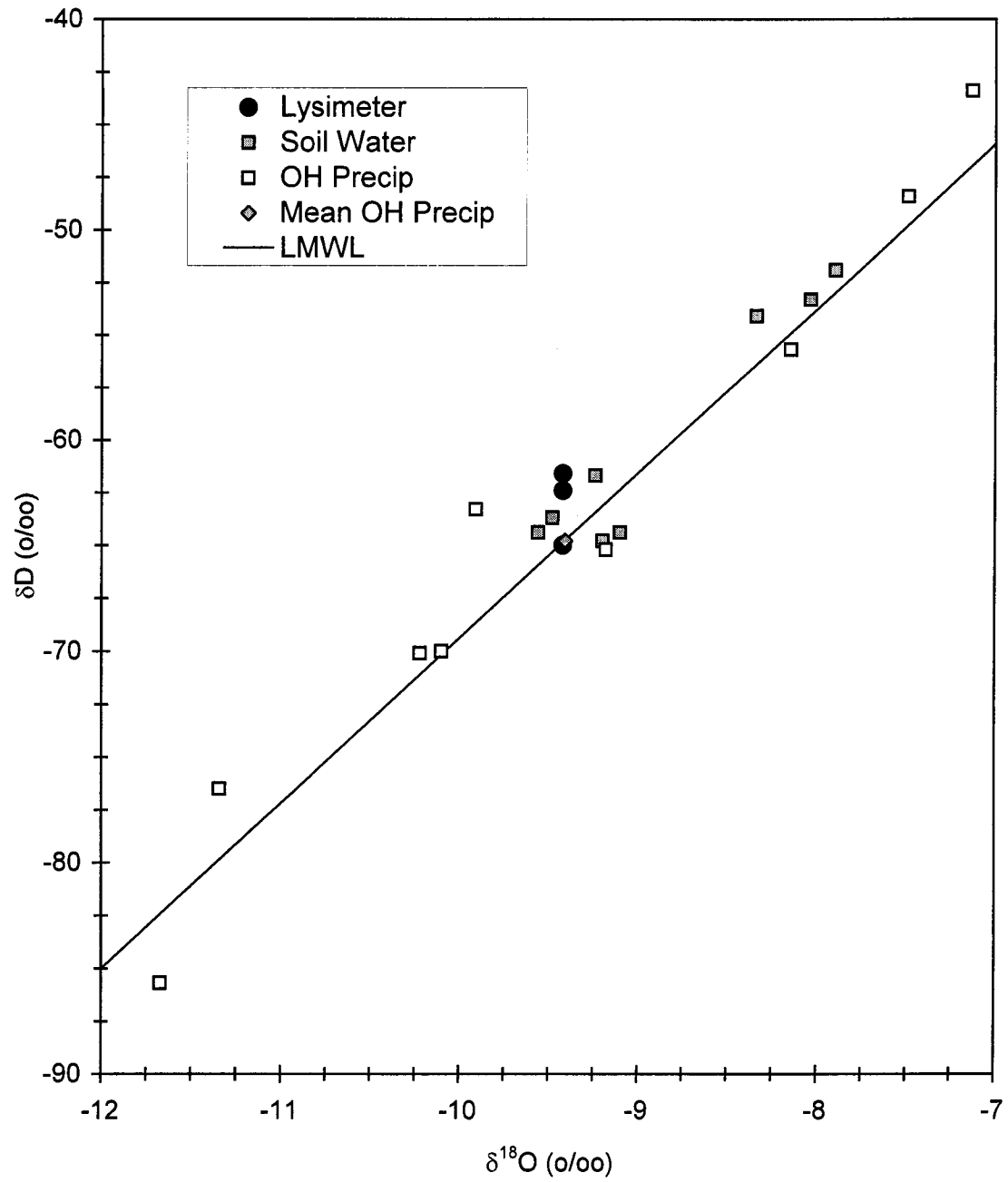


Figure 67. δD vs $\delta^{18}\text{O}$ plot of UOGW lysimeter waters with the local meteoric water line (LMWL).

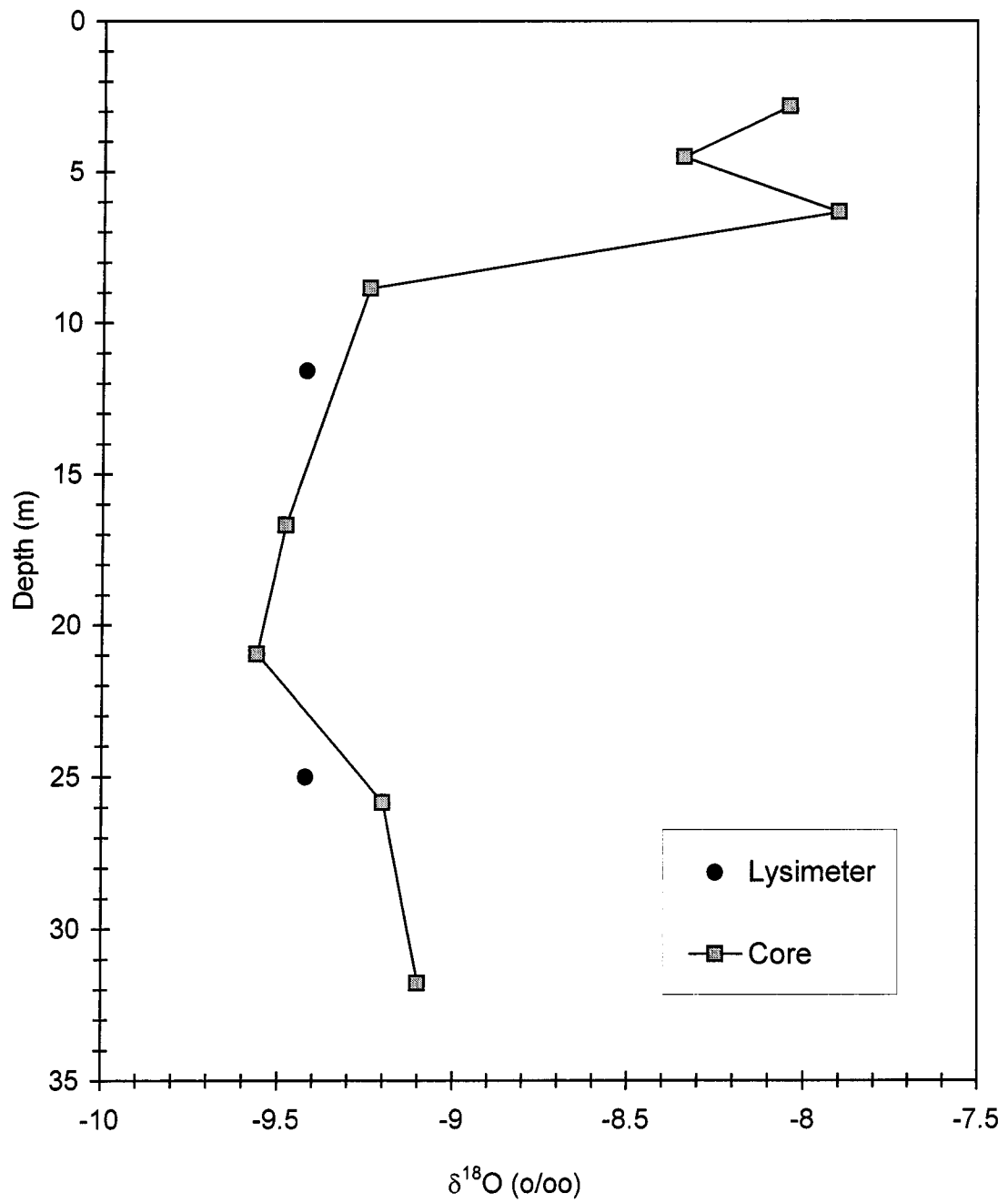


Figure 68. $\delta^{18}\text{O}$ depth profile of UOGW lysimeter waters.

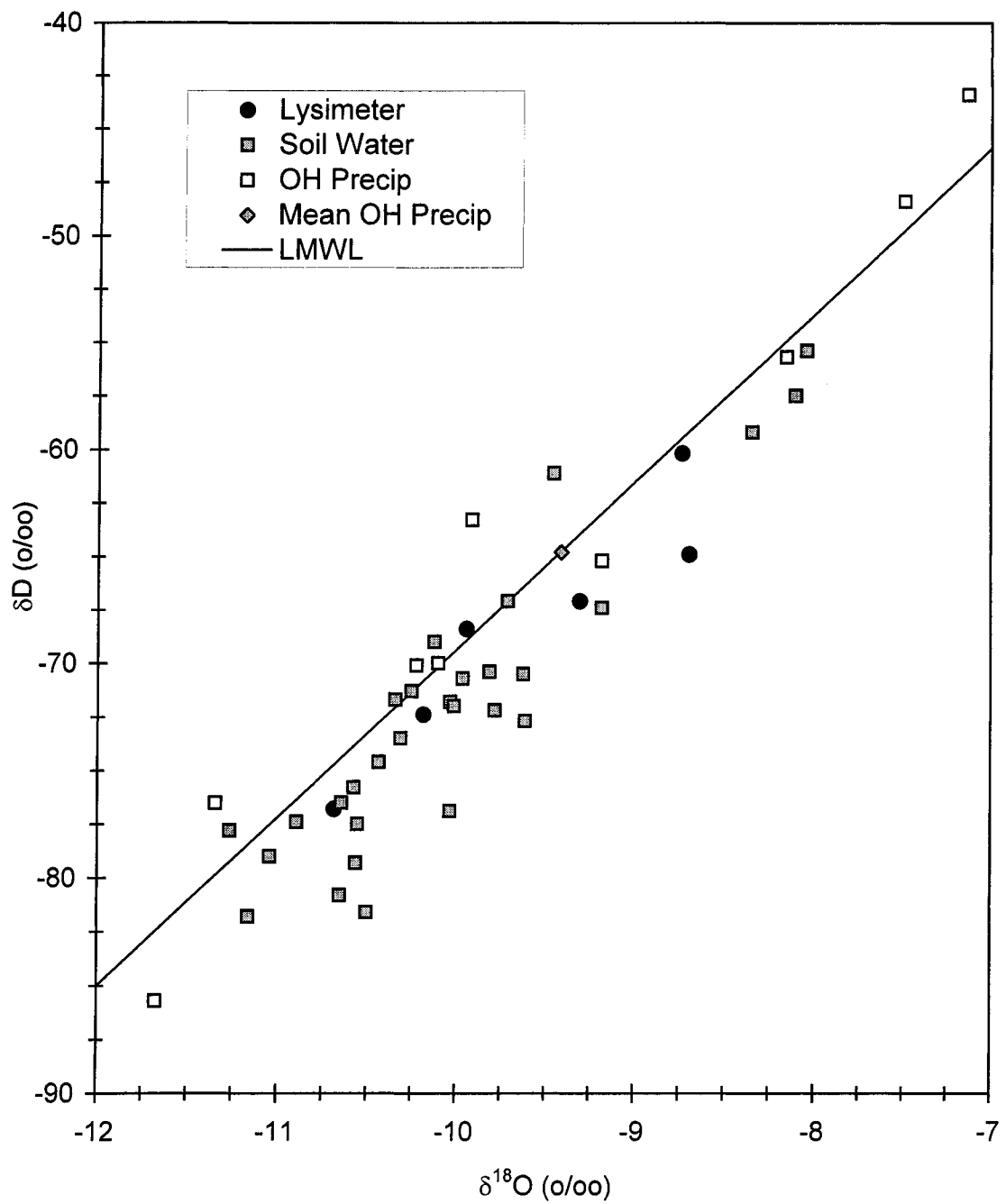


Figure 69. δD vs $\delta^{18}\text{O}$ plot of MOGW lysimeter waters with the local meteoric water line (LMWL).

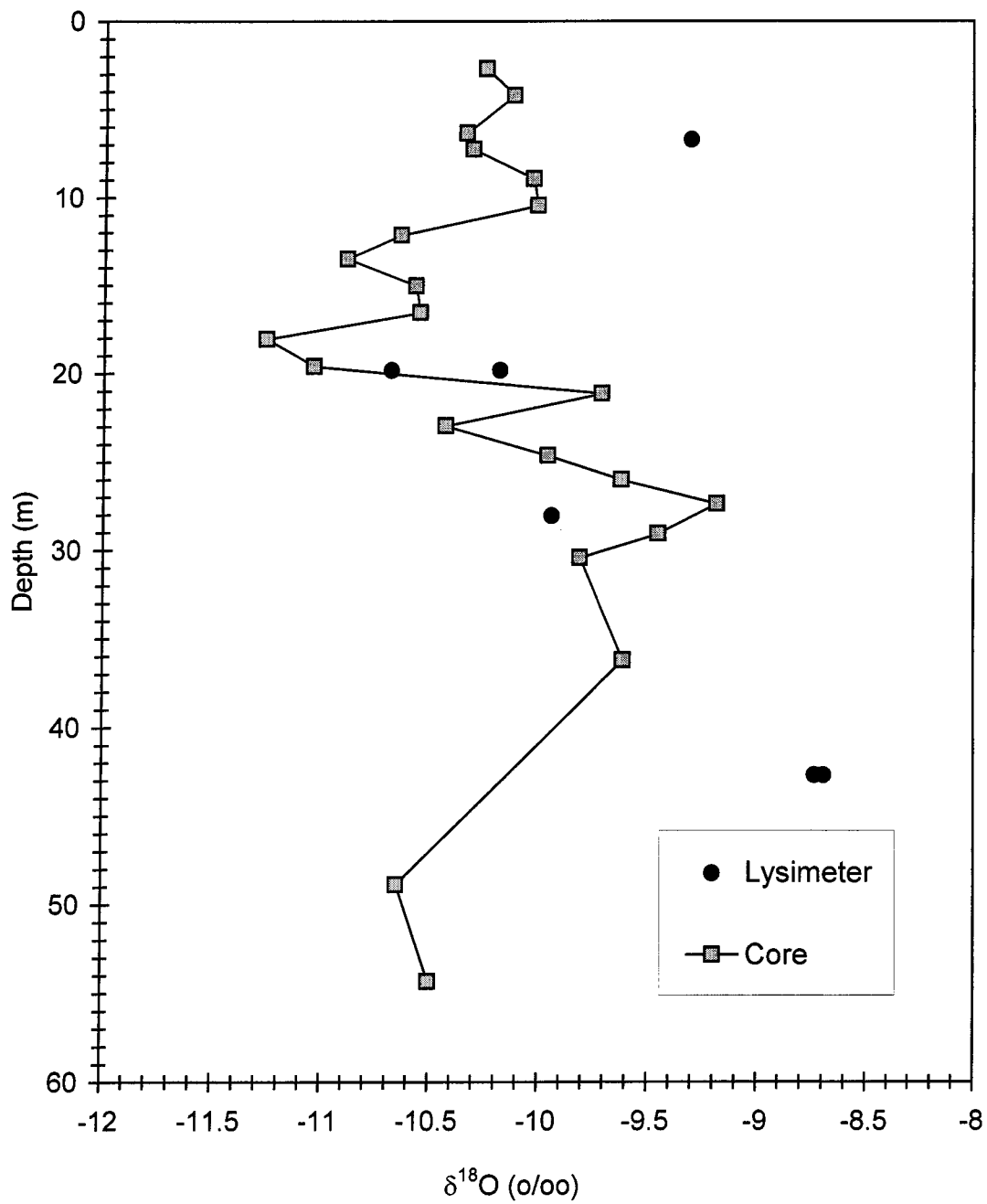


Figure 70. $\delta^{18}\text{O}$ depth profile of MOGW lysimeter waters.

LOGW-1. All the lysimeters installed at this location yielded water. On a plot of δD vs $\delta^{18}O$ (Fig. 71), the lysimeter waters are within the range of soil-water isotopic compositions, although the lysimeter waters from 6.7 m and 23.2 m plot closer to the LMWL than most of the soil waters. Plotted on a $\delta^{18}O$ depth profile (Fig. 72) of the soil-water samples, the lysimeter waters, with the exception of the 23.2 m sample, fit the profile well.

USCW. The lysimeter installed at 28.6 m (94 ft) failed to yield water. On a plot of δD vs $\delta^{18}O$ (Fig. 73), the lysimeter waters plot nearer the LMWL and are closer in isotopic composition to precipitation than the soil waters. Plotted on a $\delta^{18}O$ depth profile (Fig. 74) with the soil waters, the lysimeter waters are 1 to 3 o/oo more negative in composition than the nearest soil waters.

LSCW. With the exception of the lysimeter installed at 8.2 m (27 ft), all lysimeters installed at this location failed to yield water. The isotopic composition of the water collected remained essentially unchanged between samplings. A plot of δD vs $\delta^{18}O$ (Fig. 75) shows that the lysimeter waters are similar in composition to some of the soil waters. Plotted on a $\delta^{18}O$ depth profile (Fig. 76) of the soil waters, the lysimeter waters are within 0.6 o/oo of the nearest soil water.

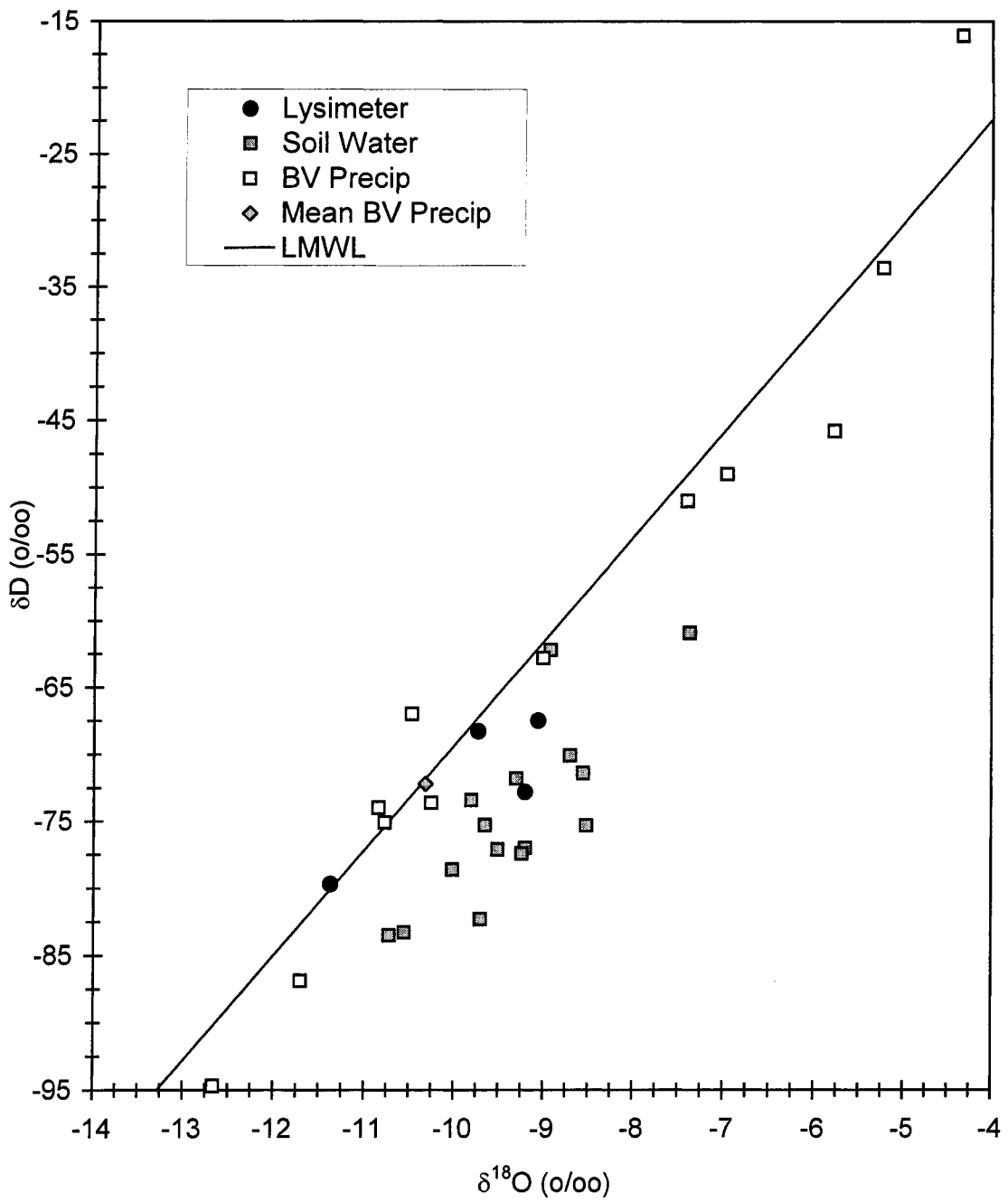


Figure 71. δD vs $\delta^{18}\text{O}$ plot of LOGW-1 lysimeter waters with the local meteoric water line (LMWL).

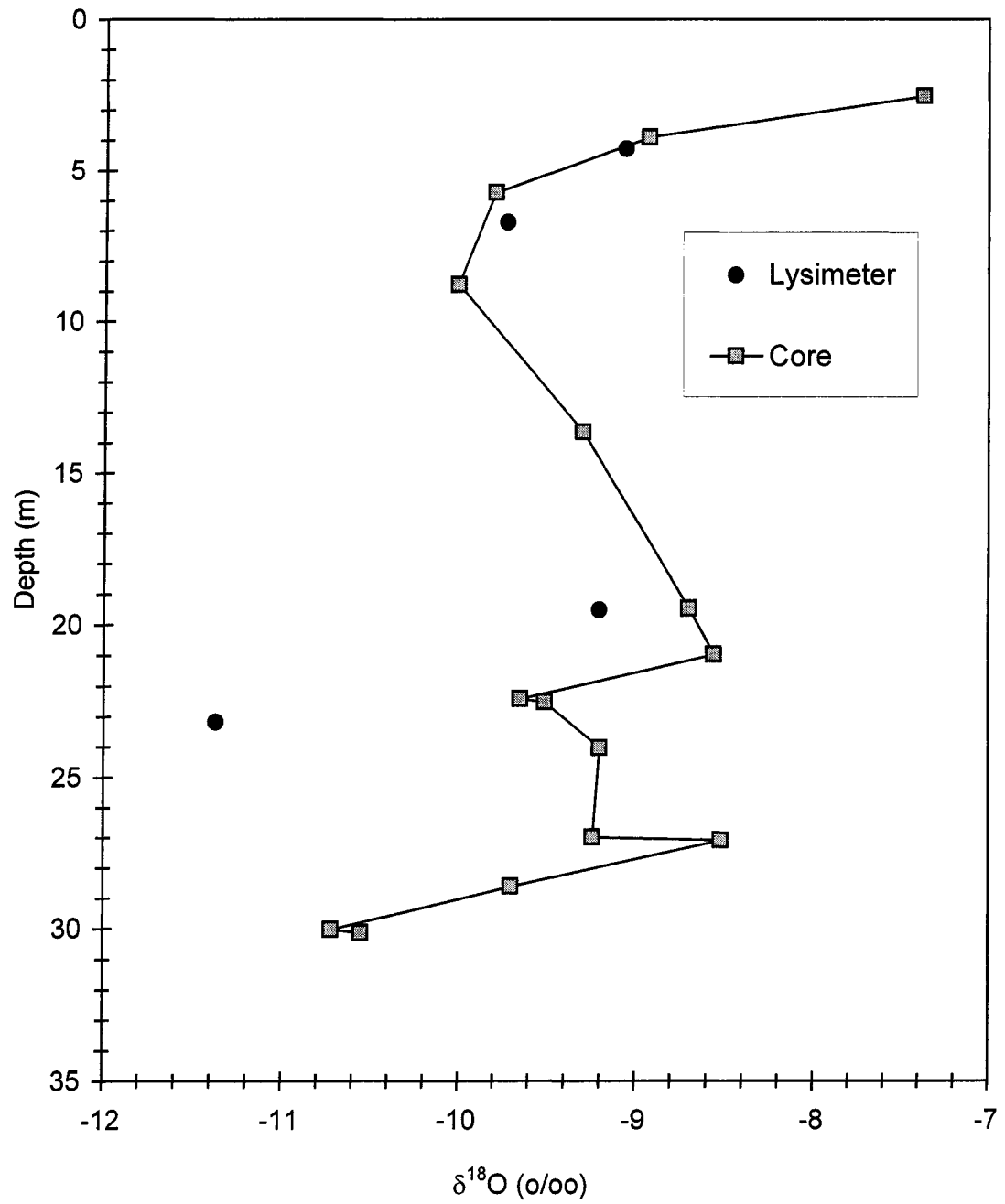


Figure 72. $\delta^{18}\text{O}$ depth profile of LOGW-1 lysimeter waters.

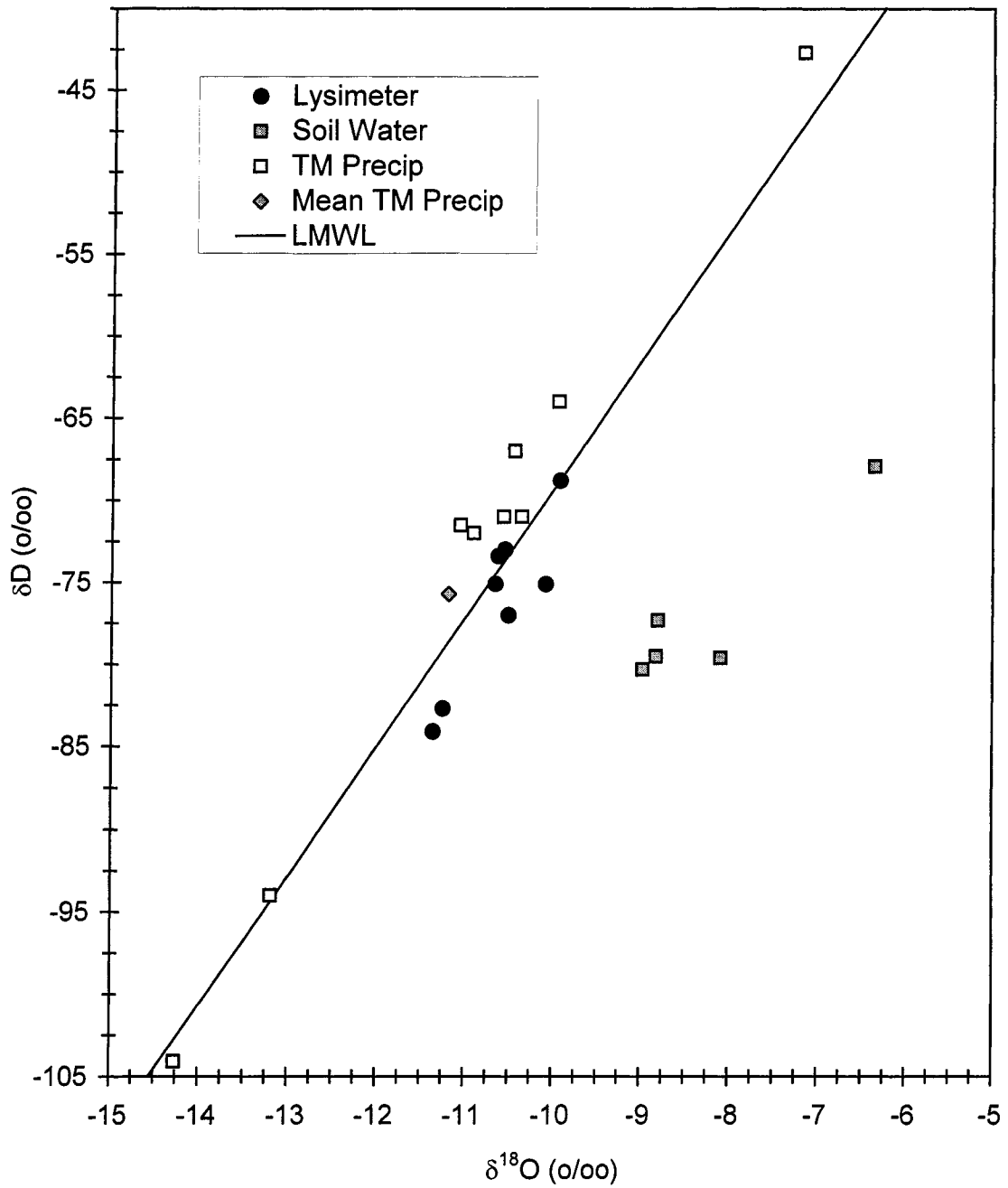


Figure 73. δD vs $\delta^{18}\text{O}$ plot of USCW lysimeter waters with the local meteoric water line (LMWL).

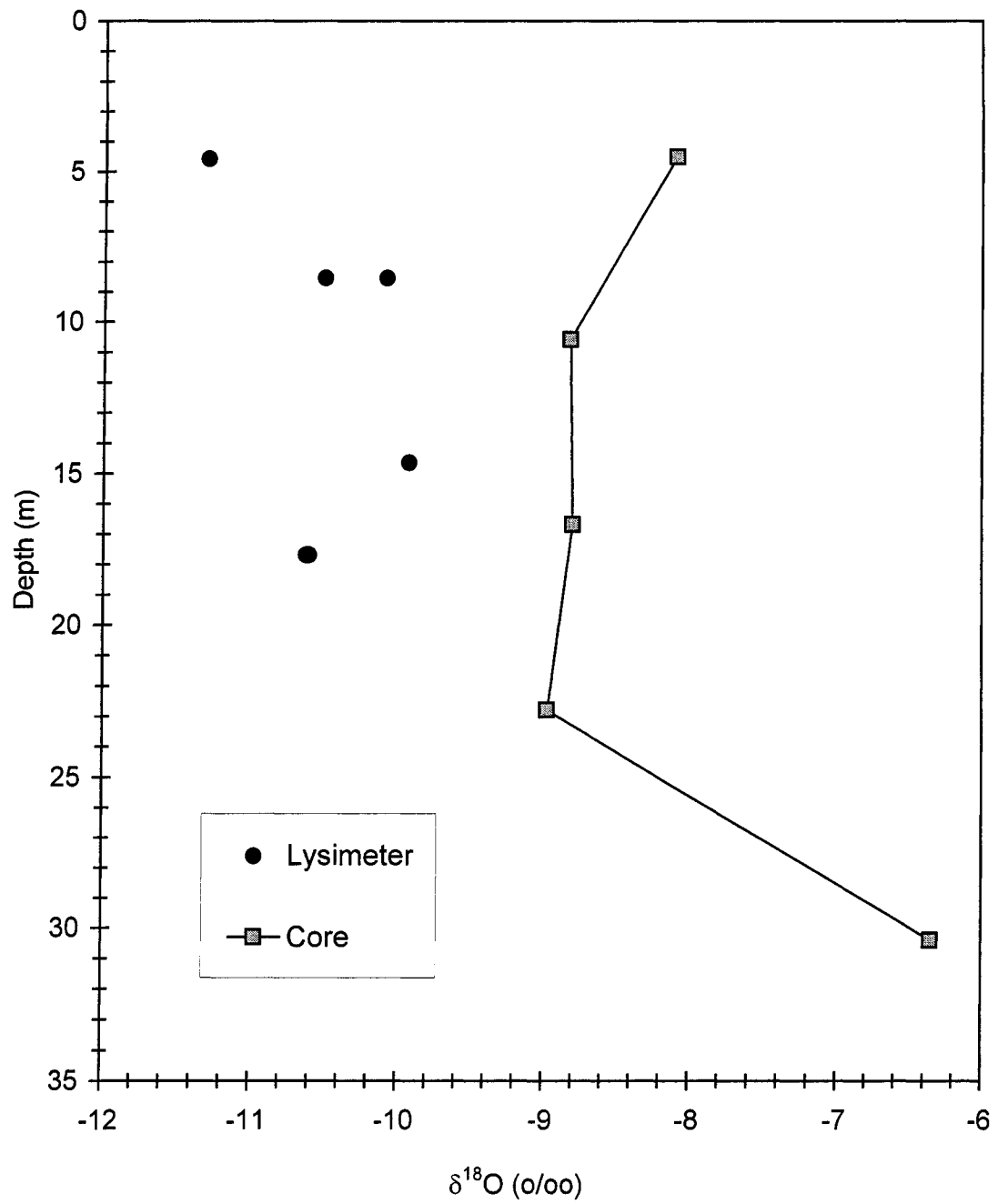


Figure 74. $\delta^{18}\text{O}$ depth profile of USCW lysimeter waters.

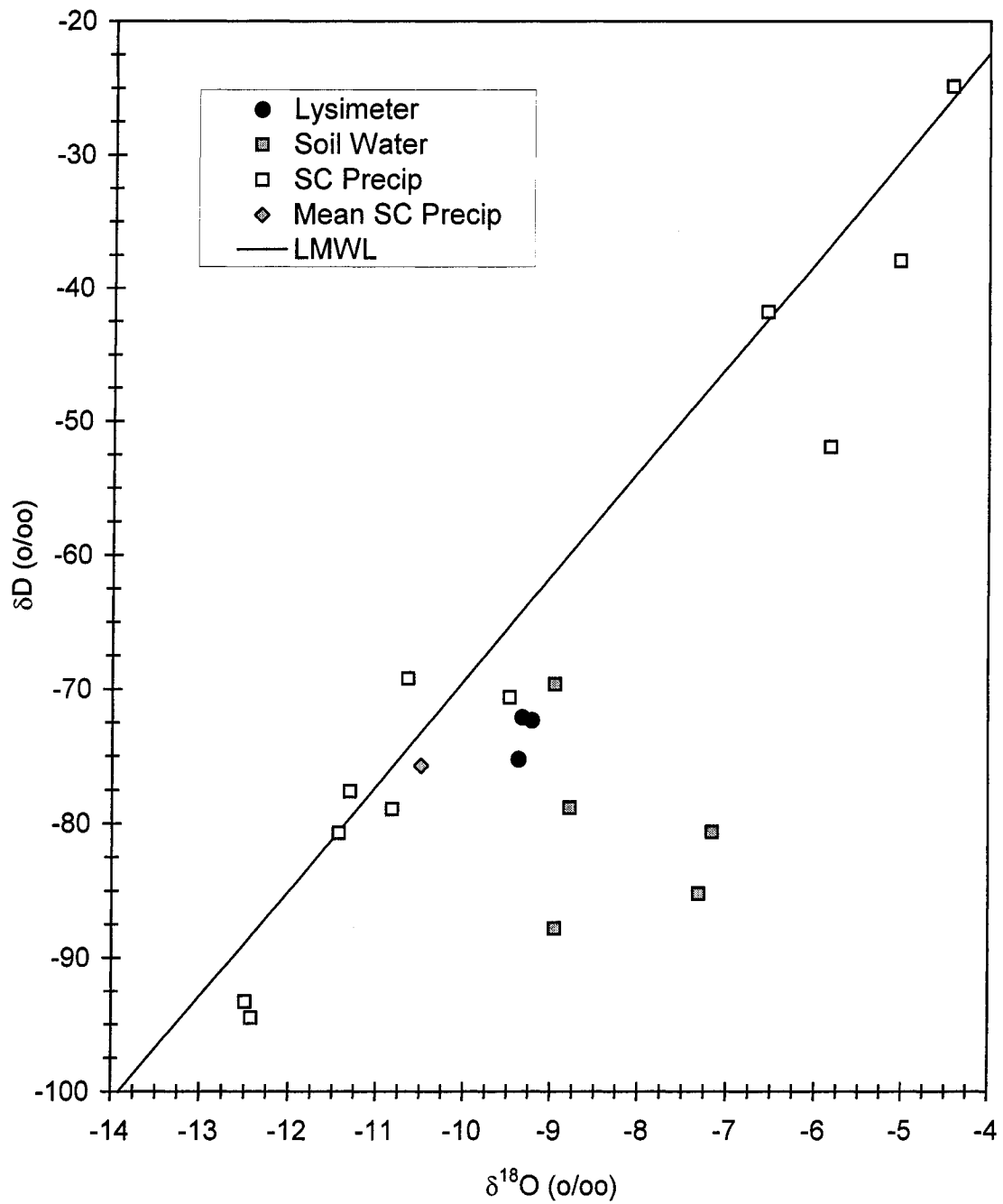


Figure 75. δD vs $\delta^{18}\text{O}$ plot of LSCW lysimeter waters with the local meteoric water line (LMWL).

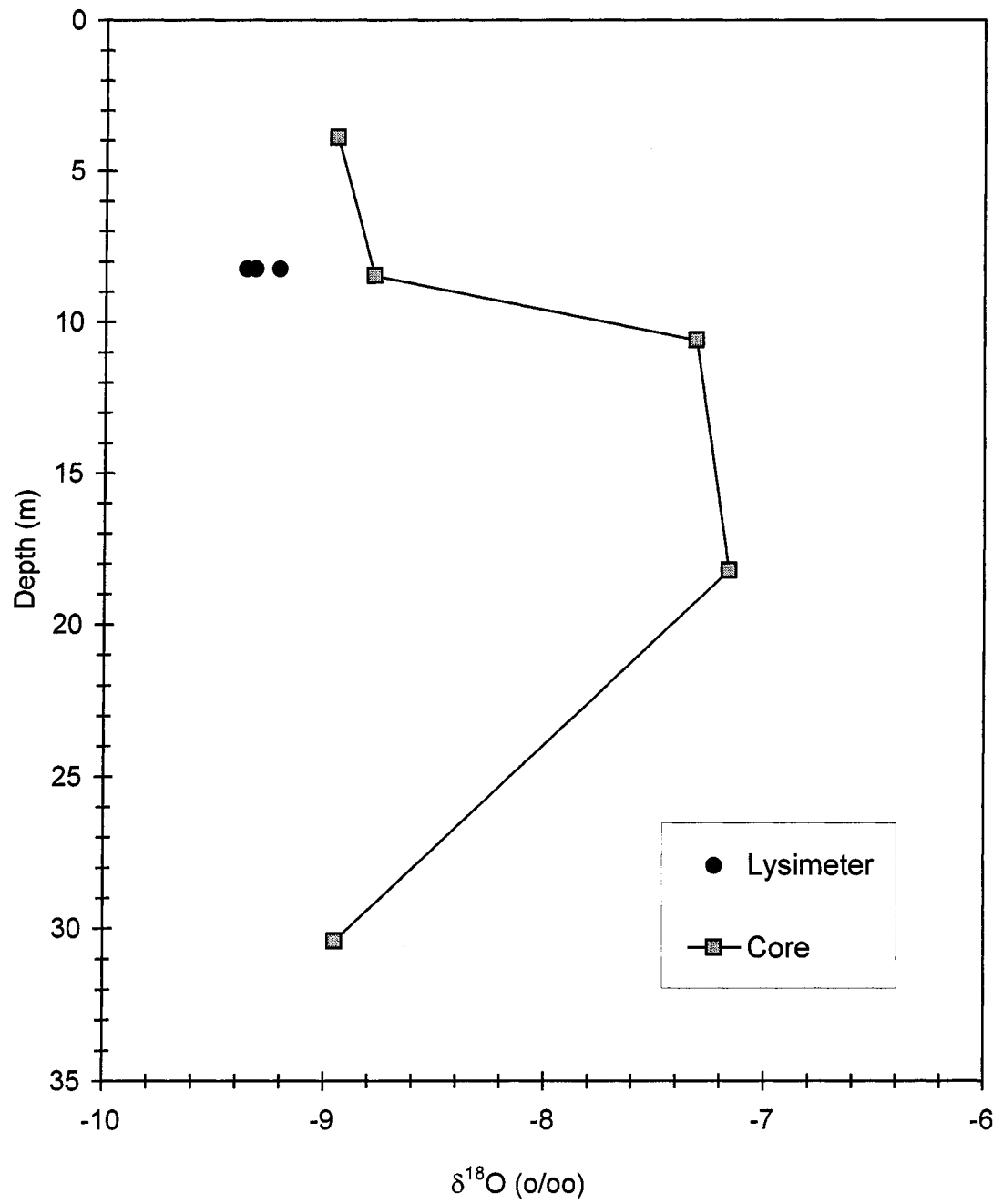


Figure 76. $\delta^{18}\text{O}$ depth profile of LSCW lysimeter waters.

Water Vapor

Water-vapor samples were collected at UOGW, MOGW, LOGW-1, and OGF. The isotopic compositions, depth, and date of collection for the water vapors are given in Table 8. The isotopic compositions of the collected water vapors were compared to the soil-water isotopic compositions and the calculated isotopic compositions of vapors in equilibrium with the soil waters. The α values used for the calculated vapor compositions were determined from the results of temperature-depth profiles (Izbicki and Michel, 2002) measured at each site. Although subsurface temperatures did fluctuate seasonally in the first few meters below land surface, temperatures remained relatively constant at greater depths and allowed vapor calculations to be made using the average temperature for each location. The average temperatures have an inverse relationship to altitude. The temperatures used were 16.5, 19, 20, and 20°C for UOGW, MOGW, LOGW-1, and OGF, respectively.

UOGW. The isotopic compositions of the vapor samples collected in October 1995 were compared to the isotopic compositions of UOGW soil waters collected in January 1995 and vapor in equilibrium with the soil waters (calculated for a temperature of 16.5°C) with a profile of $\delta^{18}\text{O}$ vs depth (Fig. 77) and a plot of δD vs $\delta^{18}\text{O}$ (Fig. 78). The isotopic compositions of the actual vapor samples are similar to the calculated vapor compositions.

Table 8. Water-vapor data.

Location	Depth	Date	δD	$\delta^{18}O$
UOGW	6.7 m (22 ft)	10/12/95	-139	-17.8
UOGW	15.9 m (52 ft)	10/12/95	-141	-18.4
UOGW	21 m (69 ft)	10/12/95	-141	-18.5
UOGW	27.7 m (91 ft)	10/12/95	-140	-19.7
UOGW	32 m (105 ft)	10/12/95	-135	-19.1
MOGW	7.9 m (26 ft)	10/25/95	-147	-19.7
MOGW	15.2 m (50 ft)	10/25/95	-147	-19.9
MOGW	24.4 m (80 ft)	10/25/95	-143	-20.5
MOGW	45.7 m (150 ft)	10/25/95	-147	-19.9
MOGW	91.5 m (300 ft)	10/25/95	-148	-19.8
MOGW	152.4 m (500 ft)	10/25/95	-149	-20.4
LOGW-1	13.1 m (43 ft)	9/14/95	-149	-19.5
LOGW-1	13.1 m (43 ft)	10/4/96	-145	-17.8
LOGW-1	13.1 m (43 ft)	1/17/97	-218	-28.6
LOGW-1	13.1 m (43 ft)	4/8/97	-180	-24.3
LOGW-1	13.1 m (43 ft)	9/97	-126	-17.1
LOGW-1	19.5 m (64 ft)	9/14/95	-151	-19.6
LOGW-1	19.5 m (64 ft)	10/4/96	-148	-20.6
LOGW-1	19.5 m (64 ft)	1/17/97	-219	-28.1
LOGW-1	19.5 m (64 ft)	4/8/97	-176	-22.2
LOGW-1	19.5 m (64 ft)	9/97	-141	-20.0
LOGW-1	23.8 m (78 ft)	9/14/95	-143	-18.9
LOGW-1	23.8 m (78 ft)	10/4/96	-144	-19.4
LOGW-1	23.8 m (78 ft)	1/17/97	-218	-28.8
LOGW-1	23.8 m (78 ft)	4/8/97	-170	-22.2
LOGW-1	23.8 m (78 ft)	9/97	-127	-18.0
LOGW-1	27.7 m (91 ft)	9/14/95	-154	-19.8
LOGW-1	27.7 m (91 ft)	11/22/95	-165	-21.0
LOGW-1	27.7 m (91 ft)	10/4/96	-149	-19.9
LOGW-1	27.7 m (91 ft)	1/17/97	-152	-22.6
LOGW-1	27.7 m (91 ft)	4/8/97	-169	-22.0
LOGW-1	27.7 m (91 ft)	9/97	-149	-19.8
LOGW-1	31.4 m (103 ft)	9/14/95	-148	-20.2
LOGW-1	31.4 m (103 ft)	10/4/96	-131	-17.8
LOGW-1	31.4 m (103 ft)	1/17/97	-159	-22.1

Table 8. Water-vapor data (cont.).

Location	Depth	Date	δD	$\delta^{18}O$
LOGW-1	31.4 m (103 ft)	4/8/97	-178	-24.4
LOGW-1	31.4 m (103 ft)	9/97	-154	-21.1
OGF	3.7 m (12 ft)	9/22/95	-169	-19.4
OGF	9.2 m (30 ft)	9/22/95	-166	-18.5
OGF	15.2 m (50 ft)	9/20/95	-149	-17.3
OGF	21.3 m (70 ft)	9/20/95	-146	-18.4
OGF	25.3 m (83 ft)	9/20/95	-149	-18.6

MOGW. The isotopic compositions of the vapor samples collected in October 1995 were compared to the isotopic compositions of MOGW soil waters collected in January 1995 and vapor in equilibrium with the soil waters (calculated for a temperature of 19°C) with a profile of $\delta^{18}O$ vs depth (Fig. 79) and a plot of δD vs $\delta^{18}O$ (Fig. 80). The isotopic compositions of the actual vapor samples are similar to the calculated vapor compositions.

LOGW-1. Vapor samples were collected at this location multiple times over a two-year period between September 1995 and September 1997. Over the two-year period, the isotopic compositions of the collected vapors varied considerably (Table 8). The isotopic compositions of the vapor samples were compared to the isotopic compositions of LOGW-1 soil waters collected in November 1994 and vapor in equilibrium with the soil waters (calculated for a temperature of 20°C) with a profile of $\delta^{18}O$ vs depth (Fig. 81) and a plot of δD vs $\delta^{18}O$ (Fig. 82). The profile and plot show a shift to more negative vapor compositions for the samples collected in January and April

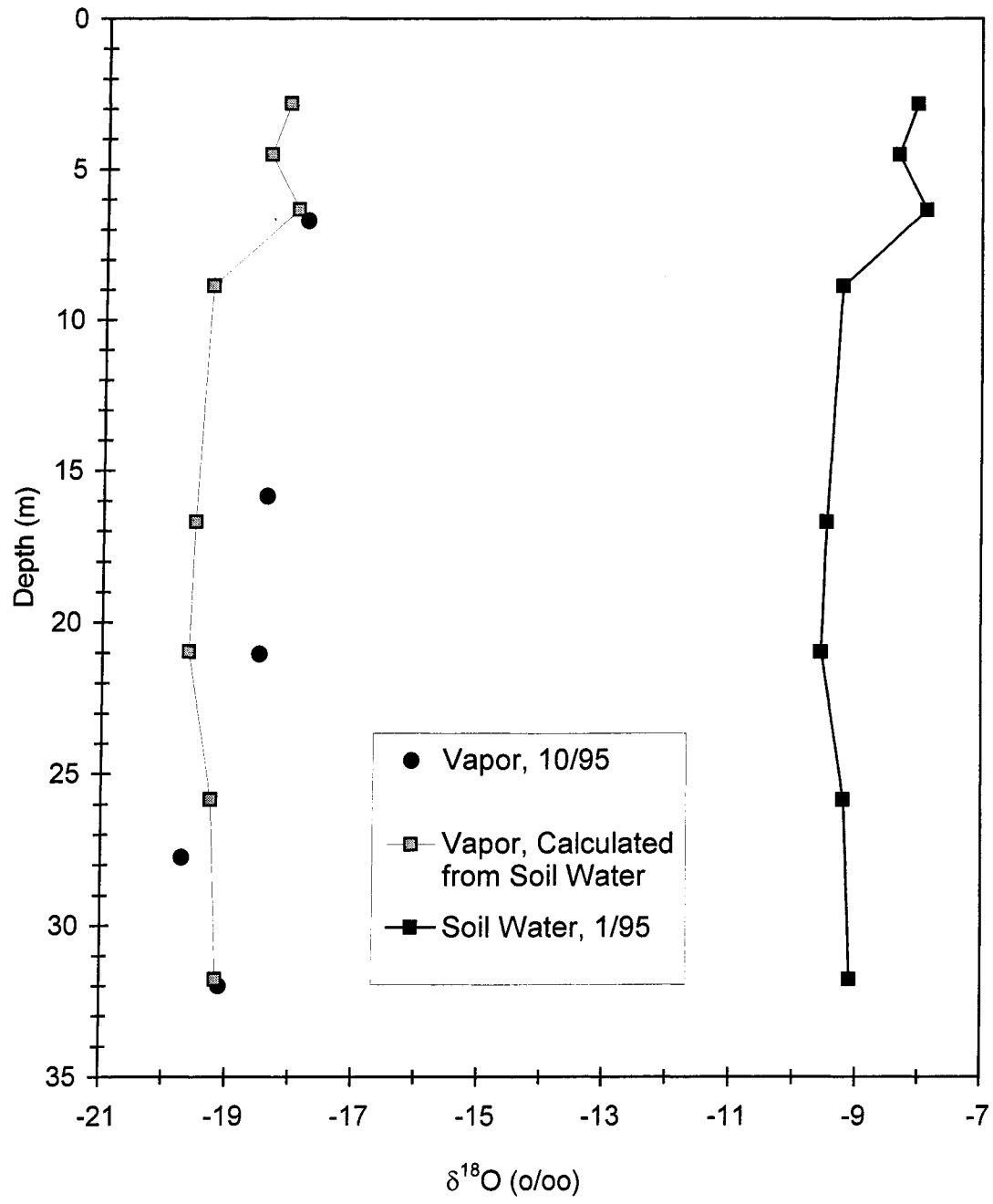


Figure 77. $\delta^{18}\text{O}$ depth profile of UOGW water-vapor samples.

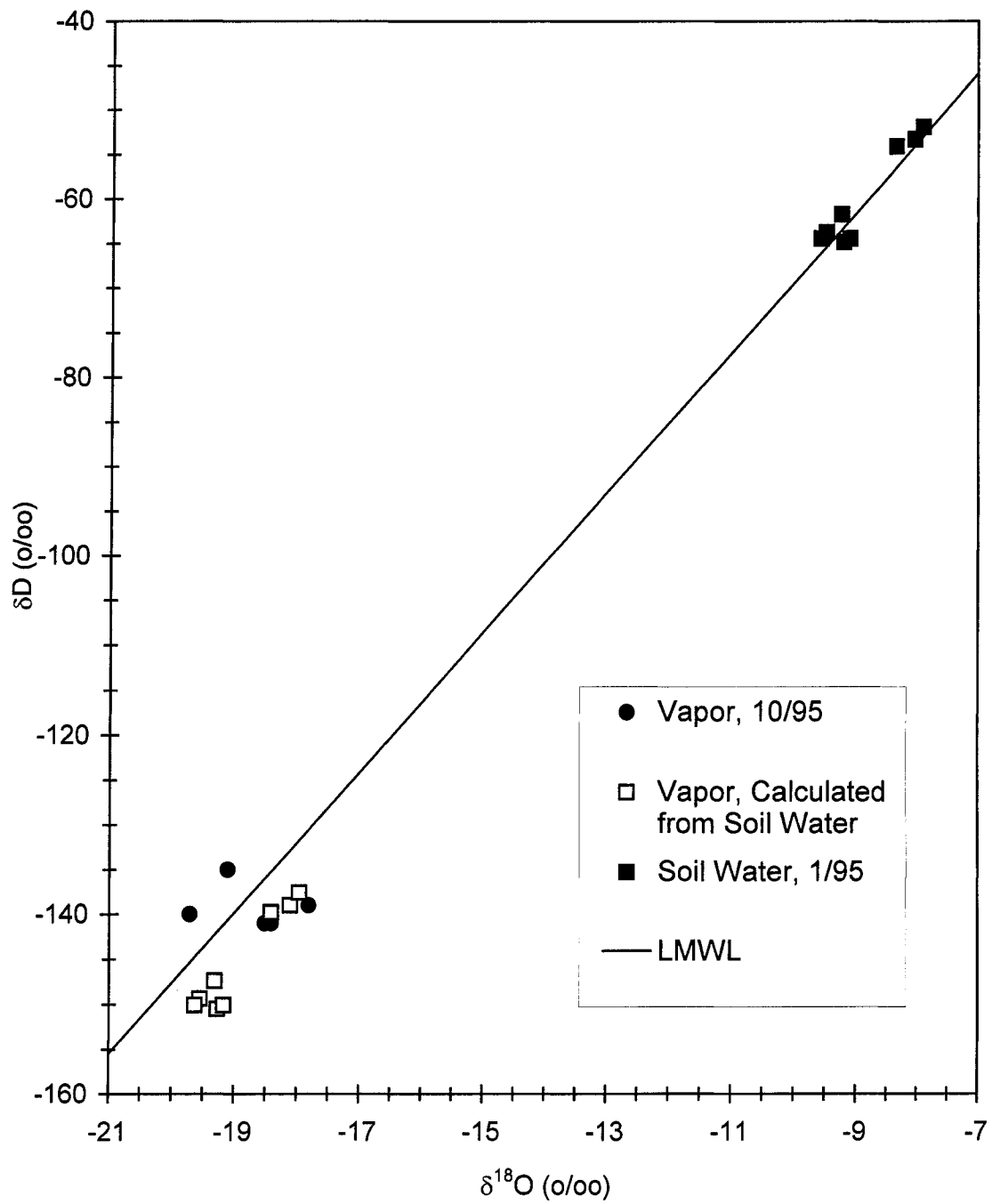


Figure 78. δD vs $\delta^{18}O$ plot of UOGW water-vapor samples with the local meteoric water line (LMWL).

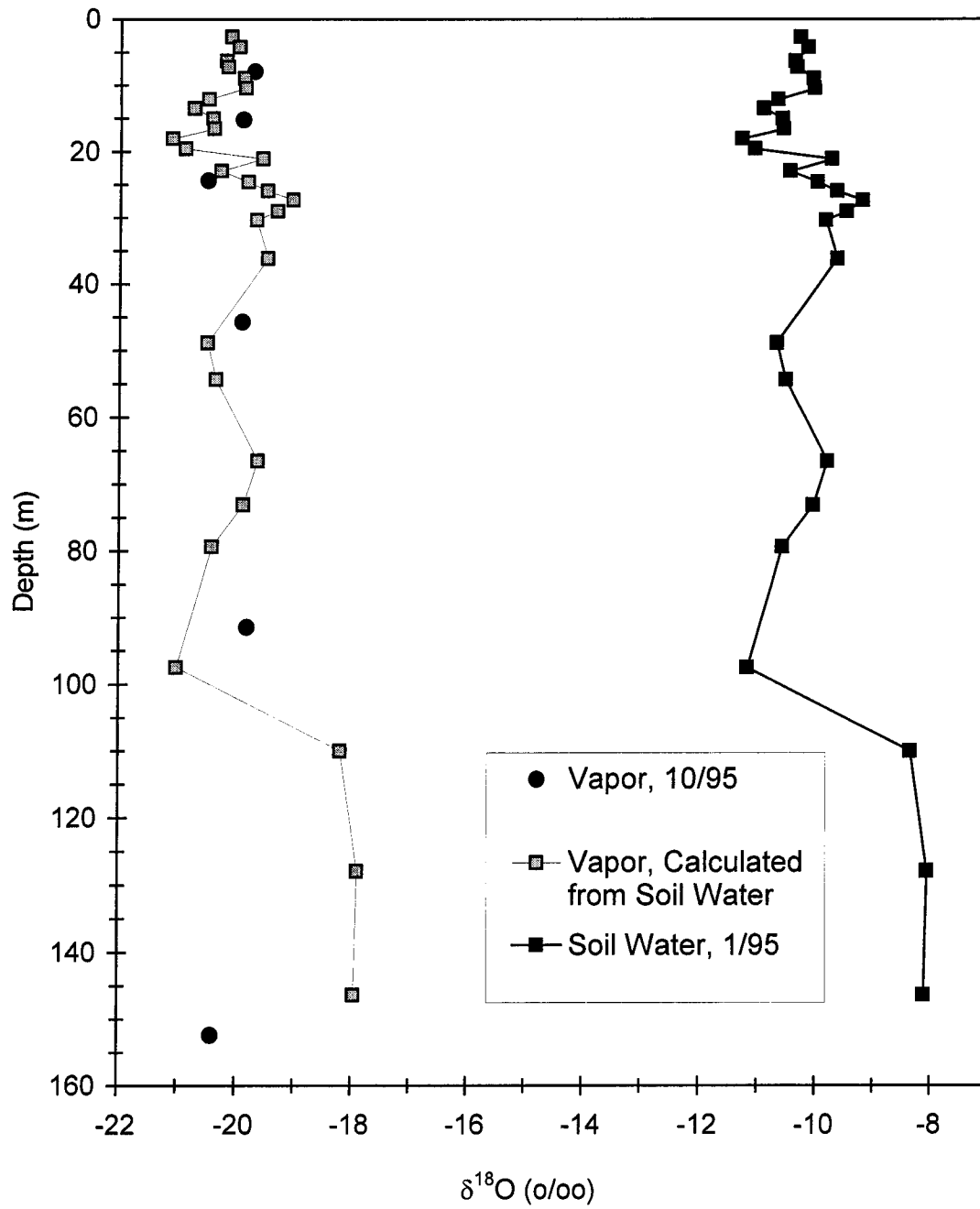


Figure 79. $\delta^{18}\text{O}$ depth profile of MOGW water-vapor samples.

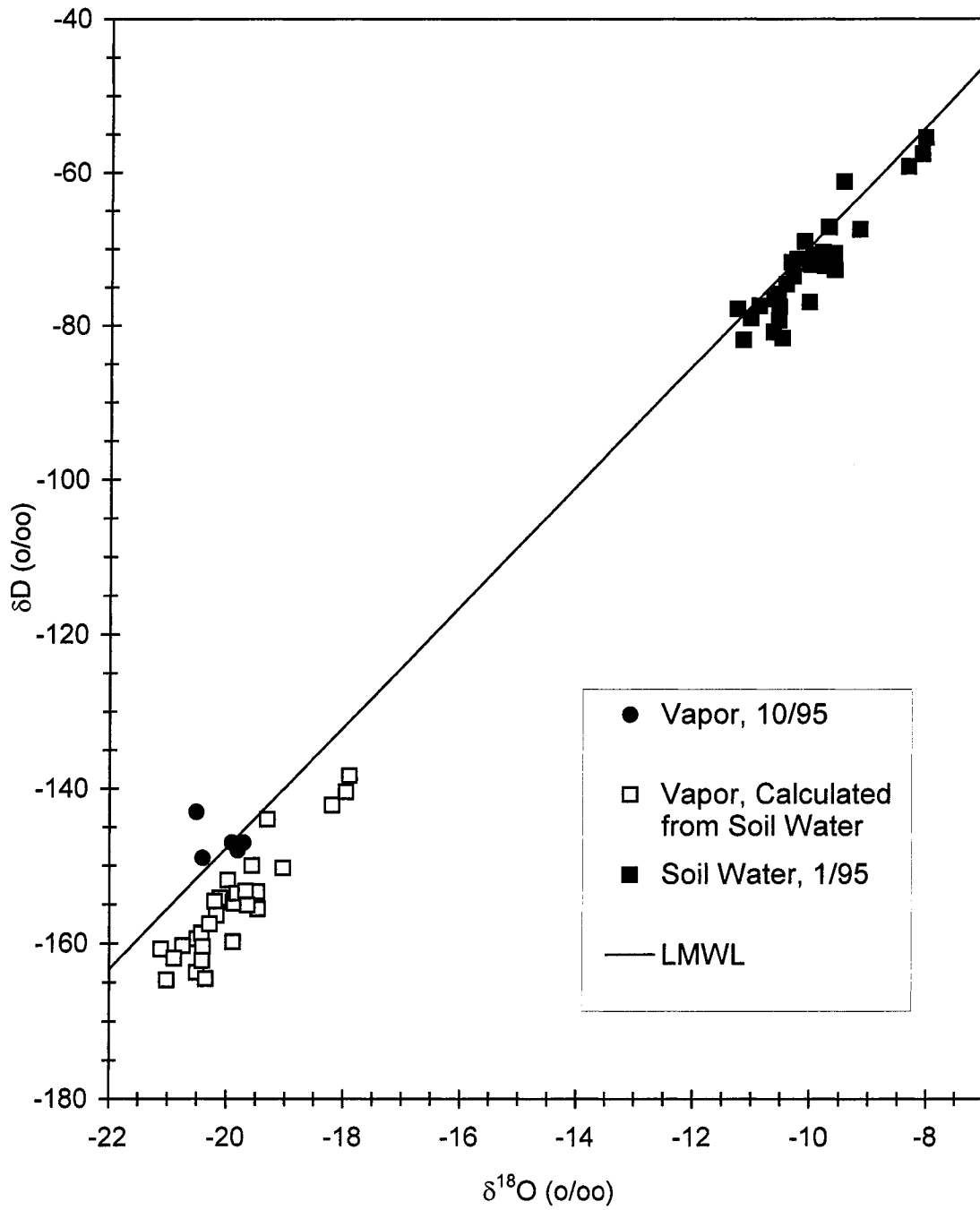


Figure 80. δD vs $\delta^{18}\text{O}$ plot of MOGW water-vapor samples with the local meteoric water line (LMWL).

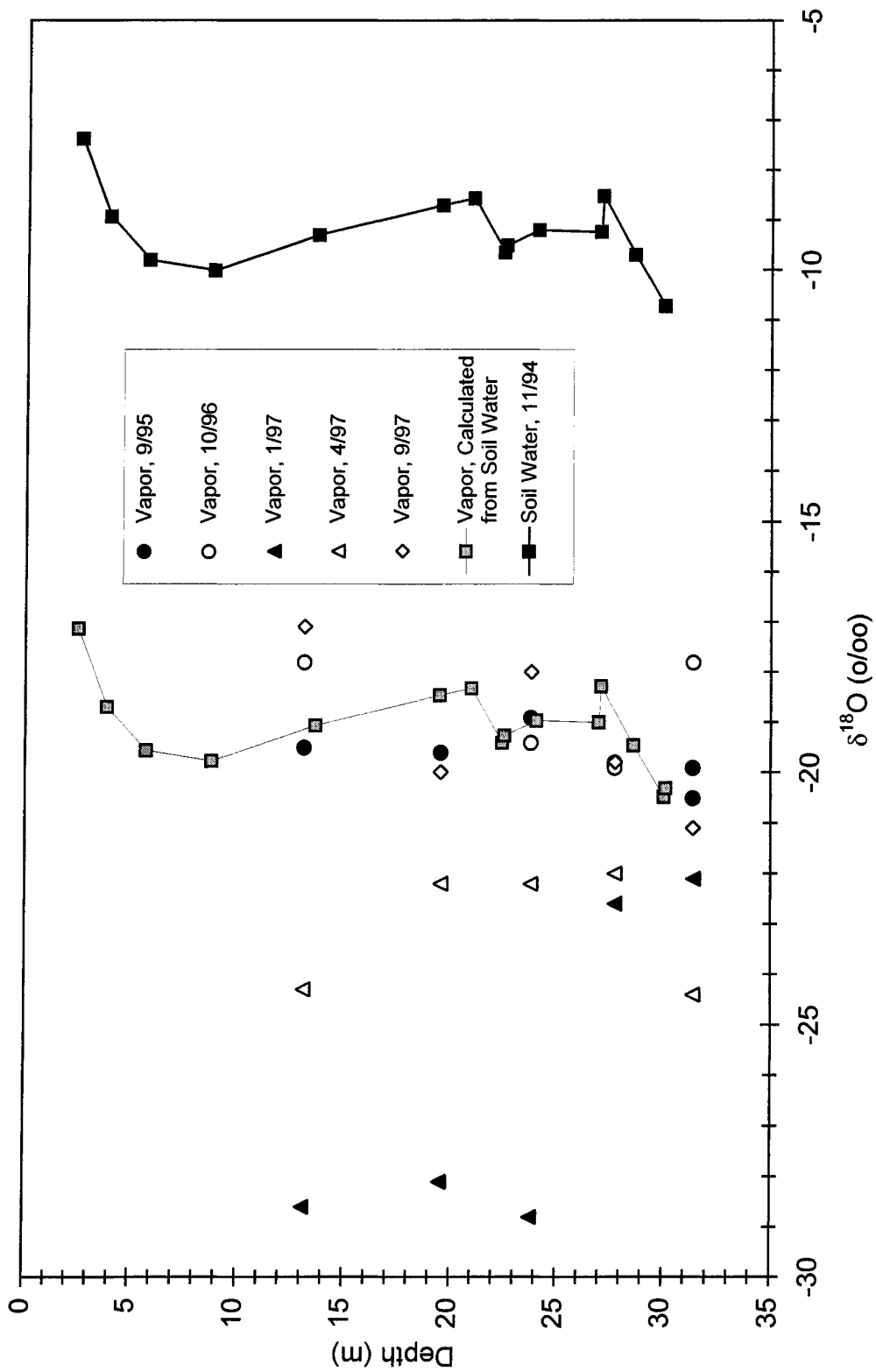


Figure 81. $\delta^{18}\text{O}$ depth profile of LOGW-1 water-vapor samples.

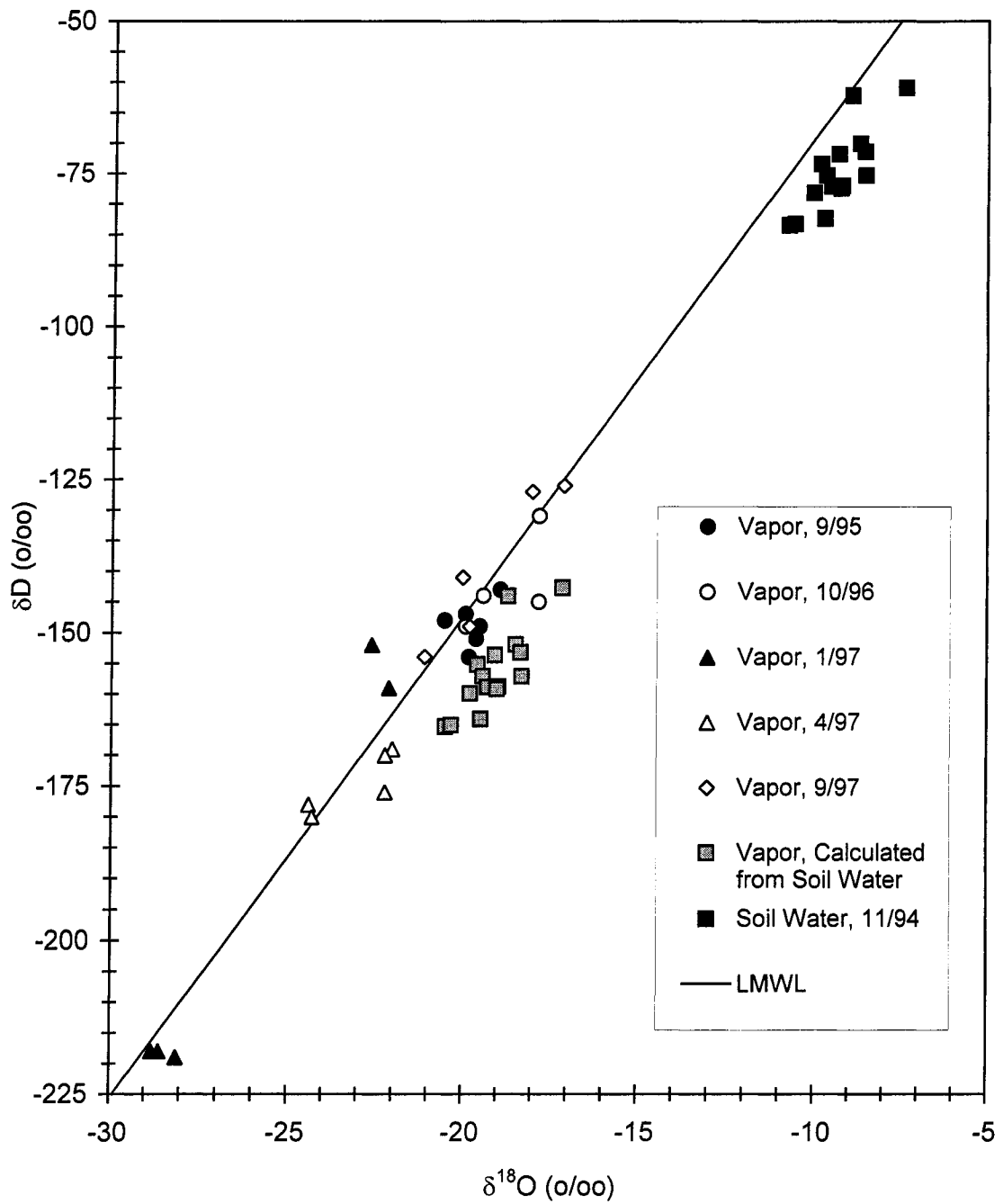


Figure 82. δD vs $\delta^{18}O$ plot of LOGW-1 water-vapor samples with the local meteoric water line (LMWL).

and a return to vapor compositions similar to the calculated compositions for the samples collected in September and October.

OGF. The isotopic compositions of vapor samples collected in September and November of 1995 were compared to the isotopic compositions of OGF soil waters collected in November 1994 and vapor in equilibrium with the soil waters (calculated for a temperature of 20°C) with a profile of $\delta^{18}\text{O}$ vs depth (Fig. 83) and a plot of δD vs $\delta^{18}\text{O}$ (Fig. 84). The isotopic compositions of the actual vapor samples are similar to the calculated vapor compositions.

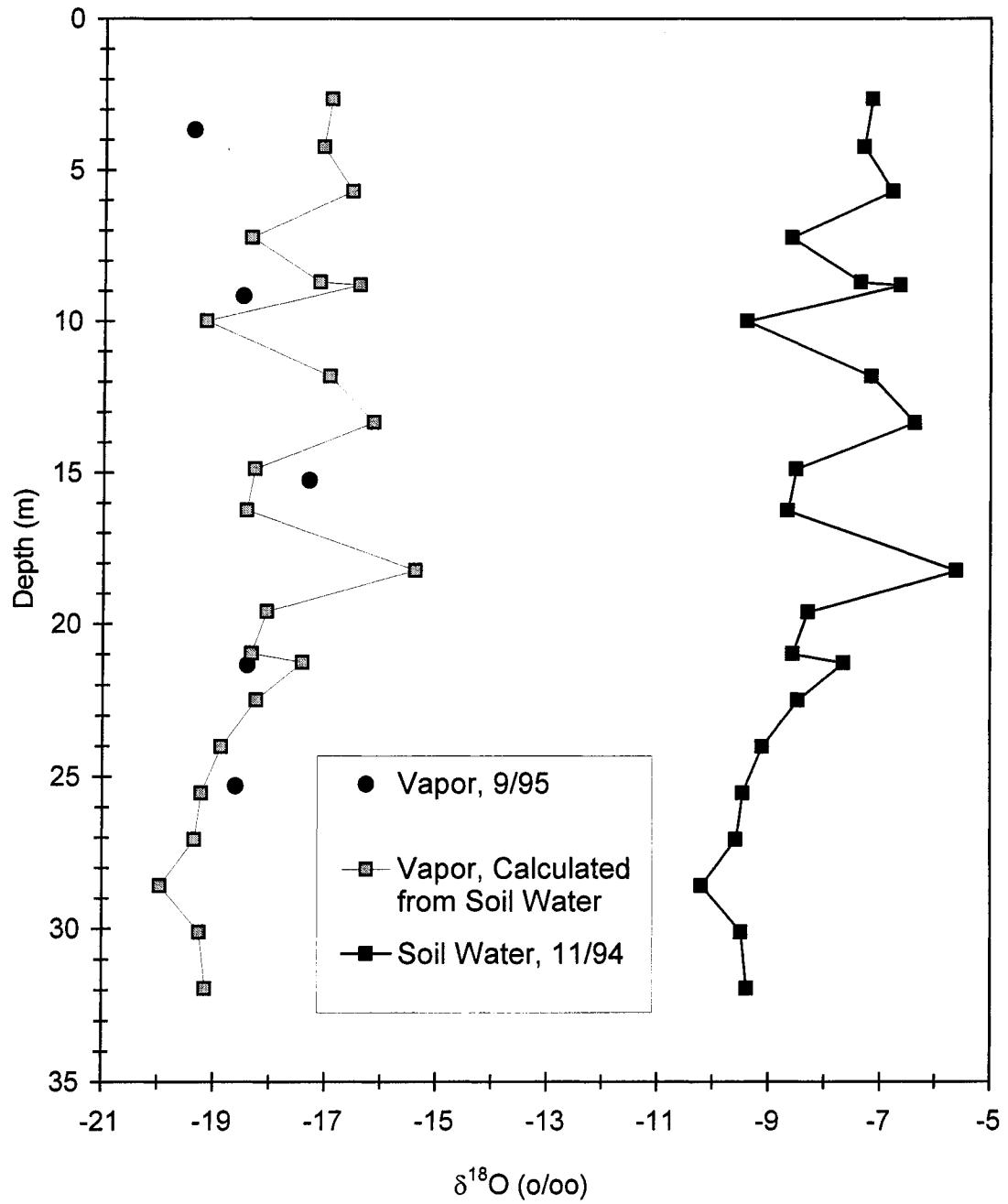


Figure 83. $\delta^{18}\text{O}$ depth profile of OGF water-vapor samples.

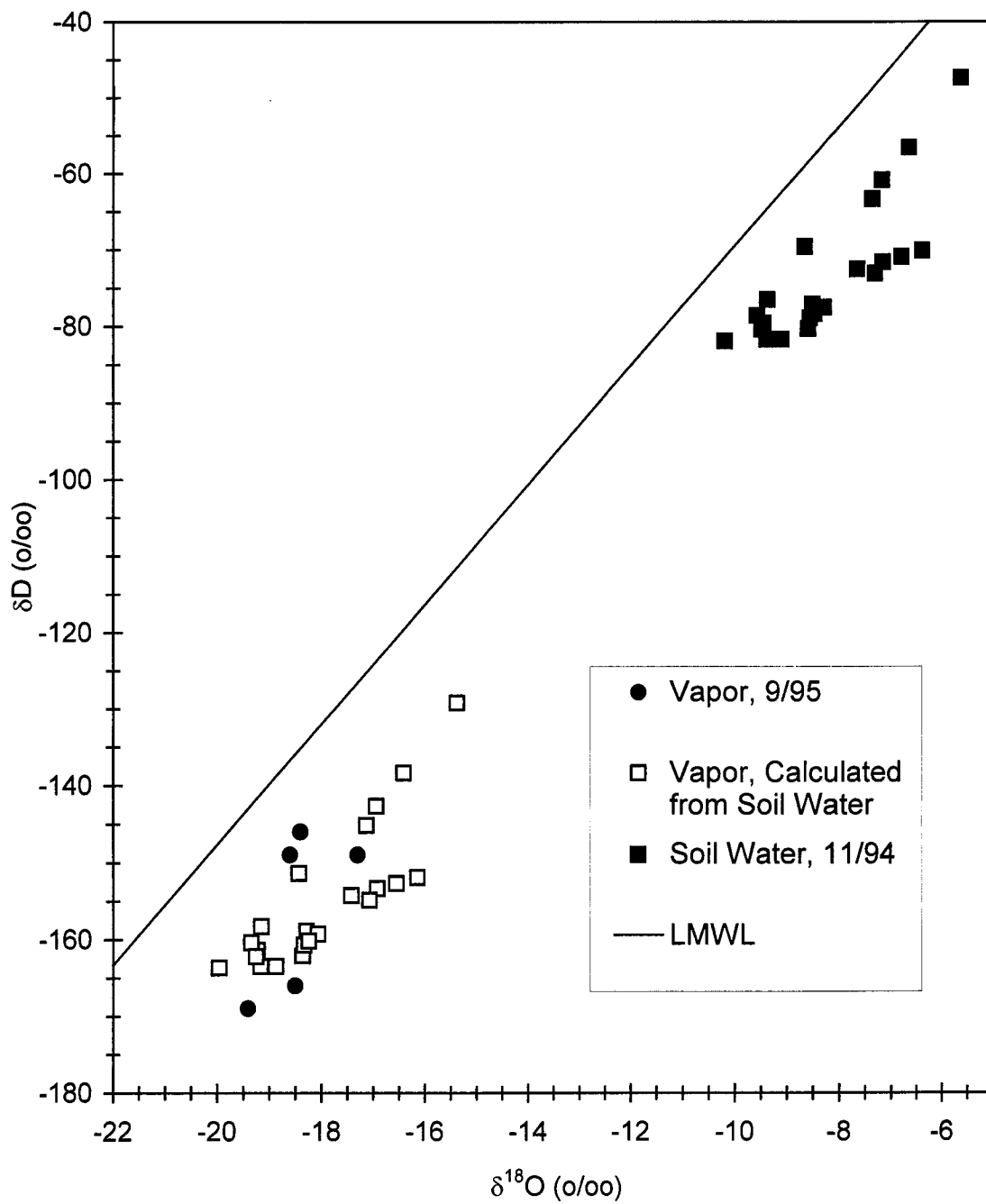


Figure 84. δD vs $\delta^{18}O$ plot of OGF water-vapor samples with the local meteoric water line (LMWL).

DISCUSSION

The data indicate that infiltrated stream water moves downward towards the water table beneath Oro Grande Wash and Sheep Creek Wash (Fig. 85), and at the upper and middle locations probably provides recharge to the regional aquifer. Beneath all control surfaces, evapotranspiration evidently has prevented infiltrated precipitation from moving beyond shallow depths. The data indicate distinct differences between control surfaces and channel locations, between locations within each channel, and between channels.

The stable-isotope data are best defined by the amount of evaporative enrichment shown by the soil waters. The evaporative enrichment is expressed numerically as the D offset from the LMWL (Table 5). For both Oro Grande Wash (Fig. 39) and Sheep Creek Wash (Fig. 40) the D offsets for the channel locations are generally less negative than those of the corresponding control surfaces. This indicates that stream water infiltrates beneath the channels rapidly and with sufficient volume to avoid substantial evaporative enrichment, in contrast to the control surfaces. The large negative D offsets of the control locations indicate that any infiltration that occurs is slow and in small amounts. Within each channel, in general, the D offsets are greater in the downstream locations. The increase in D offset with distance downstream can be explained by a combination of decrease in streamflow volume and decrease in sediment particle size. The lower volume of streamflow and decrease in sediment particle size with distance downstream slows infiltration and percolation allowing more evaporative enrichment to occur. A contribution to streamflow of local runoff, which may already have been partially

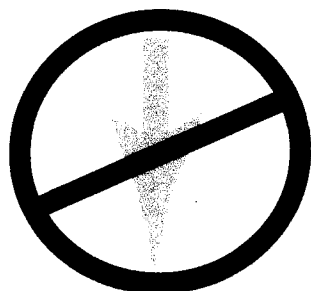
ORO GRANDE WASH AND SHEEP CREEK WASH

CONTROL LOCATIONS

RECEIVE ONLY
LOCAL PRECIPITATION



- * LOW WATER CONTENTS - MEAN OF 2.9 % BY WEIGHT
- * HIGHLY NEGATIVE SOIL-WATER POTENTIALS
- * SOIL-WATER ISOTOPIC COMPOSITIONS ARE EVAPORATIVELY ENRICHED
- * TRITIUM DETECTABLE ONLY AT SHALLOW DEPTHS (<10 m)
- * HIGH CHLORIDE CONCENTRATIONS AT SHALLOW DEPTHS



EVAPOTRANSPIRATION PREVENTS INFILTRATED PRECIPITATION FROM MOVING BEYOND SHALLOW DEPTHS

CHANNEL LOCATIONS

EXPERIENCE INTERMITTENT FLOW



- * HIGHER WATER CONTENTS - MEAN OF 4.9 % BY WEIGHT
- * SLIGHTLY NEGATIVE SOIL-WATER POTENTIALS
- * SOIL-WATER ISOTOPIC COMPOSITIONS SHOW LITTLE OR NO EVAPORATIVE ENRICHMENT
- * TRITIUM DETECTABLE TO GREATER DEPTHS (up to 36 m)
- * LOW CHLORIDE CONCENTRATIONS



INFILTRATED STREAM WATER MOVES DOWNWARD TOWARD THE WATER TABLE

Figure 85. Comparison of control and channel locations.

evaporated, could also be partially responsible for the trend toward more negative D offsets with distance downstream. A comparison of the two channels shows that the Sheep Creek Wash sites have more negative D offsets than their Oro Grande Wash counterparts. This suggests that infiltration and percolation of infiltrated waters to depths beyond the effects of evaporation occurs more rapidly beneath Oro Grande Wash.

Gravimetric-water contents (Figs. 11 and 12) of the sediment samples from beneath the channels are generally greater than those of the sediment samples from beneath the control surfaces, indicating that infiltrated stream water moves through the unsaturated zone beneath the channels. At Oro Grande Wash, water contents beneath the channel locations generally increase with distance downstream. The increase in water content is interpreted to be the result of the greater water retention capacities of the finer sediment in the downstream locations. Water contents beneath Sheep Creek Wash locations do not increase with distance downstream and are generally less than their Oro Grande Wash counterparts. The lower water contents beneath Sheep Creek Wash illustrate the differences between the two channels. Streamflow in Oro Grande Wash is confined to a channel that averages 3 m (10 ft) wide, whereas at Sheep Creek Wash, the channel is as much as 100 m (328 ft) wide and has changed location within the last 40 years (John Izbicki, personal communication, 1996). Even though average annual flow in Sheep Creek Wash is much greater than that in Oro Grande Wash, the wider, unconfined channel has resulted in a more diffuse distribution of water.

The slightly negative soil-water potentials (Figs. 13 - 22) measured in the sediment samples from beneath the channels indicate that gravity-driven flow of

infiltrated stream water toward the water table occurs beneath the channels. Many soil-water potentials of 0 kPa were recorded beneath the Oro Grande Wash channel locations. As noted previously, these values reflect the lack of sensitivity of the water-activity meter at slightly negative potentials. Although not saturated, these sediment samples were observed to be wet when their water activities were measured. Sheep Creek Wash locations generally have more negative soil-water potentials than their Oro Grande Wash counterparts. Soil-water potentials beneath the control surfaces are much more negative than soil-water potentials beneath the channels. Beneath control surfaces, soil-water potentials as low as $-17,000$ kPa were measured. The highly negative soil-water potentials measured at depths between 5 and 15 m (16 and 49 ft) beneath OGF (Fig. 18) and SCF (Fig. 22) suggest that water movement, from above and below, is toward these intervals.

Chloride concentrations (Figs. 23 - 32) also indicate that water moves downward through the unsaturated zone beneath the channels. Chloride concentrations beneath the channels are generally less than 5 mg/L, whereas intervals with concentrations exceeding 100 mg/L are present under control surfaces at depths ranging from 3 - 15 m (10 - 49 ft). The high chloride concentrations present beneath the control surfaces are the result of evapotranspiration, where evaporation and uptake of water by plants leave chloride behind to accumulate over time. The presence of the high chloride concentrations indicates that infiltrated precipitation does not move beyond shallow depths under current climatic conditions. In contrast, the low chloride concentrations beneath the upper and middle locations of both channels indicate that infiltrated stream water is moving

downward through the unsaturated zone and probably reaches the water table. Beneath the lower channel locations, intervals of higher chloride concentration are present at depths of 21 - 26 m (69 - 85 ft) and 9 - 15 m (30 - 49 ft) in LOGW-1 (Fig. 26) and LSCW (Fig. 31), respectively. The presence of higher chloride concentrations beneath the lower channel locations indicates that infiltrated stream water has reached greater depths than infiltrated precipitation beneath the corresponding control surfaces, but has not moved beyond these depths and therefore is not a source of groundwater recharge.

Tritium (Figs. 23 - 32) was not detected beyond depths of 9 m (30 ft) beneath the control surfaces, but beneath the channels it was detected at depths as great as 36.3 m (119 ft). Beneath the control surfaces tritium was not detected below the intervals of high chloride concentration, a further indication that evapotranspiration prevents infiltrated precipitation from moving beyond shallow depths and that recharge does not occur beneath the control surfaces. Beneath the channel locations, the tritium data indicate that infiltrated stream water does move downward toward the water table. The maximum depth of occurrence for detectable tritium (36.3 m (119 ft)) was at MOGW. Assuming that this tritium entered the unsaturated zone in 1953 and traveled by piston flow, the 36.3 m (119 ft) interval represents a time period of 42 years and a percolation rate of about 0.9 m per year (3 ft/year). Assuming the percolation rate remains constant, infiltrated stream water requires approximately 220 years to reach the water table beneath MOGW.

Validity of Soil-water-isotope Data

Because the accuracy of the stable-isotope data obtained from the extracted soil waters is a matter of some concern, a quality-assurance program, details of which are in Appendix A, was undertaken to assess the validity of the data. The results of the program indicate that the toluene distillation technique was effective at removing the “mobile” water from the sediment, but the isotopic compositions of waters from sediment with low water content and/or high mica content may have been altered through exchange with “bound” water adsorbed on or contained in the structures of the minerals composing the sediment. However, these results were obtained by performing rehydration experiments with oven-dried soils and may not be applicable to field conditions. The conclusion of this work is that the best test of data validity is in the degree to which the isotopic compositions of the extracted soil waters compare to the rest of the isotope dataset. If reasonable relationships are found to exist between the isotopic compositions of the extracted soil waters and the rest of the isotope dataset, then the isotope data can be compared with results from other methods. Oro Grande Wash and Sheep Creek Wash are two different environments and their datasets will be discussed individually.

Oro Grande Wash

Oro Grande Wash has a large isotope dataset consisting of data from 123 extracted soil waters and numerous precipitation, streamflow, groundwater, lysimeter-water, and water-vapor samples. Many of the soil waters have isotopic compositions almost identical to precipitation (Fig. 36). On δD vs $\delta^{18}O$ plots, the soil waters from

UOGW (Fig. 43) and some of the soil waters from MOGW (Fig. 45) plot very close to the LMWL, and statistical t-tests indicated that these soil waters are indistinguishable from precipitation. The δD and $\delta^{18}O$ depth profiles for each location (Figs. 42, 44, 46, 48, 50, and 52) are also quite similar, indicating that exchange processes, between the infiltrated stream water and bound or structural waters associated with the sediment, have not occurred. Groundwater collected at MOGW (Fig. 45) is similar in composition to the soil waters from that location. Lysimeter waters collected from the channel locations (Figs. 67 - 72) are also very close in composition to precipitation and the soil waters. Water-vapor samples (Figs. 77 - 84), specifically those collected during the same time of year as the soil waters, have compositions similar to those predicted from the soil-water-isotopic compositions, indicating that the toluene distillation technique was successful in extracting soil water from the Oro Grande Wash sediment.

In summary, the isotopic compositions of the extracted soil waters are very similar to the precipitation, lysimeter-water, and groundwater samples. Most significantly, the isotopic compositions of the extracted soil waters and vapor samples indicate equilibrium between the two phases. The isotopic compositions of the extracted soil waters are a good fit with the rest of the isotope dataset from Oro Grande Wash and can be used to interpret unsaturated-zone processes.

Sheep Creek Wash

The isotope dataset consists of data from 33 extracted soil waters and a number of precipitation, stream-water, snow, groundwater, and lysimeter-water samples. The

isotopic compositions of the soil waters are significantly evaporatively enriched when compared to precipitation (Fig. 36). The δD and $\delta^{18}O$ depth profiles for MSCW (Fig. 56), LSCW (Fig. 58), and SCF (Fig. 60) display some differences that may indicate that exchange processes, between the infiltrated stream water and bound or structural waters associated with the unsaturated-zone sediment, have occurred. Groundwater collected at MSCW (Fig. 55) is not similar in isotopic composition to most of the soil waters from that location. Lysimeter waters collected from USCW (Figs. 73 and 74) are not similar in composition to the soil waters. However, lysimeter waters collected from LSCW (Figs. 75 and 76) at a depth of 8.2 m (27 ft) are similar in composition to soil water from the same depth. Unfortunately, the Sheep Creek Wash isotopic dataset does not include water-vapor data.

Seventy percent of the soil waters were extracted from sediment with water contents less than 3%. In addition, many of the samples contain large quantities of muscovite. The Sheep Creek Wash sediment is derived mainly from Pelona schist, which is composed of 15 - 45 % muscovite (Ehlig, 1958), a mica with a clay-like structure. The low water contents and large amounts of muscovite in the Sheep Creek Wash sediment significantly affected the results of rehydration experiments performed as part of this thesis. Studies conducted by other researchers (Stewart and Stetson, 1975; Ingraham and Shadel, 1992; and Araguas-Araguas et al., 1995) report similar results for sediment with low water contents and large quantities of clay or clay-like minerals.

Overall, the Sheep Creek Wash soil waters display few of the similarities to precipitation, groundwater, and lysimeter waters that are seen in the Oro Grande Wash

dataset, but the data can be interpreted to explain the differences. However, given the low water contents of the majority of the samples and the large quantities of muscovite possessing adsorbed and structural waters that may exchange with the mobile waters (Stewart and Stetson, 1975; Ingraham and Shadel, 1992; and Araguas-Araguas et al., 1995), it is possible that the isotopic compositions of the extracted soil waters have been altered during their migration through the unsaturated zone. These possibilities must be considered when analyzing the data.

Discussions of Specific Sites

The general differences between the channel and control locations of Oro Grande Wash and Sheep Creek Wash have been discussed in the preceding pages, but each individual location is unique and will be discussed separately in the following pages.

Summit

This location is the control surface representing the wetter, more vegetated environment found in the upper reaches of Oro Grande Wash near the Cajon Pass. In spite of the greater amount of precipitation received at this location, the data indicate that infiltrated precipitation is not a source of recharge under current climatic conditions. The isotopic compositions of the soil waters (Fig. 41) display some evaporative enrichment, as evidenced by their more negative D offsets (Table 5 and Fig. 39) when compared to local precipitation and the UOGW soil waters. Tritium (Fig. 23) is not detectable beyond a depth of 8.8 m (29 ft), and elevated chloride concentrations (Fig. 23) indicate that

infiltrated precipitation has not moved beyond a depth of approximately 15 m (49 ft). Evapotranspiration evidently prevents infiltrated precipitation from reaching the water table at this location.

UOGW

The data from this location indicate that stream water derived from local precipitation infiltrates and percolates rapidly through the unsaturated zone, and probably provides recharge to the regional aquifer. The isotopic compositions of the soil waters (Fig. 43) are very similar to local bulk precipitation, and a t-test comparison of the D offsets of the soil waters to those of precipitation indicated no difference between the soil waters and precipitation. The similarity of the soil waters to local precipitation and the lack of evaporative enrichment indicate that local precipitation is the source of these waters and infiltration and percolation to depths below the influence of evaporative effects is rapid. The isotopic compositions of soil waters extracted from shallow hand-auger samples collected in January 1996, a year after the collection of core samples in January 1995, confirmed that percolation is rapid at this location. The isotopic compositions of the January 1996 soil waters were different from the isotopic compositions of the January 1995 soil waters and were very similar to winter 1995 bulk precipitation (Fig. 62). The change in isotopic composition indicates that stream water infiltrated during the winter of 1995 had displaced older soil waters and moved through the unsaturated zone at a rate of at least 3 m/year (10 ft/year).

Along with the isotope data, the coarser sediment at this location, slightly negative soil-water potentials (Fig. 14), low chloride concentrations (Fig. 24), and the presence of detectable tritium (Fig. 24) throughout the sampled depth all indicate rapid infiltration and percolation through the unsaturated zone. A percolation rate determined from the tritium data could not be calculated because the sampled interval lacks an identifiable 1964 tritium peak and the maximum depth containing detectable tritium is not known. Michel and Izbicki (1996) estimated the long-term average percolation rate beneath UOGW to be at least 1 m/year (3.3 ft/year). At a percolation rate of 1 m/year (3.3 ft/year), infiltrated stream water would require approximately 350 years to reach the water table.

MOGW

The data from this location indicate that infiltrated stream water probably provides recharge to the regional aquifer at this location. When compared to the control locations, the similarity of the isotopic compositions of the extracted soil waters (Fig. 45) to precipitation and ground water, greater gravimetric-water contents (Figs. 11 and 15), slightly negative soil-water potentials (Fig. 15), low chloride concentrations (Fig. 25), and detectable tritium (Fig. 25) present in soil waters to a depth of 36.3 m (119 ft) all indicate that infiltrated stream water moves downward through the unsaturated zone at this location.

The isotopic compositions of the soil waters (Fig. 45) fall within the range of bulk precipitation collected from the area and plot near the LMWL. The soil waters can be

divided into three groups according to depth (Table 5 and Fig. 45): 1) soil waters from depths less than 30 m (98 ft) that plot very near the LMWL with D offsets similar to precipitation, 2) soil waters from depths between 30 and 100 m (98 - 328 ft) that plot farther from the LMWL with more negative D offsets, and 3) three soil waters from depths greater than 100 m (328 ft) that plot close to the LMWL with D offsets close to precipitation, but with more positive isotopic compositions than the other soil waters. The D offsets of the three groups were compared to precipitation by statistical t-tests. The results of the t-tests indicated no statistical difference between the 0- to 30-m (0- to 98-ft) soil waters and precipitation, but the two deeper groups of soil waters were found to differ from precipitation. Therefore, the shallowest, most recent soil waters infiltrated and moved to depths below the effects of evaporation without being evaporatively enriched, whereas the deeper soil waters were evaporatively enriched. The differences seen in the soil waters indicate that climatic conditions have varied over time. The unevaporated shallow (0 - 30 m (0 - 98 ft)) soil waters are the result of more frequent and/or larger streamflow events, whereas the deeper soil waters indicate less frequent and/or smaller streamflow events. The deepest soil waters (>100 m (>328 ft)) are also of noticeably more positive isotopic compositions (Fig. 46), significantly shifted from the shallower soil waters and groundwater at this location. These soil waters may represent a preserved record of a climatic period during which storms that originated in lower latitudes delivered precipitation with more positive isotopic compositions to the area (Friedman et al., 1992).

Tritium (Fig. 25) was detectable in the soil waters to a depth of 36.3 m (119 ft), with the maximum tritium concentration (8.7 TU) located at 27.4 m (90 ft). Having both the maximum depth of occurrence and depth of maximum concentration allowed the estimation of percolation rates. Assuming the maximum tritium concentration represents waters infiltrated in 1964, and the maximum depth of occurrence represents waters infiltrated in 1953, the following percolation rates were calculated: 0.9 m/yr (3 ft/year), from 1953 through 1994 (36.3 m/42 years); 0.9 m/yr (3 ft/year), from 1964 through 1994 (27.4 m/31 years); and 0.8 m/yr (2.6 ft/year), from 1953 through 1963 (36.3 – 27.4 m/11 years). At an average percolation rate of 0.9 m/yr (3 ft/year), infiltrated stream water requires approximately 220 years to travel from land surface to the water table.

Precipitation data have been collected at the Victorville pump station since 1940 (National Oceanic and Atmospheric Administration). Combining stable-isotope, tritium, and precipitation data allowed the estimation of additional percolation rates. The δD depth profile, from land surface to maximum depth of tritium occurrence, representing a time period from 1953 through 1994, was compared to precipitation amounts from the same time period (Fig. 86). An interval of more negative δD values located at depths from 12 to 20 m (39 to 66 ft) correlates with a period of higher than average precipitation received from 1976 through 1983. From this correlation the following percolation rates were calculated: 1.0 m/yr (3.3 ft/year), from 1976 through 1983 (20 – 12 m/8 years); 1.1 m/yr (3.6 ft/year), from 1984 through 1994 (12 m/11 years); 1.1 m/yr (3.6 ft/year), from 1976 through 1994 (20 m/19 years); and 0.7 m/yr (2.3 ft/year), from 1953 through 1975 (36.3 – 20 m/23 years). From 1953 through 1975 the average percolation rate was 0.7

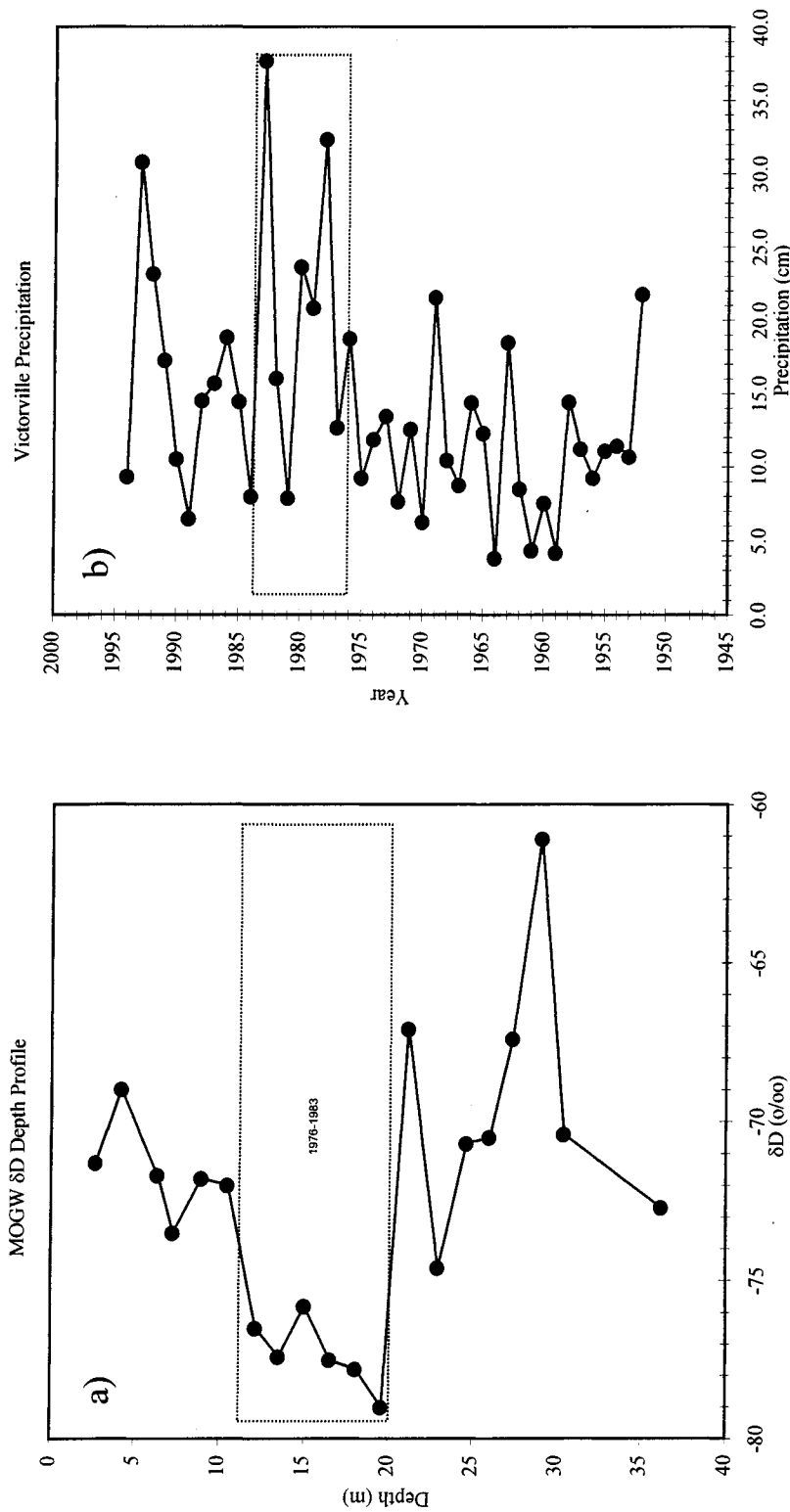


Figure 86. MOGW δD depth profile (a) compared to Victorville precipitation (National Oceanic and Atmospheric Administration) for water years 1952-1994 (b). A water year begins in November of previous year and continues through October of year indicated. An interval of more negative δD values in the depth profile (12-20 m) correlates to a period of high rainfall (1976-1983).

m/yr (2.3 ft/year), and the average percolation rate from 1976 through 1994 was 1.1 m/yr (3.6 ft/year). These rates seem reasonable because the annual rainfall from 1953 through 1975 was generally less than rainfall amounts from 1976 through 1994. These percolation rates are similar to those based solely upon the tritium data and also indicate a travel time of approximately 220 years from land surface to the water table.

The percolation rates calculated from the tritium data and the combined tritium, stable-isotope, and precipitation data relate well to the stable isotope data as they also indicate that the shallower soil waters have infiltrated and moved through the unsaturated zone more rapidly than the deeper soil waters.

The data presented in this thesis indicate that infiltrated stream water is a source of recharge at this location. However, more recent work by Michel and Izbicki (2002), using chlorofluorocarbon (CFC) data, indicates that an impermeable layer underlies this location at a depth greater than 91.5 m (300 ft). Chlorofluorocarbon concentrations were measured in soil air samples collected from the vapor samplers (Table 2) installed in the boreholes. The other locations in this study show a progressive decrease in CFC concentration with depth, but beneath MOGW concentrations drop to near zero between 91.5 and 152.4 m (300 and 500 ft). Gas diffusion calculations showed that the decrease seen in the CFC concentrations would require a laterally extensive impermeable layer beneath this location. The presence of an impermeable layer explains the shift to more positive isotopic compositions seen in the isotope depth profile (Fig. 46) for the soil waters deeper than 100 m (328 ft). The interpretation that this shift in isotopic compositions represents waters introduced under different climatic conditions is probably

correct because the CFC data indicate that infiltrated stream water does not pass through the impermeable layer. After encountering the impermeable layer, downward percolating water must flow laterally until the edge of the impermeable layer is reached and downward flow to the water table can resume. The work of Michel and Izbicki (2002) implies the existence of an impermeable layer that prevents infiltrated stream water from reaching the regional aquifer directly beneath this location, but it is unlikely that the impermeable layer exists for any great distance beneath the channel, and infiltrated stream water is probably able to reach the water table along most of the middle length of Oro Grande Wash. The work of Michel and Izbicki (2002) clearly illustrates the importance of employing as many different techniques as possible when studying the unsaturated zone.

LOGW-1

The data from this location indicate that infiltrated stream water is probably not currently a source of recharge to the regional aquifer, but that recent increases in streamflow, brought about by human influences, may provide recharge in the future.

The isotopic compositions of all of the extracted soil waters from this location (Figs. 37, 47, and Table 5), with the exception of the soil water from a depth of 3.9 m (13 ft), are more evaporatively enriched and have more negative D offsets than those from UOGW and MOGW, indicating that the rate and amount of infiltration at LOGW-1 are less than at the upstream locations. Of the four lysimeter samples collected at this location (Table 7 and Fig. 71), two, from depths of 6.7 m (22 ft) and 23 m (75 ft), are

very similar in isotopic composition to local precipitation and display little or no evaporative enrichment, whereas the remaining two are evaporatively enriched, like all but one of the soil waters. The lack of evaporative enrichment displayed by the two lysimeter waters from 6.7 m (22 ft) and 23 m (75 ft), and the soil water from 3.9 m (13 ft) indicates that these waters have infiltrated and moved through the unsaturated zone quickly, in contrast to the other soil and lysimeter waters, suggesting movement through preferential flow paths.

Unlike the other Oro Grande Wash locations, where water-vapor samples were collected once at the end of the dry season, water vapor was collected at intervals over the period of a year, October 1996 to September 1997. The isotopic compositions of the collected water vapors (Fig. 81) varied considerably over the collection period. Water-vapor samples collected at the end of the dry season, like the soil-water samples, had isotopic compositions quite similar to those calculated from the soil-water isotopic compositions. The water vapors collected during the wet season had isotopic compositions that were significantly more negative than those calculated from the soil-water isotopic compositions. At the end of the dry season, the water-vapor isotopic compositions were once again similar to the calculated values. The shift to more negative vapor compositions was observed at all depths. As discussed earlier, the fractionation factor, indicating the difference in isotopic composition between liquid water and the water vapor in equilibrium with it, is dependent upon temperature. Colder temperatures result in larger fractionation factors and more negative water-vapor isotopic compositions. However, subsurface temperatures did not fluctuate greatly at the depths

where vapors were collected. One explanation (Izbicki et al., 2000b) is that small amounts of cold water from winter rains infiltrated and moved through the unsaturated zone by preferential flow paths. The colder water was not of sufficient quantity to lower subsurface temperatures, but the colder water somehow dominated vapor processes, resulting in the more negative isotopic compositions of water vapors collected during the wet season. Over time, the cold water grew warmer and by the end of the dry season the isotopic compositions of the water vapors were again similar to the calculated compositions.

Overall, the evaporatively enriched isotopic compositions of the LOGW-1 soil waters indicate that infiltration and percolation are slower than at than the upstream locations, UOGW and MOGW, but the isotopic compositions of one soil water, two lysimeter samples, and the vapor samples indicate that some infiltrated water rapidly reaches depths of greater than 30 m (98 ft).

Gravimetric-water contents (Figs. 11 and 16) of the finer sediment at LOGW-1 are the highest of the Oro Grande Wash channel locations, with water contents as high as 20%, and soil-water potentials (Fig. 16) are slightly negative throughout most of the profile, indicating the possibility of gravity-driven downward movement of water. The presence of high chloride concentrations (Fig. 26) at depths between 21 and 26 m (69 and 85 ft) indicates that water has not moved beyond these depths for a considerable period of time, but tritium data (Fig. 26) indicates otherwise. Detectable levels of tritium are present in soil waters down to 23 m (75 ft), absent between 23 and 26 m (75 and 85 ft), and again present between 27 and 29 m (89 and 95 ft), beneath the chloride.

The stable-isotope, tritium, and gravimetric-water content data indicate that a large amount of stream water has entered the unsaturated zone beneath LOGW-1 within the last 50 years. This may be the result of human influences in recent years. Local development has resulted in large areas being paved over for parking lots and roadways. Runoff from nearby paved areas has resulted in increased streamflow. Even in the summer, thunderstorms and periodic draining of nearby water storage tanks has been observed to produce flow in the channel (John Izbicki, personal communication, 1997). Izbicki et al. (1998) suggested that the additional water provided in recent years has reactivated recharge at this location.

An explanation for the presence of tritium in soil waters beneath the interval of high chloride concentrations is dependent upon the source of the chloride. The chloride may have entered the unsaturated zone with infiltrated stream waters and indicates the maximum depth reached by the infiltrated waters, or, as suggested by Izbicki et al. (1998), it could represent a laterally extensive paleosurface. The LOGW-2 borehole was drilled to determine the lateral extent of the chloride.

LOGW-2

This site is located 45 m (148 ft) west of LOGW-1 (Fig. 7) and is 1 m (3 ft) higher in elevation. LOGW-2 was drilled to determine the lateral extent of the high chloride concentrations found at depth beneath LOGW-1. It was thought that the chloride beneath LOGW-1 could represent a laterally extensive paleosurface instead of chloride derived from infiltrated Oro Grande Wash stream water.

Overall, the isotopic compositions of the LOGW-2 soil water (Fig. 49), water contents (Fig. 17), soil-water potentials (Fig. 17), and chloride concentrations (Fig. 27) are very similar to the OGF control location, and indicate that waters infiltrated from the surface have not reached depths greater than 10 - 12 m (33 – 39 ft). High chloride concentrations are only present at depths shallower than 13 m (43 ft) and are similar in concentration and depth to those at the OGF control site (Fig. 28). Tritium (Fig. 27) was only detected at depths of 27.9 m (91.5 ft) and 31.6 m (103.6 ft).

The absence of chloride at depth beneath LOGW-2 indicates that the deep chloride at LOGW-1 is a feature associated with the channel and represents the maximum depth reached by infiltrated stream water. The soil waters containing tritium at depths of 27.9 m (91.5 ft) and 31.6 m (103.6 ft) at LOGW-2 correlate with the soil waters containing tritium found below the deep chloride at LOGW-1 (Fig. 26) and are of similar isotopic compositions. The presence of tritium at depth beneath LOGW-2 and beneath the chloride at LOGW-1 may be the result of lateral spreading of downward-percolating water from LOGW-1 or of lateral flow from an upstream location through the inclined alluvial sediment. Nimmo et al. (2002) predicted significant lateral spreading of downward-percolating waters due to the textural diversity and pronounced layer contrasts of the alluvial sediment beneath Oro Grande Wash. Even a single minimally conductive layer can account for a high degree of spreading. Lateral spreading of downward-percolating water from LOGW-1 could explain the occurrence of tritium at depth beneath LOGW-2 and could allow downward-percolating water to flow around the region of deep chloride beneath LOGW-1. Lateral flow of tritium-bearing waters from farther upstream

is another possibility. The alluvial fan sediment beneath this location dips to the north, in the direction of streamflow. Sediment variability in inclined sediment has been found to promote lateral flow of water under unsaturated conditions (Hendrickx and Walker, 1997).

In summary, the data from LOGW-2 show that the deep chloride beneath LOGW-1 is a feature associated with the channel and represents the maximum depth reached by infiltrated stream water. The presence of the deep chloride beneath LOGW-1 indicates that recharge to the regional aquifer is not likely, even though the data indicate that some infiltrated water moves rapidly to substantial depths, and that significant lateral spreading of downward-percolating from LOGW-1 and/or lateral flow of water from an upstream location occurs. However, recent increases in streamflow due to human influences may provide recharge in the future.

OGF

This location is the control site for the lower portion of Oro Grande Wash and is located on a fan surface 200 m (656 ft) west of LOGW-1 and 11 m (36 ft) higher in elevation. The data indicate that infiltrated precipitation is not a source of recharge and has not moved beyond a depth of 10 m (33 ft) for a considerable period of time. The isotopic compositions of the soil waters from this location have the most negative D offsets (Table 5 and Fig. 39), indicating the greatest evaporative enrichment, of all of the sites related to Oro Grande Wash. Gravimetric-water contents (Figs. 11 and 18) and soil-water potentials (Fig. 18) are the lowest of all of the Oro Grande Wash sites. Tritium

(Fig. 28) was not detectable in soil waters below a depth of 2.4 m (8 ft) and the high concentrations of chloride (Fig. 28) present at depths of 2 - 10 m (7 - 33 ft) indicate that any precipitation infiltrated from the surface has ultimately been lost through evapotranspiration. The amount of chloride present was estimated to represent accumulation during a period of approximately 10,000 years (Izbicki et al., 1998). The data from this control location, when compared with data from the Oro Grande Wash channel locations, indicate that intermittent streamflow in the channel is responsible for the higher water contents, less negative soil-water potentials, lower chloride concentrations, greater depths of occurrence of tritium, and the less evaporatively enriched isotopic compositions of the soil waters from the channel locations.

As indicated by the chloride data, the soil waters from OGF, specifically those from depths greater than 10 m (33 ft), are much older than the soil waters from the other Oro Grande Wash locations. The δD and $\delta^{18}O$ depth profiles (Fig. 52) display a general trend toward more negative δ values with depth. The original isotopic compositions of many of the soil waters, estimated by projection back to the LMWL along evaporative trend lines with slopes of 4, were more negative than bulk-average precipitation and most of the bulk precipitation collected during the study period. Waters infiltrated during the colder, wetter climatic conditions believed to exist in the study area prior to 10,000 years ago would have had more negative isotopic compositions. Therefore, the trend to more negative isotopic compositions with depth indicates that the source of the deeper soil waters is precipitation with more negative isotopic compositions received in the study area more than 10,000 years ago.

The large number of soil-water samples from OGF produced well-defined δD and $\delta^{18}O$ depth profiles (Fig. 52) and data trends when plotted as δD vs $\delta^{18}O$ (Fig. 51). The depth profiles display a general trend toward more negative δ values with depth, but also display a number of peaks with more positive δ values. The δD vs $\delta^{18}O$ data plot (Fig. 51) shows that the soil waters plot as 3 groups: 1) soil waters of more negative compositions plotting in a cluster below the LMWL; 2) soil waters defining a linear trend with a lower slope than the LMWL, and 3) soil waters defining a linear trend roughly parallel to, but below the LMWL. Izbicki et al. (2000b) interpreted these groups as follows: soil waters from group 1 are unaltered soil waters, soil waters from group 2 are evaporated soil waters, and soil waters from group 3 define a Rayleigh distillation line. The group 1 soil waters have the most negative isotopic compositions and plot in a cluster below the LMWL. These waters (Fig. 52) are from depths greater than 7 m (23 ft) and the majority of them are from depths greater than 19 m (62 ft). They appear to have remained relatively unaltered in isotopic composition since infiltrating and moving to depths beyond the effects of evaporation. The group 2 soil waters, from depths between 13 and 19 m (43 and 62 ft), extend away from the cluster of group 1 soil waters along an evaporative trend line with a slope less than the LMWL. These soil waters apparently underwent more evaporation than the group 1 waters and have retained their evaporatively enriched compositions. The interpretation that these soil waters define an evaporative trend is supported by the soil waters extracted from shallow hand-auger samples at this location. The shallow soil waters from the hand-auger samples extend the evaporative trend line defined by the group 2 soil waters (Fig. 66). The group 3 soil

waters, from depths between 2 and 22 m (7 and 72 ft), plot along what is interpreted to be a Rayleigh distillation line extending away from the group 1 soil waters. The isotopic compositions of these waters are very similar to some of the bulk-precipitation samples collected during the study period, and an alternative interpretation would be that the source of these soil waters was precipitation with more positive isotopic composition. However, the bulk-precipitation samples represent very small amounts of summer precipitation that was more likely to evaporate than infiltrate. In support of a Rayleigh distillation origin is the correlation of the soil waters with intervals of low water content (Fig. 18), low soil-water potential (Fig. 18), and coarser sediment (see Appendix B). The coarser, more permeable sediment associated with these depths is inferred to have allowed circulation of air, which removed water, as vapor, from the sediment. Over time, the isotopic composition of the remaining water evidently became progressively more positive along a Rayleigh distillation line, and the soil-water potentials and water contents decreased.

The interpretation that water movement in the vapor phase occurs at this location is supported by the shallow isotope-depth profiles. The shallow isotope-depth profiles from OGF (Fig. 65) display greater evaporative enrichment than the depth profiles from UOGW (Fig. 61) and MOGW (Fig. 63). The isotope maximum, located at the drying front (Fig. 3), is more evaporatively enriched at OGF than at the two channel locations (Table 6). The greater amplitude of the isotope maximum at OGF indicates that downward diffusion of the heavier isotopes in the liquid phase does not occur to the same

degree as at the wetter channel locations, suggesting that water movement in the vapor phase is the more dominant process at OGF.

In summary, isotope, tritium, and chloride data indicate that water from infiltrated precipitation has not moved beyond a depth of 10 m (33 ft) and is not a source of recharge under current climatic conditions. The soil waters from depths greater than 10 m (33 ft) display a trend to more negative isotopic compositions with depth, indicating that their source was precipitation of more negative isotopic composition received in the study area more than 10,000 years ago under wetter, colder conditions. The large number of soil-water samples also permitted the identification of Rayleigh-type enrichment of soil waters occurring in more permeable sediment layers. The presence of the Rayleigh-enriched soil waters and the highly enriched shallow-isotope depth profiles indicate that vapor transport is the dominant mode of water movement at this location.

USCW

The data indicate that recharge from infiltrated stream water is probable at USCW. The isotopic compositions of the soil waters (Fig. 53), including one sample collected by scooping a shallow depression in the channel, are evaporatively enriched, but have less negative D offsets (Table 5) than those from the SCF control location. The original isotopic compositions of the soil waters, estimated by projection back to the LMWL along evaporative trend lines with slopes of four, were considerably more negative than Table Mountain bulk-average precipitation. This suggests that the source of the soil waters was precipitation with more negative isotopic compositions. Snowmelt

is a likely source for these waters because snow collected at USCW (Fig. 53) has a more negative isotopic composition than all but one of the other precipitation samples. Lysimeter waters (Figs. 73 and 74) plot closer to the LMWL and have isotopic compositions more similar to precipitation than the soil waters, indicating less evaporative enrichment. The small degree of evaporative enrichment seen in the lysimeter waters indicates that they infiltrated more rapidly than the extracted soil waters and the shallow soil water collected at the surface.

Gravimetric-water contents (Figs. 12 and 19) and soil-water potentials (Fig. 19) are greater than those from the SCF control location (Figs. 12 and 22), indicating the contribution of infiltrated stream water. Low chloride concentrations (Fig. 29) and detectable concentrations of tritium (Fig. 29) present throughout the entire sampled interval (30.4 m (100 ft)) indicate that water is moving through the unsaturated zone. Because the maximum depth of tritium occurrence is at some depth below the sampled interval, a percolation rate could only be estimated. The maximum sampled depth (30.4 m (100 ft)) divided by the time elapsed between the onset of atmospheric nuclear testing and sample collection (43 years) indicates that the percolation rate is greater than or equal to 0.7 m/year (2.3 ft/year). A rate of 1.0 m/year (3.3 ft/year) does not seem unreasonable, and at this rate infiltrated waters require approximately 350 years to reach the water table.

All the data indicate that recharge probably occurs at this location, but the stable-isotope data also indicate that the lysimeter waters infiltrated and percolated more rapidly than the extracted soil waters. This suggests that some infiltrated waters move rapidly through the unsaturated zone by macropore flow or preferential flow paths while the

remaining waters percolate more slowly and become evaporatively enriched. Evidence for rapid percolation is supported by the presence of tritium in groundwater from a well (not a part of this study) located upstream, closer to the mountain front, from USCW (Izbicki et al., 1995). The presence of tritium in the groundwater from the well indicates that infiltrated waters reached the water table at a depth greater than 168 m (550 ft) in less than 50 years. In summary, soil-water data indicate that infiltrated stream water at USCW has an average percolation rate of approximately 1 m/year (3.3 ft/year), whereas the isotopic compositions of the lysimeter-water samples suggest that some water moves considerably faster.

MSCW

The data indicate that infiltrated stream water is moving downward toward the water table and recharge is probable beneath MSCW. The stable-isotope compositions of the soil waters from this location (Fig. 55) are evaporatively enriched, but have less negative D offsets (Table 5) than those from the SCF control surface, indicating faster infiltration and movement to depths beyond the effects of evapotranspiration. Differences in the δD and $\delta^{18}O$ depth profiles (Fig. 56) indicate that exchange between the infiltrated waters and bound waters associated with minerals in the unsaturated-zone sediment may have occurred. Gravimetric-water contents (Figs. 12 and 20) and soil-water potentials (Fig. 20) are greater than those associated with the control surface (Fig. 22) indicating the contribution of infiltrated stream water, and low chloride concentrations (Fig. 30) indicate that water is moving through the unsaturated zone

toward the water table. Tritium (Fig. 30) was not detected below 13.41 m (45 ft). The maximum depth of tritium detection (13.41 m (45 ft)) divided by the time elapsed between the onset of atmospheric nuclear testing and sample collection (43 years) gives an average percolation rate of 0.3 m/year (1 ft/year). At this rate infiltrated stream water requires more than five hundred years to reach the water table.

The average percolation rate at MSCW is one-third of the average percolation rate at MOGW. The more negative D offsets (Table 5) of the MSCW soil waters suggest that infiltration and percolation are slower than at MOGW, and the tritium data confirm this. The broader, less focused application of water to the unsaturated zone and the finer particle size of the sediment at MSCW result in slower infiltration and percolation rates even though the average annual flow of Sheep Creek Wash is more than four times that of Oro Grande Wash.

The isotopic compositions of the soil waters (Fig. 55 and Table 5) at MSCW can be separated into two groups based on their D offsets from the LMWL: 1) those with more negative D offsets plotting well off the LMWL, and 2) those with less negative D offsets plotting closer to the LMWL. The soil waters plotting closer to the LMWL are mainly those from depths greater than 42 m (138 ft). The smaller amounts of evaporative enrichment seen in the deeper soil waters indicate a greater recharge rate. These deeper waters may have originated in wetter climatic conditions when more frequent flow events supplied more infiltrated water to the unsaturated zone. Most of the deeper soil waters have more negative isotopic compositions than local bulk precipitation, and their original isotopic compositions probably were considerably more negative, indicating an origin

from precipitation and/or snowmelt of more negative isotopic composition. The percolation rate of 0.3 m/year (1 ft/year) derived from the tritium data indicates that these soil waters entered the unsaturated zone prior to 140 years ago (42 m divided by 0.3 m/year).

Unlike the soil waters, groundwater at MSCW (Fig. 55) is not evaporatively enriched and plots along the LMWL. The isotopic composition of the groundwater is similar to that of the majority of the regional aquifer, which is composed mainly of waters older than 5,000 years (Izbicki et al., 1995). Although recharge at this location is indicated, the lack of similarity between the isotopic compositions of the soil waters and groundwater suggests that any recharge contribution is of insufficient quantity and/or too areally diffuse to significantly affect the isotopic composition of the groundwater.

LSCW

At this location the data indicate that infiltrated stream water moves downward through the unsaturated zone, but has not moved beyond a depth of approximately 10 m (33 ft). Stable-isotope compositions, gravimetric-water contents, soil-water potentials, chloride concentrations, and tritium concentrations all exhibit changes at or near a depth of 10 m (33 ft). The stable-isotope compositions of the soil waters (Fig. 57) from depths less than 10 m (33 ft) have less negative D offsets, indicating less evaporative enrichment, than the deeper soil waters and more closely resemble the compositions of the precipitation, stream water, and lysimeter water (Fig. 76) collected at this location. However, the isotopic compositions of the shallow soil waters may be the result of

exchange between infiltrated waters and bound waters associated with minerals in the unsaturated zone sediment because the δD and $\delta^{18}O$ depth profiles (Fig. 58) display opposing trends at depths less than 10 m (33 ft). Water contents (Fig. 21) increase to a depth of 8.2 m (27 ft) and then decrease to a minimum at 10.3 m (34 ft). Of the five lysimeters installed, the only one to yield water was located at a depth of 8.2 m (27 ft). Soil-water potentials (Fig. 21) reach a maximum at 8.2 m (27 ft) and then shift to highly negative values at 10.3 m (33.8 ft). Tritium (Fig. 31) was detectable to a depth of 8.3 m (27 ft). The stable-isotope data are somewhat suspect, but the gravimetric-water content, soil-water potential, and tritium data indicate that infiltrated stream water has reached a depth of approximately 10 m (33 ft).

The higher chloride concentrations (Fig. 31) below 9.2 m (30 ft) indicate that infiltrated stream water has not moved to greater depths at this location. However, the chloride at this location is lower in concentration and occurs at greater depth than the chloride beneath the SCF control surface. The greater depth indicates that infiltrated stream water is able to move past the effects of evapotranspiration, and the lower chloride concentrations can be explained by channel migration. Sheep Creek Wash is located upon an active fan surface and, as mentioned previously, the channel is known to have changed location within the last 40 years and has been in existence for many thousands of years. The migration of the channel across the fan surface keeps water moving through the unsaturated zone and prevents the accumulation of high concentrations of chloride at shallow depths. The chloride present at 9 - 16 m (30 - 53 ft) beneath the present channel accumulated at a shallower depth until the channel arrived over this location and the

chloride moved to its present depth with infiltrated stream water. The chloride will continue to move downward toward the water table with the percolating water. Although water infiltrated over the last 40 to 50 years beneath the current location has only moved about 10 m (33 ft) below the surface, it seems likely that waters infiltrated beneath previous channel locations are currently providing recharge to the regional aquifer and that the lower reaches of Sheep Creek Wash represent a zone of diffuse recharge.

SCF

This site is the control surface for Sheep Creek Wash and represents the area surrounding the channel that receives only direct precipitation. The data indicate that evapotranspiration has prevented infiltrated precipitation from moving beyond a depth of 16 m (53 ft) under current climatic conditions.

The isotopic compositions of the soil waters (Fig. 59) from this location are highly evaporatively enriched and have more negative D offsets (Table 5 and Fig. 40) than the channel locations. The δD and $\delta^{18}O$ depth profiles (Fig. 60) are not similar above 7 m (23 ft), a possible indication that the isotopic compositions of the infiltrated waters have been altered by exchange with bound and structural waters associated with the sediment. The gravimetric-water contents (Fig. 22) at this location are the lowest of all the sites measured in this study. Water contents do not exceed 1.4% above depths of 17 m (56 ft). Highly negative soil-water potentials (Fig. 22) and high chloride concentrations (Fig. 32) are present between depths of 4 - 16 m (13 - 53 ft) and tritium (Fig. 28) was not detected in soil waters from depths greater than 3.7 m (12 ft).

Gravity-driven downward movement of infiltrated waters past the zones of highly negative potential is not likely and the high chloride concentrations indicate that infiltrated waters have not moved beyond a depth of 16 m (53 ft). Although the chloride concentrations are not as high as those at OGF (Fig. 28), it is assumed that the total chloride accumulation represents a time period comparable to the 10,000 years that Izbicki et al. (1998) estimated that the OGF chloride accumulation represents. Soil water from a depth of 24 m (79 ft), the only soil water sample collected beneath the high chloride concentrations, has a more negative isotopic composition, suggesting that the source of this water was precipitation received during colder, wetter conditions that existed in the study area prior to 10,000 years ago. In contrast, the more positive isotopic compositions of the shallower soil waters and the presence of detectable tritium in the shallowest soil waters indicate more recent infiltration.

Overview

To conclude this section, Figures 87 and 88 summarize the main points of the discussions of infiltration, percolation, and recharge for Oro Grande Wash and Sheep Creek Wash, respectively.

ORO GRANDE WASH

Channel incised into beheaded fan surface. Streamflow derived from local runoff.

SUMMIT & ORO GRANDE FAN CONTROL LOCATIONS



No recharge from infiltrated precipitation. Evapotranspiration prevents infiltrated precipitation from moving beyond shallow depths.



UPPER

Recharge indicated along upper channel. Infiltrated stream water requires approximately 350 years to reach the water table.



MIDDLE

Recharge indicated along middle channel, but not beneath this location due to presence of impermeable layer at depth. Infiltrated stream water requires approximately 220 years to reach the water table.



LOWER

No recharge indicated along lower channel. Recent increases in streamflow due to human influences may have activated recharge at this location.

Figure 87. Oro Grande Wash overview.

SHEEP CREEK WASH

Channel migrates across an active fan surface. Streamflow derived from mountain precipitation and snowmelt, and from local runoff.

SHEEP CREEK FAN CONTROL LOCATION



No recharge from infiltrated precipitation. Evapotranspiration prevents infiltrated precipitation from moving beyond shallow depths.



UPPER

Recharge indicated along upper channel. Infiltrated stream water requires approximately 350 years to reach the water table. Preferential flow may allow some water to reach the water table in less than 50 years.



MIDDLE

Recharge indicated along middle channel. Infiltrated stream water requires approximately 500 years to reach the water table.



LOWER

No recharge indicated at present channel location. However, lower channel area may be a zone of diffuse recharge due to infiltrated stream water from previous channel locations reaching the water table.

Figure 88. Sheep Creek Wash overview.

CONCLUSIONS

The goal of this thesis was to determine if infiltrated stream water from the two ephemeral stream channels studied, Oro Grande Wash and Sheep Creek Wash, provides recharge to the underlying regional aquifer under present-day climatic conditions. The data indicate that infiltrated stream water probably provides recharge at the upper and middle reaches of both Oro Grande Wash and Sheep Creek Wash. More recent work indicates that the presence of an impermeable layer beneath MOGW prevents recharge at that particular location, but it is likely that recharge does occur in other areas along the middle reach of Oro Grande Wash. Infiltrated stream water at the lower locations of both channels is not providing recharge, but at LOGW-1 the data suggest that downward percolation of water, which would ultimately provide recharge, has recently increased due to additional streamflow provided by human activity. At control locations, on fan surfaces away from the channels, evapotranspiration prevents infiltrated precipitation from moving beyond shallow depths.

The isotopic compositions of the extracted soil waters from Oro Grande Wash and Sheep Creek Wash, by themselves, indicate that the channel locations are different from the control locations. The isotopic compositions of the soil waters from the control locations are highly evaporatively enriched whereas the soil waters from the channel locations show little or no evaporative enrichment. This clearly indicates more rapid water movement beneath the channels. Even though it is possible that the isotopic compositions of the extracted soil waters from Sheep Creek Wash have been altered

through exchange with waters associated with the sediment in the unsaturated zone, the stable-isotope data nonetheless indicate that the channel locations differ from the control locations. The stable-isotope data also provide evidence of variation in recharge/climatic conditions at MOGW and MSCW, preferential flow at LOGW-1 and USCW, and the dominance of vapor transport at OGF.

The stable-isotope data were significantly enhanced and supported by data from other techniques. Chloride and tritium data were especially useful. Chloride data, showing an absence of high concentrations of chloride beneath the upper and middle locations of each channel, indicate that infiltrated waters are moving through the unsaturated zone to the water table. Tritium data indicate that infiltrated stream water has reached considerable depths within the last 50 years, and the data provided percolation rate estimates. Combining data was also useful. Comparison of the 50-year isotope depth profile from MOGW, as defined by tritium data, to precipitation records provided additional percolation rate estimates similar to those based on the tritium. At OGF, correlations between evaporatively enriched soil waters, low water contents, more negative soil-water potentials, and coarser sediment provide support for an apparent Rayleigh distillation process defined in an isotope data plot.

The large datasets available, particularly from Oro Grande Wash, were also beneficial for interpretations. The large number of samples from OGF allowed identification of the Rayleigh trend line on the δD vs $\delta^{18}O$ plot. With a smaller dataset this interpretation would not have been possible. However, because of the time and cost required to prepare and analyze samples, datasets of this size are not typical. The dataset

from Sheep Creek Wash was a more realistic size and provided the needed information, whereas the larger Oro Grande Wash dataset provided additional details.

Future studies would benefit from additional precipitation data. Collection of precipitation for several years prior to drilling and collection of core samples may permit the calculation of percolation rates and recharge amounts based upon correlations between precipitation and soil-water isotopic compositions. For example, at UOGW, where infiltration and percolation of water was rapid enough to avoid evaporative enrichment, several years of precipitation data prior to core collection may have allowed the identification of yearly inputs to the unsaturated zone.

In conclusion, stable-isotope data combined with data from other methods, in particular tritium and chloride data, were successfully used to determine that infiltrated stream water is a probable source of recharge along the upper and middle reaches of both Oro Grande Wash and Sheep Creek Wash.

REFERENCES CITED

- Allison, G.B., Barnes, C.J., and Hughes, M.W., 1983, The distribution of deuterium and ^{18}O in dry soils. 2. Experimental: *Journal of Hydrology*, v. 64, p. 377-397.
- Allison, G.B., Barnes, C.J., Hughes, M.W., and Leaney, F.W.J., 1984, Effect of climate and vegetation on oxygen-18 and deuterium profiles in soils, *in* *Isotope hydrology 1984*: Vienna, Austria, International Atomic Energy Agency, p. 105-123.
- Araguas-Araguas, L., Rozanski, K., Gonfiantini, R., and Louvat, D., 1995, Isotope effects accompanying vacuum extraction of soil water for stable isotope analyses: *Journal of Hydrology*, v. 168, p. 159-171.
- Barnes, C.J., and Allison, G.B., 1983, The distribution of deuterium and ^{18}O in dry soils. 1. Theory: *Journal of Hydrology*, v. 60, p. 141-156.
- Barnes, C.J., and Allison, G.B., 1984, The distribution of deuterium and ^{18}O in dry soils. 3. Theory for non-isothermal water movement: *Journal of Hydrology*, v. 74, p. 119-135.
- Barnes, C.J., and Allison, G.B., 1988, Tracing of water movement in the unsaturated zone using stable isotopes of hydrogen and oxygen: *Journal of Hydrology*, v. 100, p. 143-176.
- Barnes, C.J., and Walker, G.R., 1989, The distribution of deuterium and oxygen-18 during unsteady evaporation from a dry soil: *Journal of Hydrology*, v. 112, p. 55-67.
- Blatt, H., 1982, *Sedimentary petrology*: San Francisco, California, W.H. Freeman and Company, 564 p.
- California State Department of Water Resources, 1967, Mojave River ground water basins investigation: *Bulletin No. 84*, 151 p.
- Clark, I.D., and Fritz, P., 1997, *Environmental isotopes in hydrogeology*: Boca Raton, Florida, Lewis Publishers, 328 p.
- Cook, P.G., Edmunds, W.M., and Gaye, C.B., 1992, Estimating paleorecharge and paleoclimate from unsaturated zone profiles: *Water Resources Research*, v. 28, p. 2721-2731.

- Craig, H., 1961, Isotopic variations in meteoric waters: *Science*, v. 133, p. 1702-1703.
- Driscoll, F.G., 1986, *Groundwater and wells*: Saint Paul, Minnesota, Johnson Filtration Systems, Inc., 1089 p.
- Ehlig, P.L., 1958, *The geology of the Mount Baldy region of the San Gabriel mountains, California [Ph.D. dissert.]*: Los Angeles, California, University of California, 195 p.
- Epstein, S., and Mayeda, T., 1953, Variation of O18 content of waters from natural sources: *Geochimica et Cosmochimica Acta*, v. 4, p. 213-224.
- Friedman, I., and O'Neil, J.R., 1977, *Compilation of stable isotope fractionation factors of geochemical interest*: U.S. Geological Survey Professional Paper 440-KK, 12 p.
- Friedman, I., Smith, G.I., Gleason, J.D., Warden, A., and Harris, J.M., 1992, Stable isotope composition of waters in southeastern California 1. Modern precipitation: *Journal of Geophysical Research*, v. 97, no. D5, p. 5795-5812.
- Gat, J.R., 1981, Properties of the isotopic species of water: The "Isotope Effect", *in* Gat, J.R., and Gonfiantini, R., eds., *Stable isotope hydrology: Deuterium and oxygen-18 in the water cycle*: Vienna, Austria, International Atomic Energy Agency, Technical Report Series No. 210, p. 7-19.
- Gee, G.W., Campbell, M.D., Campbell, G.S., and Campbell, J.H., 1992, Rapid measurement of low soil water potentials using a water activity meter: *Soil Science Society of America Journal*, v. 56, p. 1069-1070.
- Hammermeister, D.P., Blout, D.O., and McDaniel, J.C., 1986, Drilling and coring methods that minimize the disturbance of cuttings, core, and rock formations in the unsaturated zone, Yucca Mountain, Nevada, *in* Proceedings of the National Water Well Association conference on characterization and monitoring of the vadose (unsaturated) zone: Worthington, Ohio, National Water Well Association, p. 507-541.
- Hendrickx, J.M.H., and Walker, G.R., 1997, Recharge from precipitation, *in* Simmers, I., ed., *Recharge of phreatic aquifers in (semi-) arid areas*: A.A. Balkema, Rotterdam, International Association of Hydrogeologists, Publication No. 19, p. 19-111.
- Hillel, D., 1982, *Introduction to soil physics*: San Diego, California, Academic Press Inc., 364 p.

- Ingraham, N.L., 1998, Isotopic variations in precipitation, *in* Kendall, C., and McDonnell, J.J., eds., *Isotope tracers in catchment hydrology*: Amsterdam, The Netherlands, Elsevier, p. 87-118.
- Ingraham, N.L., and Shadel, C., 1992, A comparison of the toluene distillation and vacuum/heat methods for extracting soil water for stable isotopic analysis: *Journal of Hydrology*, v. 140, p. 371-387.
- Izbicki, J.A., Martin, P., and Michel, R.L., 1995, Source, movement, and age of groundwater in the upper part of the Mojave River Basin, California, USA, *in* Adair, E. M., and Leibungut, C., eds., *Application of tracers in arid zone hydrology*: Wallingford, UK, International Association of Hydrological Sciences, Publication No. 232, p. 43-56.
- Izbicki, J.A., and Michel, R.L., 2002, Use of temperature data to estimate infiltration from intermittent streams in the western Mojave Desert, USA, *in* Proceedings of International Association of Hydrological Sciences conference on balancing the groundwater budget, Darwin, Australia, CD-ROM.
- Izbicki, J.A., Michel, R.L., and Martin, P., 1998, Chloride and tritium concentrations in a thick unsaturated zone underlying an intermittent stream in the Mojave Desert, southern California, U.S.A., *in* Brahana, J.V., Eckstein, Y., Ongley, C.K., Schneider, R., and Moore, J.E., eds., *Gambling with groundwater – physical, chemical, and biological aspects of aquifer-stream relations*, proceeds volume of the joint conference of the International Association of Hydrogeologists and the American Institute of Hydrology, Las Vegas, Nevada USA, 28 September – 2 October 1998: St. Paul, Minnesota, American Institute of Hydrology, p. 81-88.
- Izbicki, J.A., Clark, D.A., Pimentel, I., Land, M., Radyk, J., and Michel, R.L., 2000a, Data from a thick unsaturated zone underlying Oro Grande and Sheep Creek Washes in the western part of the Mojave Desert, near Victorville, San Bernardino County, California: U.S. Geological Survey Open-File Report 00-262, 133 p.
- Izbicki, J.A., Radyk, J.C., and Michel, R.L., 2000b, Water movement through a thick unsaturated zone underlying an intermittent stream in the western Mojave Desert, southern California, U.S.A.: *Journal of Hydrology*, v. 238, p. 194-217.
- James, A.T., and Baker, D.R., 1976, Oxygen isotope exchange between illite and water at 22°C: *Geochimica et Cosmochimica Acta*, v. 40, p. 235-239.

- Kendall, C., and Caldwell, E.A., 1998, Fundamentals of isotope geochemistry, *in* Kendall, C., and McDonnell, J.J., eds., Isotope tracers in catchment hydrology: Amsterdam, The Netherlands, Elsevier, p. 51-86.
- Kendall, C., and Coplen, T.B., 1985, Multisample conversion of water to hydrogen by Zn for stable isotope determination: *Analytical Chemistry*, v. 57, p. 1437-1440.
- Liu, B., Phillips, F., Hoines, S., Campbell, A.R., and Sharma, P., 1995, Water movement in desert soil traced by hydrogen and oxygen isotopes, chloride, and chlorine-36, southern Arizona: *Journal of Hydrology*, v. 168, p. 91-110.
- Mendez, G.O., and Christensen, A.H., 1997, Regional water table and water level changes in the Mojave River, the Morongo, and the Fort Irwin ground-water basins, San Bernardino County, California: U.S. Geological Survey Water-Resources Investigations Report 97-4189, 34 p.
- Michel, R.L., and Izbicki, J.A., 2002, Measurements of CFCs in the unsaturated zones of recharge sites in the Mojave Desert, USA: Proceedings of International Association of Hydrological Sciences conference on balancing the groundwater budget, Darwin, Australia, CD-ROM.
- Michel, R.L., Izbicki, J.A., and Martin, P., 1996, Use of tritium to estimate recharge under an intermittent wash in the Mojave Desert, Southern California (abstract): EOS, Transactions, American Geophysical Union, 1996 Fall Meeting, v. 77, no. 46, p. F263.
- National Oceanic and Atmospheric Administration, 1940-1994, California Climatological Data.
- Nimmo, J.R., Deason, J.A., Izbicki, J.A., Martin, P., 2002, Evaluation of unsaturated zone water fluxes in heterogeneous alluvium at a Mojave Basin Site: *Water Resources Research*, v. 38, no. 10, 1215.
- Nutting, P.G., 1943, Some standard thermal dehydration curves of minerals: U.S. Geological Survey Professional Paper 197-E, p. 197-217.
- Phillips, F.M., Peeters, L.A., Tansey, M.K., and Davis, S.N., 1986, Paleoclimatic inferences from an isotopic investigation of groundwater in the Central San Juan Basin, New Mexico: *Quaternary Research*, v. 26, p. 179-193.

- Plummer, L.N., Michel, R.L., Thurman, E.M., and Glynn, P.D., 1993, Environmental tracers for age dating young ground water, *in* Alley, W.M., ed., Regional ground-water quality: New York, New York, Van Nostrand Reinhold, p. 255-294.
- Rawlins, S.L., and Campbell, G.S., 1986, Water potential: Thermocouple psychrometry, *in* Klute, A., ed., Methods of soil analysis, part 1-physical and mineralogical methods (second edition): Madison, Wisconsin, Soil Science Society of America, Inc., Agronomy Series, no. 9, p. 597-618.
- Revesz, K., and Woods, P.H., 1990, A method to extract soil water for stable isotope analysis: *Journal of Hydrology*, v. 115, p. 397-406.
- Rust, B.R., 1979, Coarse Alluvial Deposits, *in* Walker, R.G., ed., Facies models: Geological Association of Canada, Geoscience Canada Reprint Series 1, p. 9-22.
- Savin, S.M., and Epstein, S., 1970, The oxygen and hydrogen isotope geochemistry of clay minerals: *Geochimica et Cosmochimica Acta*, v. 34, p. 25-42.
- Saxena, R.K., and Dressie, Z., 1983, Estimation of groundwater recharge and moisture movement in sandy formations by tracing natural oxygen-18 and injected tritium profiles in the unsaturated zone, *in* Isotope hydrology 1983: Vienna, Austria, International Atomic Energy Agency, p. 139-150.
- Scanlon, B.R., 1991, Evaluation of moisture flux from chloride data in desert soils: *Journal of Hydrology*, v. 128, p. 137-156.
- Sharp, R.P., and Nobles, L.H., 1953, Mudflow of 1941 at Wrightwood, southern California: *Bulletin of the Geological Society of America*, v. 64, p. 547-560.
- Shurbaji, A-R.M., Phillips, F.M., Campbell, A.R., and Knowlton, R.G., 1995, Application of a numerical model for simulating water flow, isotope transport, and heat transfer in the unsaturated zone: *Journal of Hydrology*, v. 171, p. 143-163.
- Smith, G.I., Friedman, I., Gleason, J.D., and Warden, A., 1992, Stable isotope composition of waters in southeastern California: 2. Groundwaters and their relation to modern precipitation: *Journal of Geophysical Research*, v. 97, no. D5, p. 5813-5823.
- Stewart, G.L., 1967, Fractionation of tritium and deuterium in soil water, *in* Stout, G. E., ed., Isotope techniques in the hydrologic cycle: Geophysical Monograph no. 11, p. 159-168.

- Stewart, G.L., and Stetson, J.R., 1975, Tritium and deuterium as water tracers in hydrologic systems: PB-248 408, National Technical Information Service, U.S. Department of Commerce, 44 p.
- Thatcher, L.L., Janzer, V.J., and Edwards, K.W., 1977, Methods for determination of radioactive substances in water and fluvial sediments: Techniques of Water-Resources Investigations of the United States Geological Survey, Chapter A-5, 95 p.
- U. S. Geological Survey, 1998, Mojave Desert Ecosystem Program, Mojave Desert Satellite Image Map, 1:750,000.
- Victor Valley Water District, 30 Sept. 2002, News.
<<http://www.vvwater.org/news.cfm?id=40>> (15 June 2004).
- Victorville, City of, 2004, Official Site for the City of Victorville.
<<http://www.ci.victorville.ca.us>> (15 June 2004).
- Walker, G.R., Woods, P.H., and Allison, G.B., 1994, Interlaboratory comparison of methods to determine the stable isotope composition of soil water: Chemical Geology (Isotope Geoscience Section), v. 111, p. 297-306.
- Weldon, R.J., and Sieh, K.E., 1985, Holocene rate of slip and tentative recurrence interval for large earthquakes on the San Andreas fault, Cajon Pass, southern California: Geological Society of America Bulletin, v. 96, p. 793-812.
- Yamanaka, T., and Yonetani, T., 1999, Dynamics of the evaporation zone in dry sandy soils: Journal of Hydrology, v. 217, p. 135-148.

APPENDIX A:
QUALITY ASSURANCE INVESTIGATIONS FOR SOIL-WATER STABLE-
ISOTOPE ANALYSES

Do the isotopic compositions of the extracted waters truly represent the soil-water isotopic composition of the material from which they were extracted? Previous studies have shown that the accuracy of the extraction technique, with respect to the isotopic composition of the extracted water, is reduced when applied to sediment with low water content and/or high clay content (Revesz and Woods, 1990; Ingraham and Shadel, 1992; Walker et al., 1994; Shurbaji et al., 1995). Also, Walker et al. (1994) found that incomplete soil-water extraction was the main reason for the large differences observed in an interlaboratory comparison of soil-water extraction techniques.

Because of the difficulties encountered in previous studies, the following procedures were included in the current study: 1) the yield of each distillation was determined; 2) duplicate distillations were performed on a random basis; 3) the water contents, the soil-water potentials, and the particle-size distributions of the samples were compared with distillation yields to determine if sample properties affected distillation yield; and 4) distillation experiments were performed to determine the accuracy and reproducibility of the technique. In the following pages, the methods, results, and conclusions about the effectiveness of the technique and the validity of the isotopic data obtained from the extracted soil waters are discussed.

Methods

Yields

The yield of each distillation was calculated based upon an expected yield determined from the amount of sample material used in the distillation and the

gravimetric-water content of the sample material. Separate subsamples from the same core sample were used for soil-water extraction and determination of gravimetric-water content. Therefore, distillation yields should be considered approximate due to the spatial variability of water content within the core materials.

Duplicate Distillations and Isotopic Analyses

Thirty-six (22%) of the samples were run in duplicate. Each duplicate distillation consisted of subsamples of material taken from the same core sample, but distilled and analyzed for isotopic composition individually. Some variation in water content and isotopic composition was possible due to spatial variability within the core sample.

Correlation of Yields to Sample Properties

The gravimetric-water contents, soil-water potentials, and fine-sediment contents (<0.074 mm) of the samples were plotted against the distillation yields to determine if any correlations between sample properties and distillation yield existed.

Distillation Experiments

Water-toluene Distillations. Mixtures of water of known isotopic composition and toluene were distilled in the absence of soil material to determine the accuracy of the extraction technique. Twelve distillations were performed, four using 2 ml of water, four using 5 ml of water, and four using 10 ml of water to determine if water amount had any effect upon the isotopic compositions of the extracted waters.

Quartz-sand Rehydration. A quartz sand was cleaned, oven-dried at 105°C, and rehydrated with water of known isotopic composition. Twelve distillations were performed, four at 2% water by weight, four at 5% water by weight, and four at 10% water by weight. After one week of equilibration time, during which they were shaken several times a day to evenly distribute water, the waters were extracted.

Field-sample Rehydration. Twelve field samples were selected to represent the range of properties seen in the sample population. The sample materials were oven-dried at 105°C and then rehydrated to their original water content with water of known isotopic composition. After one week of equilibration time, during which they were shaken several times a day to evenly distribute water, the waters were extracted. Four of the selected samples were run in duplicate. For plotting and data interpretation the averages of the duplicate distillation yields and isotopic analyses were used.

Results

Distillation Yields

Distillation yields had a range of 56.4 % to 135.8 % (Table A-1) with a mean of 100.5 % and a standard deviation of 11.6 % (a complete list of distillation yields can be found in Appendix C). A histogram of the distillation yields (Fig. A-1) indicates a normal distribution about the mean. Also, as shown in Table A-1, the distribution of yields between the two washes and individual boreholes was quite uniform.

Table A-1. Distillation yields.

Sample Set	n	Minimum % Yield	Maximum % Yield	Mean % Yield
All	149	56.4	135.8	100.5
OGW	116	56.4	107.9	99.6
SCW	33	81.7	135.8	101.0
Summit	5	84.7	122.9	98.4
UOGW	21	97.7	131.8	107.9
MOGW	40	78.2	121.7	99.5
LOGW-1	15	67.0	130.4	100.5
LOGW-2	5	92.7	100.5	95.1
OGF	30	56.4	110.5	96.4
USCW	5	91.6	111.3	99.5
MSCW	17	88.4	123.1	102.9
LSCW	5	84.8	102.5	94.8
SCF	6	81.7	135.8	106.7

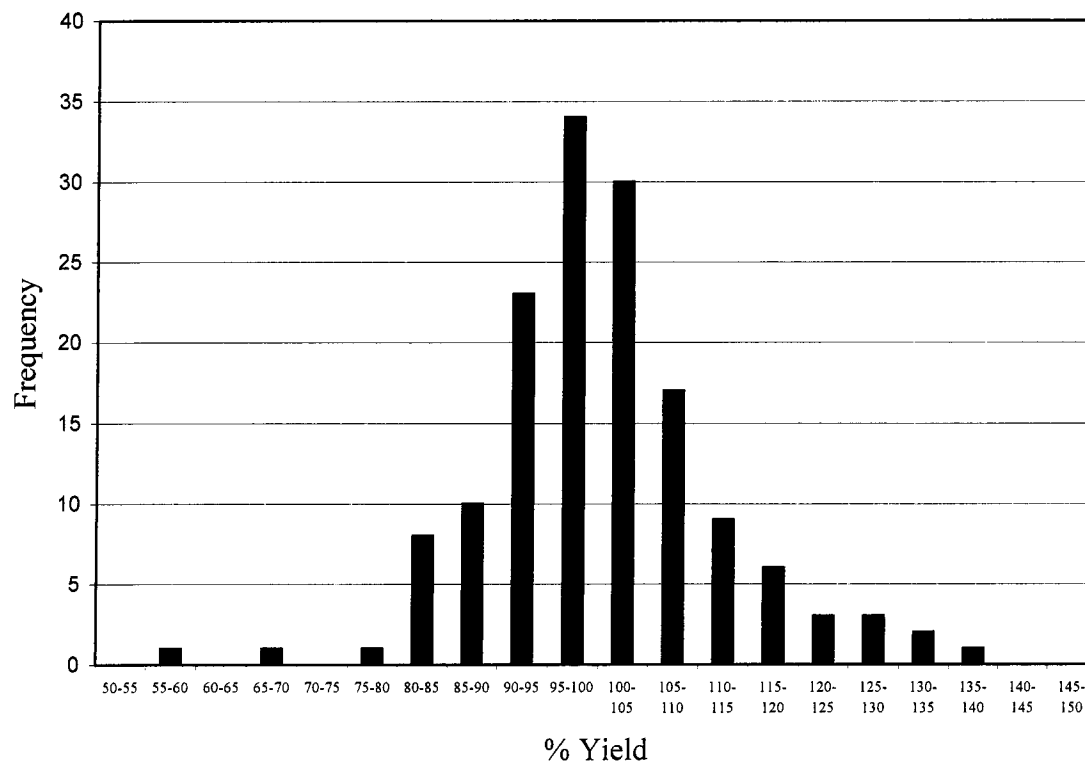


Figure A-1. Distillation yield histogram.

Duplicate Distillations and Isotopic Analyses

The results of the duplicate distillations and isotopic analyses are given in Table A-2. The mean absolute difference in yields for the 35 duplicate distillations was 7.4 % with a standard deviation of 6.2 %. The mean absolute difference in δD was 1.5 o/oo with a standard deviation of 1.3 o/oo. The mean absolute difference in $\delta^{18}O$ was 0.16 o/oo with a standard deviation of 0.12 o/oo. The standard deviations for the duplicate isotopic analyses were close to the precision of analysis.

Correlations with Sample Properties

Plots of distillation yield versus water content, soil-water potential, and percent fines (<0.074 mm) are shown in Figures A-2 through A-4. The figures show no apparent correlations between the sample properties and distillation yield.

Distillation Experiments

Water-toluene Distillations. The results of the water-toluene distillations are shown in Table A-3. The results show that the oxygen isotopic compositions of the extracted waters were slightly more positive than their original composition, but the differences were very close to the precision of analysis. The fact that all of the extracted waters had slightly more positive compositions suggests slight evaporative enrichment, possibly as a result of the paraffin treatment performed to remove residual toluene from the extracted waters.

Table A-2. Results of Duplicate* Distillations and Isotopic Analyses.

Sample ID	% Yield		δD (o/oo)		$\delta^{18}O$ (o/oo)	
	A	B	A	B	A	B
Summit 13-13.5	92.1	77.2	-74.3	-76.2	-10.22	-10.26
Summit 28-28.5	99.6	99.8	-71.3	-69.8	-9.43	-9.31
UOGW 9-9.5	97.7	99.6	-54.7	-51.8	-8.03	-8.05
UOGW 14.5-15	105.1	100.3	-51.4	-56.7	-8.15	-8.52
UOGW 28.8-29.3	107.3	114.5	-62.3	-61.1	-9.18	-9.29
MOGW 8.5-9	98.1	79.2	-71.1	-71.5	-10.18	-10.31
MOGW 20.5-21	107.1	113.2	-72.9	-70.4	-10.33	-10.34
MOGW 34-34.5	96.6	83.2	-71.0	-73.0	-10.07	-9.95
MOGW 54-54.5	107.4	96.6	-78.8	-76.1	-10.44	-10.65
MOGW 64-64.5	104.3	107.7	-80.1	-77.9	-11.14	-10.93
MOGW 69-69.5	97.9	99.6	-68.0	-66.1	-9.66	-9.76
MOGW 85-85.5	104.1	113.8	-67.7	-73.2	-9.66	-9.58
MOGW 118.5-119	102.0	90.0	-72.1	-73.3	-9.75	-9.46
LOGW1 8-8.5	96.4	98.9	-61.9	-59.8	-7.41	-7.32
LOGW1 28.5-29	132.3	123.2	-77.7	-78.4	-9.97	-10.05
LOGW2 28-28.5	95.0	94.0	-77.0	-76.8	-8.26	-8.52
LOGW2 73-73.5	91.7	93.7	-82.3	-83.1	-10.25	-10.57
OGF 43.5-44	91.6	93.2	-69.8	-70.3	-6.54	-6.21
OGF 64-64.5	86.3	79.5	-77.6	-77.4	-8.28	-8.31
OGF 78.5-79	95.4	95.7	-81.3	-82.0	-9.12	-9.09
OGF 88.5-89	95.4	97.8	-78.6	-78.5	-9.69	-9.46
OGF 93.5-94	91.8	95.1	-81.1	-82.6	-10.26	-10.13
OGF 104.5-105	96.9	97.5	-76.6	-76.3	-9.58	-9.19
USCW 54.5-55	94.9	102.9	-76.9	-77.6	-8.71	-8.88
MSCW 23.5-24	95.4	108.6	-78.7	-78.1	-8.90	-8.73
MSCW 43.5-44	95.9	104.1	-89.2	-86.2	-8.92	-8.65
MSCW 90.5-91	130.4	103.0	-88.4	-89.5	-10.95	-11.14
MSCW 109.5-110	107.2	100.6	-85.0	-84.3	-8.34	-8.35
MSCW2 259.5-260	92.6	101.7	-90.6	-87.7	-10.71	-10.68
MSCW 302.5-303	101.8	98.0	-95.2	-93.9	-11.96	-11.89
MSCW2 400.5-401	97.3	102.7	-89.4	-88.5	-10.91	-10.98
LSCW 34.5-35	82.6	87.0	-85.1	-85.2	-7.08	-7.54
LSCW 59.5-60	94.6	101.8	-80.9	-80.3	-7.25	-7.06
LSCW 99.5-100	102.5	NA	-88.2	-87.4	-8.80	-9.09
SCF 17.5-18	71.0	92.3	-77.6	-77.0	-6.65	-6.60
SCF 47.5-48	99.2	109.3	-88.4	-89.3	-7.87	-7.85

*A and B are separate subsamples taken from the same core.

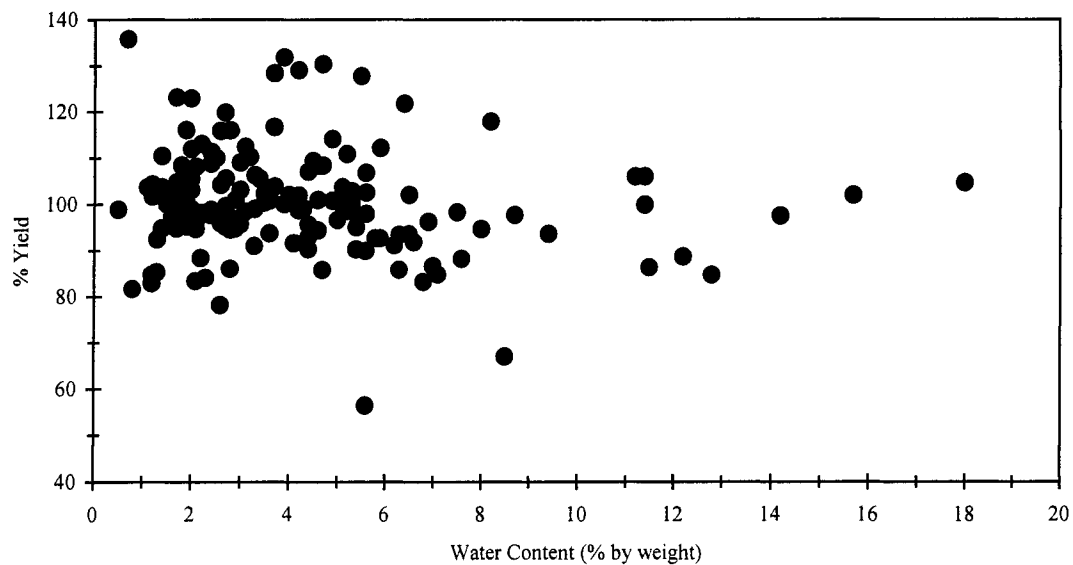


Figure A-2. Distillation yield versus water content.

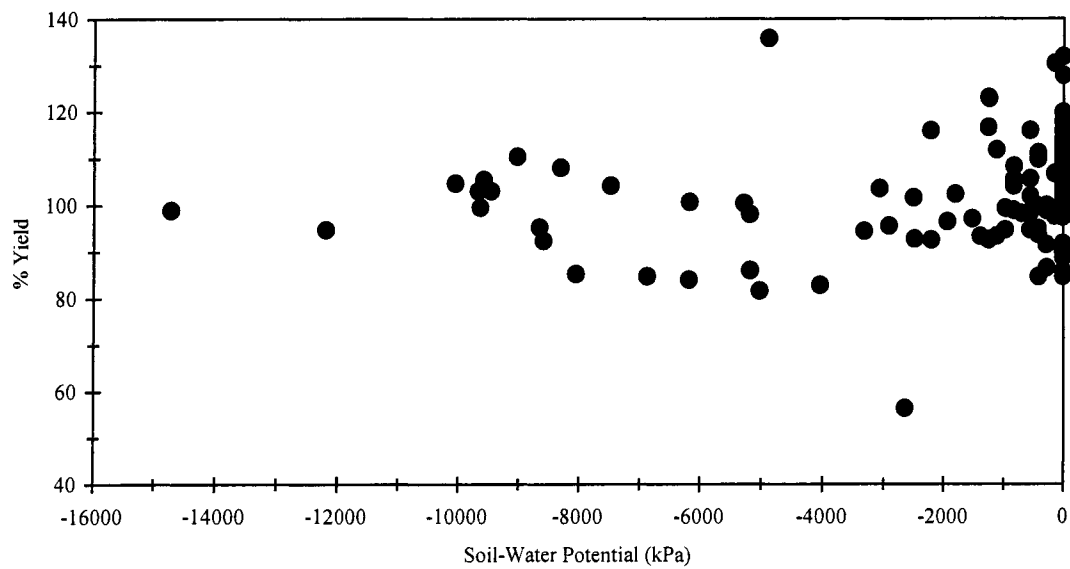


Figure A-3. Distillation yield versus soil-water potential.

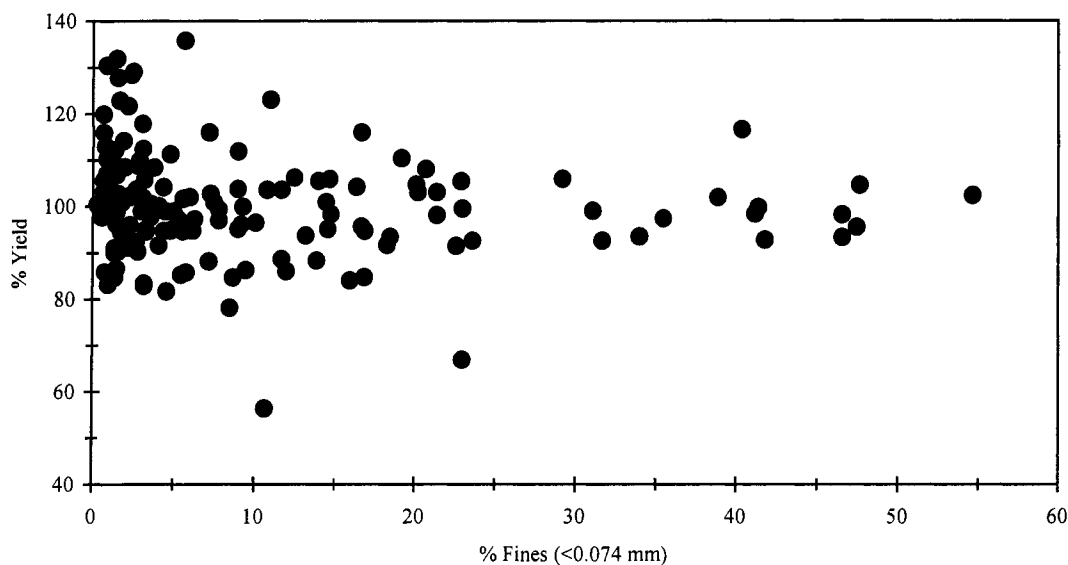


Figure A-4. Distillation yield versus percent fines.

Quartz-sand Rehydrations. The results of the twelve quartz-sand rehydrations are given in Table A-4. Almost all of the extracted waters had slightly more negative isotopic compositions than their original composition, but the differences were close to the precision of analysis. Distillation yields were, with one exception, slightly greater than 100 %, indicating that small amounts of toluene had been decanted with the water.

Field-sample Rehydrations. The results of the field-sample rehydrations are shown in Table A-5. The extracted waters from all of the samples had more negative isotopic compositions than their original composition. The depletions observed in the extracted waters were as great as 9.8 o/oo and 2.53 o/oo for δD and $\delta^{18}O$, respectively.

Table A-3. Results of water-toluene distillations. Isotopic composition of water used for all distillations was defined as -81.5 o/oo and -11.64 o/oo for δD and $\delta^{18}O$, respectively.

Sample ID	δD	$\delta^{18}O$	% Yield
2 ml #1	-82.9	-11.44	98.4
2 ml #2	-82.5	-11.46	113.6*
2 ml #3	-81.4	-11.39	104.8
2 ml #4	-83.4	-11.37	106.1
2 ml Mean	-82.6	-11.42	105.7
5 ml #1	-83.4	-11.44	102.1
5 ml #2	-82.2	-11.50	103.0
5 ml #3	-82.6	-11.46	104.4
5 ml #4	-82.6	-11.60	101.7
5 ml Mean	-82.7	-11.50	102.8
10 ml #1	-83.9	-11.43	101.0
10 ml #2	-82.8	-11.47	102.6
10 ml #3	-82.5	-11.48	104.3
10 ml #4	-84.7	-11.62	102.3
10 ml Mean	-83.5	-11.50	102.6

*An obvious excess of toluene was decanted from the collection funnel with the extracted water.

The mean absolute difference in yields for the 4 duplicate distillations was 1.5 % with a standard deviation of 0.8 %. The mean absolute difference in δD for the 4 duplicate distillations was 0.5 o/oo with a standard deviation of 0.3 o/oo. The mean absolute difference in $\delta^{18}O$ for the 4 duplicate distillations was 0.19 o/oo with a standard deviation of 0.22 o/oo. A δD vs $\delta^{18}O$ plot of the results (Figure A-5) compared to the original isotopic composition of the rehydrating water shows that the extracted waters had more negative compositions. The three driest samples, with hydration levels of 2 % or less, had the most negative isotopic compositions, but above the 2 % level of hydration there

Table A-4. Results of quartz-sand rehydration distillations. Isotopic composition of water used for rehydration was defined as -81.5 o/oo and -11.64 o/oo for δD and $\delta^{18}O$, respectively.

Sample ID	δD	$\delta^{18}O$	% Yield
2 % #1	-83.8	-11.88	102.6
2 % #2	-85.8	-11.96	102.4
2 % #3	-83.2	-11.77	107.1*
2 % #4	-83.1	-11.68	99.6
2 % Mean	-84.0	-11.82	102.9
5 % #1	-82.3	-11.83	102.3
5 % #2	-82.7	-11.50	103.1
5 % #3	-84.3	-11.67	101.8
5 % #4	-83.4	-11.58	101.7
5 % Mean	-83.2	-11.65	102.2
10 % #1	-84.1	-11.77	101.0
10 % #2	-84.8	-11.74	101.9
10 % #3	-81.8	-11.72	100.9
10 % #4	-84.4	-11.63	102.6
10 % Mean	-83.8	-11.72	101.6

*An obvious excess of toluene was decanted from the collection funnel with the extracted water.

was no correlation between water content and isotopic depletion. The distillation yields for most of the samples were slightly greater than 100 %, but four of the distillations had yields of less than 100 %. Incomplete extraction of the rehydrating water would result in more negative isotopic compositions of the extracted waters relative to their original composition. To check for possible incomplete water extraction, the δD and $\delta^{18}O$ depletions of the extracted waters were plotted against several Rayleigh recovery curves (Figure A-6). The amount of depletion seen in the extracted waters with distillation yields less than 100 % was greater than that predicted by the Rayleigh recovery curves,

Table A-5. Results of field-sample rehydration distillations. Isotopic composition of water used for rehydration was defined as -81.5 o/oo and -11.64 o/oo for δD and $\delta^{18}O$, respectively.

Sample ID	% Water (by wt.)	δD	$\delta^{18}O$	% Yield
MOGW 80.5-81A*	3.3	-83.2	-12.31	101.9
MOGW 80.5-81B*	3.3	-83.9	-12.37	102.4
MOGW 69-69.5	2.4	-83.7	-12.17	102.7
USCW 54.5-55	2.7	-83.8	-12.07	100.2
OGF 28.66-29A*	1.4	-91.1	-13.66	92.7
OGF 28.66-29B*	1.4	-91.0	-14.17	94.8
UOGW 9.5-10	4.2	-85.6	-12.04	102.6
OGF 83.5-84	4.7	-82.3	-11.70	102.2
MSCW 159.5-160	2.0	-89.5	-12.91	105.1
MSCW 240.5-241	5.4	-83.8	-12.18	102.4
OGF 68.5-69A*	5.6	-82.5	-11.90	103.3
OGF 68.5-69B*	5.6	-83.3	-11.75	101.0
SCF 47.5-48	1.2	-91.3	-13.87	98.5
LOGW 73.33-73.66	18.0	-84.7	-12.48	99.1
MSCW 302.5-303A*	11.4	-85.2	-12.24	102.9
MSCW 302.5-303B*	11.4	-84.8	-12.19	101.8

*Indicates that rehydration was performed in duplicate for that sample. A and B are separate subsamples from the same core.

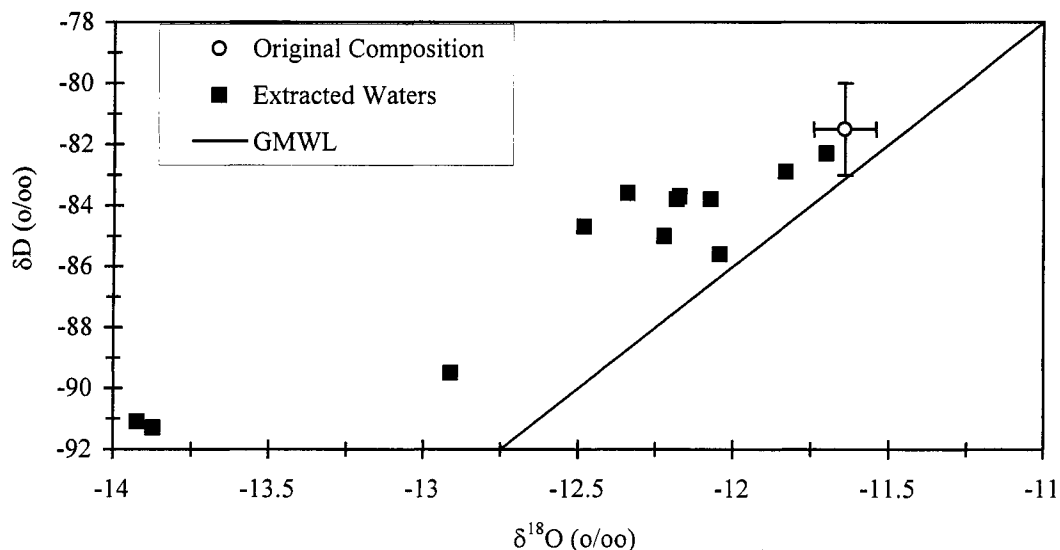
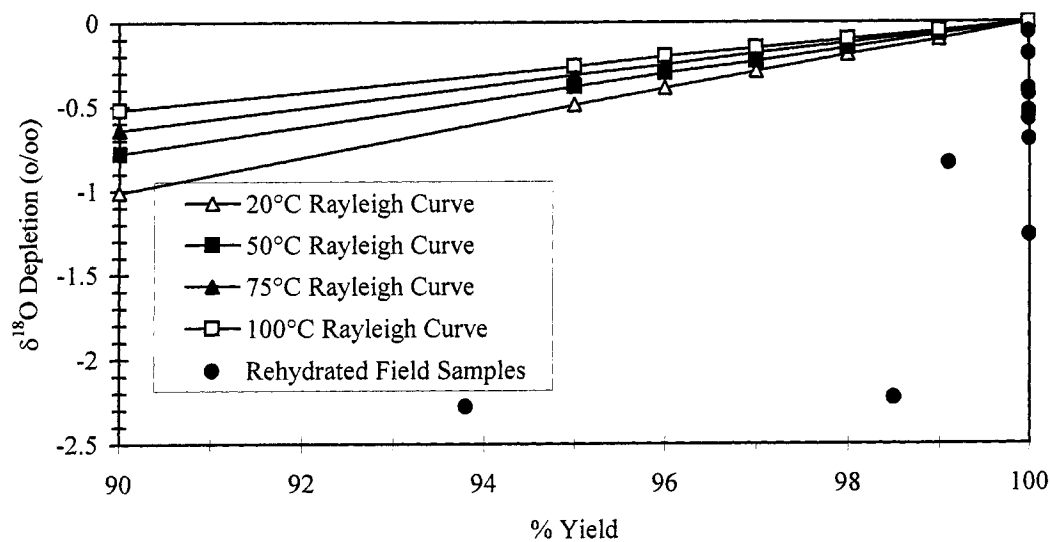


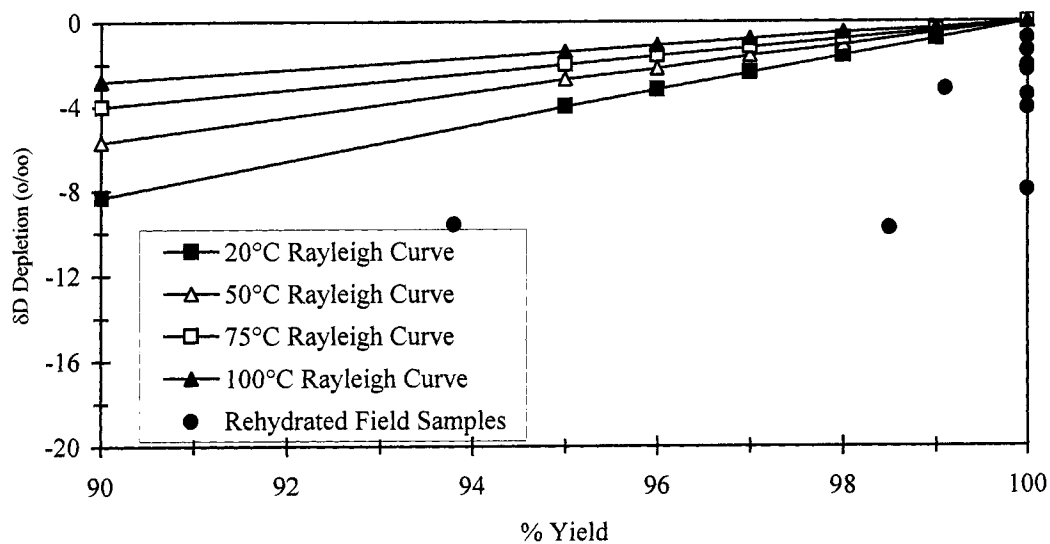
Figure A-5. δD vs $\delta^{18}O$ plot of field-sample rehydration results. Error bars on original composition indicate the precision of analysis at the 1-sigma level.

therefore ruling out incomplete extraction as the cause of the observed isotopic depletions.

Another factor that was considered as a possible cause of the observed depletions in the isotopic compositions of the extracted rehydrating waters was the original composition of the soil waters (field isotopic composition, before oven-drying). It is possible that the amount of isotopic depletion seen in the extracted water could be related to the difference between the original field isotopic composition of the sample and the isotopic composition of the rehydrating water. The amount of isotopic depletion versus the difference between field isotopic composition and rehydrating water isotopic composition was examined (Figure A-7). The majority of the field waters had more positive isotopic compositions than the rehydrating water. Although the sample with the

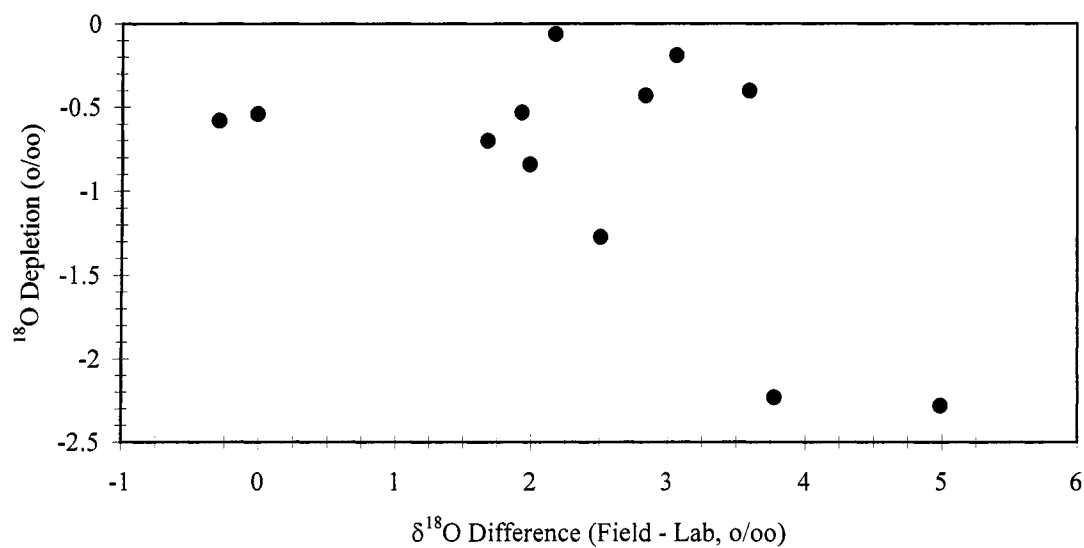


a) ^{18}O depletion versus distillation yield.

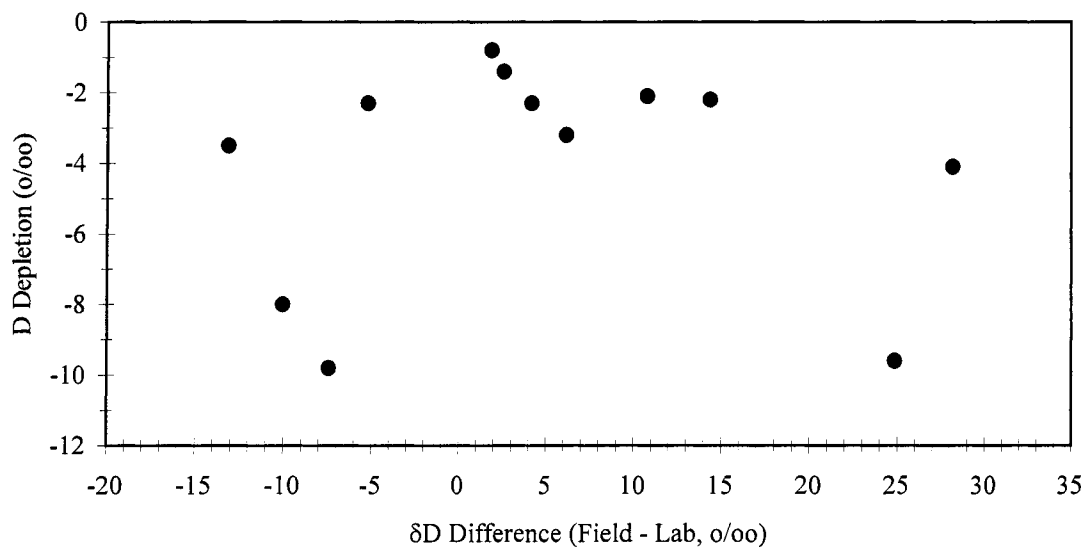


b) D depletion versus distillation yield.

Figure A-6. Isotopic depletion versus distillation yield. As predicted by Rayleigh curves and observed in rehydrated field samples.



a) ^{18}O depletion versus $\delta^{18}\text{O}$ difference between field and laboratory rehydrating water.



b) D depletion versus δD difference between field and laboratory rehydrating water.

Figure A-7. Isotopic depletion versus difference in isotopic composition between field and laboratory rehydrating water.

largest difference between field $\delta^{18}\text{O}$ and rehydrating water $\delta^{18}\text{O}$ did undergo the greatest depletion, the rest of the samples showed no correlation.

Discussion

The toluene distillations appear to have been effective at removing water from the sample materials. The normal distribution of yields about the mean, the similarity of yields and isotopic compositions of the waters from the samples distilled in duplicate, and the lack of correlation between sample properties and distillation yields suggest that the range of the yields is the result of natural variation in the water content of the sample materials.

The water-toluene distillation results indicated that slight evaporative enrichment might occur as a result of the distillation and paraffin treatment. However, the observed effects were very close to the precision of analysis. The quartz-sand rehydrations showed the toluene distillation method to be effective at removing and preserving the original isotopic composition of the hydrating water. The results of the field-sample rehydrations were less successful because all of the extracted waters displayed varying amounts of isotopic depletion relative to the original isotopic composition of the hydrating water. The results of the rehydration experiments were not unlike those seen in other studies, where the differences in isotopic composition have been attributed to the exchange of the hydrating water with water associated with minerals in the sample materials (Stewart and Stetson, 1975; Ingraham and Shadel, 1992; and Araguas-Araguas et al., 1995). Oven drying at 105°C does not completely remove the water contained in the sample materials.

Water remains adsorbed on the surfaces, between the layers, or in the structures of the minerals composing the sample. At 105°C, quartz or feldspar contains about 0.5 % water by weight and clay minerals can contain as much as 16 % by weight of adsorbed, interlayer, and structural water (Nutting, 1943). At high water content and/or low clay content, the isotopic effects of exchange with the “bound” waters associated with the sample materials are negligible, but at low water content and/or high clay content, the bound waters become a significant percentage of the total water in the sample and the isotopic effects of exchange between the mobile and bound waters are observed. Isotopic exchange between adsorbed and interlayer waters and mobile water or water vapor occurs almost immediately (Stewart, 1967; Savin and Epstein, 1970; and Stewart and Stetson, 1975), whereas exchange with structural waters may or may not occur. Isotopic exchange between structural waters found in clay and clay-like minerals is thought to be controlled by the accessibility of the structural waters (Stewart, 1967; and James and Baker, 1976). Fresh, unweathered mineral surfaces with no structural imperfections permit little access of mobile waters to the structural waters, whereas weathered mineral surfaces or those with structural imperfections allow access of mobile waters to the structural waters.

Sample materials from the study area contain small amounts of clay, but some samples, particularly those from Sheep Creek Wash, contain large amounts of muscovite, a clay-like mineral. The muscovite is obtained from weathering of the Pelona schist, which contains between 15 and 45 % muscovite (Ehlig, 1958). A correlation between the relative proportions of muscovite in the field rehydration samples and the amount of

isotopic depletion observed in the extracted waters is not apparent. It is likely that mineral condition, and not amount, is the factor controlling the amount of isotopic depletion observed. Because the investigations required to determine the accessibility of the structural waters contained in the sample materials are beyond the scope of this thesis, all that can be said is that the results of the field-sample rehydration experiments indicate that contact with minerals contained in the unsaturated-zone sediment may have altered the isotopic compositions of the extracted soil waters.

The results of the rehydration experiments performed in this and other studies suggest that interaction between the hydrating waters and bound waters remaining in the sample materials can produce significant changes in the isotopic composition of the hydrating water. However, it is uncertain how applicable the results of the rehydration experiments are to field conditions. Under field conditions, the isotopic compositions of the mobile and bound waters in the unsaturated zone probably had reached a state of equilibrium. The rehydration procedure undoubtedly disturbed any equilibrium that existed in the sample materials. The removal of water by oven-drying, rehydration with water that may or may not have been similar in isotopic composition to the original water, and a relatively short period of equilibration may have produced isotopic effects not representative of field conditions. Under field conditions, the interaction of mobile and bound waters may produce isotopic effects of smaller magnitude than those observed in the rehydration experiments.

Conclusions

A mean distillation yield of 100.5 %, a normal distribution of distillation yields about the mean, a lack of correlation between sample properties and distillation yield, and the results of duplicate distillations and isotopic analyses all indicate that the toluene distillations were successful at removing the mobile water from the sample materials. It seems unlikely that incomplete extraction of soil water is a factor to be considered when assessing the validity of the isotopic data obtained from the extracted soil waters in this study. However, the results of the rehydration experiments suggest that the isotopic compositions of the extracted soil waters can be altered through interaction with waters adsorbed on the surfaces or contained in the structures of the minerals composing the unsaturated-zone sediment. Waters extracted from sediment with low water and/or high muscovite content may have undergone the largest alterations in isotopic composition, but the results of the rehydration experiments may not be applicable to field conditions.

It is not possible to determine the effect, if any, that interaction with minerals contained in the unsaturated-zone sediment had upon infiltrated waters, but it is possible to compare the isotopic compositions of the extracted soil waters with the isotopic compositions of precipitation, streamflow, snow, lysimeter samples, and water vapor collected as part of the study. Comparison with the water-vapor samples should be particularly useful, because the isotopic composition of vapor should reflect the isotopic composition of soil water. If comparisons within the stable-isotope dataset are favorable, then the stable-isotope data should be compared and combined with other hydrologic, geologic, and geochemical information.

In conclusion, a careful comparison of the isotopic compositions of the extracted soil waters with the isotopic compositions of other water samples collected as part of the study, and the relationships existing between them, should indicate the validity of the soil-water data. If agreement within the stable-isotope dataset exists, then the isotopic data can be compared and combined with the results of other hydrologic, geologic, and geochemical methods to interpret the processes occurring in the unsaturated zone beneath the stream channels.

APPENDIX B:

CORE AND HAND-AUGER MATERIAL PARTICLE-SIZE DISTRIBUTIONS

Table B1. Particle-size distributions of core and hand-auger materials

Sample ID	Depth	Percent Distribution					
		>16 mm	Gravel 4-16 mm	2-4 mm	Sand 2-0.35 mm	Sand 0.35-0.074 mm	Very Fine Sand, Silt & Clay <0.074 mm
SUMMIT 8-8.5	2.52 m (8.25 ft.)	0.0	4.4	16.5	67.7	9.9	1.5
SUMMIT 13-13.5	4.04 m (13.25 ft.)	0.0	10.0	15.0	64.0	9.6	1.4
SUMMIT 23-23.5	7.09 m (23.25 ft.)	0.0	1.9	4.7	67.3	25.0	1.1
SUMMIT 28-28.5	8.61 m (28.25 ft.)	0.0	2.9	11.4	64.9	19.5	1.3
SUMMIT 48-48.5	14.71 m (48.25 ft.)	0.0	15.3	21.5	50.3	11.2	1.7
UOGW 6"	0.15 m (0.5 ft.)	0.0	5.3	11.5	64.5	17.2	1.5
UOGW 12"	0.3 m (1 ft.)	0.0	11.9	10.4	58.8	16.7	2.2
UOGW 18"	0.46 m (1.5 ft.)	0.0	2.8	7.6	67.4	19.2	3.0
UOGW 24"	0.61 m (2 ft.)	0.0	4.7	17.6	60.4	14.1	3.2
UOGW 30"	0.76 m (2.5 ft.)	0.0	3.0	9.4	65.8	18.8	3.0
UOGW 36"	0.91 m (3 ft.)	0.0	1.8	13.2	57.3	23.3	4.4
UOGW 42"	1.07 m (3.5 ft.)	0.0	15.9	9.6	55.7	15.9	2.9
UOGW 48"	1.22 m (4 ft.)	0.0	2.2	15.7	63.8	15.2	3.1
UOGW 54"	1.37 m (4.5 ft.)	0.0	10.1	10.0	50.7	25.4	3.8
UOGW 60"	1.52 m (5 ft.)	0.0	9.6	10.5	65.0	14.0	0.9
UOGW 72"	1.83 m (6 ft.)	0.0	7.6	15.3	63.6	12.2	1.3
UOGW 84"	2.13 m (7 ft.)	0.0	11.2	11.9	58.8	14.5	3.6
UOGW 96"	2.44 m (8 ft.)	0.0	10.4	16.4	56.9	14.4	1.9
UOGW 108"	2.74 m (9 ft.)	0.0	3.7	17.7	63.8	13.4	1.4
UOGW 9-9.5	2.82 m (9.25 ft.)	0.0	5.1	13.2	56.0	22.0	3.7
UOGW 14.5-15	4.5 m (14.75 ft.)	0.0	10.5	16.8	60.3	10.8	1.6
UOGW 20.5-21	6.33 m (20.75 ft.)	0.0	5.7	13.5	72.1	8.1	0.6
UOGW 28.8-29.3	8.86 m (29.05 ft.)	0.0	8.9	11.1	66.9	12.1	1.0
UOGW 54.5-55	16.69 m (54.75 ft.)	0.0	33.5	17.5	37.9	9.3	1.8
UOGW 68.5-69	20.96 m (68.75 ft.)	0.0	57.5	10.3	20.6	9.2	2.4

Sample ID	Depth	Percent Distribution					
		>16 mm	Gravel 4-16 mm		2-4 mm	2-0.35 mm	Sand 0.35-0.074 mm
UOGW 84.5-85	25.84 m (84.75 ft.)	30.2	11.5	8.4	25.6	19.3	5.0
UOGW 104-104.5	31.78 m (104.25 ft.)	24.2	20.9	14.2	27.7	10.5	2.5
MOGW 6" *	0.15 m (0.5 ft.)	0.0	12.4	4.7	49.5	30.3	3.1
MOGW 12" *	0.3 m (1 ft.)	0.0	1.5	7.8	66.5	21.9	2.3
MOGW 18" *	0.46 m (1.5 ft.)	0.0	3.3	9.0	59.4	25.5	2.8
MOGW 24" *	0.61 m (2 ft.)	0.0	1.9	6.5	59.8	29.8	2.0
MOGW 30" *	0.76 m (2.5 ft.)	0.0	1.4	10.3	82.7	5.3	0.3
MOGW 36" *	0.91 m (3 ft.)	0.0	6.7	13.8	72.4	6.9	0.2
MOGW 42" *	1.07 m (3.5 ft.)	0.0	0.4	3.1	83.4	12.3	0.8
MOGW 48" *	1.22 m (4 ft.)	0.0	1.2	10.9	76.2	10.7	1.0
MOGW 54" *	1.37 m (4.5 ft.)	0.0	1.2	12.4	76.5	9.2	0.7
MOGW 60" *	1.52 m (5 ft.)	0.0	7.0	17.9	64.4	10.0	0.7
MOGW 66" *	1.68 m (5.5 ft.)	0.0	7.1	17.3	68.4	6.5	0.7
MOGW ~72" *	1.83 m (6 ft.)	0.0	3.9	12.8	74.8	7.8	0.7
MOGW 72" *	1.83 m (6 ft.)	0.0	0.0	2.5	61.0	27.8	8.7
MOGW 84" *	2.13 m (7 ft.)	0.0	26.5	11.5	44.4	16.1	1.5
MOGW 96" *	2.44 m (8 ft.)	0.0	9.2	11.4	59.8	18.3	1.3
MOGW 8.5-9	2.67 m (8.75 ft.)	0.0	3.7	4.7	47.2	32.7	11.7
MOGW 13.5-14	4.19 m (13.75 ft.)	0.0	0.0	1.3	33.9	57.5	7.3
MOGW 20.5-21	6.33 m (20.75 ft.)	0.0	5.0	9.4	66.9	17.8	0.9
MOGW 23.5-24	7.24 m (23.75 ft.)	0.0	23.4	26.9	37.3	11.6	0.8
MOGW 29-29.5	8.92 m (29.25 ft.)	0.0	8.6	5.7	67.6	16.5	1.6
MOGW 34-34.5	10.44 m (34.25 ft.)	0.0	22.0	19.7	49.4	7.5	1.4
MOGW 39.5-40	12.12 m (39.75 ft.)	0.0	1.9	11.1	73.2	12.8	1.0
MOGW 44-44.5	13.49 m (44.25 ft.)	0.0	0.3	10.0	76.4	10.2	3.1
MOGW 49-49.5	15.02 m (49.25 ft.)	36.3	28.4	7.3	19.6	7.3	1.1

Sample ID	Depth	Percent Distribution					
		Gravel			Sand		Very Fine Sand, Silt & Clay < 0.074 mm
		>16 mm	4-16 mm	2-4 mm	2-0.35 mm	0.35-0.074 mm	
MOGW 54-54.5	16.54 m (54.25 ft.)	0.0	2.0	15.5	70.4	10.8	1.3
MOGW 59-59.5	18.06 m (59.25 ft.)	0.0	19.6	19.6	51.7	7.6	1.5
MOGW 64-64.5	19.59 m (64.25 ft.)	0.0	0.9	4.6	47.3	32.5	14.7
MOGW 69-69.5	21.11 m (69.25 ft.)	0.0	12.7	6.4	56.1	23.3	1.5
MOGW 75-75.5	22.94 m (75.25 ft.)	0.0	34.8	16.6	31.1	15.2	2.3
MOGW 80.5-81	24.62 m (80.75 ft.)	0.0	13.6	16.4	47.5	21.1	1.4
MOGW 85-85.5	25.99 m (85.25 ft.)	0.0	16.9	17.6	55.4	8.8	1.3
MOGW 89.5-90	27.36 m (89.75 ft.)	0.0	33.5	13.7	35.6	13.9	3.3
MOGW 95-95.5	29.04 m (95.25 ft.)	0.0	2.9	4.8	10.7	62.7	18.9
MOGW 99.5-100	30.41 m (99.75 ft.)	0.0	0.0	5.3	29.3	53.7	11.7
MOGW 118.5-119	36.2 m (118.75 ft.)	0.0	33.7	16.3	36.2	11.5	2.3
MOGW 160-160.5	48.86 m (160.25 ft.)	0.0	0.7	2.0	14.4	48.9	34.0
MOGW 178	54.34 m (178.25 ft.)	0.0	0.0	6.8	63.2	22.2	7.8
MOGW 218-218.5	66.54 m (218.25 ft.)	0.0	4.0	14.3	53.0	21.5	7.2
MOGW 239.5-240	73.09 m (239.75 ft.)	0.0	5.8	10.3	61.8	18.9	3.2
MOGW 260-260.5	79.34 m (260.25 ft.)	0.0	5.1	6.0	46.0	34.4	8.5
MOGW 320	97.48 m (319.75 ft.)	0.0	0.0	0.9	62.1	31.4	5.6
MOGW 360.7-361.2	110.05 m (360.95 ft.)	0.0	1.7	8.0	60.8	28.0	1.5
MOGW 419.3-419.8	127.91 m (419.55 ft.)	0.0	39.8	23.1	26.0	8.9	2.2
MOGW 480-480.5	146.42 m (480.25 ft.)	0.0	9.9	2.8	43.4	34.4	9.5
LOGW 8-8.5	2.52 m (8.25 ft.)	0.0	7.5	17.3	68.0	6.6	0.6
LOGW 12.5-13	3.89 m (12.75 ft.)	0.0	8.4	9.1	59.6	22.0	0.9
LOGW 18.5-19	5.72 m (18.75 ft.)	0.0	0.6	2.4	77.7	18.8	0.5
LOGW 28.5-29	8.77 m (28.75 ft.)	0.0	13.5	5.1	68.3	11.5	1.6
LOGW 44.5-45	13.64 m (44.75 ft.)	0.0	0.0	0.8	5.3	55.0	38.9
LOGW 63.66-64	19.46 m (63.83 ft.)	0.0	0.0	1.7	47.2	43.6	7.5

Sample ID	Depth	Percent Distribution					
		>16 mm	Gravel 4-16 mm	2-4 mm	2-0.35 mm	Sand 0.35-0.074 mm	Very Fine Sand, Silt & Clay < 0.074 mm
LOGW 68.5-69	20.96 m (68.75 ft.)	0.0	0.0	0.7	19.8	61.2	18.3
LOGW 73.33-73.66	22.41 m (73.5 ft.)	0.0	0.0	0.5	7.8	44.0	47.7
LOGW 73.66-74	22.51 m (73.83 ft.)	0.0	0.0	1.0	11.3	52.2	35.5
LOGW 78.66-79	24.03 m (78.83 ft.)	0.0	12.3	1.3	8.6	48.6	29.2
LOGW 88.33-88.66	26.98 m (88.5 ft.)	0.0	0.0	0.4	19.3	57.7	22.6
LOGW 88.66-89	27.08 m (88.83 ft.)	0.0	0.0	0.0	25.5	59.7	14.8
LOGW 93.66-94	28.61 m (93.83 ft.)	0.0	0.0	1.2	16.3	59.5	23.0
LOGW 98.33-98.66	30.03 m (98.5 ft.)	0.0	0.9	0.0	0.6	51.9	46.6
LOGW 98.66-99	30.13 m (98.83 ft.)	0.0	0.0	0.0	3.2	50.2	46.6
LOGW2 8-8.5	2.52 m (8.25 ft.)	0.0	18.3	16.6	42.3	19.2	3.6
LOGW2 28-28.5	8.61 m (28.25 ft.)	0.0	20.0	22.3	41.0	13.4	3.3
LOGW2 48-48.5	14.71 m (48.25 ft.)	0.0	0.0	1.0	13.4	43.8	41.8
LOGW2 73-73.5	22.33 m (73.25 ft.)	0.0	0.0	0.5	10.7	65.2	23.6
LOGW2 103-103.5	31.48 m (103.25 ft.)	0.0	1.6	2.1	36.2	43.2	16.9
OGF 6" *	0.15 m (0.5 ft.)	0.0	2.5	3.0	41.3	39.2	14.0
OGF 12" *	0.3 m (1 ft.)	0.0	0.0	5.6	42.7	35.7	16.0
OGF 18" *	0.46 m (1.5 ft.)	0.0	0.0	4.6	41.7	33.6	20.1
OGF 24" *	0.61 m (2 ft.)	0.0	0.0	4.2	40.6	34.5	20.7
OGF 30" *	0.76 m (2.5 ft.)	0.0	4.3	5.7	39.9	30.9	19.2
OGF 36" *	0.91 m (3 ft.)	0.0	0.0	6.1	39.6	32.9	21.4
OGF 42" *	1.07 m (3.5 ft.)	0.0	5.4	5.4	29.9	36.3	23.0
OGF 48" *	1.22 m (4 ft.)	0.0	2.0	4.8	31.6	38.7	22.9
OGF 52" *	1.37 m (4.5 ft.)	0.0	0.0	6.7	34.7	38.4	20.2
OGF 8.33-9	2.64 m (8.67 ft.)	0.0	12.2	7.7	36.4	34.5	9.2
OGF 13.66-14	4.22 m (13.83 ft.)	0.0	0.0	4.2	24.7	54.4	16.7
OGF 18.33-19	5.69 m (18.67 ft.)	0.0	6.0	12.0	58.2	21.0	2.8

Sample ID	Depth	Percent Distribution						
		Gravel			Sand		Very Fine Sand, Silt & Clay < 0.074 mm	
		>16 mm	4-16 mm	2-4 mm	2-0.35 mm	0.35-0.074 mm		
OGF 23.33-24	7.22 m (23.67 ft.)	0.0	0.8	1.6	44.4	47.4	5.8	
OGF 28.33-28.66	8.69 m (28.5 ft.)	0.0	2.6	9.0	51.4	28.0	9.0	
OGF 28.66-29	8.79 m (28.83 ft.)	0.0	7.0	6.5	51.5	28.8	6.2	
OGF 32.5-33	9.98 m (32.75 ft.)	0.0	0.0	0.7	9.9	48.2	41.2	
OGF 38.5-39	11.81 m (38.75 ft.)	0.0	7.6	17.8	56.8	16.4	1.4	
OGF 43.5-44	13.34 m (43.75 ft.)	0.0	4.6	9.5	63.6	19.6	2.7	
OGF 48.5-49	14.86 m (48.75 ft.)	0.0	0.0	1.4	32.5	53.6	12.5	
OGF 53-53.5	16.23 m (53.25 ft.)	0.0	6.9	6.3	34.8	40.0	12.0	
OGF 59.5-60	18.22 m (59.75 ft.)	0.0	1.5	4.2	62.8	26.0	5.5	
OGF 64-64.5	19.59 m (64.25 ft.)	0.0	6.2	12.2	57.7	20.7	3.2	
OGF 68.5-69	20.96 m (68.75 ft.)	0.0	0.9	3.7	49.9	34.8	10.7	
OGF 69.5-70	21.27 m (69.75 ft.)	0.0	0.0	2.2	50.5	44.6	2.7	
OGF 73.5-74	22.48 m (73.75 ft.)	0.0	0.4	4.8	57.8	31.4	5.6	
OGF 78.5-79	24.01 m (78.75 ft.)	0.0	0.0	0.4	4.3	47.8	47.5	
OGF 83.5-84	25.53 m (83.75 ft.)	0.0	0.0	4.0	25.7	50.4	19.9	
OGF 88.5-89	27.06 m (88.75 ft.)	0.0	0.0	0.5	28.7	60.7	10.1	
OGF 93.5-94	28.58 m (93.75 ft.)	0.0	0.5	0.7	18.8	61.5	18.5	
OGF 98.5-99	30.11 m (98.75 ft.)	0.0	0.0	1.1	36.4	47.9	14.6	
OGF 104.5-105	31.94 m (104.75 ft.)	0.0	0.0	2.1	59.4	32.2	6.3	
USCW 14.5-15	4.5 m (14.75 ft.)	0.0	6.2	17.0	60.6	14.4	1.8	
USCW 34.5-35	10.59 m (34.75 ft.)	0.0	10.1	20.7	49.5	15.6	4.1	
USCW 54.5-55	16.69 m (54.75 ft.)	0.0	11.8	20.4	49.2	14.1	4.5	
USCW 74.5-75	22.79 m (74.75 ft.)	0.0	40.4	14.0	28.2	12.6	4.8	
USCW 99.5-100	30.41 m (99.75 ft.)	0.0	26.5	14.0	41.6	13.1	4.8	
MSCW 23.5-24	7.24 m (23.75 ft.)	0.0	29.7	16.6	29.9	17.8	6.0	

Sample ID	Depth	Percent Distribution					
		Gravel		Sand		Very Fine Sand, Silt & Clay < 0.074 mm	
		>16 mm	4-16 mm	2-4 mm	2-0.35 mm		0.35-0.074 mm
MSCW 33.5-34	10.29 m (33.75 ft.)	0.0	2.9	9.0	43.5	37.4	7.2
MSCW 43.5-44	13.34 m (43.75 ft.)	0.0	8.7	12.2	28.8	40.4	9.9
MSCW 59.5-60	18.22 m (59.75 ft.)	0.0	0.0	4.9	43.2	37.4	14.5
MSCW 90.5-91	27.67 m (90.75 ft.)	0.0	0.4	1.9	6.4	50.9	40.4
MSCW 99.5-100	30.41 m (99.75 ft.)	0.0	0.0	0.4	30.5	58.1	11.0
MSCW 109.5-110	33.46 m (109.75 ft.)	0.0	14.9	12.7	40.3	23.1	9.0
MSCW 139.5-140	42.61 m (139.75 ft.)	0.0	1.0	0.8	11.1	55.4	31.7
MSCW 159.5-160	48.7 m (159.75 ft.)	0.0	0.0	0.1	36.3	54.6	9.0
MSCW 179.5-180	54.8 m (179.75 ft.)	0.0	2.0	8.3	64.1	22.7	2.9
MSCW 199.5-200	60.9 m (199.75 ft.)	0.0	3.9	13.2	48.1	27.0	7.8
MSCW2 201.5-202	61.51 m (201.75 ft.)	0.0	3.1	1.0	6.0	58.8	31.1
MSCW 240.5-241	73.4 m (240.75 ft.)	0.0	1.2	8.4	54.8	32.3	3.3
MSCW2 259.5-260	79.19 m (259.75 ft.)	0.0	1.1	12.1	47.8	33.7	5.3
MSCW 302.5-303	92.3 m (302.75 ft.)	0.0	0.0	1.0	3.4	54.2	41.4
MSCW2 320.5-321	97.64 m (320.75 ft.)	0.0	1.3	9.3	38.2	37.3	13.9
MSCW2 400.5-401	122.18 m (400.75 ft.)	0.0	1.3	7.2	59.3	28.1	4.1
LSCW 12.5-13	3.89 m (12.75 ft.)	0.0	12.7	15.7	52.8	14.4	4.4
LSCW 27.5-28	8.46 m (27.75 ft.)	0.0	1.5	6.8	34.8	43.7	13.2
LSCW 34.5-35	10.59 m (34.75 ft.)	0.0	2.7	9.5	34.1	36.8	16.9
LSCW 59.5-60	18.22 m (59.75 ft.)	0.0	0.4	3.8	31.3	43.1	21.4
LSCW 99.5-100	30.41 m (99.75 ft.)	0.0	0.0	0.0	3.1	42.2	54.7
SCF 7.5-8	2.36 m (7.75 ft.)	0.0	22.8	10.1	42.6	18.8	5.7
SCF 12.5-13	3.89 m (12.75 ft.)	0.0	0.0	0.2	28.1	60.9	10.8
SCF 17.5-18	5.41 m (17.75 ft.)	0.0	12.3	11.8	55.3	16.0	4.6
SCF 22.5-23	6.94 m (22.75 ft.)	0.0	15.5	8.2	49.9	21.4	5.0

Sample ID	Depth	Percent Distribution					
		>16 mm	Gravel 4-16 mm		2-4 mm	2-0.35 mm	Sand 0.35-0.074 mm
SCF 47.5-48	14.56 m (47.75 ft.)	0.0	4.4	3.3	26.0	49.9	16.4
SCF 78.5-79	24.01 m (78.75 ft.)	0.0	11.4	4.3	39.9	27.7	16.7

* Hand-auger sample

APPENDIX C:
CORE AND HAND-AUGER SAMPLE DATA

Table C1. Core and hand-auger sample data: gravimetric-water contents, soil-water potentials, soil-water extraction distillation yields, and isotopic compositions of extracted soil waters

Sample ID	Depth	Water Content (% by weight)	Soil-Water Potential (kilopascals)	Distillation Yield (%)	δD (o/oo)	$\delta^{18}O$ (o/oo)
SUMMIT 8-8.5	2.52 m (8.25 ft.)	7.0	-272	86.6	-76.6	-10.08
SUMMIT 13-13.5 #	4.04 m (13.25 ft.)	7.1	-409	84.7	-75.3	-10.24
SUMMIT 23-23.5	7.09 m (23.25 ft.)	5.6	-136	97.9	-72.3	-9.49
SUMMIT 28-28.5 #	8.61 m (28.25 ft.)	5.1	0	99.7	-70.6	-9.37
SUMMIT 48-48.5	14.71 m (48.25 ft.)	2.0	-1230	122.9	-73.3	-9.41
UOGW 6"	0.15 m (0.5 ft.)	3.9	0	131.8	-77.1	-9.91
UOGW 12"	0.3 m (1 ft.)	6.2	0	91.2	-63.4	-6.33
UOGW 18"	0.46 m (1.5 ft.)	2.0	-821	99.0	-67.7	-7.66
UOGW 24"	0.61 m (2 ft.)	1.9	-544	105.7	-73.5	-9.42
UOGW 30"	0.76 m (2.5 ft.)	1.8	-817	108.4	-74.1	-9.61
UOGW 36"	0.91 m (3 ft.)	2.6	-822	104.2	-76.8	-10.19
UOGW 42"	1.07 m (3.5 ft.)	2.5	-409	110.0	-73.5	-10.09
UOGW 48"	1.22 m (4 ft.)	3.1	0	112.4	-76.7	-10.27
UOGW 54"	1.37 m (4.5 ft.)	4.7	0	108.4	-77.2	-10.44
UOGW 60"	1.52 m (5 ft.)	4.4	0	107.1	-75.9	-10.47
UOGW 72"	1.83 m (6 ft.)	4.6	0	100.9	-72.7	-10.26
UOGW 84"	2.13 m (7 ft.)	8.7	0	97.7	-77.3	-10.76
UOGW 96"	2.44 m (8 ft.)	4.9	0	114.1	-75.5	-10.12
UOGW 108"	2.74 m (9 ft.)	5.9	0	112.2	-72.3	-10.32
UOGW 9-9.5 #	2.82 m (9.25 ft.)	4.2	-545	98.7	-53.3	-8.04
UOGW 14.5-15 #	4.5 m (14.75 ft.)	5.3	0	102.7	-54.1	-8.34
UOGW 20.5-21	6.33 m (20.75 ft.)	5.2	NA	98.5	-51.9	-7.90

Sample ID	Depth	Water Content (% by weight)	Soil-Water Potential (kilopascals)	Distillation Yield (%)	δD (o/oo)	$\delta^{18}O$ (o/oo)
UOGW 28.8-29.3 #	8.86 m (29.05 ft.)	5.2	0	110.9	-61.7	-9.24
UOGW 54.5-55	16.69 m (54.75 ft.)	4.6	NA	94.3	-63.7	-9.48
UOGW 68.5-69	20.96 m (68.75 ft.)	3.7	NA	128.4	-64.4	-9.56
UOGW 84.5-85	25.84 m (84.75 ft.)	4.2	NA	NA	-64.8	-9.20
UOGW 104-104.5	31.78 m (104.25 ft.)	4.2	NA	129.0	-64.4	-9.10
MOGW 6" *	0.15 m (0.5 ft.)	4.2	0	101.9	-73.4	-7.79
MOGW 12" *	0.3 m (1 ft.)	3.5	0	102.3	-50.6	-3.93
MOGW 18" *	0.46 m (1.5 ft.)	5.4	0	90.3	-58.6	-6.73
MOGW 24" *	0.61 m (2 ft.)	4.6	0	108.5	-63.3	-7.66
MOGW 30" *	0.76 m (2.5 ft.)	3.5	0	100.4	-64.4	-7.09
MOGW 36" *	0.91 m (3 ft.)	4.3	0	NA	-66.1	-7.70
MOGW 42" *	1.07 m (3.5 ft.)	4.7	0	85.8	-65.8	-7.43
MOGW 48" *	1.22 m (4 ft.)	3.7	0	103.8	-71.3	-8.57
MOGW 54" *	1.37 m (4.5 ft.)	3.4	0	105.5	-69.3	-8.91
MOGW 60" *	1.52 m (5 ft.)	3.0	0	103.1	-67.6	-8.65
MOGW 66" *	1.68 m (5.5 ft.)	2.6	0	115.9	-67.5	-8.85
MOGW ~72" *	1.83 m (6 ft.)	2.7	0	119.9	-64.5	-8.45
MOGW 72" *	1.83 m (6 ft.)	12.8	0	84.7	-66.3	-9.02
MOGW 84" *	2.13 m (7 ft.)	5.0	0	NA	-67.7	-8.98
MOGW 96" *	2.44 m (8 ft.)	4.5	0	109.4	-66.3	-8.65
MOGW 8.5-9 #	2.67 m (8.75 ft.)	12.2	0	88.7	-71.3	-10.25
MOGW 13.5-14	4.19 m (13.75 ft.)	5.3	0	102.8	-69.0	-10.12
MOGW 20.5-21 #	6.33 m (20.75 ft.)	3.2	0	110.2	-71.7	-10.34
MOGW 23.5-24	7.24 m (23.75 ft.)	2.2	0	113.0	-73.5	-10.31
MOGW 29-29.5	8.92 m (29.25 ft.)	4.4	NA	90.3	-71.8	-10.03

Sample ID	Depth	Water Content (% by weight)	Soil-Water Potential (kilopascals)	Distillation Yield (%)	δD (o/oo)	$\delta^{18}O$ (o/oo)
MOGW 34-34.5 #	10.44 m (34.25 ft.)	5.6	0	89.9	-72.0	-10.01
MOGW 39.5-40	12.12 m (39.75 ft.)	6.8	NA	83.1	-76.5	-10.64
MOGW 44-44.5	13.49 m (44.25 ft.)	8.2	0	117.9	-77.4	-10.89
MOGW 49-49.5	15.02 m (49.25 ft.)	5.6	NA	NA	-75.8	-10.57
MOGW 54-54.5 #	16.54 m (54.25 ft.)	6.5	0	102.0	-77.5	-10.55
MOGW 59-59.5	18.06 m (59.25 ft.)	5.6	-137	106.8	-77.8	-11.26
MOGW 64-64.5 #	19.59 m (64.25 ft.)	11.2	0	106.0	-79.0	-11.04
MOGW 69-69.5 #	21.11 m (69.25 ft.)	2.4	0	98.8	-67.1	-9.71
MOGW 75-75.5	22.94 m (75.25 ft.)	4.0	NA	102.0	-74.6	-10.43
MOGW 80.5-81	24.62 m (80.75 ft.)	3.3	0	91.0	-70.7	-9.96
MOGW 85-85.5 #	25.99 m (85.25 ft.)	3.0	0	109.0	-70.5	-9.62
MOGW 89.5-90	27.36 m (89.75 ft.)	3.3	NA	99.0	-67.4	-9.18
MOGW 95-95.5	29.04 m (95.25 ft.)	5.2	0	NA	-61.1	-9.45
MOGW 99.5-100	30.41 m (99.75 ft.)	5.1	NA	103.7	-70.4	-9.81
MOGW 118.5-119 #	36.2 m (118.75 ft.)	2.6	NA	96.0	-72.7	-9.61
MOGW 160-160.5	48.86 m (160.25 ft.)	9.4	NA	93.6	-80.8	-10.65
MOGW 178	54.34 m (178.25 ft.)	2.8	NA	97.1	-81.6	-10.50
MOGW 218-218.5	66.54 m (218.25 ft.)	7.6	NA	88.2	-72.2	-9.78
MOGW 239.5-240	73.09 m (239.75 ft.)	2.1	NA	83.4	-76.9	-10.03
MOGW 260-260.5	79.34 m (260.25 ft.)	2.6	NA	78.2	-79.3	-10.56
MOGW 320	97.48 m (319.75 ft.)	8.0	NA	94.7	-81.8	-11.16
MOGW 360.7-361.2	110.05 m (360.95 ft.)	6.9	NA	96.2	-59.2	-8.34
MOGW 419.3-419.8	127.91 m (419.55 ft.)	6.4	NA	121.7	-55.4	-8.04
MOGW 480-480.5	146.42 m (480.25 ft.)	11.5	NA	86.3	-57.5	-8.10
LOGW1 8-8.5 #	2.52 m (8.25 ft.)	2.4	-136	97.7	-60.9	-7.37

Sample ID	Depth	Water Content (% by weight)	Soil-Water Potential (kilopascals)	Distillation Yield (%)	δD (o/oo)	$\delta^{18}O$ (o/oo)
LOGW1 12.5-13	3.89 m (12.75 ft.)	4.7	-136	130.4	-62.2	-8.93
LOGW1 18.5-19	5.72 m (18.75 ft.)	5.3	NA	100.0	-73.4	-9.80
LOGW1 28.5-29 #	8.77 m (28.75 ft.)	5.5	0	127.8	-78.1	-10.01
LOGW1 44.5-45	13.64 m (44.75 ft.)	15.7	NA	102.0	-71.8	-9.30
LOGW1 63.66-64	19.46 m (63.83 ft.)	3.6	NA	101.0	-70.1	-8.70
LOGW1 68.5-69	20.96 m (68.75 ft.)	6.6	0	91.8	-71.4	-8.56
LOGW1 73.33-73.66	22.41 m (73.5 ft.)	18.0	0	104.7	-75.3	-9.65
LOGW1 73.66-74	22.51 m (73.83 ft.)	14.2	0	97.5	-77.1	-9.51
LOGW1 78.66-79	24.03 m (78.83 ft.)	11.4	NA	106.0	-77.0	-9.20
LOGW1 88.33-88.66	26.98 m (88.5 ft.)	4.3	-275	91.6	-77.4	-9.24
LOGW1 88.66-89	27.08 m (88.83 ft.)	3.1	-551	98.4	-75.3	-8.52
LOGW1 93.66-94	28.61 m (93.83 ft.)	8.5	NA	67.0	-82.3	-9.70
LOGW1 98.33-98.66	30.03 m (98.5 ft.)	6.3	-1378	93.4	-83.5	-10.72
LOGW1 98.66-99	30.13 m (98.83 ft.)	7.5	-687	98.3	-83.3	-10.55
LOGW2 8-8.5	2.52 m (8.25 ft.)	1.9	-5268	100.5	-81.5	-9.47
LOGW2 28-28.5 #	8.61 m (28.25 ft.)	2.8	-3305	94.5	-76.9	-8.39
LOGW2 48-48.5	14.71 m (48.25 ft.)	4.4	-2474	92.9	-83.6	-9.93
LOGW2 73-73.5 #	22.33 m (73.25 ft.)	5.9	-2196	92.7	-82.7	-10.41
LOGW2 103-103.5	31.48 m (103.25 ft.)	2.9	-958	94.8	-81.2	-10.80
OGF 6" *	0.15 m (0.5 ft.)	2.7	-822	105.6	-85.3	-9.56
OGF 12" *	0.3 m (1 ft.)	2.3	-6171	84.1	-36.6	-1.16
OGF 18" *	0.46 m (1.5 ft.)	1.7	-10043	104.8	-53.0	-3.53
OGF 24" *	0.61 m (2 ft.)	2.1	-8292	108.1	-66.9	-6.02
OGF 30" *	0.76 m (2.5 ft.)	1.4	-9013	110.5	-67.9	-6.31

Sample ID	Depth	Water Content (% by weight)	Soil-Water Potential (kilopascals)	Distillation Yield (%)	δD (o/oo)	$\delta^{18}O$ (o/oo)
OGF 36" *	0.91 m (3 ft.)	1.6	-9661	103.1	-73.1	-7.71
OGF 42" *	1.07 m (3.5 ft.)	2.7	-9629	99.6	-72.6	-8.38
OGF 48" *	1.22 m (4 ft.)	2.0	-9570	105.5	-70.3	-8.27
OGF 52" *	1.37 m (4.5 ft.)	2.0	-9450	103.1	-70.2	-8.64
OGF 8.33-9	2.64 m (8.67 ft.)	2.1	NA	96.2	-71.6	-7.16
OGF 13.66-14	4.22 m (13.83 ft.)	3.0	NA	95.7	-73.1	-7.31
OGF 18.33-19	5.69 m (18.67 ft.)	2.4	NA	108.8	-70.9	-6.79
OGF 23.33-24	7.22 m (23.67 ft.)	6.3	NA	85.8	-80.3	-8.60
OGF 28.33-28.66	8.69 m (28.5 ft.)	1.9	-8641	95.3	-63.4	-7.37
OGF 28.66-29	8.79 m (28.83 ft.)	1.4	-12187	94.8	-56.6	-6.65
OGF 32.5-33	9.98 m (32.75 ft.)	5.3	NA	98.5	-81.7	-9.40
OGF 38.5-39	11.81 m (38.75 ft.)	3.6	-6161	100.8	-60.9	-7.18
OGF 43.5-44 #	13.34 m (43.75 ft.)	1.3	-8580	92.4	-70.1	-6.38
OGF 48.5-49	14.86 m (48.75 ft.)	3.3	NA	106.3	-77.1	-8.52
OGF 53-53.5	16.23 m (53.25 ft.)	2.8	-5167	86.1	-69.6	-8.67
OGF 59.5-60	18.22 m (59.75 ft.)	1.3	-8038	85.3	-47.4	-5.62
OGF 64-64.5 #	19.59 m (64.25 ft.)	1.2	-4029	82.9	-77.5	-8.30
OGF 68.5-69	20.96 m (68.75 ft.)	5.6	-2631	56.4	-78.9	-8.57
OGF 69.5-70	21.27 m (69.75 ft.)	1.1	NA	103.7	-72.5	-7.66
OGF 73.5-74	22.48 m (73.75 ft.)	1.2	-2489	101.7	-78.4	-8.48
OGF 78.5-79 #	24.01 m (78.75 ft.)	4.4	-2894	95.6	-81.7	-9.11
OGF 83.5-84	25.53 m (83.75 ft.)	4.7	-1090	NA	-79.6	-9.46
OGF 88.5-89 #	27.06 m (88.75 ft.)	5.0	-1928	96.6	-78.6	-9.58
OGF 93.5-94 #	28.58 m (93.75 ft.)	6.5	-1106	93.5	-81.9	-10.20
OGF 98.5-99	30.11 m (98.75 ft.)	2.7	NA	95.2	-80.4	-9.49
OGF 104.5-105 #	31.94 m (104.75 ft.)	1.6	-1511	97.2	-76.5	-9.39

Sample ID	Depth	Water Content (% by weight)	Soil-Water Potential (kilopascals)	Distillation Yield (%)	δD (o/oo)	$\delta^{18}O$ (o/oo)
USCW 14.5-15	4.5 m (14.75 ft.)	4.9	0	100.8	-79.6	-8.09
USCW 34.5-35	10.59 m (34.75 ft.)	4.1	-274	91.6	-79.5	-8.82
USCW 54.5-55 #	16.69 m (54.75 ft.)	2.7	-274	98.9	-77.3	-8.80
USCW 74.5-75	22.79 m (74.75 ft.)	2.4	-411	111.3	-80.3	-8.97
USCW 99.5-100	30.41 m (99.75 ft.)	1.7	-549	94.8	-67.9	-6.35
MSCW 23.5-24 #	7.24 m (23.75 ft.)	1.7	-549	102.0	-78.4	-8.82
MSCW 33.5-34	10.29 m (33.75 ft.)	2.8	-549	116.0	-88.2	-9.51
MSCW 43.5-44 #	13.34 m (43.75 ft.)	3.9	-274	100.0	-87.7	-8.79
MSCW 59.5-60	18.22 m (59.75 ft.)	2.9	NA	101.0	-87.2	-10.11
MSCW 90.5-91 #	27.67 m (90.75 ft.)	3.7	-1247	116.7	-89.0	-11.05
MSCW 99.5-100	30.41 m (99.75 ft.)	1.7	-1239	123.1	-83.2	-7.71
MSCW 109.5-110 #	33.46 m (109.75 ft.)	1.7	NA	103.9	-84.7	-8.35
MSCW 139.5-140	42.61 m (139.75 ft.)	5.8	-1240	92.7	-88.9	-10.65
MSCW 159.5-160	48.7 m (159.75 ft.)	2.0	-1102	111.9	-91.5	-9.13
MSCW 179.5-180	54.8 m (179.75 ft.)	1.3	NA	102.4	-89.1	-11.70
MSCW 199.5-200	60.9 m (199.75 ft.)	1.7	-962	99.4	-89.9	-10.77
MSCW2 201.5-202	61.51 m (201.75 ft.)	4.3	NA	99.1	-93.1	-11.24
MSCW 240.5-241	73.4 m (240.75 ft.)	5.4	-412	95.0	-86.7	-11.65
MSCW2 259.5-260 #	79.19 m (259.75 ft.)	1.8	NA	97.2	-89.2	-10.70
MSCW 302.5-303 #	92.3 m (302.75 ft.)	11.4	-412	99.9	-94.6	-11.93
MSCW2 320.5-321	97.64 m (320.75 ft.)	2.2	NA	88.4	-96.8	-11.80
MSCW2 400.5-401 #	122.18 m (400.75 ft.)	1.5	NA	100.0	-89.0	-10.95
LSCW 12.5-13	3.89 m (12.75 ft.)	2.1	-412	94.7	-69.6	-8.95
LSCW 27.5-28	8.46 m (27.75 ft.)	3.6	-411	93.8	-78.8	-8.78

Sample ID	Depth	Water Content (% by weight)	Soil-Water Potential (kilopascals)	Distillation Yield (%)	δD (o/oo)	$\delta^{18}O$ (o/oo)
LSCW 34.5-35 #	10.59 m (34.75 ft.)	1.2	-6867	84.8	-85.2	-7.31
LSCW 59.5-60 #	18.22 m (59.75 ft.)	2.2	-5171	98.2	-80.6	-7.16
LSCW 99.5-100 #	30.41 m (99.75 ft.)	5.6	-1795	102.5	-87.8	-8.95
SCF 7.5-8	2.36 m (7.75 ft.)	0.7	-4871	135.8	-78.4	-7.48
SCF 12.5-13	3.89 m (12.75 ft.)	1.4	-3050	103.7	-78.3	-6.53
SCF 17.5-18 #	5.41 m (17.75 ft.)	0.8	-5011	81.7	-77.3	-6.63
SCF 22.5-23	6.94 m (22.75 ft.)	0.5	-14715	98.9	-81.4	-6.51
SCF 47.5-48 #	14.56 m (47.75 ft.)	1.2	-7463	104.3	-88.9	-7.86
SCF 78.5-79	24.01 m (78.75 ft.)	1.9	-2206	116.0	-92.4	-8.59

Duplicate soil water extractions were performed and the values for distillation yield, δD and $\delta^{18}O$ are averages.

* Hand-auger sample